THE UNIVERSITY *of* EDINBURGH

THE UNIVERSITY *of* EDINBURGH

The Impact of Thiosulfate Sulfurtransferase (TST) on Metabolic Dysfunction-Associated Steatotic Liver Disease (MASLD) and the Metabolic Benefits of Calorie Restriction

Shaden Melhem

Thesis for the Degree of Doctor of Philosophy (PhD)

The University of Edinburgh

2024

Declaration

I declare the following:

(a) This thesis has been composed by myself.

(b) All work presented in this thesis was performed by the myself unless where explicitly stated otherwise.

(c) This work has not been submitted for any other degree or professional qualification.

(d) Any included publications are my own work, except when indicated throughout the thesis and summarised and clearly identified on the declarations page of the thesis.

Shaden Melhem

October, 2024

Dedication

This work is dedicated to all students in Palestine who lost everything and did not get to graduate this year. My achievements feel incomplete without yours. I hope we will see peace one day.

Shaden

Poster/oral presentations and publications

Publications related to this PhD:

1. **Shaden Melhem***, Yang Luo*, Laurent Chatre, Martin Feelisch, Nicholas Morton, Amalia M. Dolga, Harry van Goor. Thiosulphate Sulfurtransferase: Biological Roles and Therapeutic Potential. *Under review,* Redox Biology.

2. Luo Y, Chatre L, **Melhem S**, Al-Dahmani ZM, Homer NZM, Miedema A, et al. Thiosulfate sulfurtransferase deficiency promotes oxidative distress and aberrant nrf2 function in the brain. Redox Biology. 2023; 68:102965.

3. Yang Luo, Angélica María Sabogal-Guáqueta, Anneke Miedema, **Shaden Melhem**, Robin van der Straat, Zayana M. Al-Dahmani, Marina Trombetta-Lima, Matthew R. Groves, Martin Feelisch, Nicholas M. Morton, Laurent Chatre, Harry van Goor, Amalia M. Dolga. Thiosulfate Sulfurtransferase Protects Neuronal Cells Against Ferroptosis. *Under review,* Redox Biology.

Oral / poster presentations related to this PhD:

1. Oral presentation: Thiosulfate Sulfurtransferase (TST) Deficiency Improves the Metabolic Benefits of Calorie Restriction in Male Mice.

The 26th International Conference on Redox Medicine 2024, Paris, France

2. Oral presentation: HepaRG Bioenergetics in MASLD

Halt-RONIN consortium Meeting 2024, Edinburgh, UK

3. Poster presentation: TST deficiency enhances the metabolic benefits of calorie restriction in mice

BHF-PhD student conference 2024, Bristol, UK

4. Poster presentation: Meeting 2024, Edinburgh, UK

3. Poster presentation: TST deficiency enhances the metabolic benefits of calorie restriction in mice.

CVS symposium 2024- Edinburgh, UK

5. Poster presentation: The role of thiosulfate sulfur transferase (TST) in MASLD.

BHF-PhD student conference 2022, Leeds, UK

6. Poster presentation: The role of thiosulfate sulfur transferase (TST) in MASLD.

CVS symposium 2022, Edinburgh, UK

Abstract

Metabolic dysfunction-associated steatotic liver disease (MASLD) affects 20-30% of adults in western countries and is closely linked to obesity and type 2 diabetes. Hydrogen sulfide (H_2S), once solely perceived as toxic, is now recognised for its role in various physiological and pathological processes. H_2S donors have shown promise in treating fatty liver disease and reducing blood pressure in animal models, but their therapeutic use is hindered by challenges in H_2S pharmacokinetics. The sulfur oxidation pathway (SOP), which regulates H_2S levels through its disposal, has been underexplored as a potential route to therapeutic H_2S elevation. Thiosulfate sulfurtransferase (TST), a mitochondrial enzyme, is part of the SOP and metabolises H_2S, indirectly, to prevent toxicity. Previous work leading up to this thesis showed that *TST* mRNA levels were upregulated during the early steatosis stage of MASLD in humans. Given the previously identified metabolic protective effect of adipose tissue TST elevation, I hypothesised that elevation of hepatic TST in early MASLD was a protective mechanism, counteracting declining liver function in MASLD. Improved metabolic health following calorie restriction (CR) is mediated in part through increased hepatic production of H_2S. *Tst*$^{-/-}$ mice exhibited elevated systemic H_2S levels, therefore I hypothesised they may have an enhanced response to CR.

In chapters 3 and 4, I tested the hypothesis that elevated hepatic TST expression in MASLD offered protection against MASLD development using a liver-specific overexpression mouse model (Liv_hTST). Male and female C57BL/6J and Liv_hTST mice were fed either a control diet or MASLD-inducing GAN diet for 20 weeks. Systemic and hepatic sulfide levels were measured, fat and lean mass assessed, and glucose tolerance evaluated. *In vitro*, HepaRG cells with TST overexpression were tested for lipid accumulation, oxidative stress, and mitochondrial function. Results showed sex-specific effects on sulfide levels and glucose tolerance, with protective effects against fibrosis in male mice *in vivo*, and a worsening of the impaired lipid metabolism and mitochondrial function *in vitro*. This research addresses the gap in understanding of the protective role ascribed to elevated TST expression against steatogenic liver changes in MASLD and revealed novel sex-specific effects on systemic sulfide levels, glucose tolerance, and fibrosis.

In chapter 5, I investigated whether *Tst*$^{-/-}$ mice experienced enhanced metabolic benefits from CR due to their elevated systemic sulfide. Ten-week-old male and female C57BL/6J and *Tst*$^{-/-}$ mice underwent 4-week 30% CR. Indirect calorimetry, glucose tolerance, H_2S production, and disposal (SOP) enzyme levels were assessed. *Tst*$^{-/-}$ males had higher systemic but similar hepatic sulfide levels compared to C57BL/6J males, confirming previous work. CR did not affect sulfide levels but improved glucose tolerance in *Tst*$^{-/-}$ males, despite their resistance to fat mass loss. Energy expenditure and substrate utilisation were similar between genotypes. Females were unaffected by the lack of TST and had lower levels of hepatic H_2S metabolism enzymes. Our findings suggested mechanisms beyond hepatic sulfide modulation mediate CR benefits. Understanding the novel role of elevated systemic H_2S and TST deficiency in maintaining fat mass and concurrent metabolic benefits with CR may inform H_2S -targeted therapeutic strategies in the future.

Lay Summary

Fatty liver disease affects 20-30% of adults in developed countries and is closely linked to obesity and type 2 diabetes. Hydrogen sulfide (H_2S), a gas once thought to be harmful, is now known to play important roles in the body. Sulfide releasing medicines have shown promise in treating fatty liver disease and lowering blood pressure in animal studies, but their use in humans is complicated by how the body handles sulfide. Thiosulfate sulfurtransferase (TST) is an enzyme that helps prevent high sulfide levels and prevent its toxicity. Research suggests that increased liver TST levels may help protect against damage in fatty liver disease.

I tested whether increasing TST levels in the liver could protect against fatty liver disease. I used mice with high TST levels and fed them either a normal diet or a fatty diet that makes the disease happen sooner. I measured sulfide levels, body fat, and glucose levels. In lab tests, we also looked at how cells with high TST handled fat and energy. I found that TST affects sulfide levels and glucose differently in males and females, with some protective effects in males.

I also studied mice lacking the TST gene to see if they had better metabolic responses to calorie restriction (CR) due to their high sulfide levels. We put these mice and normal mice on a reduced-calorie diet for 4 weeks and measured various health markers. Mice without the TST gene had higher sulfide levels in their blood but not in the liver. CR improved their glucose levels but they lost less weight. Our findings suggest that factors other than sulfide levels in the liver contribute to the benefits of CR. This work will guide future studies aimed at understanding the role of sulfide in CR and may help scientists find ways to design drugs to make people benefit more from CR diets.

Acknowledgments

I would like to thank the British Heart Foundation (BHF) for funding and supporting this PhD. I would also like to thank my supervisors, Prof. Nik Morton, Prof. Ruth Andrew, Prof. Jonathan Fallowfield and Prof. Timothy Kendall for their support and guidance through these years of developing as a scientist, their patience and encouragement made this experience a valuable learning opportunity and a journey of personal and professional growth. A special thank you to Nik Morton, who is the primary supervisor of this work, for treating me like a scientist from day one, and allowing me to experience things for myself, which has made me much more confident and competent in the lab, and as a person as well.

I would also like to thank Prof. Roland Stimson, the chair of my committee for these years, for leading the process of yearly reviews with most kindness and professionalism. I extend my thanks and appreciation to Dr. Lenny Nelson, whose energy, enthusiasms, and knowledge had a big impact on me and I am grateful for knowing you and your research group. A massive thank you to Rod Carter who helped me make sense of some challenges and was always ready to discuss my research with me.

I would like to extend my heartfelt thanks to all BVS staff for their invaluable assistance with the animal work throughout my research. Especially Ami Onishi, your professionalism, dedication, and support were instrumental in ensuring the success of this aspect of my project. I am truly grateful for your expertise and kindness. I would also like to Thank Harry and Yang from the University of Groningen for our shared work and for supporting my academic career.

These years were filled with great moments, but also brought more stress and anxiety than I could have imagined. I feel incredibly fortunate to have met friends who became the backbone of this journey. Everyone in office W3.15, especially Kalyani, Bronwyn, and Hongling, thank you for always being there for me. Your kindness and the purity of your hearts are truly rare and something I deeply cherish.

These acknowledgments would not be complete without thanking Ibrahim who unconditionally supported me in every way possible! and Khansa who was always the kindest and helped me forget about the stress, and all my friends whose names are not mentioned who checked on me constantly especially during the last year.

Living in Edinburgh is one of the best things about this PhD. I am deeply grateful to Elsbeth and Douglas Currie for their support and generosity during my PhD. Your home provided comfort, encouragement, and a sense of belonging that made all the difference.

Finally, my dear family, no words can express my love and gratitude for you, my dear sisters and brother and my lovely nephew and niece. My mom "Nihad", and my dad "Saleh", none of this would be possible without your unconditional love and support, and without your patience and prayers. I hope my work makes you proud!

Table of Contents

List of Figures

List of Tables

List of abbreviations

Abbreviation	Description
AD	Alzheimer'S Disease
AL	Ad Libitum
ALD	Alcohol-Related Liver Disease
AMLN	Amylin Liver NASH
AMPK	AMP-Activated Protein Kinase
ANCOVA	Analysis of Co-Variants
ANOVA	Analysis of Variance
AOC	Area of the Curve
BMI	Body Mass Index
BSA	Bovine Serum Albumin
CBS	Cystathionine Synthase
CCl4	Carbon Tetrachloride
CO	Carbon Monoxide
COPD	Chronic Obstructive Pulmonary Disease
COX	Cytochrome C Oxidase
CPT1	Carnitine Palmitoyltransferase 1
CR	Calorie Restriction
CSE or CTH or CGL	Cystathionine Gamma Lyase
DMSO	Dimethylsulfoxide
DNL	*De novo* Lipogenesis
ECM	Extracellular Matrix
EE	Energy Expenditure
ER	Endoplasmic Reticulum
ETC	Electron Transport Chain
ETHE1	Ethylmalonic Encephalopathy Protein 1
FAO	Fatty Acid Oxidation
FCCP	Carbonyl Cyanide-P-Trifluoromethoxyphenylhydrazone
FDFT1	Farnesyl-Diphosphate Farnesyltransferase 1
FFAs	Free Fatty Acids
GAN	Gubra Amylin NASH
GFP	Green Fluorescent Protein
GK	Glucokinase
GSH	Glutathione
H&E	Hematoxylin and Eosin
H_2S	Hydrogen Sulfide
HCC	Hepatocellular Carcinoma
HFD	High Fat Diet
HFHC	High-Fat, High-Cholesterol

HFHF	High-Fat, High-Fructose
HPR101	Progenitor HepaRG
HPR116	Differentiated HepaRG
HSCs	Hepatic Stellate Cells
IL-6	Interleukin-6
iPSCs	Induced Pluripotent Stem Cells
IRI	Ischemia-Reperfusion Injury
IRS1	Insulin Receptor Substrate 1
ISCs	Iron-Sulfur Clusters
KCs	Kupffer Cells
LDL	Low-Density Lipoprotein
Liv_hTST	Liver- Specific Human TST Overexpression
LPON	Lactate, Pyruvate, Octanoate, Ammonia
LV	Lentivirus
MASH	Metabolic Dysfunction-Associated Steatohepatitis
MASLD	Metabolic Dysfunction-Associated Steatotic Liver Disease
MBB	Monobromobimane
MetALD	Metabolic Dysfunction and Alcoholic Liver Disease
metHb-SH	Methemoglobin-Sulfide Intermediate Complexes
mg	Milligram
mL	Millilitre
mM	Millimolar
MMPs	Matrix Metalloproteinases
MPST	Mercaptopyruvate Sulfurtransferase
mtDNA	Mitochondrial DNA
mTORC1	mTOR Complex 1
NAD+	Nicotinamide Adenine Dinucleotide
NAFLD	Non-Alcoholic Fatty Liver Disease
NaHS	Sodium Hydrosulfide
NAS	NASH Activity Score
NASH	Non-Alcoholic Steatohepatitis
ng	Nanogram
NMDA	N-Methyl-D-Aspartic Acid
NO	Nitric Oxide
NRF2	Nuclear Factor Erythroid 2-Related Factor 2
OCR	Oxygen Consumption Rate
OGTT	Oral Glucose Tolerance Test
OXPHOS	Oxidative Phosphorylation
Pen Strep	Penicillin-Streptomycin
PEPCK	Phosphoenolpyruvate Carboxykinase
PRDX3	Peroxiredoxin 3

PSR	Picrosirius Red
PTMs	Post-Translational Modifications
RBCs	Red Blood Cells
RER	Respiratory Exchange Ratio
RNS	Reactive Nitrogen Species
ROS	Reactive Oxygen Species
RSS	Reactive Sulfur Species
SAAs	Sulfur-containing Amino Acids
SCFAs	Short-Chain Fatty Acids
SIRT	Sirtuin
SLD	Steatotic Liver Disease
SOD	Superoxide Dismutase
SOP	Sulfide Oxidation Pathway
SQOR or SQRDL	Sulfide Quinone Oxidoreductase
T2D	Type 2 Diabetes
TAA	Thioacetamide
TD-NMR	Time Domain-Nuclear Magnetic Resonance
TGF-β	Transforming Growth Factor-Beta
TNF-α	Tumour Necrosis Factor-Alpha
TSP	Transsulfuration Pathway
TST	Thiosulfate Sulfurtransferase
VSMCs	Vascular Smooth Muscle Cells

1 Chapter 1: Introduction

1.1 Metabolic dysfunction-associated steatotic liver disease (MASLD)

1.1.1 From NAFLD to MASLD; updated nomenclature

Multinational liver societies have agreed to update the nomenclature of Non-Alcoholic Fatty Liver Disease (NAFLD) to better reflect its metabolic origins and reduce associated stigma (1). The new terminology introduces Metabolic Dysfunction-Associated Steatotic Liver Disease (MASLD) in place of NAFLD and Metabolic Dysfunction-Associated Steatohepatitis (MASH) to replace Non-Alcoholic Steatohepatitis (NASH). Additionally, a new category, Metabolic Dysfunction and Alcoholic Liver Disease (MetALD), has been established to address cases where both metabolic factors and moderate alcohol consumption contribute to liver disease. These changes aim to improve risk stratification, guide treatment approaches, and enhance understanding of liver disease aetiology (2, 3).

The term "non-alcoholic" has faced criticism for failing to accurately represent the disease's underlying causes and for potentially stigmatising patients, including those with alcohol-related liver disease, while "fatty" may also be seen as derogatory (1). A recent survey revealed that more than 60% of participants considered the terms "non-alcoholic" and "fatty" as stigmatising (4). Moreover, the restrictive alcohol intake limits in the definition of MASLD have excluded many patients from clinical trials, despite their elevated risk of liver-related outcomes (5). Steatotic Liver Disease (SLD) is a new umbrella term introduced to encompass liver conditions characterised by fat accumulation, regardless of the cause. It distinguishes between MASLD, which is linked to metabolic issues like obesity and diabetes, and Alcohol-Related Liver Disease (ALD), caused by excessive alcohol consumption. The term SLD was introduced to recognise the biological overlap between these conditions and simplify their classification while reducing stigma associated with previous terminology. This change aims to improve diagnosis and treatment by grouping similar liver diseases under a single category (2, 5).

1.1.2 MASLD; definition and epidemiology

MASLD is characterised by the accumulation of fat in more than 5-10% of hepatocytes. As illustrated in Figure 1.1, a more severe form of MASLD is MASH, which is characterised by

lobular inflammation and hepatocyte enlargement (6). MASH is less prevalent than MASLD and it can rapidly progress to chronic fibrosis and liver cirrhosis (7).

Among adults, the global prevalence of MASLD is approximately 32%, with a higher prevalence in males (40%) compared to females (26%) (8). Global MASLD prevalence increased from 25.26% in 1990–2006 to 38.00% in 2016–2019 (8). MASLD prevalence varies significantly by region, ethnicity, obesity rates, genetic variations, and socioeconomic conditions. The highest MASLD prevalence is in south and north America at 35.7% and 35.3%, respectively; with similar prevalence in Europe and Asia at 30.9% and 30.5%, respectively; and lowest in Africa at 28.2%, based on a recent systematic review and meta-analysis by Le *et al.* (9). MASLD affects 80-90% of obese adults, 30-50% of patients with diabetes, and up to 90% of patients with hyperlipidemia (10). If current trends continue, the prevalence of MASLD is expected to rise significantly in various regions by 2030 (11, 12). These projections are largely based on rising obesity rates, indicating a parallel increase in MASLD prevalence (9, 13).

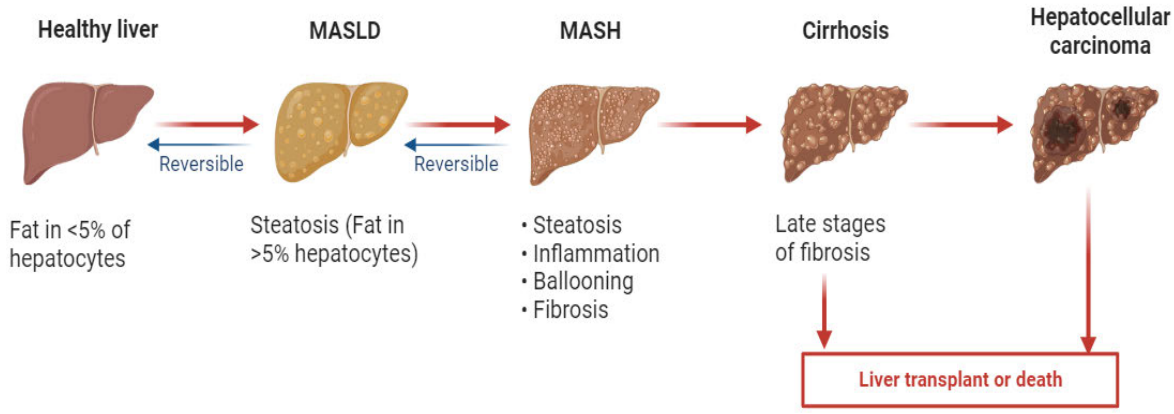

Figure 1.1 A schematic view of metabolic dysfunction-associated steatotic liver disease (MASLD) spectrum. Image adapted and updated from Biorender.com.

Metabolic dysfunction-associated steatotic liver disease (MASLD), progresses through several stages, starting with simple steatosis, where fat accumulates in more than 5% of liver cells without significant inflammation or damage. The liver may appear enlarged and pale yellow, with fat vacuoles visible within hepatocytes. If left untreated, it can advance to metabolic dysfunction-associated steatohepatitis (MASH), characterised by inflammation and hepatocyte injury, giving the liver a more inflamed, reddish appearance. Histologically, this stage shows ballooning hepatocytes and possible early fibrosis. As the disease progresses, fibrosis develops, visible by scarring of liver tissue due to ongoing inflammation. The liver may begin to shrink and harden, with collagen deposition forming fibrous bands. Continued damage leads to cirrhosis, where extensive fibrosis impairs liver function. At this stage, the liver is shrunken, hard, with regenerative nodules surrounded by thick fibrotic bands. The

final stage, hepatocellular carcinoma (HCC), involves the development of malignant tumours due to chronic liver damage and cirrhosis and requires liver transplant (14).

1.1.3 Pathophysiology and risk factors of MASLD

The pathophysiology of MASLD involves complex interactions among environmental factors, diet, lifestyle, metabolism, genetic variants, and gut microbiota. The earlier "two-hit" model was once widely used to explain the progression of MASLD to MASH. This model suggested that lipid accumulation in the liver (the "first hit") makes it more susceptible to additional damaging factors (the "second hit"), such as oxidative stress and inflammation (15). However, this theory is now viewed as too simplistic, the "multi-hit" model is now more accepted, recognising that various pathogenic drivers, such as mitochondrial ATP depletion, glutathione depletion, hypoxia, dysregulated adipokines, and a high-fructose diet, contribute to disease progression (16). Central to this progression is the liver's inability to manage excess free fatty acids and metabolic substrates, which leads to toxic lipid accumulation (17). This "substrate overload" causes oxidative stress, hepatocellular injury, inflammation, and fibrosis, which may ultimately progress to cirrhosis or HCC (18).

1.1.3.1 Lipotoxicity and insulin resistance

The pathogenesis of MASLD and its progression MASH is intricately linked to metabolic dysfunction, primarily driven by insulin resistance and lipid accumulation in the liver. Insulin resistance is a hallmark feature in individuals with obesity and type 2 diabetes (T2D), with estimates suggesting that over 70% of individuals with T2D have MASLD, and nearly half may progress to MASH (19). Insulin, a hormone crucial for regulating glucose and lipid metabolism, becomes less effective in insulin-resistant states, particularly affecting glucose uptake in insulin-sensitive tissues like adipose tissue and the liver (20).

In healthy conditions, insulin promotes lipid storage and inhibits lipolysis in adipose tissue, helping to maintain energy balance after meals (21). However, in insulin resistance, this process becomes dysfunctional. The adipose tissue's ability to store lipids becomes overwhelmed, leading to an increased release of free fatty acids (FFAs) into the bloodstream. These FFAs are taken up by the liver, where they accumulate and lead to ectopic fat deposition (22). This lipid overload is central to the concept of "lipotoxicity," where the excessive accumulation of saturated fatty acids in hepatocytes induces cellular damage through

mechanisms involving endoplasmic reticulum (ER) stress, oxidative stress, and mitochondrial dysfunction (23).

Lipotoxicity contributes to the activation of inflammatory pathways, such as the release of pro-inflammatory cytokines like tumour necrosis factor-alpha (TNF-α) and interleukin-6 (IL-6). These cytokines, which are secreted by dysfunctional adipose tissue, further impair insulin signalling in the liver and exacerbate hepatic inflammation (24). TNF-α promotes lipolysis, increasing the delivery of FFAs to the liver, while IL-6 enhances hepatic insulin resistance and steatosis (18, 25). Together, these factors create a vicious cycle where increased FFA influx and lipotoxicity perpetuate liver injury.

The liver plays a crucial role in lipid and glucose homeostasis by adapting to varying metabolic states. Under normal conditions, hepatocytes can switch between synthesising fatty acids during feeding and oxidising them during fasting, depending on the body's energy demands (18, 25). However, in insulin-resistant states, this adaptive capacity is impaired. The liver becomes inefficient at oxidising fatty acids, leading to incomplete fatty acid oxidation and the accumulation of toxic lipid species such as diacylglycerols (DAGs) and ceramides (26, 27), which worsens hepatic insulin resistance and drives further hepatic inflammation and fibrosis.

In addition to these metabolic disturbances, the gut-liver axis also plays a significant role in the progression of MASLD. Poor dietary habits common in MASLD patients, such as high consumption of fructose and saturated fats, can alter the gut microbiota. This leads to a decrease in beneficial short-chain fatty acids (SCFAs) and an increase in gut permeability, allowing translocation of bacterial endotoxins into the liver (28). These endotoxins, in turn, trigger inflammatory pathways that activate hepatic stellate cells, driving the production of collagen and leading to fibrosis, a key feature in the progression from simple steatosis to MASH (28).

Furthermore, adipokines, hormones produced by adipose tissue, play crucial roles in the pathogenesis of MASLD. Leptin, typically elevated in obesity, promotes inflammation and fibrosis in the liver, while adiponectin, which is reduced in MASLD, normally has protective effects by enhancing insulin sensitivity and suppressing hepatic fat accumulation (29). The imbalance between these adipokines further promotes liver injury.

Skeletal muscle insulin resistance also plays a significant role in MASLD. Skeletal muscle is responsible for a large proportion of postprandial glucose disposal, primarily through insulin-stimulated glucose uptake *via* GLUT4 transporters (30). In insulin-resistant states, this process

is impaired, leading to reduced glucose utilisation in muscle and a compensatory increase in glucose production by the liver (31). This drives further metabolic disturbances, including increased *de novo* lipogenesis (DNL) in the liver (32), which further exacerbates hepatic fat accumulation.

Ultimately, the combination of insulin resistance, lipotoxicity, chronic inflammation, and mitochondrial dysfunction leads to a progressive accumulation of fat in the liver, advancing from simple steatosis (fat accumulation without inflammation) to MASH, characterised by liver inflammation, hepatocyte injury, and fibrosis. If left unchecked, this process can lead to more severe outcomes such as cirrhosis and hepatocellular carcinoma (HCC), highlighting the complex and multifactorial nature of MASLD pathogenesis.

1.1.3.2 Mitochondria dysfunction and oxidative stress

Mitochondrial dysfunction and oxidative stress are closely related processes, and they can influence each other in a bidirectional manner, creating a vicious cycle, especially in the context of MASLD and MASH.

Under normal physiological conditions, mitochondria are essential for the β-oxidation of fatty acids (FA), ATP production, and the regulation of reactive oxygen species (ROS), ensuring a balance between fat metabolism and energy production in hepatocytes (33). However, mitochondrial dysfunction leads to a cascade of toxic events, including impaired fatty acid oxidation (FAO), ATP depletion, and increased oxidative stress, all of which contribute to hepatic steatosis. In MASLD and MASH, mitochondrial abnormalities such as structural damage, reduced respiratory chain activity, and increased membrane permeability are commonly observed (33). For example, patients with MASH exhibit enlarged and swollen mitochondria, loss of cristae, and the presence of paracrystalline inclusion bodies, all indicative of mitochondrial damage (33).

When FAO is compromised, as seen in both clinical and experimental models of MASLD (34), fatty acids accumulate in hepatocytes, contributing to hepatic steatosis. Mitochondrial abnormalities in the respiratory chain enzyme complexes (I, III, IV, and V) have been documented in MASH patients (35), and these defects correlate with insulin resistance, higher levels of pro-inflammatory cytokines such as TNF-α, and increased fibrosis (35). These findings are mirrored in animal models, such as leptin-deficient C57BL/6J *Lep*^{ob}/*Lep*^{ob} mice,

which exhibit impaired FAO and altered mitochondrial respiration, further supporting the link between mitochondrial dysfunction and lipid accumulation in the liver (36).

Several molecular mechanisms underline this mitochondrial dysfunction in MASLD and MASH. One critical factor is the depletion of nicotinamide adenine dinucleotide (NAD+), a cofactor essential for the activity of sirtuins, a family of enzymes involved in regulating mitochondrial function and oxidative stress (37). In particular, reduced SIRT3 activity, which is vital for the breakdown of FFAs, exacerbates mitochondrial dysfunction in the context of a high-fat diet, leading to the accumulation of fatty acids in the liver (38, 39). Additionally, alterations in mitochondrial membrane composition, such as changes in cardiolipin, a phospholipid crucial for mitochondrial function, further impair ATP production and increase ROS production, promoting apoptosis and cell death (40, 41). Elevated levels of ceramides, which are associated with saturated fatty acid intake, also contribute to mitochondrial fragmentation and exacerbate liver damage in MASLD (41).

Oxidative stress, characterised by excessive ROS production, is another major consequence of mitochondrial dysfunction in MASLD and MASH. ROS, such as superoxide anion, hydrogen peroxide, and hydroxyl radicals, are by products of impaired electron flow in the mitochondrial respiratory chain (42). When mitochondria are unable to neutralise excessive ROS, oxidative damage occurs, affecting mitochondrial DNA, proteins, and lipids (42, 43). One of the most harmful aspects of oxidative stress is its ability to damage mitochondrial DNA (mtDNA) (33, 44). As ROS escape from the electron transport chain, they induce mutations in mtDNA, further impairing mitochondrial function. This damage disrupts the electron transport chain, increasing the leakage of electrons and perpetuating a cycle of ROS overproduction and mitochondrial damage (45-47). Over time, this cycle overwhelms the liver's antioxidant defence mechanisms, such as superoxide dismutase (SOD) and catalase, leading to a failure in ROS detoxification and worsening oxidative stress (46).

Impaired FAO and increased ROS production in mitochondria disrupt insulin signalling pathways, contributing to systemic metabolic dysfunction. For instance, mitochondrial defects in the carnitine palmitoyltransferase 1 (CPT1) enzyme, responsible for transporting long-chain fatty acids into mitochondria for oxidation, lead to decreased FAO and the accumulation of acylcarnitines (48, 49), which further impairs mitochondrial function and exacerbates insulin resistance. This metabolic dysfunction not only promotes fat accumulation in the liver but also contributes to the systemic inflammation observed in MASLD and MASH.

1.1.3.3 Hepatic inflammation and fibrosis

MASLD progresses due to a combination of inflammation and fibrosis, with chronic lipid accumulation in hepatocytes playing a central role. The excessive fat in liver cells triggers cellular stress and injury, which activates an inflammatory response. Immune cells, particularly macrophages and neutrophils, are recruited to the liver and release pro-inflammatory cytokines such as TNF-α, IL-6, and IL-1β. This creates a sustained inflammatory environment that exacerbates hepatocellular damage and advances disease progression (24).

The inflammation process in MASLD involves a delicate balance between pro- and anti-inflammatory signals. When the pro-inflammatory signals from stressed or damaged hepatocytes overwhelm the anti-inflammatory responses, inflammation becomes chronic. This involves key players such as Kupffer cells (KCs), hepatic stellate cells (HSCs), myofibroblasts, and immune cells like T cells, natural killer cells, and T regulatory cells (50, 51). Additionally, mitochondrial dysfunction and oxidative stress, by-products of lipid overload, play a significant role by generating ROS, oxidised lipids, and aldehydes, which contribute to sustained liver inflammation and further damage (43, 52).

Activated HSCs play a pivotal role in fibrosis development by transitioning from a quiescent to a fibrogenic state under the influence of persistent inflammation. These activated HSCs produce large amounts of collagen, predominantly types I and III, which contributes to the formation of fibrous scar tissue(53). In addition to cytokines, factors like transforming growth factor-beta (TGF-β) are crucial in promoting HSC activation and driving the ECM synthesis that underpins fibrosis (24).

Hepatocyte apoptosis, often induced by oxidative stress and inflammation, plays an important role in perpetuating fibrosis. Damaged hepatocytes release danger-associated molecular patterns (DAMPs), which further stimulate inflammatory pathways and activate HSCs (54). This ongoing cycle of damage and repair leads to fibrosis, with extracellular matrix (ECM) remodelling becoming dysregulated. In a healthy liver, ECM balance is maintained by matrix metalloproteinases (MMPs) and their inhibitors (TIMPs). However, in MASLD, this balance shifts, with an increase in TIMP expression and a reduction in MMP activity, leading to excessive ECM accumulation (54).

As MASLD advances to MASH, the inflammatory response escalates. Various factors contribute to this process, including poor dietary habits, such as a Western diet high in saturated

fats and omega-6 fatty acids. These dietary components increase systemic and hepatic inflammation, while a higher ratio of omega-6 to omega-3 polyunsaturated fatty acids is associated with MASLD progression (55).

In conclusion, the progression of MASLD from simple steatosis to MASH and fibrosis is driven by a complex interaction between inflammation, oxidative stress, and fibrosis. Persistent inflammation activates hepatic stellate cells, leading to excessive ECM deposition and scarring. If left unchecked, fibrosis can progress to cirrhosis, significantly increasing the risk of liver failure and liver-related mortality. Early interventions targeting inflammation and fibrosis are crucial to halting or reversing disease progression.

1.1.3.4 Genetic and environmental factors

Certain genetic variants significantly influence the occurrence and severity MASLD. Research has identified several genetic variants associated with the progression of liver damage in MASH patients. For instance, the Farnesyl-Diphosphate Farnesyltransferase 1 (FDFT1) rs2645424 variant was found to be positively associated with the NASH Activity Score (NAS), indicating its role in disease severity (56). Moreover, the *PNPLA3* gene variant has been shown to play a significant role in the progression of histological damage in both adults and children, with homozygosity for the G allele being associated with an increased risk of hepatocytes ballooning, lobular inflammation, and fibrosis (11, 12, 57). Additionally, the variant rs1260326 of *GCKR* has been suggested to facilitate the progression of MASLD towards MASH (58, 59).

HSD17B13 is a liver-specific protein associated with lipid droplets that plays a role in the metabolism of steroids, pro-inflammatory lipid mediators, and retinol. The most well-studied variant of *HSD17B13*, known as rs72613567, has a prevalence ranging from 5% in Africa to 34% in East Asia (60). Loss-of-function variants in *Hsd17b13* have been linked to a decreased risk of MASLD, especially in HFD-induced obese mice where *Hsd17b13* knockdown significantly improved hepatic steatosis without affecting body weight, adiposity, or glycemia (61).

MASLD development is influenced by many other risk factors, including sex, age, race/ethnicity, diet, physical activity, sleep, gut microbiota, and obesity. Men have a higher prevalence and risk of severe liver fibrosis compared to premenopausal women, while postmenopausal women share similar risks with men due to the protective role of oestrogen

(62). Hispanics show the highest prevalence of MASLD, partly due to genetic factors like the I148M variant of *PNPLA3* (63). Diets high in fructose increase MASLD risk (64), while omega-3 fatty acids and a Mediterranean diet can reduce it (64). Physical inactivity and poor sleep also increase MASLD risk through their effects on metabolic processes and inflammation (65). Gut microbiota imbalances and oxidative stress further contribute to liver damage (66).

It is important to understand the interplay between genetic factors, lifestyle, and other factors and disease progression, understanding the determinants of these conditions is essential for developing personalised treatment strategies and advancing the management of patients with MASLD and MASH.

1.1.4 *In vivo* mouse models of MASH

The field of MASLD research has dramatically improved in the last 20 years, mainly thanks to the development and characterisation of animal models that display specific features of human pathology. Despite differences between species, all important physiological similarities exist between humans and mice. The mouse is an ideal and economic model to study both the onset and the progression of liver disease because of the low number of animals needed and the reduced husbandry costs compared with larger animals like monkeys or pigs. Finally, the mouse liver has an extraordinary regenerative capacity, allowing for a better study of liver injury/repair dynamics (67).

1.1.4.1 Genetic mouse models of MASLD/MASH

Table 1.1 provides a summary of various genetic mouse models used in MASH research. Each model is characterised by specific features that contribute to our understanding of MASLD's development and progression to MASH. The key features of these models include metabolic alterations, liver inflammation, fibrosis, and other pathological markers relevant to MASLD/ MASH.

Table 1.1 The main genetic mouse models of MASH.

Model	Diet/genetic manipulation	Key features	References
C57BL/6J *Lep^{db}/Lep^{db}* mice with iron supplementation	Homozygous for the autosomal recessive diabetic gene (*db*). High iron content	Hepatocellular ballooning, increased oxidative stress, inflammasome activation, impaired mitochondrial biogenesis, and fatty acid β-oxidation, activation of pro-inflammatory mediators.	(68-70)
***foz/foz* mice**	Spontaneous deletion in *Alms1* gene; HFD	Hyperphagic, obese, glucose intolerant, insulin resistance, decreased adiponectin, increased cholesterol, hepatic steatosis, inflammation, fibrosis.	(71-73)
***Ldlr$^{-/-}$* / *Ldlr$^{-/-}$*. Leiden mice**	Knockout of LDL receptor gene; HFC diet (21% milk butter, 0.2% cholesterol) or "diabetogenic" diet.	Obesity, insulin resistance, hyperinsulinemia, dyslipidemia, steatosis, inflammation, fibrosis, atherosclerosis. HFD leads to severe hyperinsulinemia.	(74-76)
Apolipoprotein E2 knock-in (*APOE2*ki) mice	Human *APOE2* gene knock-in; high-fat/high-cholesterol diet (42% energy as milk fat, 0.2% cholesterol)	Early inflammation indicative of MASH, compared to C57BL/6 mice which develop simple steatosis.	(75, 77, 78)
Apolipoprotein E-deficient (*ApoE$^{-/-}$*) mice	Absence of *ApoE*; Western-type, cholesterol-enriched diet (42% energy as fat, 1.25% cholesterol)	Hypercholesterolemia, atherosclerosis, obesity, abnormal glucose tolerance, hepatomegaly, MASH with steatosis, hepatocyte ballooning, inflammation, fibrosis.	(79, 80)

1.1.4.2 Chemically-induced mouse models of MASLD/MASH

Table 1.2 outlines various chemical and environmental models used to study MASLD/MASH. These models utilise specific chemicals, conditions, or dietary modifications to induce liver damage, inflammation, and fibrosis, mimicking the key pathological features of MASLD/MASH.

Table 1.2 The main chemically-induced mouse models of MASLD/ MASH.

Model	Chemical/condition	Key features	References
Carbon Tetrachloride (CCl4) administration	CCl4 injection (0.4 mL/kg) twice a week for 6 weeks CCl4 + LXR agonist + HFD	Increased serum aminotransferase and alkaline phosphatase, disturbed liver antioxidative status, extensive fibrosis. Insulin resistance, macrovesicular hepatic steatosis, hepatocyte ballooning, inflammation, fibrosis, elevated TNF-α and IL-6, increased expression of mRNAs related to lipogenesis, oxidative stress, fibrosis, and steatosis.	(81)
Thioacetamide (TAA) administration in combination to fast-food diet	TAA (75 mg/kg, intraperitoneally, three times a week) + fast food diet (12% SFA, 2% cholesterol, high fructose corn syrup) for 8 weeks	Hepatic inflammation, hepatocellular ballooning, collagen deposition, bridging fibrosis.	(82)

1.1.4.3 Diet-induced mouse models of MASH

A review by Flessa *et al.* (83) explored the different diet-induced MASLD/ MASH models, a summary of each diet, it's components, Phenotypic Outcomes, duration to effect and general remarks is provided in Table 1.3

Table 1.3 Overview of dietary-induced mouse models of MASLD/MASH.

Model Type	Key Characteristics	Outcomes	Time Frame	References
Methionine and choline deficient diet (MCD)	High sucrose (40%), moderate fat (10%), lacks methionine and choline.	Hepatic steatosis, inflammation, fibrosis, increased AST/ALT, oxidative stress.	Inflammation: 2 weeks; Fibrosis: 6 weeks.	(84-86)
Atherogenic diet (High cholesterol and high cholate)	High cholesterol (1-1.25%) and cholate (0.5%)	Progressive steatosis, fibrosis, inflammation, hepatocellular ballooning	6-24 weeks; ballooning: 24 weeks	(68, 87)
High-fat (HF) atherogenic diet	60% fat (cocoa butter), high cholesterol and cholate	Steatosis, MASH lesions, insulin resistance, oxidative stress, hepatic stellate cell activation	34 weeks	(68, 87)
High-fat, high-cholesterol (HFHC) diets	33% kcal fat, 1% cholesterol or 45% kcal fat, 0.12% cholesterol	Weight gain, hepatic lipid accumulation, steatosis, inflammation, fibrosis, hypercholesterolaemia, obesity	7-20 weeks	(84, 88, 89)
High-fat, high-fructose (HFHF) diets	58-60% kcal fat, 42 g/L carbohydrates (55% fructose, 45% sucrose)	Weight gain, insulin resistance, hepatic steatosis, inflammation, oxidative stress, fibrogenesis	16 weeks	(90, 91)
Amylin liver NASH (AMLN) model	40% fat (18% trans-fat), 22% fructose, 2% cholesterol	Steatosis, necroinflammation, fibrosis, cirrhosis, periportal inflammation, hepatocellular ballooning	30 weeks; accelerated in *ob/ob* mice: 8 weeks	(92)

Gubra Amylin NASH (GAN) diet	40% fat (saturated, no trans-fat), 22% fructose, 10% sucrose, 2% cholesterol	Steatosis, fibrotic MASH, lobular inflammation, hepatocyte ballooning, body weight gain, glucose intolerance	16-28 weeks; Severe form: 38 weeks	(93, 94)

While genetic and chemical models have their advantages in MASH research, diet-induced mouse models offer a more relevant, cost-effective, and ethically favourable approach that closely mimics the human condition. In this study we are utilising the Gubra Amylin NASH (GAN) diet (94) which arguably comes closest to modelling human MASH due to its composition mirroring the western diet high in fats and sugars.

1.1.5 *In vitro* models of MASLD

In vitro modeling of MASLD provides a valuable alternative to *in vivo* studies, addressing some of the limitations associated with animal models while offering significant insights into disease mechanisms (95). Although *in vivo* models, particularly rodents, have enhanced our understanding of MASLD pathogenesis and the evaluation of therapeutic targets, they are constrained by species-specific differences that limit their translatability to humans. *In vitro* models, on the other hand, have evolved to replicate many hallmarks of MASLD, offering a more ethically sound, cost-effective, and scalable approach for research.

Table 1.4 provides a summary of the different *in vitro* models used in MASLD research, highlighting their key features, advantages, and limitations.

Table 1.4 *In vitro* models for studying MASLD/ MASH

Model Type	Description	Advantages	Limitations	References
Simple hepatocyte models	**Primary hepatocytes**: Isolated from human/animal liver tissue.	Retain liver-specific functions.	Limited lifespan	(96)
	Hepatoma cell lines: (e.g., HepG2, Huh7, HepaRG) immortalised cells.	Easy to culture HepaRG cells retain high metabolic	May not fully represent the human disease.	(97-99)

		activity like human hepatocytes.		
Co-culture models	**Hepatocyte-stellate cell co-cultures**	Study liver cell interactions during MASLD.	More complex setup.	(100, 101)
	Hepatocyte-Kupffer cell co-cultures	Allows study of fibrosis and inflammation.	Lack full physiological relevance.	(102, 103)
3D Spheroid and organoid models	**Hepatocyte spheroids**: 3D spherical clusters.	Improved cell-cell/matrix interactions.	Complex and may require advanced culturing techniques.	(104-106)
	Liver organoids: Mini-liver structures derived from stem cells or primary cells.	Better physiological relevance than 2D models.		
Induced pluripotent stem cells (iPSCs)	iPSCs differentiated into hepatocyte-like cells to model patient-specific MASLD.	Enables personalised disease modelling. Can represent patient-specific characteristics.	Differentiation protocols can be complex. Cells may not fully mature into hepatocytes.	(107, 108)

1.2 Hydrogen sulfide (H_2S)

1.2.1 H_2S biosynthesis and catabolism

Hydrogen sulfide (H_2S), once perceived solely as a noxious gas, has gained recognition for its involvement in a broad spectrum of physiological and pathophysiological processes. Among its notable roles is its function as a regulator of insulin activity within tissues such as the liver, adipose tissue, and the pancreas (109, 110).

Endogenous H_2S is produced both enzymatically and non-enzymatically. H_2S is formed non-enzymatically by thiol-containing compounds, primarily cysteine, interacting with various molecules. Mammalian tissues produce H_2S primarily through this interaction, facilitated by iron and vitamin B6 (111), except for the liver and kidneys where enzymatic pathways predominate. The study of Bianco et al. (112) demonstrated that red blood cells (RBCs) are involved in sulfide catabolism through the formation of methemoglobin-sulfide intermediate complexes (metHb-SH) highlighting the contribution of RBCs to sulfide catabolism (113, 114).

Enzymatically, a trio of key enzymes governs H_2S biosynthesis: cystathionine synthase (CBS), cystathionine gamma lyase (CSE or CTH or CGL) predominantly located in the cytoplasm, and mercaptopyruvate sulfur transferase (MPST), present in both cytoplasm and mitochondria (115). *In vivo*, CBS and CSE catalyse the conversion of sulfur-containing amino acids (SAAs), specifically L-cysteine, into H_2S, while MPST generates H_2S from 3-mercaptopyruvate as shown in Figure 1.2. These enzymes are distributed across diverse tissues, each governing tissue-specific regulation of H_2S production. All three H_2S-producing enzymes; CSE, CBS, and MPST are detectable in the liver, however, CSE is about 60 times more abundant than CBS in murine liver (116), and its knockout reduces H_2S production by over 90% (117, 118). In contrast, CBS is the main H_2S-producing enzyme in the brain (119) and the kidney (120).

Given the toxic potential of elevated H_2S concentrations and their lethal implications (121), swift oxidation of H_2S occurs, primarily within the liver and gastrointestinal tissues, to preserve physiological equilibrium (122). H_2S emerges as the sole inorganic substrate subject to mitochondrial oxidation, a phenomenon reflective of its ancient origin in the evolution of the bacterial/mitochondrial system during a period when the Earth harboured abundant sulfur and oxygen had not yet assumed its role as the principal substrate for electron transport-mediated respiration (123). The catabolism of H_2S is orchestrated through three key mitochondrial enzymes constituting the sulfide oxidation pathway (SOP). These enzymes, namely ethylmalonic encephalopathy protein 1 (ETHE1, also known as persulfide dioxygenase: PSO), sulfide quinone oxidoreductase (SQOR, also known as SQRDL), and thiosulfate sulfurtransferase (TST, also known as rhodanese), mediate a sequence of enzymatic reactions that ultimately oxidise sulfide, progressing from sulfide to sulfite, thiosulfate, and sulfate. Subsequently, these oxidised forms are excreted in the urine, effectively maintaining H_2S levels within a safe range. For instance, human blood typically contains H_2S concentrations of around

10–100 μmol/L (124), although ongoing discussions persist regarding the robustness of quantification methodologies for systemic and tissue-specific H_2S levels.

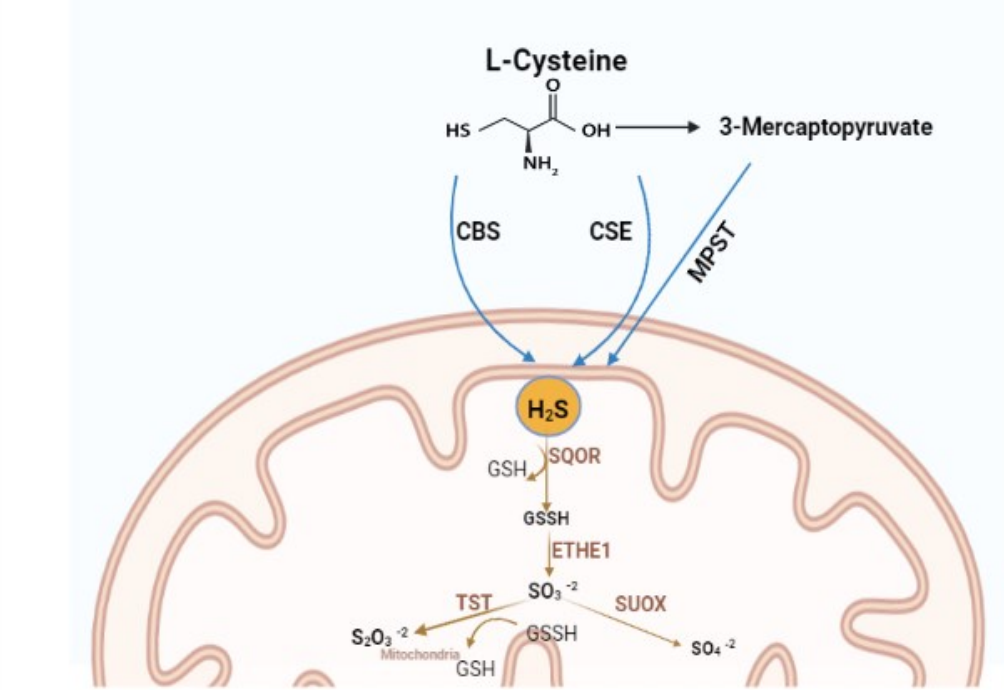

Figure 1.2 A schematic view of hydrogen sulfide (H_2S) biosynthesis and catabolism *via* enzymatic pathways. Created in BioRender.com.

The schematic shows enzymatic pathways for endogenous H_2S production, and the mitochondrial pathway for H_2S catabolism. CBS, cystathionine β-synthase; CSE, cystathionine γ-lyase; MPST, mercaptopyruvate sulfurtransferase; SQOR, sulfide quinone reductase; GSSH, glutathione persulfide; ETHE1, persulfide dioxygenase; TST, thiosulfate sulfur transferase.

1.2.2 Mechanisms of H_2S signalling in biological systems

H_2S is now recognised as the third gasotransmitters, joining carbon monoxide (CO) and nitric oxide (NO). Like H_2S, CO and NO are toxic at high concentrations, produced endogenously within the body, and can freely cross cell membranes to exert biological effects. These gases are highly reactive, generating various metabolites collectively known as reactive sulfur species (RSS), reactive oxygen species (ROS), and reactive nitrogen species (RNS) (125).

Interestingly, each gasotransmitter can regulate the production of the others; H_2S influences NO production through multiple mechanisms, and appears to increase CO production *via* activation of the nuclear factor erythroid 2-related factor 2 (*Nrf2*) pathway, which upregulates heme oxygenase enzymes that generate CO (126). Although understanding the exact dynamics

of H_2S-NO-CO interactions is challenging, this cross-talk plays an important role in various biological processes, particularly in the cardiovascular system, where it regulates inflammation, blood vessel formation, vasodilation, and protection from ischemia-reperfusion injury (127).

Figure 1.3 provides a summary of the main mechanisms by which H_2S acts as a signalling molecule. In various systems, H_2S exerts its functions primarily through persulfidation. Persulfidation, also known as protein sulfhydration is a reversible post-translational modification that can occur on any cysteine residue (128). Persulfidation was first introduced by Mustafa *et al.* (129) and later recognised as a way to understand H_2S signalling mechanisms (130-132). Persulfidation involves the conversion of the thiol group (R-SH) in cysteine into a persulfide group (R-S-SH). Before this conversion, the thiol group must first be oxidised to form derivatives like sulfenic acid (R-SOH), a disulfide (R-S-S-R), or S-nitrosothiol (R-SNO). These derivatives can then react with H_2S to create a persulfidated protein residue. Persulfidation of cysteine residues induces conformational changes in protein structure, thereby altering protein activity (133). For example, H_2S modifies specific cysteine residues in NRF2 through persulfidation, it facilitates the dissociation of NRF2 from its repressor, KEAP1. This release allows NRF2 to translocate to the nucleus, where it binds to antioxidant response elements (AREs) in the promoters of target genes, leading to their upregulation. Additionally, persulfidation can protect NRF2 from degradation, ensuring its accumulation and activity, especially under oxidative stress conditions. This mechanism is vital for the cellular defence system, as it boosts the expression of genes involved in combating ROS and maintaining redox balance (134, 135). It is worth noting that despite the identification of many proteins as targets for persulfidation, challenges persist in accurately pinpointing specific proteins and conducting in-depth mechanistic studies. These challenges stem from issues related to method specificity and the instability of persulfides, which is beyond the scope of this project but has been reviewed comprehensively by Liu *et al.* (136).

H_2S can also modulate ion channels and was the first endogenous gas identified to open ATP-sensitive K^+ channels in vascular smooth muscle cells (137, 138). Finally, H_2S can directly influence the function of the mitochondria by modulating mitochondrial respiration (139), regulating mitochondrial membrane potential (140), modulating mitochondrial oxidative stress (141). The exact mechanisms and chemistry behind all these signalling mechanisms is beyond

the scope of this project, the next section explores the physiological functions exerted by H_2S signalling in various biological systems.

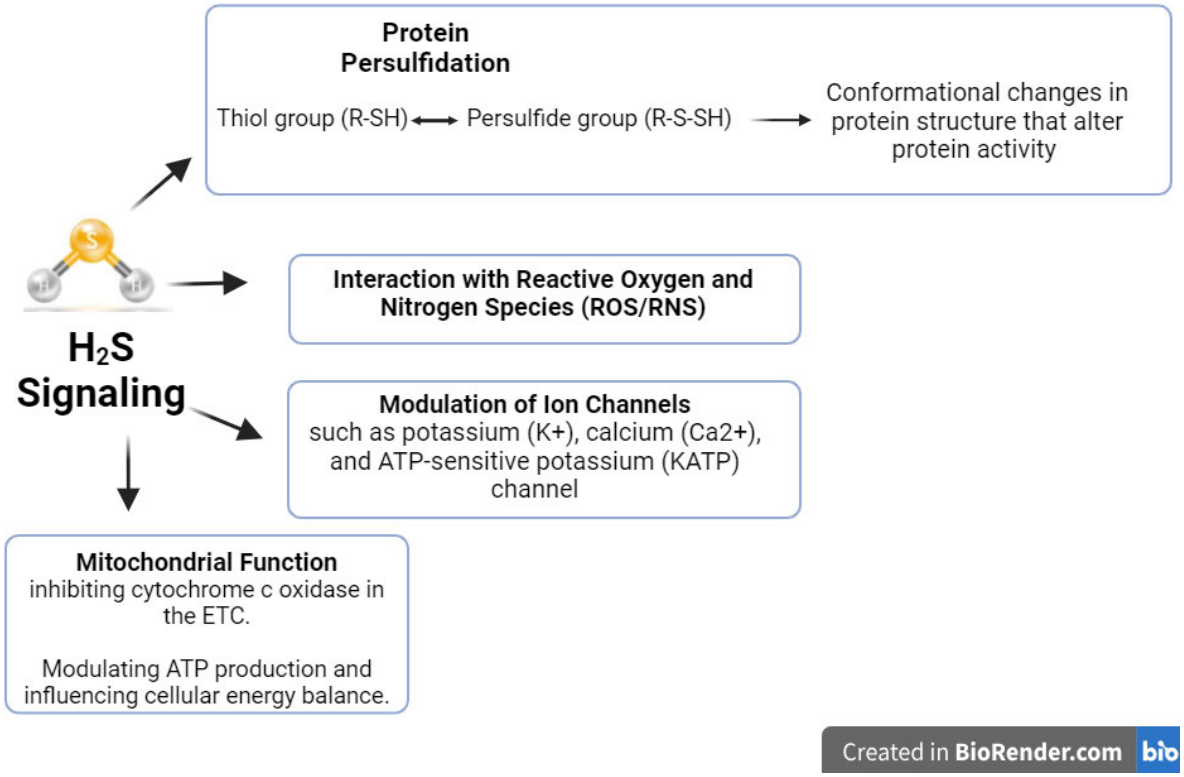

Figure 1.3 A schematic view of the main mechanisms of H_2S signalling in biological systems. Created in BioRender.com.

1.2.3 The physiological functions of H_2S

The initial investigations into the physiological role of H_2S involved inhibiting endogenous production through the silencing of *Cse* or *Cbs* genes, along with the augmentation of H_2S levels *via* exogenous administration of H_2S donors. In a seminal contribution by Abe and Kimura in 1996 (142) the proposition that H_2S operates as an innate neuromodulator influencing cognitive function was first substantiated. This revolutionary work was rapidly succeeded by their demonstration of the role of H_2S as a vasodilator in vascular smooth muscle (143) and its subsequent identification as a protective agent for neurons against oxidative stress (144). These discoveries triggered increasing scientific interest in H_2S, leading to a comprehensive exploration of its extensive spectrum of physiological impacts across diverse biological processes and pathologies.

H_2S has a significant impact on cardiovascular function by affecting KATP (potassium ATP) channels in vascular smooth muscle cells (VSMCs), effectively regulating their activity and influencing vascular tone (143). This modulation of KATP channels by H_2S contributes to the control of blood pressure, vascular resistance, and overall cardiovascular function. Additionally, H_2S offers protection against oxidative stress (145) which can damage blood vessels and contribute to heart disease. It also has anti-inflammatory properties that help prevent the development of atherosclerosis (146). During ischemia-reperfusion injury, which occurs when blood supply returns to the tissue after a period of ischemia or lack of oxygen, H_2S acts as a cardioprotective agent, reducing tissue damage and improving recovery (147, 148).

H_2S functions as a neuromodulator, influencing the activity of neurons and synapses. Kimura *et al.* (142) discovered that H_2S enhances the response of N-methyl-D-aspartic acid (NMDA) receptors, promoting long-term potentiation in the hippocampus, which is critical for learning and memory (142). In Alzheimer's disease (AD), the most common neurodegenerative disease, Giovinazzo *et al.* (149) investigated the neuroprotective effects of H_2S in an AD mouse model (3xTg-AD) with specific Tau protein mutations and showed that H_2S prevents Tau protein hyperphosphorylation through S-sulfhydration of GSK3β and that binding between CSE and WT Tau reduces Tau protein levels. Moreover, administering the H_2S donor GYY4137 improved motor and cognitive functions in the AD mice, and increased Tau protein S-sulfhydration.

In the kidneys, CSE, CBS, and MPST enzymes are present. In human renal tissues, CSE is found in the glomerulus and tubulointerstitial, with 75% of renal cells and 87% of endothelial cells expressing this enzyme (150). CBS is highly expressed in renal proximal tubular cells (151). Similarly, in mice kidneys, CBS is predominantly located in the outer renal cortex, while CSE is found in the inner cortex and medulla, particularly in the proximal straight tubule (152). Additionally, MPST is localised in the proximal tubular epithelium (153). In both human and rat renal tissue, CBS was abundantly expressed in renal tubular epithelial cells, with its expression negatively correlating with the severity of kidney disease (151). This evidence suggests that these enzymes are abundant in the kidneys and play critical roles in kidney function.

In the respiratory system, H_2S helps regulate airway tone and inflammation, making it relevant in conditions like asthma and chronic obstructive pulmonary disease (COPD) (154). H_2S

relaxes the smooth muscles of the airways, facilitating better airflow and reducing the symptoms of bronchoconstriction. It also protects the lungs from oxidative stress, which is a common feature of many respiratory diseases. H_2S has shown promise in managing obstructive respiratory diseases, pulmonary fibrosis, emphysema, pancreatic inflammatory/respiratory lung injury, pulmonary inflammation, bronchial asthma, and bronchiectasis (155).

The complex interactions between H_2S and various signalling molecules underscore the intricate nature of its physiological functions. Importantly, in multiple tissues, it has been shown that H_2S exhibits a biphasic effect: at low concentrations, it enhances mitochondrial respiration, while at higher concentrations, it inhibits the respiratory chain at mitochondrial complex IV, leading to cytotoxicity and degeneration (156). Therefore, it is essential to identify the concentrations at which H_2S exerts beneficial effects to avoid toxicity.

1.2.4 H_2S function in liver disease and metabolic regulation

In the liver, CSE is the primary enzyme responsible for H_2S production, CSE protein level is 60 times higher than CBS in the liver (116). The liver plays a major role in regulating glucose and lipid metabolism and antioxidant defence (157). It is also the principal organ for production and clearance of H_2S under basal conditions (158, 159). Impaired hepatic H_2S catabolism is reported in many forms of liver disease such as MASLD and hepatic cirrhosis (160).

H_2S has been implicated in liver disease, mainly through the genetic manipulation of enzymes involved in the production of H_2S such as CBS and CSE. In addition, the administration of exogenous H_2S donors showed therapeutic efficacy for fatty liver disease in rodents. Watanabe *et al.*(161) observed the emergence of severe hepatic steatosis in mice deficient in *Cbs* (*Cbs*$^{-/-}$). Concurrently, Namekata *et al.* (162) documented increased oxidative stress and lipid accumulation within the hepatic tissue of these *Cbs*$^{-/-}$ mice. The authors of the latter study suggested that the hepatic steatosis might be attributable to hyperhomocysteinaemia in these mice. Nevertheless Namekata *et al.* (162) did not further explore the involvement of H_2S in the altered hepatic lipid metabolism observed in *Cbs*$^{-/-}$ mice.

Subsequently, Li *et al.* (163) reported a 1.5-fold elevation in MPST protein levels in WT mice subjected to HFD compared to those on chow diet. Furthermore, they noted a substantial augmentation of MPST within the cytoplasm of hepatocytes displaying steatosis in MASLD patients relative to hepatocytes from healthy individuals. Li *et al.* (163) also reported that adenovirus-mediated RNA interference partial knockdown of *Mpst* (achieving a 40% reduction

at the mRNA level and a 60% decrease at the protein level) resulted in a reduction in hepatic steatosis in HFD-fed mice, as evidenced by diminished triglyceride and total cholesterol levels, as well as histological analyses *via* hematoxylin and eosin (H&E) and Oil Red O staining. The authors claimed that the mechanism by which elevated MPST contributed to steatosis was *via* the inhibition of CSE-mediated H_2S production.

Moreover, Mani *et al.* (118) showed diverse effects of *Cse* knockdown on lipid metabolism in mouse liver. Their findings indicated that $Cse^{-/-}$ mice did not significantly differ from WT mice in terms of liver lipid content when placed on a standard diet. However, when exposed to HFD, $Cse^{-/-}$ mice displayed significantly enlarged livers and increased hepatocyte fat deposition. The production of H_2S was further diminished in HFD-fed $Cse^{-/-}$ mice relative to $Cse^{-/-}$ mice on chow diet. Collectively, these findings led Mani *et al.* (118) to conclude that $Cse^{-/-}$ mice exhibited normal fat metabolism under standard dietary conditions but were unable to effectively metabolise excess fat resulting from HFD consumption. These findings suggested that the H_2S-producing enzymes, CBS, CSE may inhibit while MPST enables the impairment of hepatic lipid metabolism in response to HFD.

In rats with liver fibrosis, plasma H_2S levels are reduced, and inhibiting H_2S production further increases fibrotic markers in cirrhotic livers (164). The protective role of H_2S is supported by evidence showing that CBS deficiency leads to increased oxidative stress, inflammation, and fibrosis (165), while CSE knockout exacerbates liver fibrosis by reducing H_2S levels (166). This suggests that the H_2S system plays a protective role in liver fibrosis, though the specific roles of H_2S -producing enzymes in different liver cells require further investigation.

Increasing H_2S concentrations is not always a therapeutic strategy, Zhang *et al.* (167) found that increasing H_2S concentration, both exogenous (*via* Sodium hydrosulfide (NaHS)) and endogenous (*via CSE* knockout), impairs glucose uptake and glycogen storage by inhibiting glucokinase (GK) activity. Furthermore, Zhang *et al.* (167) reported that H_2S decreased insulin-stimulated glucose consumption. The study suggests that H_2S inhibits the activation of AMP-activated protein kinase (AMPK), which plays a key role in insulin sensitivity. When AMPK is inhibited, gluconeogenic enzyme phosphoenolpyruvate carboxykinase (PEPCK) activity is increased, promoting glucose production, and exacerbating insulin resistance. Interestingly, H_2S also promotes glycogenolysis, further increasing glucose output from the liver (167). In fasting conditions, H_2S was shown to enhance glucose production *via* gluconeogenesis, while also inhibiting glycogen storage. The findings demonstrate that H_2S disrupts glucose

homeostasis by decreasing glucose uptake and promoting both gluconeogenesis and glycogenolysis, leading to elevated blood glucose levels, a hallmark of insulin resistance (167).

Similarly, Carter *et al.* (168) found that *Tst* knockout (*Tst*$^{-/-}$) mice, which are characterised by elevated systemic sulfide levels, exhibit increased hepatic glucose and show reprogramming of amino acid metabolism that supports gluconeogenesis, along with a shift in pyruvate metabolism toward aspartate production. These mice exhibited abnormal hepatic lipid accumulation and impaired glucose tolerance under standard chow diet.

The conflicting results regarding the effects of H_2S in various studies can be attributed to multiple factors. One of the main reasons is the dose-dependent nature of H_2S, where low levels can be beneficial due to its anti-inflammatory and antioxidant properties, while higher levels may cause toxicity by inhibiting mitochondrial respiration (127, 169). Additionally, H_2S has tissue-specific effects, showing protective benefits in cardiovascular health but potentially promoting fat accumulation and glucose production in the liver. Variations in genetic models, enzyme expression, and experimental conditions contribute to these discrepancies, as different methods of H_2S administration or genetic knockouts can lead to opposing results (170). Moreover, the balance between H_2S production and disposal plays a crucial role in determining its effects, as impaired sulfide disposal can lead to metabolic dysfunction despite normal sulfide levels (168). These factors collectively explain the varying conclusions across studies on the effects of H_2S. The next section provides an overview of the most recent approaches for H_2S elevation.

1.2.5 Pharmacological elevation of H_2S has multiple metabolic effects

The development of H_2S-based therapeutics for treating liver disease has made significant advances, with a focus on creating physiologically stable H_2S donors that can deliver the gas at the desired concentrations to the target tissues. Natural sulfur-containing organic compounds, like those found in garlic and cruciferous vegetables, as well as inorganic sulfide salts, such as Na_2S and NaHS, have been explored (147, 171, 172). However, their limitations, including poor water solubility, and the rapid fluctuation of H_2S levels after administration, highlight the need for more refined H_2S delivery systems that can mimic the controlled release seen in endogenous H_2S production.

To address these challenges, synthetic H_2S donors, such as Lawesson's reagent derivatives like GYY4137 and dithiolthiones (DTTs), have been developed. GYY4137, known for its high-

water solubility and slow but prolonged H_2S release, has become a valuable tool to study the effects of H_2S in various physiological contexts (173). However, concerns remain about the potential confounding effects of residual dichloromethane in GYY4137 preparations, which can produce carbon monoxide, another gas signalling molecule (173). Despite the promising results of such studies, very few H_2S donors were validated as therapeutic strategies and it remains the case that the pharmacokinetics of sulfide donors, due to the nature of H_2S as a labile gas, are difficult to control and measure. An aspect of considerable significance is the limited attention afforded to the oxidation of H_2S by sulfur oxidation enzymes (SOP enzymes), an oversight that ignores a very significant regulatory process influencing effective concentrations of H_2S. NaHS, the first widely used H_2S donor in biological studies, remains one of the most common choices due to its simple structure and clear reaction byproducts, aiding in the understanding of H_2S's biological effects. However, NaHS's high water solubility results in rapid absorption and metabolism, causing tissue H_2S levels to drop quickly (173).

H_2S has shown protective effects against liver IR injury. In animal models, administering H_2S donors like NaHS further reduces injury severity (174, 175). Administering NaHS, has been shown to improve liver function and reduce fibrosis and portal hypertension in mice with carbon tetrachloride-induced liver damage. Similar results have been observed in rat models, with compounds like diallyl trisulfide (DATS) and S-allyl-cysteine (SAC) also reducing fibrosis by increasing H_2S levels (160). Proteomics and metabolomics studies on a MASLD mouse model revealed that H_2S treatment primarily impacts pathways related to fat digestion and absorption, fatty acid metabolism, glutathione metabolism, cytochrome P450 drug metabolism, and steroid hormone biosynthesis (176).

Additionally, H_2S donors are increasingly being studied as pre-treatment agents before tissue transplants due to their protective properties. In animal studies, H_2S pre-treatment improved lung function, reduced oxidative stress, and suppressed apoptosis and inflammation. These protective effects are likely due to the modulation of NF-κB and NRF2 pathways, which regulate inflammation and antioxidant defences (177). Additionally, H_2S donors have been shown to improve vascular function and promote anti-apoptotic signalling pathways, further enhancing tissue survival post-transplant (178).

In conclusion, pharmacological elevation of H_2S levels has demonstrated promising therapeutic potential in both preclinical and clinical studies. Understanding its protective mechanisms against liver injury will facilitate the development of novel therapeutic

interventions. Despite the promising results of such studies, very few H_2S donors were validated as therapeutic strategies and it remains the case that the pharmacokinetics of sulfide donors, due to the nature of H_2S as a labile gas, are difficult to control and measure. An aspect of considerable significance is the limited attention afforded to the oxidation of H_2S by sulfur oxidation enzymes (SOP enzymes), an oversight that ignores a significantly influence on the effective concentrations of H_2S.

1.3 Thiosulfate sulfur transferase (TST)

1.3.1 The structure of TST

Thiosulfate sulfur transferase (TST, EC 2.8.1.3), also known as rhodanese, is a member of the SOP enzymes primarily localised within mitochondria, as documented by Nagahara *et al.* (153). This enzyme facilitates the catalysis of H_2S by transferring a sulfur atom from a sulfane-containing donor to a nucleophilic acceptor.

The *hTST* gene is located on chromosome 22 (22q12.3), the protein (TST, EC 2.8. 1.1) comprises 297 amino acid residues and possesses a molecular weight of 35.6 kDa (179, 180). TST exhibits substantial sequence homology, sharing up to 66% sequence similarity, with another important sulfurtransferase known as MPST, as illustrated in Figure 1.4. Interestingly, in various species including humans and mice, the *Tst* gene consistently resides near the *Mpst* gene, although with opposite transcriptional orientations (181).

In rats and mice, TST protein is a 33-kDa, 320 amino acid protein (gene symbol *Tst*, ENSMUSG00000026882), and a search of the protein database reveals its presence in a wide variety of species. The 3-D structure of human TST protein has not been characterized, however, a predicted structure by "AlphaFold structure prediction" is available online (https://alphafold.ebi.ac.uk/entry/Q16762). At the present time, there is no evidence for alternative splicing or polymorphism in the TST gene. Homology studies suggest that TST is a member of the cdc25-like phosphatase family (182), a prediction that was supported by the recent solution of the crystal structure of thiosulfate sulfurtransferase. X-ray crystallography revealed that the fold of the protein was nearly identical to that of MPST, and TST was found to have a bidomain structure consisting of an N-terminal rhodanese domain and a C-terminal domain that hosts the active site; Cys-248 (or 247 in bovine TST) (183, 184).

Notably, Nagahara *et al.* (185) reported an elevation in *Tst* mRNA and protein levels in livers obtained from *Mpst* knockout (*Mpst*$^{-/-}$) mice in comparison to their WT counterparts. Conversely, in *Tst* knockout (*Tst*$^{-/-}$) mice, Carter *et al.* (168) documented reduced levels of *Mpst* mRNA but an increase in MPST protein levels. These findings suggest the existence of a compensatory mechanism and imply a potential interaction between *Tst* and *Mpst* on translational and posttranslational levels. This interaction warrants consideration when developing transgenic mouse models and investigating the mechanistic actions of either of these genes or their respective proteins.

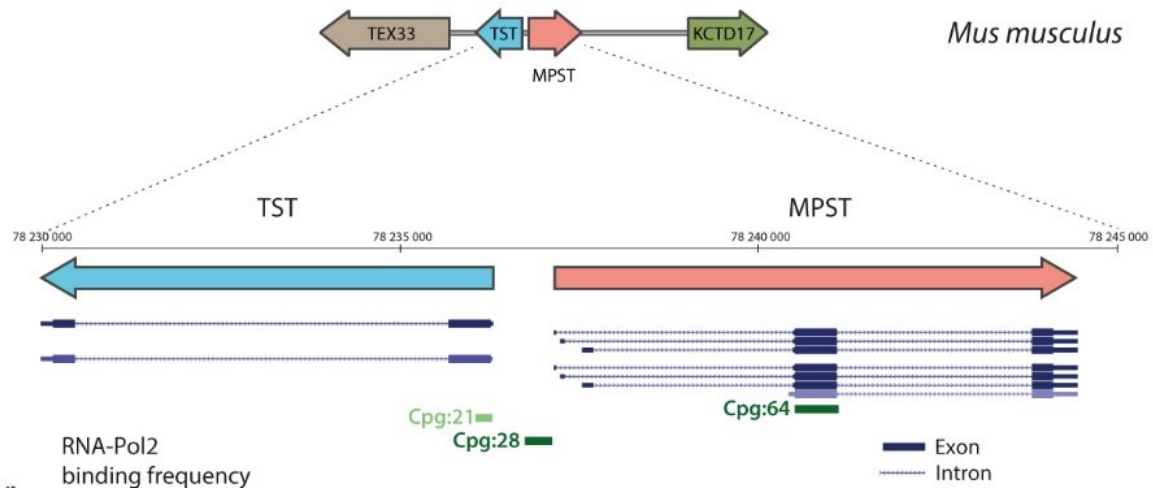

Figure 1.4 Alignment of *Tst* and *Mpst* genes on mouse chromosome 15.

Arrows represent transcriptional direction. Adapted from Pedre and Dick (181).

1.3.2 The enzymatic activity of TST

TST was first described for its cyanide detoxification enzymatic activity (179). The enzymatic activity of TST involves the transfer of sulfur atoms from a donor (such as a sulfate ester or a cysteine residue) to an acceptor nucleophile (such as an amine or a thiol group). TST was first described for its cyanide detoxification enzymatic activity (186). The cyanide detoxifying enzymatic activity of TST involves the following reaction:

Thiosulfate (S2O3^2-) + Cyanide ion (CN^-) ↔ Sulfite (SO3^2-) + Thiocyanate (SCN^-)

This reaction reversable and is also used as the basis of an assay to measure rhodanese activity *in vitro* (187, 188). Substrate specificity in TST, and all other sulfutrtansferases, is determined by residues on an active-site loop where catalytic cysteine resides. Studies showed that the

Cys^{247} residue is a catalytic site of TST (189, 190) and that the positive charges of the Arg^{186} and Lys^{249} in the CRKGVT motif interact with the negative charge of the substrate which is oxygen or thiosulfate (191).

TST undergoes significant modulation of enzymatic activity through post-translational modifications (PTMs). While traditionally recognised for its role in cyanide detoxification, TST is multifunctional in biological contexts. It facilitates detoxification processes, mediates the transportation of sulfur and selenium in bioavailable forms, and contributes to the restoration of iron-sulfur clusters (ISCs) within various proteins, including aconitase and mitochondrial respiratory complexes (187). Notably, phosphorylation of TST at key residues, such as Ser38 and Ser160, has been identified as a critical PTM, potentially influencing its enzymatic activity and interactions (192). Ser38, situated in a region linked to protein-protein interactions, and Ser160, near the catalytic domain, may modulate substrate binding or catalytic efficiency. These phosphorylation events are thought to be regulated by mitochondrial signalling pathways, such as AMPK during energy stress or PKA during metabolic shifts, underscoring TST's adaptive role in cellular metabolism (193). Additionally, PTMs may enhance TST's capacity to regulate redox balance and facilitate sulfide detoxification, processes critical to maintaining mitochondrial integrity and function under metabolic or oxidative stress (179). These modifications emphasise TST's dynamic role in mitochondrial regulatory networks and its potential as a therapeutic target for metabolic disorders.

1.3.3 The function of TST in metabolism

In a study conducted by Morton *et al.* (194), *TST* was identified as a significant genetic determinant associated with "healthy leanness" in mice. Notably, the study revealed that adipose tissue-specific overexpression of *TST* conferred a protective effect on mice subjected to a HFD, resulting in several favourable outcomes, including a substantial reduction in fat mass gain, mitigation of hyperglycaemia, enhanced insulin sensitivity, and a decrease in mean adipocyte size (194). Furthermore, Morton *et al.* (194) reported correlations between *TST* expression levels in human adipose tissue and several key metabolic markers. Specifically, *TST* expression exhibited a negative correlation with body mass index (BMI) and a positive correlation with insulin receptor substrate 1 (*IRS1*) and adiponectin, the latter being recognized for its protective role against diabetes and inflammation associated with obesity (195). These observations positioned *TST* as one of the relatively few known positive predictors of metabolic

health, thereby underscoring its potential significance as a promising drug target for addressing conditions such as obesity, diabetes, and fatty liver disease.

The absence of ETHE1 in mice leads to premature mortality, primarily attributed to the toxic effects of sulfide accumulation (196). Conversely, the deletion of the *Tst* gene results in a *via*ble condition characterised by elevated H_2S levels (194). Notably, *Tst* mRNA exhibits its highest expression levels in the liver relative to other tissues, as depicted in Figure 1.5.

Morton *et al.* (194) demonstrated that *Tst*$^{-/-}$ mice displayed impaired glucose tolerance when subjected to a HFD in contrast to C57BL/6N control mice. Importantly, the administration of thiosulfate, a substrate for TST, ameliorated HFD-induced glucose intolerance in C57BL/6N mice but had no such effect in *Tst*$^{-/-}$ mice. These findings underscore the central role of *Tst* in mediating the beneficial metabolic effects of H_2S. Moreover, *Tst*$^{-/-}$ mice exhibited only subtle alterations in adipose tissue, hinting at a non-adipose origin for impaired glucose homeostasis and emphasising the liver's potential significance in driving this phenotype (194). Consequently, our research group investigated the consequences of global *Tst* gene knockdown (*Tst*$^{-/-}$ mice) on hepatic metabolism, as detailed in Carter *et al.* (168). In this study, it was observed that *Tst*$^{-/-}$ mice displayed a ten-fold elevation in systemic plasma sulfide levels and a twenty-fold increase in thiosulfate, a metabolite of H_2S, compared to control C57BL/6J mice. To elucidate the liver's contribution to this sulfide elevation, sulfide levels were quantified in the inferior vena cava, revealing a three-fold increase in *Tst*$^{-/-}$ mice. This did not mirror the extent of elevation observed in circulating plasma. Furthermore, hepatocytes cultured from *Tst*$^{-/-}$ and control mice exhibited similar sulfide levels, suggesting the liver's ability to maintain a consistent sulfide concentration despite elevated circulating sulfide levels (168). *Tst*$^{-/-}$ mice showed significantly higher hepatocyte production of cysteine and glutathione (GSH) compared to controls, both under basal conditions and after stimulation of sulfur amino acid metabolism with methionine (168). This suggests an enhanced liver capacity to process sulfide into cysteine and glutathione (168).

1.4 Calorie restriction

Ever since McCay *et al.* (197) made the initial observation of prolonged lifespan following calorie restriction (CR) in rodents in 1935, a wave of scientific investigations into the underlying mechanisms and potential benefits of CR intervention has been growing. CR, defined as the reduction of food intake without malnutrition, can improve metabolic health,

enhance stress resistance, reduce inflammation, and enhance cellular repair processes (198). These benefits of CR have been reported across a wide range of model organisms, including yeast (199), *C. elegans* (200), drosophila (201), and rodents (202-204). It is important to note the various types of dietary restriction which could include whole food intake restriction or restriction of specific food types like protein or carbohydrates. In this project I use calorie restriction (CR) to refer to whole-calorie restriction without malnutrition unless otherwise mentioned.

Research has shown that CR can be an effective strategy for improving various aspects of metabolic health. It often leads to weight loss and a reduction in body fat, which is associated with improved insulin sensitivity, glucose regulation, and lipid profiles. Several studies have demonstrated the benefits of CR in mitigating the risk factors associated with metabolic diseases such as type 2 diabetes, obesity, and cardiovascular disease (205). In humans, CR was found to improve insulin sensitivity and reduced the risk of developing diabetes (206). Similarly, the CALERIE (Comprehensive Assessment of Long-term Effects of Reducing Intake of Energy) trials have provided valuable insights into the positive effects of CR on metabolic parameters (207, 208). However, it is important to note that the implementation of CR should be carefully monitored and tailored to individual needs, considering factors like age, sex, and baseline health status (206, 208-210).

Currently, there is no approved therapy for MASLD, and weight reduction is commonly recommended, although its efficacy has not been well-documented. CR has been shown to have a beneficial impact on hepatic steatosis, a hallmark of MASLD, by promoting weight loss and reducing overall body fat (211). The reduction in calorie intake leads to a negative energy balance, prompting the utilisation of stored fat, including the fat accumulated in the liver. Several studies have indicated that CR can improve liver function, reduce liver fat accumulation, and mitigate inflammation in the liver (198). CR is also associated with enhanced insulin sensitivity and improved glucose regulation, which are essential for managing MASLD and preventing its progression to more severe conditions such as MASH and fibrosis. While CR can be an effective approach to combat fatty liver, it should be implemented under the guidance of a healthcare professional to ensure that essential nutrients are adequately maintained, and overall health is safeguarded.

Despite the overwhelming evidence of the advantages of CR in humans (208, 212), challenges related to compliance hinder its widespread application in clinical settings. CR may also be of

high risk in conditions accompanied by extensive weight loss such as cachexia, immunocompromised disease, and advanced age (207). It is therefore essential to understand the underlying mechanisms of CR benefits for targeted dietary or pharmacological approaches.

1.4.1 Possible mechanisms of CR benefits

As CR limits caloric intake, it usually results in substantial weight loss that alters various metabolic pathways. Even though there are reductions in anabolic pathways (energy expenditure), the levels of available FFAs, gluconeogenic amino acids, and sterols are elevated under CR. Multiple studies have reported reduced metabolic rate as an adaptation to CR in rodents (213), non-human primates (214, 215) and humans (216). Although animals adapt to CR by initially reducing their basal metabolic rate, this change is typically transient, returning to normal within weeks as they adjust to the new caloric intake (217). However, during the initial adaptive period, animals lose body mass, particularly fat mass, which is recognized as a beneficial aspect of CR. This reduction in fat mass results from the depletion and insufficient replenishment of glycogen stores, leading to increased fatty acid mobilization from adipose tissue to meet energy demands. Eventually, energy intake and expenditure balance, and body mass stabilises or even increases.

CR is known to have a range of benefits across different species, and several mechanisms have been proposed to explain these effects. One prominent theory is mitohormesis, introduced by Sinclair (218). The mitohormesis concept stems from hormesis (219) where mild stressors prompt adaptations that enhance stress resistance. The mitohormesis theory suggests that increased production of reactive oxygen and nitrogen species (RONS) due to increased mitochondrial fatty acid oxidation triggers slight oxidative stress, subsequently prompting adaptive antioxidant mechanisms (218, 220).

The mammalian target of rapamycin (mTOR) pathway is crucial for nutrient sensing and regulating cellular growth. CR inhibits mTOR complex 1 (mTORC1), which suppresses the synthesis of proteins, lipids, and nucleotides while promoting autophagy and cellular maintenance (221-223). Additionally, the AMPK-mTOR-Sirtuin (SIRT) pathway plays a significant role in CR (224). Activation of AMPK inhibits mTOR, leading to increased expression of SIRT proteins, which in turn further activates AMPK in a positive feedback loop (224, 225). This pathway regulates key processes such as glycogen synthesis, fatty acid oxidation, and insulin sensitivity.

In addition to stimulating mitochondrial biogenesis and enhancing oxidative phosphorylation (OXPHOS), CR is associated with an increase in mitochondrial mass (226). However, some age-related increases in mitochondrial mass might be due to dysfunctional mitochondria, potentially harming cells. Studies in both rodents and humans, particularly older subjects, have shown increased mitochondrial mass during CR. This increase in mitochondrial mass is linked to the *Sirt1/Pgc-1α* pathway, which regulates several mitochondrial genes (227). In young rodents, CR leads to elevated levels of *Pgc-1α, Sirt1*, and *Tfam* mRNA (228), an increase in mitochondrial genes, and a decrease in cytochrome b mRNA, suggesting a denser and more homogeneous mitochondrial population.

Sirtuin3 (SIRT3), a Mitochondrial NAD+ -dependent protein deacetylase, plays a crucial role in regulating mitochondrial protein acetylation and malonylation, influencing ROS production and mitochondrial dynamics (229, 230). In *Sirt3*$^{-/-}$ mice, some beneficial effects of CR, such as reduced mitochondrial ROS production and decreased protein hyperacetylation, are lost (231). Proteomic analysis indicates that CR regulates acetylation levels of mitochondrial proteins involved in metabolism and translation, and these effects are absent in *Sirt3*$^{-/-}$ mice (231). Lastly, the SKN1/NRF2 pathway is another potential mediator of CR benefits. NRF2 acts as a central transcription factor in the phase II antioxidant and detoxification response, regulating genes involved in counteracting oxidative stress, such as haem oxygenase-1 (HO-1), NAD (P) H dehydrogenase quinone 1 (NQO-1), and glutathione transferases (232, 233). While NRF2 is critical for CR's protective effects against carcinogenesis, its role in longevity effects appears limited. The process of mitohormesis can be affected by antioxidants like vitamin C, vitamin E, and N-acetyl cysteine (NAC), which counteract oxidative stress (232, 233).

1.4.2 The link between the transsulfuration pathway and CR

The transsulfuration pathway (TSP) plays a critical role in converting homocysteine into cysteine, which is essential not only for protein synthesis but also for producing the antioxidant glutathione (GSH) and H_2S. H_2S has been shown to confer several physiological benefits, including stress resistance and lifespan extension in model organisms like yeast, worms, fruit flies, and mice (233-236). Ground-breaking research by Hine and Mitchell identified H_2S as a conserved mechanism driving the longevity and health span improvements linked to CR (235, 236).

In mice, Hine *et al.* (236) demonstrated that CR increased the expression of CSE and CBS enzymes in the liver, leading to higher endogenous hepatic H_2S production, which was crucial for the protective effects of CR (236). These benefits include resistance to ischemia-reperfusion injury (IRI) and protection against oxidative damage, with H_2S likely playing a role by interacting with mitochondrial components such as the enzyme SQOR. SQOR transfers electrons from H_2S to the electron transport chain, and its loss eliminates the protective effects of H_2S during IRI (236). Further studies indicated that manipulating TSP components can enhance or block the benefits of CR, highlighting the pivotal role of H_2S in these effects. The upregulation of H_2S production appears to be triggered by cysteine deprivation, which is influenced by stress responses and the mTORC1 pathway (236). Supplementing sulfur amino acids or inhibiting CSE in the liver diminished H_2S production and negated CR's protective effects against liver damage. Moreover, transcriptomics analysis of graded CR interventions showed that hepatic *Cse* was upregulated in mice livers after 2 weeks on 10%, 20%, 30% or 40% CR, indicating an activation in the H_2S production pathway (237), indicating a vital role of H_2S elevation in achieving the benefits of CR.

1.5 Hypotheses and aims

Given the evidence that mitochondrial TST modulates H_2S levels, with consequent impact on liver function in particular, this thesis set out to test two major hypotheses relating to the role of either hepatic elevation of TST activity on development of MASLD, or the effect of TST deficiency on the H_2S-mediated process of hepatic metabolism in the context of calorie restriction.

Hypothesis 1 (Chapters 3 and 4): Increased hepatic thiosulfate sulfurtransferase (TST) activity ameliorates development of metabolic dysfunction-associated steatotic liver disease (MASLD) *in vitro* and *in vivo*.

Aims

1. Determine the expression profiles of TST and the other 6 key proteins of H_2S metabolism in the liver across the MASLD spectrum in humans and mouse MASLD models.

2. Define the impact of liver specific TST over-expression on MASLD development and hepatic metabolism in mice *in vivo*.

3. Determine whether TST overexpression ameliorates the adverse effects of fat accumulation in human HepaRG cells *in vitro*.

Hypothesis 2 (Chapter 5): Elevation of sulfide levels in TST deficient mice improves the metabolic benefits of CR in mice.

Aims:

1. Define the impact of *Tst* knockout on glucose homeostasis in response to 30% CR in male and female mice.

2. Define the impact of *Tst* knockout on whole body energy homeostasis in response to 30% CR in male and female mice.

3. Determine the effects of 30% CR on the expression of the transsulfuration pathway (TSP) enzymes in male and female mice.

2 Chapter 2: Materials and Methods

2.1 Experimental animals

2.1.1 The *Tst*$^{-/-}$ mouse model

Tst$^{-/-}$ mice were previously generated and described as a full *Tst* deletion (*Tst*$^{tm1(KOMP)Vlcg}$). Sperm from viable heterozygote mice were used to fertilise C57BL/6N embryos at the University of Edinburgh Genetic Intervention and Screening technologies (GIST) facility. *Tst*$^{-/-}$ mice and age-matched littermate controls were placed on experimental diets at approximately 8-10 weeks of age. Mice in this study originated from C57BL/6N *Tst*$^{-/-}$ mice (194) backcrossed onto a C57BL/6J genetic background for more than 10 generations.

2.1.2 The Liv_hTST mouse model

The Liv_hTST mouse model was generated after successful revival of a unique genetic model of hepatic TST overexpression: the *hTST* allele: floxed-STOP-CAG-h*TST*mCherry by *in vitro* fertilisation (IVF) at the Genetic Intervention and Screening Technology (GIST) facility at the University of Edinburgh. Three homozygous (2 x *hTST* alleles) female mice were initially bred with three male heterozygous albumin-Cre mice that causes expression of CRE-recombinase selectively in the liver (238). All offspring were then genotyped using Transnetyx. The h*TST* allele responds to Cre recombinase by excising a STOP signal upstream of a strong CAG promoter, which then drives high expression of the human *TST* gene and has a Green fluorescent protein (GFP) reporter downstream (non-fused) as shown in Figure 2.1.

The desired allele combination was Albumin-*Cre*$^{+/-}$*hTST*$^{+/flox}$, meaning non-homozygous expression of CRE, and a single allele of *hTST* to achieve non-maximal overexpression. Genotyping for allele specific markers identified 4 genotypes as described in Table 2.1. Only 2 were included in this study, the "**Liv_hTST**" as a model for liver-specific overexpression of hTST and the Cre^{+} "**control**" as a control group.

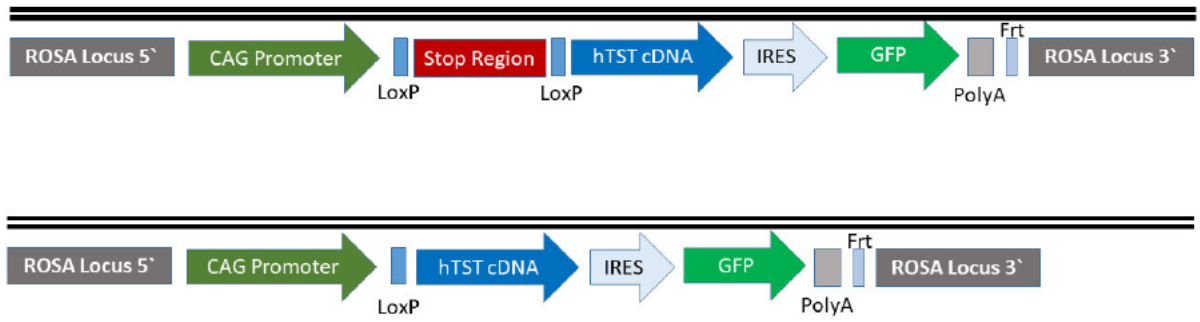

Figure 2.1 Targeting strategy to generate the *hTST* flox allele

The targeting vector contains the CAG promoter, the lox P sites (light blue boxes) flanking the stop region, when these animals are bred with Cre^{+} mice, the Cre recombinase enzyme recognizes the loxP sites and excises the stop region. This allows the downstream gene of interest (*hTST*) to be expressed under the control of the CAG promoter in the offspring, effectively activating hTST in liver tissue only.

Table 2.1 Genotype and characteristics of experimental groups used and excluded from the study.

Group	**Genotype**	***hTST* Allele Status**	**Cre Presence**	***hTST* Overexpression**
Liv_hTST	$Cre^{+}\ hTST^{flox/+}$	One *hTST* allele, one WT allele (heterozygous for *hTST* overexpression)	Present	Yes (Liver-specific)
Control	$Cre^{+}\ hTST^{+/+}$	Two WT alleles, no *hTST* overexpression	Present	No
Excluded	$Cre^{+}\ hTST^{flox/flox}$	two *hTST* alleles, (homozygous for *hTST* overexpression)	Present	Yes
Excluded	$Cre^{-}\ hTST^{flox/+}$	One hTST allele, one WT allele (no hTST overexpression)	Absent	No

2.2 Colony maintenance

Mice were housed in ventilated cages of 3-6 individual littermates until intervention at the Bioresearch and Veterinary Services (BVS) at the University of Edinburgh in a controlled environment (19-21°C and 50% humidity) with standard light conditions of 12 hours light (7 am-7 pm) and 12 hours dark (7 pm-7 am) cycles. When not in an experiment, mice had *ad libitum* access to water and food, and standard chow diet (CRM, Special Diet Service, Essex, UK). Eight to ten-week-old male and female mice were used for all experiments unless otherwise indicated.

Experiments were performed according to the UK Animals (Scientific Procedures) Act 1986 under a valid and active project license (PPL: PP5702478) and personal license (PIL: I37595510) and with the approval of the ethics committee of the University of Edinburgh.

2.3 Genotyping

Mouse pups were genotyped by Transnetyx (Memphis, TN, USA) shortly after being weaned around age 21 days. In short, an ear clip was taken and sent to Transnetyx, where DNA extraction was performed by an automated process and pre-designed probes were used to determine the genotype of the animal. Mouse genotypes from were determined using real time PCR with specific probes designed for each gene. Transnetyx TaqMan assays target specific sets of DNA sequence, generating millions of copies of the target DNA molecule analysed in a real-time fluorescent readout throughout the reaction as it occurs. These assays are built in such a way that they must bind to the target molecule of interest 5' to 3' end and the specificity of the reaction comes from the fluorescent-labelled probe. The sequences of primers and reporters used to genotype the *Tst*$^{-/-}$ and the Liv_hTST mouse lines are available confidentially upon request (Transnetyx confidentiality agreement does not allow publicly sharing these sequences).

2.4 Diet interventions

2.4.1 Calorie restriction (CR) diet

All experiments involving dietary intervention started at age 8-10 weeks. Before starting the mice on CR diets, mice were housed individually and fed a control diet (Research Diets,

D09100304, New Brunswick, NJ, USA) *ad libitum*, and daily food intake was determined by weighing the food remaining in each cage each day. Following one week of single housing, all mice were switched to CR diet (Research Diets, D09100304, administered at 70% of each mouse's daily *ad libitum* diet consumption, to achieve a 30% CR) for 4 weeks. Mice were single-housed and fed their food portions daily at 4:30-5 pm. Mice weight loss was monitored and recorded every 2-3 days. A weekly non-invasive assessment of fat/lean mass and body fluid was performed using TD-NMR (Minispec LF90II, Bruker Optics, Billerica, MA, USA).

2.4.2 Gubra Amylin NASH (GAN) diet

During the feeding time of this study (20 weeks), mice were given *ad libitum* access to either a control diet (Research Diets, D09100304) (Table 2.2) which was used as a "chow" diet for mice in the Liv_hTST study, or Gubra Amylin MASH (GAN) diet (Research Diets, D09100310), containing 40 kcal% fat (palm Oil), 20 kcal% fructose and 2% cholesterol, which was used to induce MASLD, full details of the components of the GAN diet are provided in Table 2.3.

Table 2.2 The components of the control diet (Research Diets, D09100304) used as "chow" in this study.

Description	Ingredients	Grams
Protein	Casein, Lactic, 30 Mesh	200.00
Protein	Cystine, L	3.00
Carbohydrate	Starch, Corn	350.00
Carbohydrate	Dextrose, Monohydrate	169.00
Carbohydrate	Sucrose, Fine Granulated	100.00
Carbohydrate	Lodex 10	85.00
Fiber	Solka Floc, FCC200	50.00
Fat	Soybean Oil, USP	25.00
Fat	Lard	20.00
Mineral	S10026B	50.00

Vitamin	Choline Bitartrate	2.00
Vitamin	V10001C	1.00
Dye	Dye, Red FD&C #40, Alum. Lake 35-42%	0.03
Dye	Dye, Yellow FD&C #5, Alum. Lake 35-42%	0.03
	Total:	**1055.05**

Table 2.3 The components of the Gubra Amylin NASH (GAN) diet (Research Diets, D09100310) used in this study.

Class description	**Ingredients**	**Grams**
Protein	Casein, Lactic, 30 Mesh	200.00
Protein	Cystine, L	3.00
Carbohydrate	Fructose	200.00
Carbohydrate	Sucrose, Fine Granulated	100.00
Carbohydrate	Lodex 10	100.00
Fiber	Solka Floc, FCC200	50.00
Fat	Palm Oil, Bleached, Deodorized	135.00
Fat	Soybean Oil, USP	25.00
Fat	Lard	20.00
Mineral	S10026B	50.00
Vitamin	Choline Bitartrate	2.00
Vitamin	V10001C	1.00
Special	Cholesterol, NF	18.00
Dye	Dye, Blue FD&C #1, Alum. Lake 35-42%	0.03
Dye	Dye, Red FD&C #40, Alum. Lake 35-42%	0.03
	Total:	**904.05**

2.5 *In vivo* techniques

2.5.1 Oral glucose tolerance test (OGTT)

On the morning of an oral glucose tolerance test (OGTT), mice were weighed, and their body composition was assessed using TD-NMR. Mice were then individually housed and subjected to a 5-hour fasting period, typically between 8 am and 1 pm, with unrestricted access to water. Before administering glucose, mice were bled by tail vein nick, and blood, glucose levels were measured, and a baseline blood sample was obtained before glucose administration for further analysis.

During the OGTT, a glucose solution (comprising 20% glucose (Sigma-Aldritch, G8270) in ultra-pure water at a dosage of 3 mg/g of lean mass was administered by oral gavage, with the volume of glucose administered being calculated based on each mouse's lean mass. Glucose concentrations were monitored, and blood samples were collected at designated time intervals of 15-, 30-, 60-, and 120-minutes following glucose administration.

Throughout the entirety of the experimental procedure, glucose levels were determined using a glucometer (Accu-Chek Performa Nano, Accu-Chek), and blood samples were procured *via* a single tail-venesection technique using microvette EDTA-coated capillary tubes (Sarsted, Nümbrecht, Germany, 16.444.100), with immediate storage on ice. Upon the conclusion of the experimental protocol, blood samples underwent centrifugation at 2000 RFC for 10 minutes at 4°C to isolate the plasma fraction, which was subsequently stored at -80°C for subsequent insulin quantification.

Glucose levels at different time points after the gavage were used to calculate glucose tolerance, which was determined by the area of the curve (AOC), calculated by subtracting the baseline glucose levels from the area under the curve (AUC) to avoid false results generated by different baseline glucose levels (239).

2.5.2 Time-domain nuclear magnetic resonance (TD-NMR)

Body composition, encompassing parameters such as fat, lean, and free body fluid mass, was quantified in mice utilising time domain-nuclear magnetic resonance (TD-NMR), facilitated by the Bruker minispec LF50 system operating at a frequency of 7.5 MHz and magnetic field strength of 0.175T, as previously described (240). This non-invasive methodology was applied

to conscious mice, with measurements conducted under conditions of physical restraint to minimise motion artifacts.

2.5.3 Animal culls and sample collection

Mice were culled at the end of each experiment by cervical dislocation (schedule 1 method), death was confirmed by decapitation. Blood was collected before culling and was treated as described at the end of section 2.6.1 for further biochemical analysis. In CR intervention experiments, mice were fed at 4-5 pm and culled the next day around 9 am, which is considered a "fasting state". In the GAN experiments, mice were culled while on *ad-libitum* diet.

Tissues dissected were liver, kidney, quadricep, heart, subcutaneous WAT (sWAT), gonadal WAT (gWAT) as form of visceral fat, and brain. Tissues for protein analysis were frozen in dry ice and stored at -80°C. The remaining sWAT, gWAT, liver, quadriceps, and kidney were fixed in 4% paraformaldehyde (PFA) for 24 hours, then transferred to 70% ethanol, and stored at 4°C for further histological analysis.

2.5.4 Indirect calorimetry

Male and female *ad libitum* and CR- fed mice were housed individually in Promethion CORE system cages (Sable Systems International, Las Vegas, USA) at the beginning of the experiment for one week during which they were still on *ad libitum* diet and again during week 4 of calorie restriction at which they were at 70% diet (30% CR).

At each time point, mice entered the cages around 11 am on day one and were housed for 3-4 nights (four days in total). The first 24 hours of data were not used for analysis to allow habituation to the new cages during day one. Before and after indirect calorimetry housing, each mouse was weighed, and body composition determined by TD-NMR.

Measurements of energy expenditure, oxygen consumption, carbon dioxide production, and physical activity were analysed using ExpeData software (Sable Systems International, Las Vegas, USA, v1.9.27) according to the manufacturer's instructions.

2.6 Biochemical assays

2.6.1 Plasma Insulin ELISA

Insulin levels from plasma samples collected during the OGTTs were quantified using the Ultra-Sensitive Mouse Insulin ELISA Kit (Crystal Chem, Zaandam, Netherlands, 90080), following the manufacturer's prescribed procedures designed for measurements within the low range. Specifically, 5 µL of the sample was used without dilution. Additionally, standards were prepared and utilised; the standard curve was generated through serial 1:2 dilutions of a known insulin stock provided in water, with resultant concentrations ranging from 0.1 to 6.4 ng/mL.

The absorbance values were recorded at 450 nm using the Optimax tunable microplate reader (Molecular devices, USA). The insulin concentrations were extrapolated by reference to the standard curve. Homeostatic Model Assessment for Insulin Resistance (HOMA-IR) and Matsuda index were calculated as previously described (241, 242).

2.7 Molecular Biology

2.7.1 Protein collection and quantification

All tissue samples were promptly stored at -80°C upon harvest for subsequent analysis. Approximately 50 mg of liver tissue was transferred to Eppendorf safety lock tubes (Eppendorf, Stevenage, UK) containing RIPA base buffer (RIPA Lysis Buffer System, Santa Cruz Biotechnology, Texas, USA, sc-24948A). Complete RIPA buffer was prepared on the day of tissue homogenisation by adding 10 µL of the provided PMSF solution and one tablet of protease inhibitor (Roche cOmplete ULTRA tablets, Sigma-Aldritch, 5892970001) per 10 mL of RIPA buffer, and 0.1% β-mercaptoethanol. Ice-cold complete RIPA buffer was added to each tissue sample, followed by incubation for 10 minutes on ice. Subsequently, tissue homogenisation was done using stainless steel beads and a TissueLyser II (Qiagen, Hilden, Germany) at 30 Hz for 15 seconds (x2), cooling down the samples on ice in between the runs. Homogenates were then centrifuged at 13200 rpm for 10 minutes at 4°C to collect the supernatant which was stored at -80°C for further analysis.

Protein quantification was performed using the Bio-Rad Protein assay (Bio-Rad, California, USA, 5000001) according to the manufacturer's instructions. Samples were diluted 1:20 in complete RIPA buffer to ensure that absorption remained within the linear range of the standard

curve prepared with bovine serum albumin (BSA, Merck, Dorset, UK, A3294) diluted in complete RIPA buffer to achieve a standard curve of 0-1.2 mg/mL. A total of 5 µL of either standard or sample was added to a 96-well plate (ELISA Microplates, Greiner bio-one, Kremsmünster, Austria). Then, 25 µL of solution A was added to each well and briefly mixed, followed by the addition of 200 µL of solution B. The plate was incubated at room temperature for at least 15 minutes. Absorption at 750 nm was measured using a plate spectrophotometer (Molecular Devices OPTImax microplate reader and software, Molecular Devices, Wokingham, UK). Sample concentrations were determined based on the standard curve and adjusted for dilution factors.

2.7.2 Western blotting

For SDS polyacrylamide gel electrophoresis, lysates were diluted to equal protein concentration in lysis buffer plus 4 X SDS loading buffer (Bio-Rad, California, USA, 1610747). 1% β-mercaptoethanol was added to the lysates. Samples were boiled for 5 minutes, cooled on ice for one minute, vortexed, and equal amounts of protein (15 µg per lane) were loaded onto 10% acrylamide/bis-acrylamide gels (30% acrylamide, Sigma-Aldrich) and separated by electrophoresis. Chameleon® Duo Pre-stained Protein Ladder (LI-COR Biosciences, Nebraska, USA, 928-60000) was also run on all gels. Gels were transferred overnight using a Bio-Rad wet transfer system onto AmershamHybond – P membranes (GE Healthcare, Illinois, USA).

All membranes were blocked in Tris buffered saline with 0.01% tween (TBST, containing 5% skimmed milk powder (Marvel skimmed milk powder) for one hour and then rinsed in TBST. Blocked membranes were then incubated with the appropriate primary antibody in TBST containing 5% BSA overnight at 4°C. Following three 5-minute washes with TBST, blots were incubated with secondary antibodies with an appropriate green or red fluorescent, at room temperature for 2 hours in TBST containing 5% BSA. Membranes were washed three times in TBST then scanned using the LI-COR Odyssey scanner (LI-COR Biosciences, USA). Image Studio software (LI-COR Biosciences, USA, v5.2) was used to quantify band intensity. For normalisation to a house keeping protein, the individual band intensity of β-actin or GAPDH was used for each sample. Primary antibodies used in this study are listed in Table 2.4, and the secondary antibodies are listed in Table 2.5.

Table 2.4 The primary antibodies used for this study

Primary Antibodies	Supplier	Catalogue Number
TST	Proteintech, (Manchester, UK)	66018-1-Ig
MPST	Abcam, Cambridge, UK	Ab224043
CSE	Proteintech, Manchester, UK	12217-1-AP
CBS	Proteintech, Manchester, UK	14787-1-AP
SQRDL	Proteintech, Manchester, UK	17256-1-AP
SUOX	Proteintech, Manchester, UK	15075-1-AP
ETHE1	Proteintech, Manchester, UK	27786-1-AP
GAPDH	Proteintech, Manchester, UK	60004-1-Ig
β-actin	Proteintech, Manchester, UK	66009-1-Ig

Table 2.5 The secondary antibodies used for this study

Secondary Antibodies	Supplier	Catalogue Number
IRDye 800CW Goat anti-Rabbit	LI-COR Biosciences, Nebraska, USA	926-32211
IRDye 680RD Donkey anti-Mouse	LI-COR Biosciences, Nebraska, USA	926-68072

2.8 *In vitro* techniques

2.8.1 Progenitor HepaRG (HPR101) culture and differentiation to differentiated HepaRG (HPR116)

A vial of HPR101 progenitor HepaRG cells at P12 from Biopredic International, France was used to create a bank of HPR101 progenitor cells which then were used for differentiation and the production of differentiated HepaRG cells (HPR116) as described in section 2.8.2.

2.8.1.1 HepaRG cell thawing and seeding

HepaRG growth medium (see table 2.6 for media preparation) was pre-warmed in a 37°C water bath. A sterile 50 mL tube was prepared with 4.5 mL of the warmed growth medium per 0.5 mL of HepaRG cryovial, ensuring a 1/10 dilution. The cryovial was quickly transferred from the liquid nitrogen tank to the 37°C water bath, ensuring it was only at room temperature for a few seconds. While holding the vial's tip, it was gently agitated, taking care not to submerge it completely. When a small crystal of ice remained (after 80 to 100 seconds), the vial was removed from the water bath, wiped with 70% ethyl alcohol absorbent paper, and placed under a laminar flow hood. The cell suspension was transferred into the tube containing the warmed growth medium. The cell suspension was homogenised thoroughly by pipetting up and down using a 5- or 10-mL pipette. Cells were counted using trypan blue and Bio-Rad TC10 automated cell counter (Bio-Rad, California, USA) to assess cell number and viability, which needed to be at least 1 million and 85%, respectively. The cells were then transferred into a 25 cm^2 flask, gently rocked to distribute them evenly, and placed in a 37°C incubator with 5% CO_2 and saturating humidity. Six hours after seeding, cell morphology was observed under a phase-contrast microscope, and the medium was renewed. The thawed cells were maintained in HepaRG growth medium for 7 days prior to trypsinisation, with the medium being renewed every 2 to 3 days after microscopic observation.

2.8.1.2 HepaRG cells expansion

After cell thawing and seeding, the expansion of HPR101 cells was performed as described in the schematic in Figure 2.2.

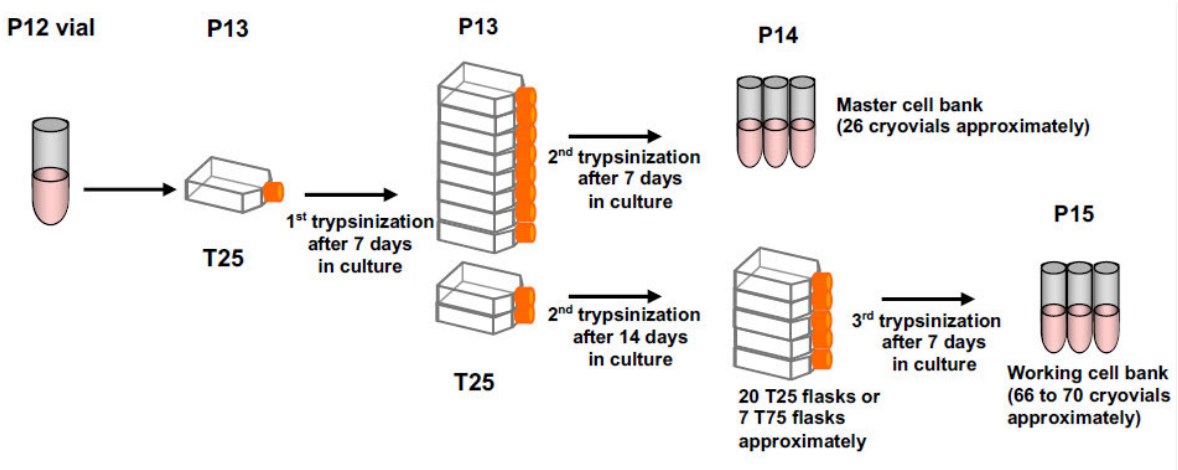

Figure 2.2 A schematic overview of the protocol for creating a bank of progenitor HepaRG cells (HPR101), this schematic was provided by Biopredic, France.

The first subculture was performed on day 7. Subsequently, cells were sub cultured every 14 days for expansion and/or differentiation. Trypsinisation of HepaRG cells was always carried out on day 14, except for the first passage after thawing and when cells were being prepared for freezing. Following the appropriate period of cell proliferation, subculturing was conducted to expand the cells, establish a master or working cell bank, or differentiate the cells.

2.8.1.3 HepaRG cells differentiation

HepaRG cells were maintained in growth medium (see table 2.6 for media preparation) for 14 days, with the medium renewed every 2 to 3 days. To induce differentiation, the growth medium was replaced with differentiation medium (see table 2.6 for media preparation), and the cells were maintained in this medium for an additional 14 days. The differentiation medium was renewed every 2 to 3 days. After 14 days in the differentiation medium, differentiated cells were maintained in the differentiation medium for up to 4 weeks, or frozen as described in section 2.8.1.4 and stored in liquid nitrogen for future use.

Table 2.6 Preparation and storage of undifferentiated HepaRG media

Media type	Preparation steps	Supplier	Storage
HepaRG growth media	ADD711 supplement was added to one bottle of 500 mL basal medium (MIL700).	BioPredic, lle et Vilaine, France	Stored at +4°C for up to one month.

HepaRG differentiation media	ADD721 supplement was added to one bottle of 500 mL basal medium (MIL700)	BioPredic, lle et Vilaine, France	Stored at +4°C for up to one month.

2.8.1.4 HepaRG cells freezing

A 20% Dimethylsulfoxide (DMSO) freezing medium was prepared by mixing HepaRG growth medium with 20% DMSO (Sigma-Aldrich, 472301), using half of the required total volume. Both the HepaRG growth medium and the 20% DMSO freezing medium were placed at 4°C. The cell suspension was centrifuged at 500 RCF for 3 minutes at 4°C, and the cell pellet was resuspended in HepaRG growth medium to half of the required total volume. The cell suspension was kept on ice. The 20% DMSO freezing medium was slowly added to the cell suspension, while mixing, to achieve a final DMSO concentration of 10%. Cells were frozen at a density of 1.5 million cells per 500 µL vial. The vials were transferred into Cryo 1°C freezing containers, "Mister Frosty", and placed at -80°C overnight. The following day, the containers were transferred into liquid nitrogen for long-term storage.

2.8.2 Differentiated HepaRG culture and maintenance

The preparation of the medium involved mixing Williams' Medium E with 1% GlutaMAX (ThermoFisher, Massachusetts, USA, 32551020), and 1% penicillin/streptomycin (pen/strep) (ThermoFisher, 15140122) was added if HepaRG supplements did not contain antibiotics. The HepaRG supplement was thawed in a 37°C water bath and then mixed with 100 mL of base medium to prepare the working medium, which was stored at 4°C for up to one month.

For thawing and counting HepaRG cells on Day 0, the HepaRG Thaw, Plate, & General Purpose (GPS) working medium (see Table 2.7 for medium preparation) was pre-warmed in a 37°C water bath. Nine millilitres of this medium were pipetted into a sterile 50 mL falcon tube per HepaRG cryovial. After removing the cryovial from liquid nitrogen, the cap was briefly loosened to release internal pressure before placing the vial in the water bath at 37°C. The cryovial was gently agitated for 1 to 2 minutes, then wiped with 70% ethyl alcohol and transferred under a laminar flow hood. The semi-thawed cell suspension was then mixed with the pre-warmed medium in a 1:10 ratio and centrifuged at 360 RCF for 2 minutes. The supernatant was aspirated, and the cell pellet was resuspended in HepaRG (GPS) Medium, followed by gradual mixing with 9 mL of additional medium.

For cell seeding, the cell suspension was diluted to achieve a concentration of 80,000 cells/well, with each well receiving 100 µL. The 96-well plate was pre-wetted with medium, allowed to equilibrate for 10 minutes, and then seeded with cells, which were incubated at 37°C with 5% CO_2 and 100% relative humidity.

Media changes were conducted the next day by replacing the medium with fresh medium (100 µL/well). After two days, the medium was changed again under a laminar flow hood, and on Day 3, the HepaRG Maintenance/Metabolism working medium (3M) was introduced (see Table 2.7 for medium preparation). All experiments were conducted on day 7, when CYP activities peak in the HepaRG culture according to Biopredic's protocol (Biopredic International, France).

Table 2.7 Preparation and storage of differentiated HepaRG media

Media type	**Preparation steps**	**Supplier**	**Storage**
HepaRG Thawing/Plating/General Purpose Medium (GPS)	1. HepaRG GPS supplement (ADD670) was thawed in a +37°C water bath. 2. Thawed supplement was added to 100 mL of base medium (Williams E with GlutaMAX).	BioPredic, lle et Vilaine, France	Stored at +4°C for up to one month.
HepaRG Maintenance/Metabolism Medium (3M)	1. HepaRG (3M) supplement (ADD620) was thawed in a +37°C water bath. 2. Thawed supplement was added to 100 mL of base medium (Williams E with GlutaMAX).	BioPredic, lle et Vilaine, France	Stored at +4°C for up to one month.

2.8.3 Stable transfection of HepaRG cells

HepaRG progenitor cells (HPR101) were thawed at a density of 2-3*10^4 cells/cm². The following day, the cell culture medium was changed. One week after seeding HPR101 cells, lentivirus was added at a multiplicity of infection (MOI) of approximately 1.6 (10 million infectious units to 6 million cells). Five days post-transduction, lentiviral uptake was confirmed by imaging the GFP reporter in both plasmids under a microscope. Cells were then sorted *via* FACS based on GFP expression, to select cells with high GFP expression for further culture. Finally, the transfected HPR101 cells were differentiated into HepaRG cells as detailed in section 2.8.1.3.

2.8.4 Seahorse extracellular flux analysis

To evaluate cellular respiratory function, oxygen consumption rate (OCR) was measured during a mitochondrial stress test using the Seahorse XFe24 Analyser (Agilent, USA). All washing, incubation, and drug preparation steps were performed with Seahorse XF base media (Agilent, 102353-100) supplemented with 2 mM pyruvate (Sigma-Aldritch, P5280), 10 mM glucose (Sigma-Aldritch, G8270), and 2 mM GlutaMAX (Gibco, 35050-038). The following drug concentrations were utilised during the mitochondrial stress: 2 µM oligomycin (Sigma-Aldritch, 75351), 1 µM carbonyl cyanide-p-trifluoromethoxyphenylhydrazone (FCCP) (Sigma-Aldritch, C2920), and 0.5 µM rotenone (Sigma-Aldritch, R8875) combined with 0.5 µM antimycin A (Sigma-Aldritch, A8674). The seeding density for HepaRG cells was optimised by our group to 80.000 cells/ well for a 96-well plate. Cells were seeded and maintained as described in 2.8.2 until day 7, after which different treatments were applied for 72 hours and the seahorse assay ran at day 10.

Each drug solution (75 µL) was loaded into separate injection ports of the Seahorse cartridge and calibrated in the seahorse analyser. Cells were washed three times with 500 µL Seahorse media and then left in 525 µL of media. After a 30-minute incubation at 37 ºC in a CO_2-free incubator, the plate was placed in the Seahorse analyser, where OCR was measured during the mitochondrial stress test at 37 ºC and normalised to cell number. The data generated was plotted and analysed using Wave desktop software (Agilent, California, USA, v 2.6.3).

Figure 2.3 illustrates the components of the electron transport chain (ETC) targeted during the mitochondrial stress test and how to calculate several parameters from the OCR measured

during different stages of the test. Basal respiration, representing the cells' OCR under normal conditions, is directly measured at the beginning. ATP-linked respiration is determined by subtracting the OCR after oligomycin injection (which inhibits ATP synthase) from the basal OCR. Proton leak, which reflects the OCR not associated with ATP production, is calculated by subtracting the non-mitochondrial OCR from the oligomycin-inhibited OCR. Maximal respiration, indicating the highest possible OCR when the ETC is fully activated, is determined by subtracting the non-mitochondrial OCR from the FCCP-stimulated OCR. The difference between maximal and basal respiration gives the spare respiratory capacity, which measures the cell's ability to meet increased energy demands. Finally, non-mitochondrial respiration, which accounts for OCR from processes outside the mitochondria, is measured after the addition of rotenone and antimycin A, which inhibit mitochondrial respiration. These calculations provide a comprehensive assessment of mitochondrial function.

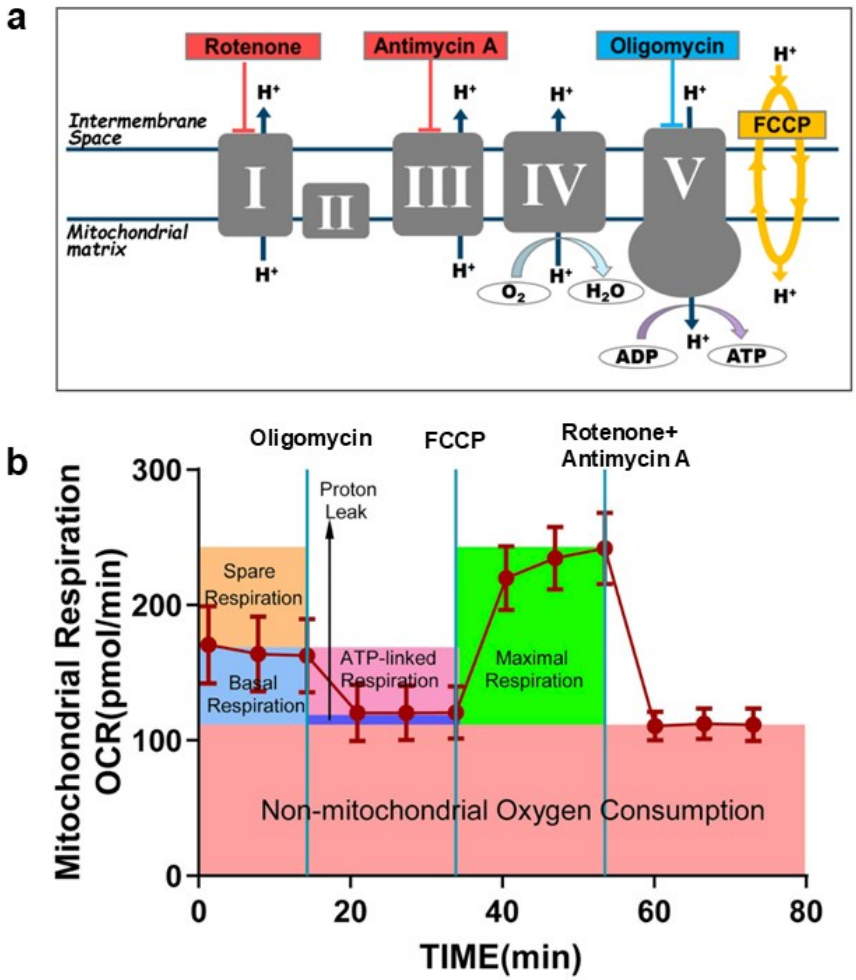

Figure 2.3 Mechanisms and targets of drugs in the Seahorse XF cell mitochondrial stress test: Impact on electron transport chain complexes and the calculations of various parameters. Images extracted from Agilent.com

a. The complexes of the Electron Transport Chain (ETC) and the action targets of the drugs used in the Seahorse XF Cell Mito Stress Test Kit. Oligomycin, which inhibits ATP synthase (complex V), is the first drug injected after basal measurements. It reduces electron flow through the ETC, leading to a decrease in mitochondrial respiration, or oxygen consumption rate (OCR). This reduction is directly linked to the cell's ATP production. The second injection, carbonyl cyanide-4-(trifluoromethoxy) phenylhydrazone (FCCP), acts as an uncoupling agent. FCCP disrupts the proton gradient and mitochondrial membrane potential, allowing uninhibited electron flow through the ETC. This causes oxygen consumption at complex IV to reach its maximum level. The FCCP-stimulated OCR is used to calculate spare respiratory capacity, which is the difference between maximal and basal respiration. This capacity reflects the cell's ability to meet increased energy demands or cope with stress. The third and final injection is a combination of rotenone, a complex I inhibitor, and antimycin A, a complex III inhibitor. This mixture completely halts mitochondrial respiration, allowing the calculation of non-mitochondrial respiration driven by processes outside the mitochondria (243, 244).

b. The calculation of basal respiration, ATP-linked respiration, maximal respiration, spare respiratory capacity, and non-mitochondrial respiration during the mitochondrial stress test.

2.8.5 Lipid staining and quantification in cell culture

Neutral lipid staining was performed on differentiated HepaRG cultured and maintained as described in section 2.8.2. For lipid imaging, cells were seeded and treated in Ibidi black 96 well culture plates with round wells and a flat, clear bottom for high throughput microscopy (Ibidi, Gräfelfing, Germany). Different treatments were applied on day 7 and lipid staining performed at day 10 using the HCS LipidTOX Deep Red Neutral Lipid Stain (Invitrogen, Massachusetts, USA, H34477) according to the manufacturer's instructions. Briefly, cells were fixed using a 3.0–4.0% formaldehyde solution, incubated for 15 minutes at room temperature. The fixative was then removed, and cells were rinsed with the provided buffer 2–3 times before staining. The neutral lipid stain, LipidTOX, was diluted 1:1000 in PBS, and 100 µL was added to each well after removing the buffer from the rinsed cells. Additionally, nuclei stain was added to each well (Hoechst, ThermoFisher, 33258) at a concentration of 10 µg/mL. Plates were sealed with film, incubated for at least 30 minutes at room temperature, and imaged without washing, followed by image acquisition and analysis. LipidTOX Deep Red neutral lipid stain was imaged with filter sets appropriate for Alexa Fluor 647 dye. Hoechst stain was imaged using blue fluorescence (excitation at ~350 nm, emission at ~461 nm). Images were collected by Dr. Justyna Cholewa-Waclaw at the high content screening facility at the University of Edinburgh using Opera Phenix Plus (Revvity) with 20x water objective (NA 1.0). Analysis was performed by Dr. Justyna Cholewa-Waclaw using Harmony software (Revvity). Briefly, cell nuclei were segmented to identify single cells. Lipid droplets were segmented with spot finding algorithm and morphology of spots was measured such as number of spots, total spot area and spot intensity.

2.8.6 Reactive oxygen species staining and quantification in cell culture

The Cellular Reactive Oxygen Species (ROS) Detection Assay Kit was used to determine total cellular ROS (Abcam, Cambridge, UK, ab186029). For ROS imaging, cells were seeded and treated in Ibidi black 96 well culture plates with round wells and a flat, clear bottom for high throughput microscopy (Ibidi, Germany). Different treatments were applied on day 7 and lipid staining performed at day 10 using the Abcam Deep Red ROS Stain according to the manufacturer's instructions. Cells cultured or treated were incubated with the ROS reagents for 45 minutes at 37°C and 5% CO_2 before being imaged. Images were collected by Dr. Justyna Cholewa-Waclaw at the high content screening facility at the University of Edinburgh using

Opera Phenix Plus (Revvity) with 20x water objective (NA 1.0). Analysis was performed by Justyna Cholewa-Waclaw using Harmony software (Revvity).

2.9 Histology

2.9.1 Fixing, paraffin blocking, and sectioning

Mouse tissue fixed in formalin were processed and embedded in paraffin at the QMRI Histology Facility, University of Edinburgh. The paraffin-embedded tissues were then sectioned into 5 μm slices using a Leica RM2125 RTS Microtome (Leica Biosystems, Nussloch, Germany) and mounted onto slides. One section from each tissue was hematoxylin and eosin (H&E) -stained, and one section was picrosirius red (PSR)- stained by the QMRI histology facility. Stained sections were imaged by Prof. Timothy Kendall (University of Edinburgh) using a NanoZoomer whole-slide scanner (Hamamatsu, Shizuoka, Japan).

2.9.2 PSR and lipid quantification in liver sections

The PSR and lipid quantification were performed as described by Kendall *et al.* (245). Briefly, a duplexed classification script was used to assess the raw.ndpi scans of PSR-stained sections. First, a 'whole tissue' classifier was applied, and small artifacts were removed from the mask based on size. Next, a second pixel classifier of the random trees (RTrees) type, with 'gaussian' and 'weighted deviation' features selected, was applied. This classifier, pretrained by a pathologist (Prof. Timothy Kendall, University of Edinburgh), categorised pixels within the 'whole tissue' masked area into histological classes: 'fat,' 'psr,' and 'other tissue'. The total number of pixels for each class and the percentage of fat and PSR-positive pixels were calculated. Whole-slide scan processing was performed using QuPath (v.0.2.3) (246).

2.10 Whole blood and liver tissue MBB derivatisation

Blood samples (5 μL) were derivatised with monobromobimane (MBB) by the addition of 20 μL of 160 mM EPPS (4-(2-hydroxyethyl)-1-piperazine propanesulfonic acid, 16 mM DTPA (diethylenetriaminepentaacetic acid) pH 8.0, 20 μL acetonitrile, and 5 μL 46 mM MBB. Reaction vials were capped tightly and vortexed for one minute and incubated protected from light at room temperature for 10 minutes. 1 mL ethyl acetate was added to stop the reaction. The reaction vials were centrifuged at 1800 rpm (350 g) for 7 minutes to separate aqueous and

organic layers. The organic layer was collected from each extraction, transferred to a 1.5 mL glass vial and the solvent was evaporated completely under a nitrogen stream. Acetonitrile (100 µL) was added to each vial, and the solvent was again evaporated to remove any traces of ethyl acetate. Dried MBB-derivatives were stored at -20 °C until analysed.

Frozen livers (~25 mg, exact weight recorded) were homogenised in 160 mM EPPS, 16 mM DTPA and MBB, pH 8.0 buffer (300 µL) and acetonitrile (300 µL) with 46 mM MBB (25 µL) for 25 minutes, at room temperature in the dark. The reaction was stopped with ethyl acetate (1 mL), the mixture centrifuged (400 g for 15 minutes at 4 °C), and the upper organic layer (~800 µL) passed through a 96-well Filter+ Plate (Biotage, Sweden), along with an MBBr-derivatised calibration curve of a mixture of Sulfide, thiosulfate, glutathione, L-Cysteine, sulfite and sulfate (0, 0.01, 0.025, 0.05, 0.1, 0.25, 0.5, 1, 2.5, 5, 10, 20, 90 and 100 µM), followed by PLD+ extraction (Biotage, Sweden), reduction to dryness. Dried MBB-derivatives were stored at -20 °C until analysed by LC-MS.

2.11 Liquid Chromatography-Mass Spectrometry (LC-MS) quantification of sulfur compounds in blood and tissue

Samples were analysed on an I-Class UPLC system (Waters, UK) on a 16 minutes chromatographic run using an HSS T3 (2.1 x 150 mm; 1.8 mm) column kept at 50 °C. MBB-thiosulfate was eluted using water (0.1% formic acid) / methanol (0.1% formic acid) system at 0.4 mL/minutes from 0-100% methanol over 6 minutes, re-equilibrating to 0% methanol at 15 minutes. Multiple reaction monitoring parameters for the thiosulfate MBB derivative was m/z 303.0 → 205.1 on a QTrap 6500+ (AB Sciex) with the following compound settings: declustering potential -65 V, collision exit potential -15 V, collision energy -18 V. Source conditions were -4.5 kV ion spray voltage, 600 °C temperature, gases (GS1=40, GS2=60, Curtain gas= 40 units). Analyst v1.7 was used for instrument control and data acquisition. Data analysis was carried out using MultiQuant v3.0 (AB Sciex). Linear regression analysis of the peak areas of MBB-thiosulfate was used to calculate the quantity of thiosulfate in each sample, corrected for tissue mass.

2.12 Statistical analysis

The power calculation for this study was performed using the software G*Power (version 3.1.9.6), leveraging data from a comparable study that evaluated the effects of the GLP1R agonist liraglutide on MASLD in mice. In that study, four groups were compared: a low-fat diet control group, a high-fat diet (HFD) vehicle group, and two treatment groups receiving liraglutide or elafibranor. The NAS (NAFLD Activity Score) was the primary outcome measure, with mean scores of 0.1 (low-fat diet), 5.1 (HFD vehicle), 4.0 (HFD + liraglutide), and 3.6 (HFD + elafibranor), indicating a 22% reduction in NAS with liraglutide and a 30% reduction with elafibranor. Using these NAS scores, we calculated an estimated effect size of 1.82 with the G*Power tool. A stringent power level was set to 0.95 and an error probability (α) of 0.05. This stringent power level was chosen to ensure robustness in the event of subject loss, accounting for potential data attrition (~10%). With these parameters, the calculation indicated that a sample size of 8 mice per group would be sufficient to detect significant differences between groups.

All statistical analyses and graphing were performed by GraphPad Prism 10 software (Boston, Massachusetts USA, www.graphpad.com). The values are represented as mean ± SEM (standard error of mean). A value of $P < 0.05$ was considered significant. Analyses comparing the interaction of two or three factors, a two-way or three-way analysis of variance (ANOVA) was used, respectively, to compare the significance of contribution to variance by each factor, and if there is a significant interaction between the factors (e.g., diet*sex*genotype). A mixed-fitted model was used instead of two-way ANOVA or three- way ANOVA if any values were missing. All statistical and post hoc tests are indicated in the legend of each graph.

3 Chapter 3: The impact of hepatic TST overexpression on MASLD progression in mice

3.1 Introduction

MASLD starts as a simple lipid accumulation (>5%), and can progresses to steatohepatitis, and liver fibrosis, and if untreated leads to cirrhosis and irreversible liver damage. Mechanistically, the critical contributors to MASLD are lipid metabolism dysfunction, oxidative stress, insulin resistance and fibrosis (43, 59). The liver plays a major role in regulating glucose and lipid metabolism and antioxidant defence (157, 159). It is also the principal organ for production and clearance of H_2S under basal conditions (158). H_2S plays a significant role in liver function and disease. The enzyme CSE is the primary source of H_2S in the liver, with *Cse* knockout studies confirming its importance in maintaining liver health especially when challenged with HFD (161). H_2S is crucial for regulating glucose and lipid metabolism, and its impaired catabolism is linked to liver diseases such as MASLD and cirrhosis (160, 165, 247).

3.1.1 The protective role of TST in adipose tissue and the liver

A growing body of preclinical evidence suggests that H_2S donors have the potential to prevent or reverse MASLD and MASH (248-251). However, the therapeutic use of H_2S is limited by its toxicity at high concentrations, which constrains the effective dosing of H_2S donors (252).

H_2S is oxidised in the mitochondria through the SOP, which involves several key enzymes: SQOR, ETHE1, SUOX, and TST (Figure 1.2). Among these, TST plays a distinctive role; unlike other SOP enzymes, TST not only facilitates the conversion of H_2S but also channels its sulfur into several beneficial mitochondrial processes, such as maintaining iron-sulfur clusters in the respiratory chain (253, 254), and detoxifying reactive oxygen species (255).

Overexpression of *Tst* appears to be metabolically protective (194), while its deficiency may contribute to the development of liver disease (168). Research by Morton *et al.* (194) showed that adipose tissue- specific overexpression of *Tst* conferred a protective effect on mice subjected to HFD, resulting in a reduction in fat mass gain, mitigation of hyperglycaemia, enhanced insulin sensitivity, and a decrease in mean adipocyte size compared to control mice (194). Furthermore, *TST* expression in human adipose tissue was positively correlated with beneficial metabolic markers like insulin receptor substrate 1 (IRS1) and adiponectin, both of

which are linked to protection against conditions such as diabetes and MASLD (256). These findings position *TST* as a potential key player in maintaining metabolic health and indicate that its overexpression in other tissues might serve as a therapeutic target for preventing liver-related metabolic disorders (194).

Conversely, the lack of TST was associated with adverse metabolic outcomes and liver dysfunction. *Tst*$^{-/-}$ mice displayed impaired glucose tolerance when subjected to HFD in contrast to control mice (168). Importantly, the administration of thiosulfate, a substrate for TST, ameliorated HFD-induced glucose intolerance in control mice but not in *Tst*$^{-/-}$ mice (168). Impaired glucose homeostasis in the absence of TST suggests a role for TST in normal metabolic processes, particularly in the liver where it is most highly expressed relative to other tissues (Figure 3.1).

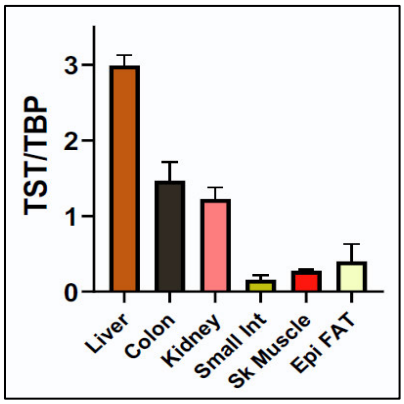

Figure 3.1 *Tst* mRNA in C57Bl/6J different tissues (adapted from Carter *et al.* (168)).

Comparison of *Tst* mRNA levels across liver, colon, kidney, small intestine, skeletal muscle and epididymal fat from male C57BL/6J mice measured by real time-PCR and normalised to *Tbp* mRNA. Data are represented as mean ± SEM, n=4. Sk: skeletal, Epi: epidermal, Int: intestine. TST: thiosulfate sulfurtransferase, TBP: TATA-Box Binding Protein.

3.1.2 The MASH-inducing GAN diet

The GAN diet induces key histopathological features of MASH in mice, such as steatosis, hepatocyte ballooning, lobular inflammation, and fibrosis, essential for accurately modelling human MASH (94). Liver biopsies from GAN-fed mice display similar dynamics in differentially expressed genes involved in key metabolic and histopathological features of MASH as observed in human patients (94). Additionally, the GAN diet induces many other aspects of the metabolic syndrome, including increased body weight, impaired glucose tolerance, and insulin resistance, providing a comprehensive model for liver and systemic MASH pathophysiology (94).

The GAN diet effectively models the progression MASLD to MASH. When C57BL/6 mice are fed the GAN diet for 28 weeks, they develop severe steatosis, moderate-to-severe lobular inflammation, mild-to-moderate fibrosis, and no hepatocyte ballooning (93). Extending the diet to 38 weeks leads to fibrotic MASH, mirroring the histopathological characteristics seen in human MASH patients, including significant increases in hepatic lipid accumulation, inflammation, and collagen deposition (93). Liver biopsies from GAN-fed mice for 38 weeks reveal similar gene expression changes to those observed in MASH patients, underscoring the diet's relevance in modelling MASLD-MASH progression (94). In accordance with FDA guidelines banning trans-fats, the GAN diet substitutes trans-fats with saturated fats (e.g., palm oil), making it highly relevant for studying diet-induced MASH. The GAN diet induces the progression of MASH, including advanced stages such as fibrotic MASH and liver lesions, over a prolonged period (28 weeks), reflecting the chronic nature of the disease in humans.

Based on our observation of an early increase in TST expression at the boundary of steatosis/MASH (see 3.4.1), in this study, the dietary exposure time was set to 20 weeks to best capture these early stages of MASLD, and thus to test the hypothesised protective role of TST at this critical disease transition period.

3.2 Hypothesis and aims

Hypothesis: The hepatic elevation of TST expression at the steatosis/MASH transition is a protective mechanism that counteracts disease progression

Aims:

1. Assessment of *TST* mRNA and protein expression across MASH stages in human patients and in the STAM mouse model of MASH.
2. Creation and validation of a new mouse model with hepatic overexpression of human *TST*: Liv_hTST mice.
3. Assessment of the metabolic profile and sulfide levels in male and female control and Liv_hTST mice at baseline
4. Assessment of the metabolic profile and sulfide levels in male and female control and Liv_hTST mice after 20 weeks on a MASLD-inducing GAN diet.

5. Quantification of liver lipids and fibrosis after 20 weeks on GAN diet to evaluate the effect of hepatic TST overexpression on fat accumulation and fibrosis progression.

3.3 Experimental design

3.3.1 Determination of the expression profile of TST at the early stages of human and mouse MASLD

The subset of SteatoSITE patient cohort (consisting of n=692 individuals; complete details available at https://steatosite.com/) with available bulk RNA sequencing data was employed to determine the expression patterns of key genes participating in the biosynthesis (*CBS*, *CTH* or *CSE*, *SQOR* or *SQRDL*, *MPST*) and catabolism (*TST*, *SUOX*, and *ETHE1*) of H_2S across distinct stages of MASLD in humans. The bioinformatics analysis related to this dataset was performed by Prof. Jonathan Fallowfield's group (Dr. Maria Ramos, University of Edinburgh) upon our request.

To gain insights into H_2S/ TST contribution to MASLD initiation and progression in mice, a well-established mouse model (STAM MASH mouse model (SMC Laboratories Inc., Tokyo, Japan) (257) that mirrors the different stages of MASH (Figure 3.2) was used. The model was created by using both the effect of a single subcutaneous injection of 200 μg of the chemical toxin streptozotocin (STZ) (at birth) and HFD (for up to 20 weeks) on C57BL/6 mice with measurements conducted at the 5 different time points (4, 6, 8, 12 and 20 weeks on HFD). All the steps shown in Figure 3.2 up until harvesting the liver tissue were performed by the SMC laboratories, our laboratory purchased frozen liver samples from different stages of MASH and I have performed all the following analysis (western blotting). Additionally, I have added liver samples from age and sex-matched C57BL/6 on chow diet as a healthy control. Liver tissues from 6 time points (n= 5 per time point) were obtained, and TST, MPST, CSE, CBS, SOUX and SQRDL were quantified by western blot as described in section 2.7.1 and 2.7.2. β-actin or GAPDH were used as a loading control to normalise the levels of protein detected.

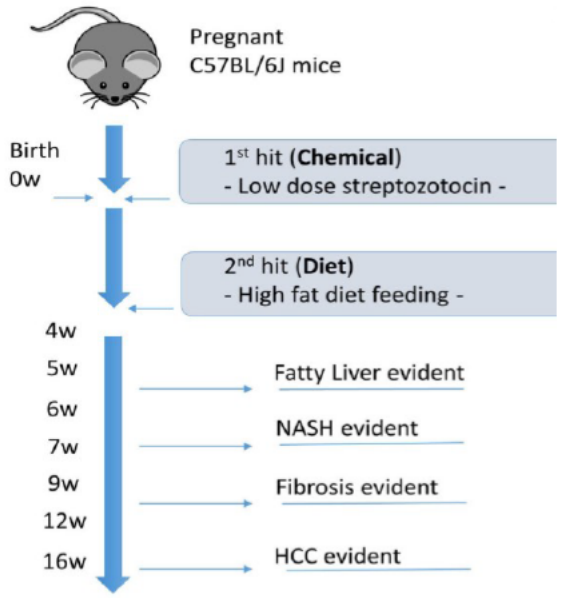

Figure 3.2 Illustration of STAM mouse model (adapted from Fujii *et al.* (255)).

The model was created by SMC Laboratories Inc., Tokyo, Japan by using both the effect of the chemical toxin streptozotocin (STZ) (0 week) and high fat diet (4 weeks) on C57BL/6 male mice with measurements conducted at the 5 different time points. A total of 42 cryo-preserved tissues were harvested from the mice Frozen liver samples were purchased for further analysis. (n=5 per timepoint). NASH: nonalcoholic steatohepatitis, HCC: hepatocellular carcinoma.

3.3.2 Validation of a novel liver-specific hTST overexpressing mouse line

A new and unique mouse model (Liv_hTST) featuring liver-specific overexpression of the human *TST* gene (*hTST*) was employed (full details of the generation of this mouse model are provided in section 2.1.2).

The liver-specific induction of hTST in Liv_hTST mice was confirmed, as hTST protein was only overexpressed in the livers and not overexpressed in the kidneys or hearts of these mice (Figure 3.3 a and b). Previous findings indicated that TST deficiency led to a compensatory increase in MPST protein, despite reduced *Mpst* mRNA levels due to proximal promoter interference (168) raising the possibility of post-translational co-regulation between these two paralogues. To investigate this, MPST protein levels were measured in Liv_hTST mouse tissues (Figure 3.4 c and d). No co-regulation of MPST was found in the kidneys or hearts of Liv_hTST mice. However, MPST protein levels were higher in the livers of Liv_hTST mice, showing a 1.7-fold increase in males and a 1.5-fold increase in females compared to controls (Figure 3.4 c and d).

Endogenous mouse TST (mTST) levels in Liv_hTST mice were comparable to those in control male and female mice (Figure 3.3 a and b). In contrast, hTST protein levels in the Liv_hTST livers were approximately 6.0-fold higher in males and 6.5-fold higher in females compared to endogenous mTST levels (Figure 3.3 e). Additionally, MPST levels in Liv_hTST livers were elevated by 1.4-fold in males and 1.7-fold in females compared to control livers (Figure 3.4 e).

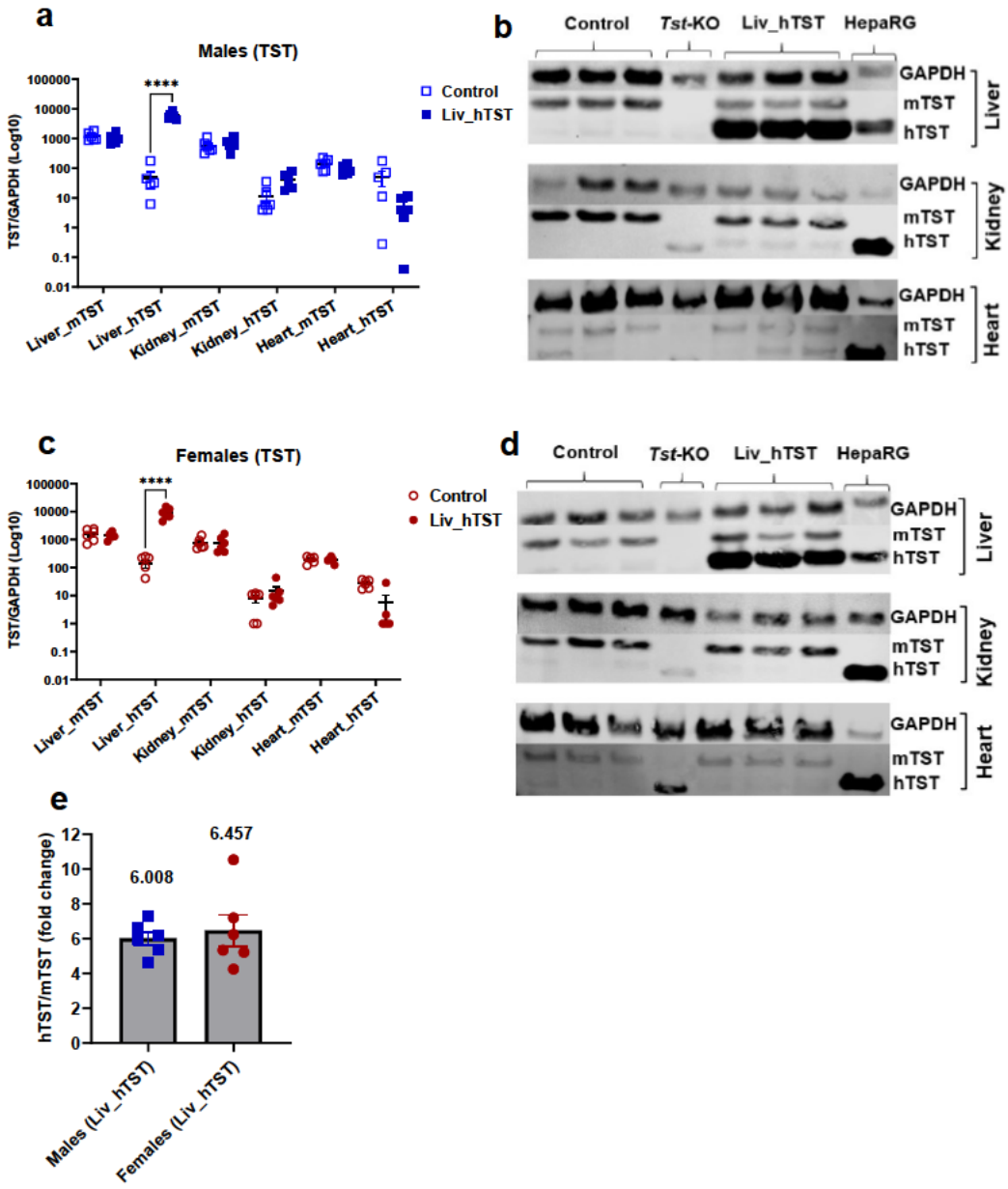

Figure 3.3 TST protein in liver, kidney, and heart tissue of Liv_hTST and control male and female mice.

TST protein level, relative to GAPDH endogenous control in liver, kidney, and heart tissue of (a) male and (c) female Liv_hTST and control mice. (b) and (d) Representative blots for males and females respectively (blots were cropped to show the bands of interest, all bands were blotted on the same membrane at the same time). (e) Fold change calculated as human TST (hTST)/ mouse TST (mTST) ratio in each of the Liv_hTST mice (from the same blot), numbers above each bar represent the mean value. Data in a-c are shown as log10-transformed intensities to normalise the wide range of signal intensities due to the lack of human TST signal in control mice. HepaRG, a human hepatocytes cell line and a mouse *Tst*- knockout sample were included to distinguish the mouse from human TST protein. (n=6/ group). Data are mean ± SEM, two-way ANOVA with Tukey's post hoc tests were performed on the original (non-transformed) intensity values to determine statistical significance: ****P≤ 0.0001. *Tst*-KO: liver sample from a global *Tst* knockout mouse from the same strain, sex, and age. *Tst*: Thiosulfate sulfurtransferase.

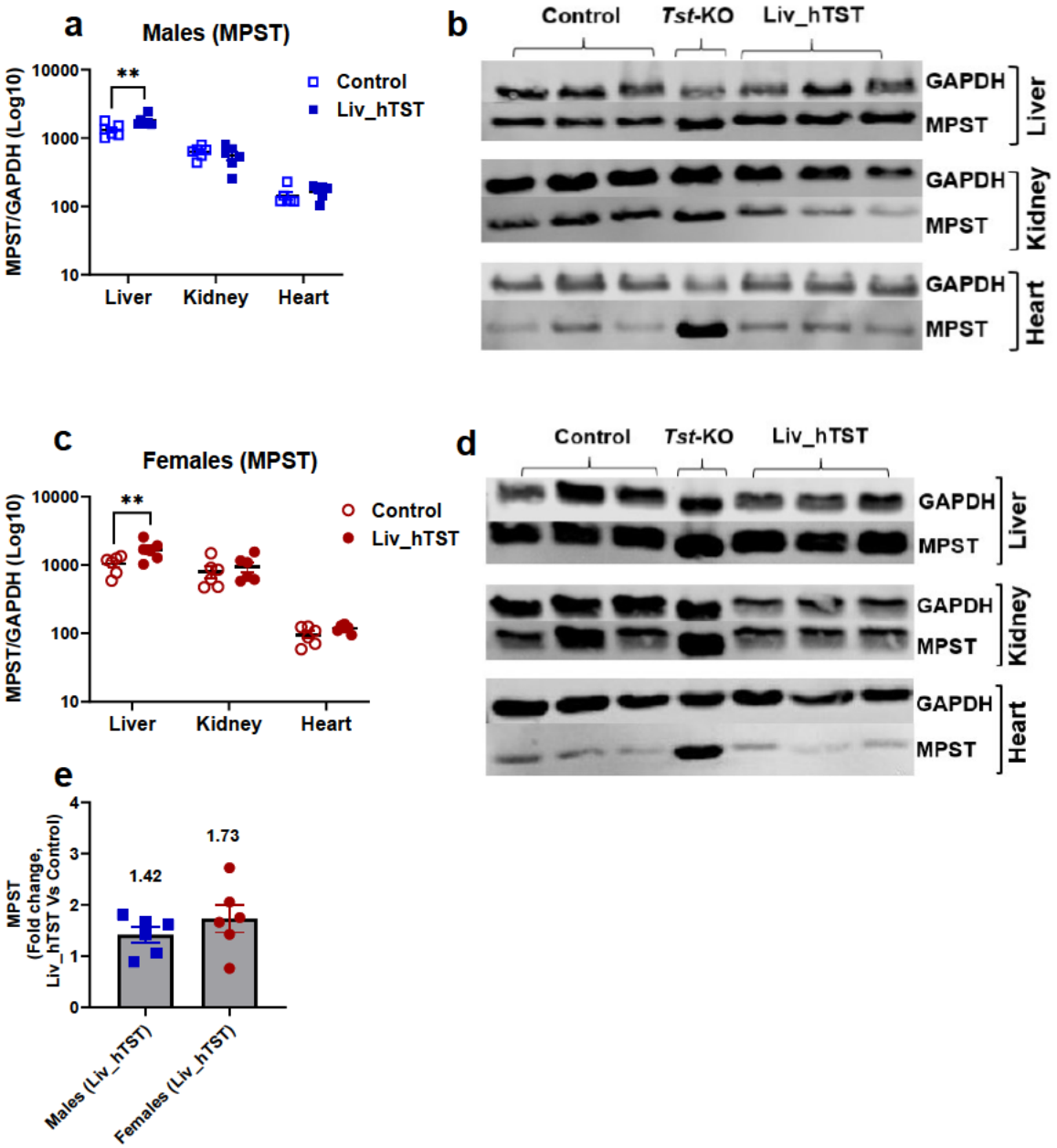

Figure 3.4 MPST protein in liver, kidney, and heart tissue of Liv_hTST and control male and female mice.

MPST protein level, relative to GAPDH endogenous control in liver, kidney, and heart tissue of (a) male and (c) Female Liv_hTST and control mice. (b) and (d) Representative blots for males and females respectively (blots were cropped to show the bands of interest, all were blotted on the same membrane at the same time). (e) Fold change of MPST levels in Liv_hTST mice compared to control mice, numbers above each bar represent the mean value. Data in a-c are shown as log10-transformed intensities to normalise the wide range of signal intensities. (n=6/ group). Data are mean ± SEM, Two-way ANOVA, with Tukey's post hoc tests were performed on the original (non-transformed) intensity values to determine statistical significance: **P≤ 0.01. *Tst*-KO: liver sample from a global *Tst* knockout mouse from the same strain, sex, and age. *Tst*: Thiosulfate sulfurtransferase.

3.3.3 The effects of liver TST overexpression on the development of steatosis in mice

The schematic in Figure 3.5 illustrates the experimental plan for this study.

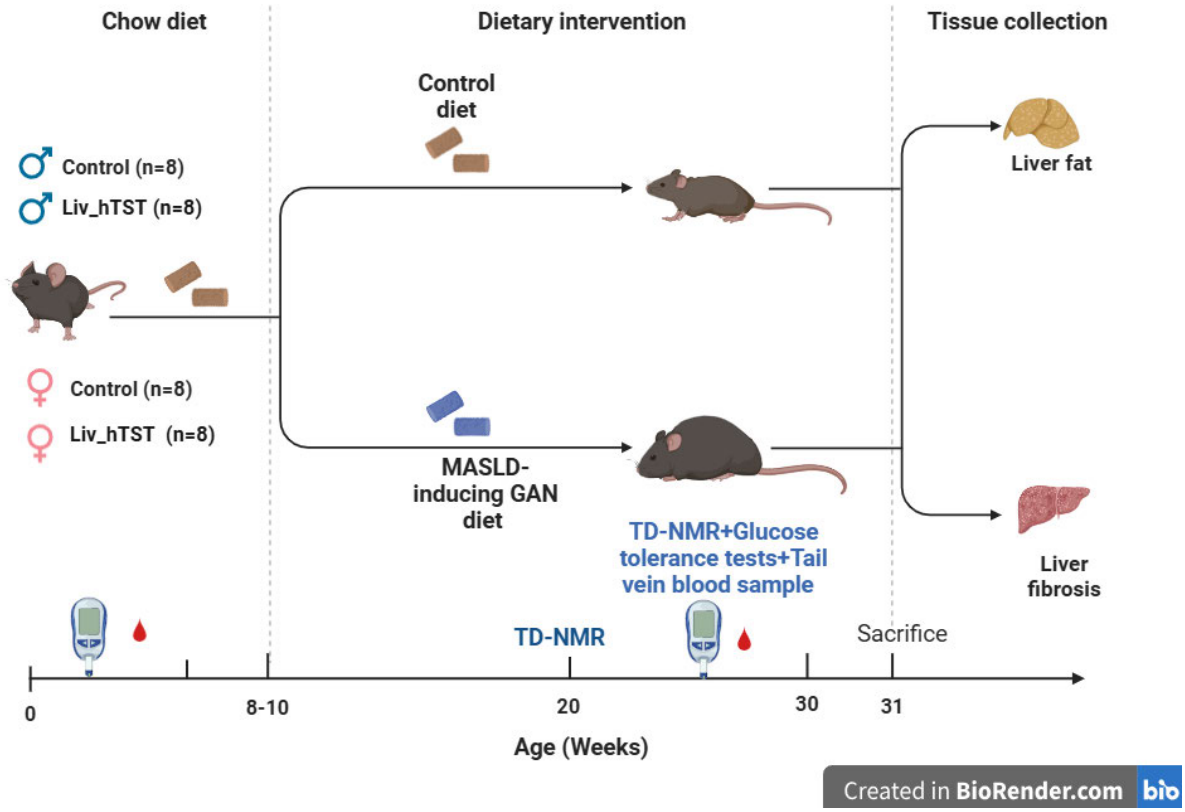

Figure 3.5 Experimental design of investigations into the effect of hepatic hTST overexpression on metabolic regulation and MASLD progression in Liv_hTST and control mice.

The study involved cohorts of Liv-hTST and control male and female mice (n=8 per group). Diet interventions started at 8-10 weeks of age. The experimental groups were exposed to the MASH inducing Gubra Amylin NASH (GAN) diet (Research Diets #D0910030), which is referred to as "GAN", or a control low fat diet (Research Diets #D09100304: 10% kcal (low fat diet), which is referred to as "Chow". Baseline measurements: body weight, fat and lean mass, glucose tolerance tests, and venous blood sulfide and thiosulfate levels. Post-diet measurements: Body weight, fat and lean mass, glucose tolerance tests, venous blood sulfide and thiosulfate levels and sulfide and thiosulfate levels in liver tissue, quantification of total hepatic lipid, and hepatic fibrosis. Body weight was recorded every week, TD-NMR quantification of fat and lean mass was carried out 3 times, at baseline, after 10 weeks and after 20 weeks of dietary intervention. "Systemic" sulfide and thiosulfate levels refer to MBB-derivatised blood samples taken from tail-vein of all mice at 1 pm at baseline (age 8-10 weeks before dietary intervention) and again at 1 pm after 20 weeks of diet intervention (age 28-30 weeks). Liv_hTST: liver specific overexpression of the human TST protein, control: *Cre*$^{+}$ control mice without overexpression of hTST. TD-NMR: Time-domain nuclear magnetic resonance.

3.4 Results

3.4.1 TST is upregulated at the early stages of MASLD in humans and in the STAM mouse model

The initial phases of MASLD, encompassing isolated steatosis in the absence of fibrosis, exhibit significant elevation in the mRNA levels of genes responsible for H_2S production, namely *CBS*, *SUOX*, and *MPST*. Among these, *CBS* demonstrates the most substantial degree of overexpression (as depicted in the heatmap provided in Figure 3.6). In contrast, within the group of enzymes associated with H_2S catabolism, an increased expression is exclusively observed for *TST* during the early stages of MASLD. This finding has prompted us to hypothesise that the upregulation of *TST* function is to protect against the progression of steatosis/MASH to advanced fibrosis and cirrhosis by counteracting the increased H_2S production in MASLD patients.

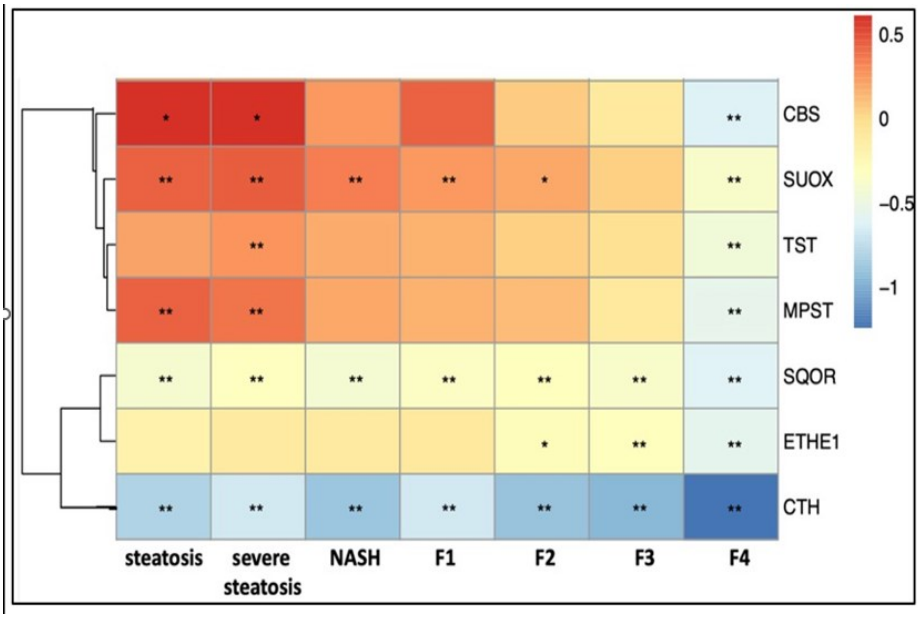

Figure 3.6 Expression of genes involved in H_2S production and catabolism through different stages of MASLD in humans.

Bulk RNA-sequencing data from 692 human liver samples from patients with different stages of MASLD. F1, F2, F3 and F4 refer to fibrosis stages as assessed by MASH-Clinical Research Network (CRN) scoring system (F1=mild fibrosis, F4= cirrhosis). *P≤ 0.05, ** P≤ 0.01 at a false discovery rate (FDR) < 0.05. Pheatmap in R (v1.0.12) was used to represent the logarithmic fold-change compared to healthy controls (logFC) of the contrasts. The heatmap was produced and shared with permission by Prof. Jonathan Fallowfield's group namely Dr. Maria Ramos.

In the STAM mouse model that mirrors the different stages of MASLD, I found that in congruence with the mRNA data from human MASH spectrum analysis (Figure 3.6), the levels of TST protein exhibited an increase during the initial phases of MASLD and persisted at elevated levels compared to the healthy control group (as depicted in Figure 3.7 a). MPST protein levels did not display a significant change except for a reduction at the most severe stage (Figure 3.7 b). The levels of SUOX and SQRDL proteins did not manifest a distinct early response but exhibited an increase during later stages, particularly after 12 weeks on HFD regimen (Figure 3.7 c and d). The protein levels of CSE exhibited a significant increase during the early stages of MASLD progression (Figure 3.7 e). While CBS displayed a decrease consistent with the progression of the disease (Figure 3.7 f).

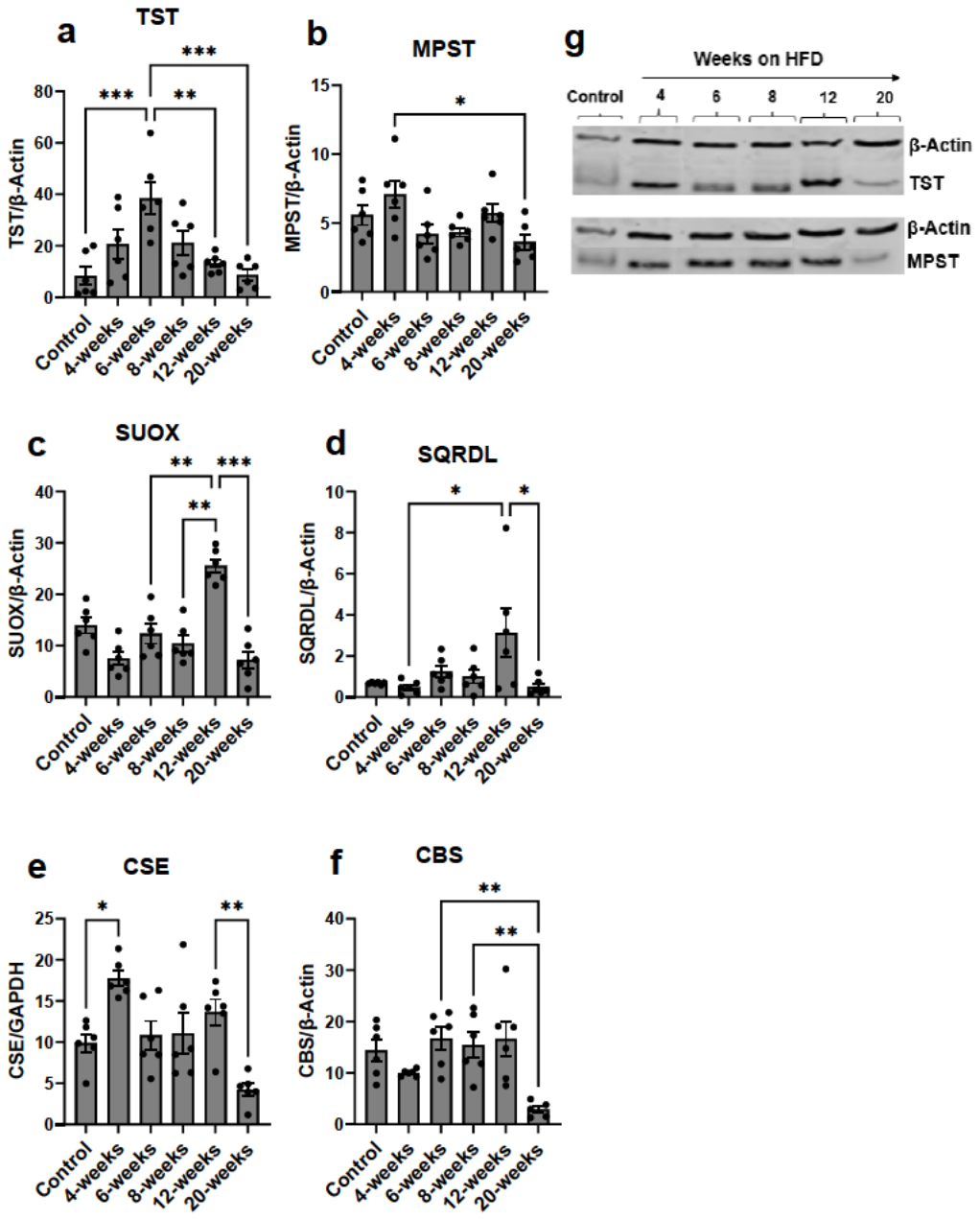

Figure 3.7 Quantification of proteins involved in H_2S production and oxidation through different stages of MASLD in the STAM mouse model.

Protein levels of (a) Thiosulfate sulfurtransferase (TST), (b) 3-mercaptopyruvate sulfurtransferase (MPST), (c) Sulfite oxidase (SUOX), (d) Sulfide quinone reductase-like protein (SQRDL), (e) Cystathionine γ-lyase (CSE), and (f) Cystathionine β-synthase (CBS) across five distinct time points of high fat diet, relative to a control group comprising healthy liver specimens. (n=6 per timepoint). Data represented as mean ± SEM. Data were analysed using one-way analysis of variance (ANOVA), with Tukey post-hoc tests. * P≤0.05, ** P≤0.01, ***P≤ 0.001. All proteins are normalised to β_actin loading control, except for CSE normalised to GAPDH because of the similarity in size with β_actin. (g) Representative western blot images for TST and MPST, blots for the other proteins are not available in logical order and are available upon request.

3.4.2 Hepatic hTST overexpression does not impact systemic or hepatic sulfide levels in mice

High systemic sulfide and thiosulfate levels were found in mice deficient in TST, giving evidence the protein is involved in sulfide breakdown (168). This implies higher liver TST might lead to greater sulfide clearance. To assess the changes in systemic and hepatic sulfide and thiosulfate levels in control and Liv_hTST mice at baseline and after 20 weeks of diet interventions, MBB-derivatised sulfide and thiosulfate from venous blood and liver homogenates were quantified using LC-MS as described in sections 2.10 and 2.11.

Hepatic hTST overexpression did not impact systemic levels of sulfide in male or female mice (Figure 3.8, a and c respectively), or thiosulfate in male or female mice (Figure 3.8 b, and d respectively) at baseline or after 20 weeks of diet intervention. However, a sex-specific difference in the dynamics of diet-sulfide interaction emerged; in male mice, systemic sulfide levels significantly increased on a chow diet, but this increase was prevented by the GAN diet (Figure 3.8 a and e). In contrast, in female mice, systemic sulfide levels significantly increased after 20 weeks of GAN diet, with no such increase after 20 weeks of chow diet (Figure 3.8 c and e). Since genotype did not affect sulfide levels at baseline or post-20 weeks of diet intervention, control, and Liv_hTST were combined to further confirm the opposing effects of diet in male and female mice (Figure 3.8 e).

Systemic thiosulfate levels were not affected by diet or genotype in male mice (Figure 3.8 b) and were reduced after 20 weeks in female mice independently of diet and genotype (Figure 3.8 d).

Hepatic sulfide levels were reduced by GAN diet in all mice independent of sex or genotype or diet (Figure 3.9 a). At the end of the experiment, females of both genotypes and regardless of diet, exhibit lower thiosulfate levels compared to males (Figure 3.9 b).

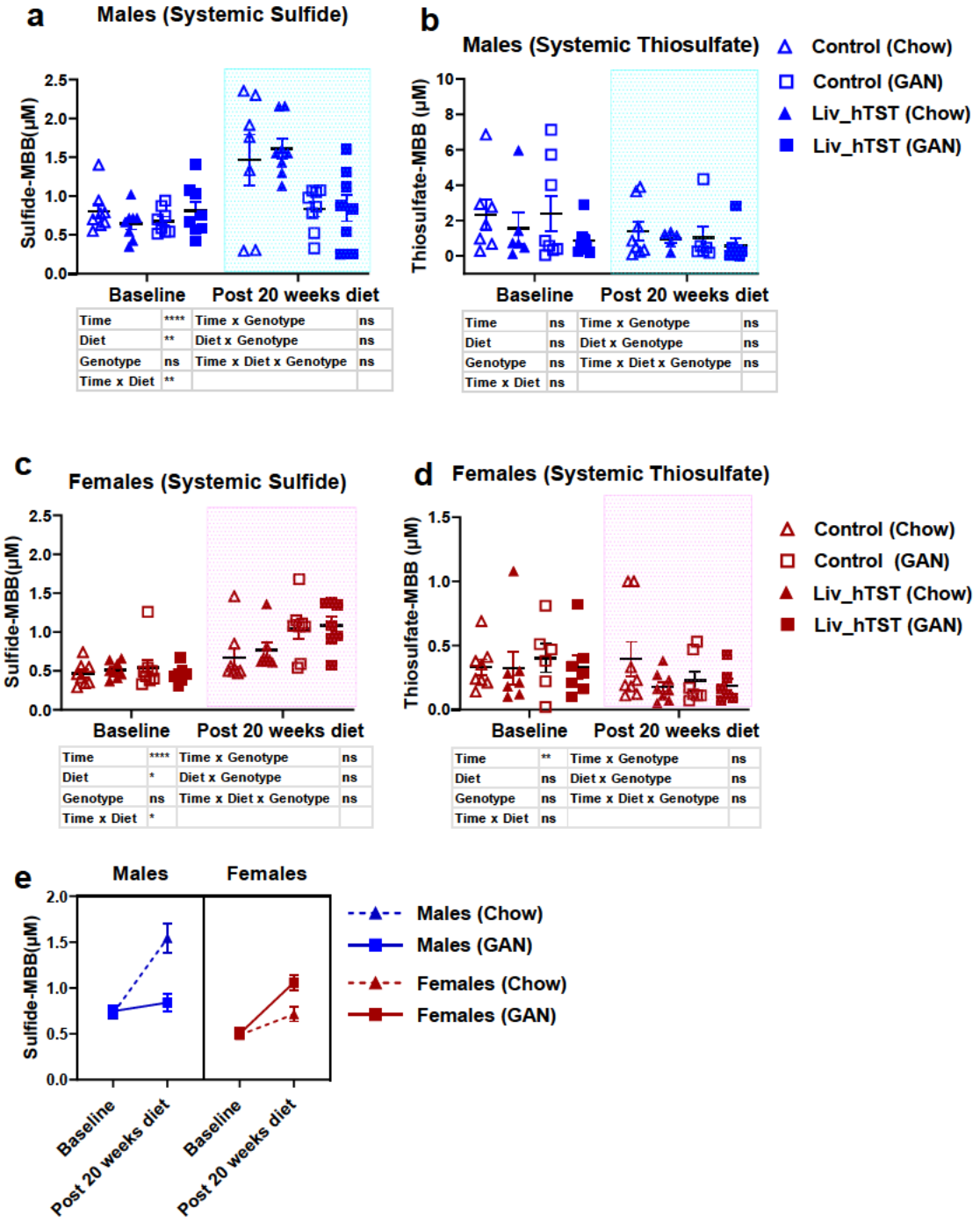

Figure 3.8 Systemic sulfide and thiosulfate levels in male and female control and Liv_hTST mice on chow or GAN diet

Systemic sulfide and thiosulfate in males (a and b respectively) and females (c and d respectively) at baseline (2 months old) and after 20 weeks of being on either chow or GAN diet. (n= 8 per group). (e) combined analysis of males and females of both genotypes to confirm the effect of diet regardless of genotype (n=16 per group). Data represented as mean ± SEM. Significant effects of diet and/or sex and/ or genotype were determined by fitting a mixed-effect analysis model with Tukey's post hoc tests. ns; P>0.05, *P≤ 0.05, **P≤ 0.01, ***P≤ 0.001, ****P≤ 0.0001. MMB: Monobromobimane, µM: micromolar.

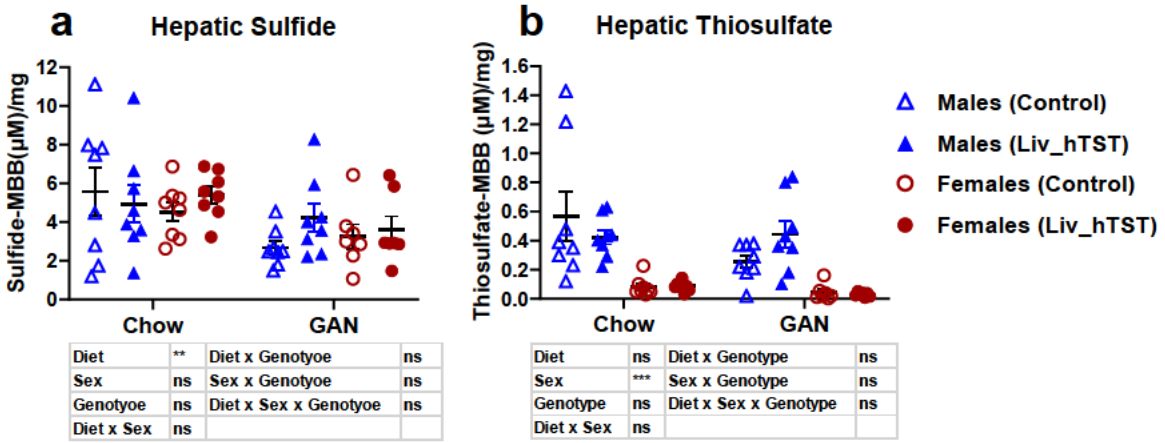

Figure 3.9 Hepatic sulfide and thiosulfate levels in male and female control and Liv_hTST mice at the end of the experiment after 20 weeks on either chow or GAN diet.

MBB- derivatised hepatic sulfide and thiosulfate (a and b respectively) levels in control and Liv_hTST male and female mice after 20 weeks of being on either chow or GAN diet, quantified in homogenised liver tissue. (n=8 per group). Data represented as mean ± SEM. Significant effects of diet and/or sex and/ or genotype were determined by fitting a mixed-effect analysis model with Tukey's post hoc tests. ns; $P > 0.05$, *$P \leq 0.05$, **$P \leq 0.01$, ***$P \leq 0.001$. MMB: Monobromobimane, µM: micromolar, mg: milligram.

3.4.3 Hepatic hTST overexpression did not impact weight, fat, and lean mass at baseline or after 20 weeks GAN diet intervention.

Hepatic TST overexpression did not affect the baseline weight (Figure 3.10, a, d, g and j), fat mass (Figure 3.10, b, e, h, and k) or lean mass (Figure 3.10, c, f, I and l) of male or female Liv_hTST mice compared to their control counterparts.

To evaluate the effect of elevated hepatic hTST levels on body weight and composition during a 20-week GAN dietary intervention, body weight was monitored and TD-NMR was used to quantify fat and lean mass in mice at baseline and after 20 weeks of diet exposure. Both male and female mice of both genotypes on the GAN diet showed a significant increase in body weight compared to those on the control diet (Figure 3.10 a, d, g, and j). This weight gain was accompanied by an increase in fat mass in both male (Figure 3.10 b, e) and female mice (Figure 3.10 h, k). There was no significant increase in lean mass in either genotype in male mice (Figure 3.10 c and f), while only Liv_hTST females gained significant lean mass after GAN diet compared to their counterparts on chow diet (Figure 3.10, i and l). It is important to note that Liv_hTST females on chow diet had less lean mass compared to control females on chow diet to start with (Figure 3.10, l).

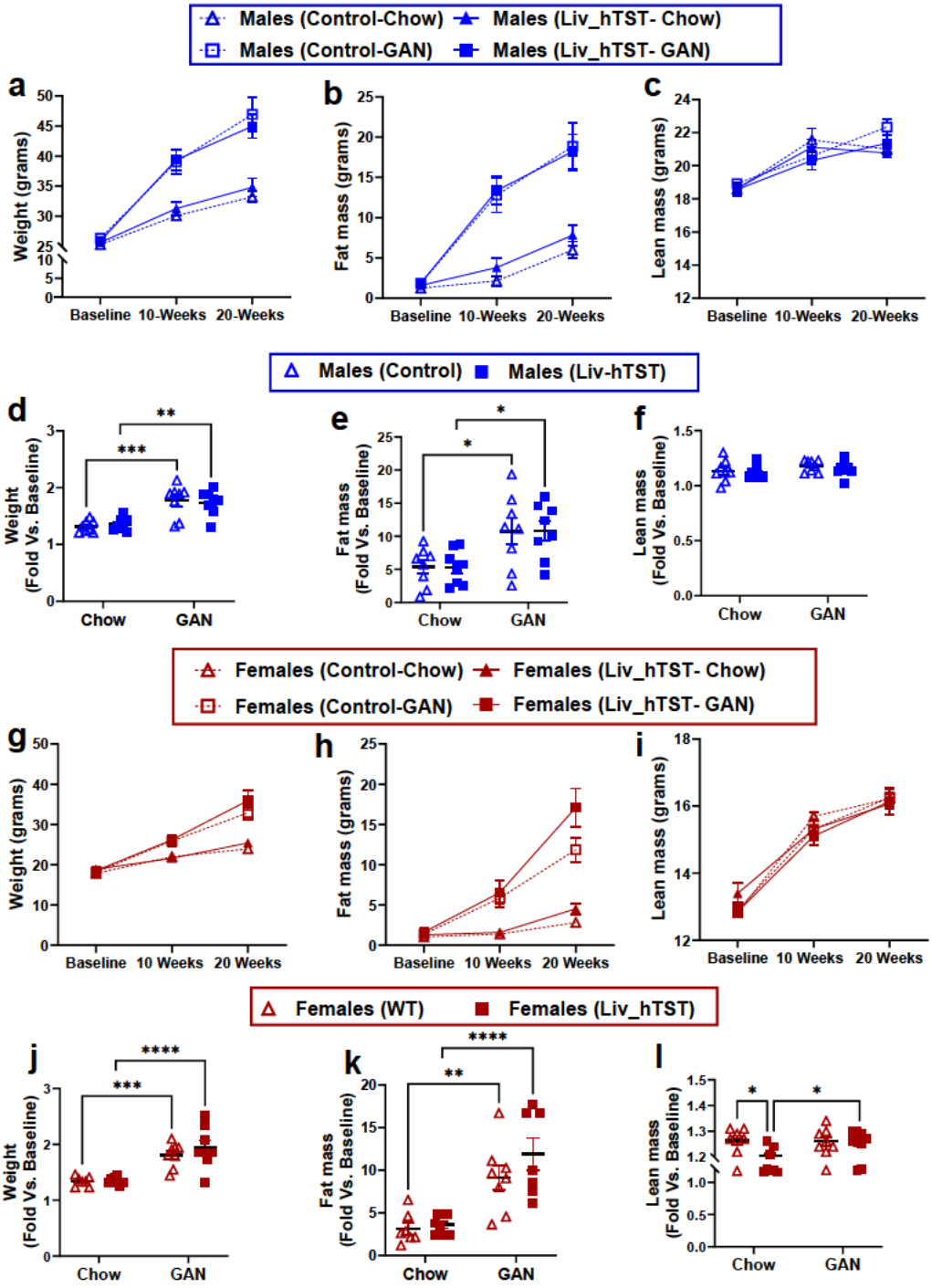

Figure 3.10 Weight gain in Liv_hTST and control male and female mice following 20 weeks on GAN or control (Chow) diet.

Weight gain plotted in grams for males (a) and females (g) and as a fold change vs. baseline in males (d) and females (j). Fat mass gain plotted in grams for males (b) and females (h) and as a fold change vs. baseline in males (e) and females (k). Lean mass plotted in grams for males (c) and females (i) and as a fold change vs. baseline in males (f) and females (l). (n=8 per group). Data represented as mean ± SEM. Significant effects of diet and/or genotype were determined by two-way ANOVA with Tukey's post hoc tests. ns; $P > 0.05$, *$P \leq 0.05$, **$P \leq 0.01$, ***$P \leq 0.001$, ****$P \leq 0.0001$.

3.4.4 Hepatic hTST overexpression does not impact the glucose tolerance of male or female mice at baseline

To evaluate the effect of elevated hepatic hTST levels on glucose tolerance and insulin secretion at baseline, oral glucose tolerance tests (OGTTs) were performed and indicated that the hepatic overexpression of hTST did not exert any effect on the baseline (before diet interventions) glucose tolerance (Figure 3.11 a and c) or insulin secretion (Figure 3.11 b and d) in either male or female mice. The glucose and insulin calculated area of the curve (AOC) from female mice OGTTs were lower than males regardless of genotype (Figure 3.11 c, and d).

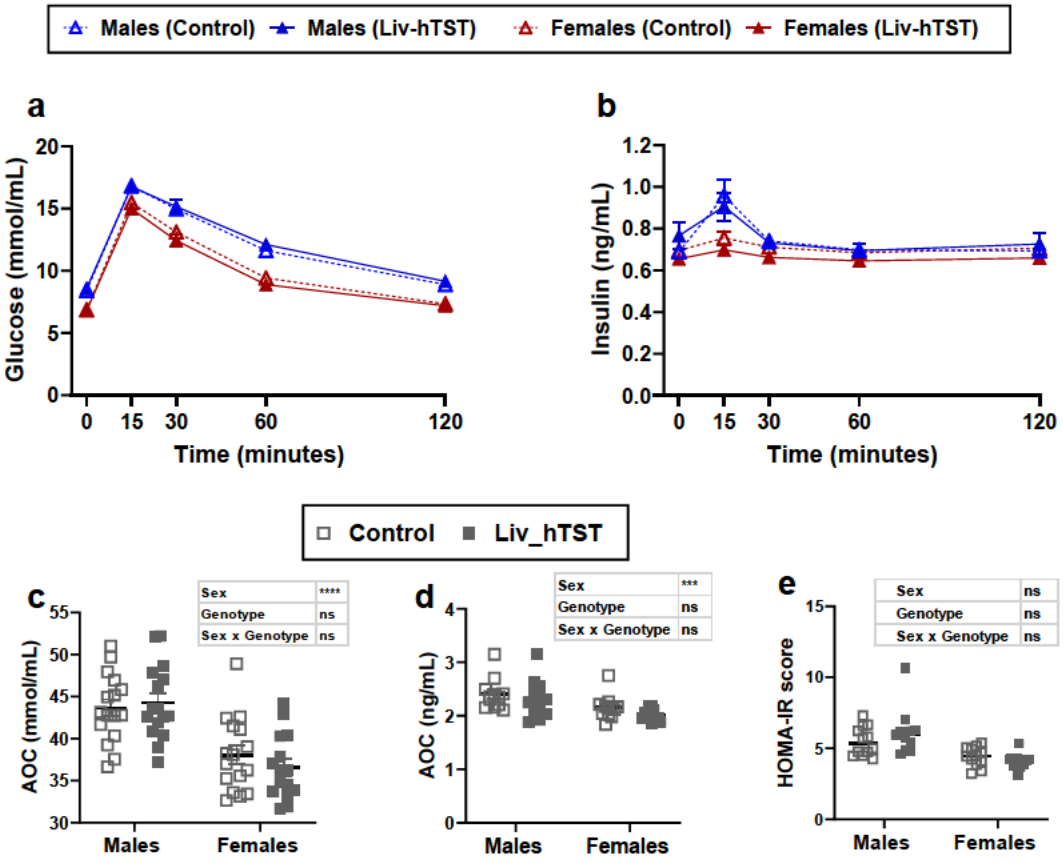

Figure 3.11 Hepatic hTST overexpression does not affect glucose tolerance in male or female mice at baseline

Oral glucose tolerance tests (OGTTs) were performed at baseline on male and female mice of control and Liv_hTST backgrounds, (a) blood glucose concentrations (mmol/mL) during the OGTT, (b) plasma insulin concentrations (ng/mL) during the OGTT. (c) Area of the glucose curve, (d) area of the insulin curve, (e) HOMA-IR score (n=8 per group). Data represented as mean ± SEM. Significant effects of genotype and/ or sex were determined by two-way ANOVA with Tukey's post hoc tests. ***P≤ 0.001, ****P≤ 0.0001. n=16 per group. mmol: millimole, mL: millilitre, ng: nanogram, AOC: area of the curve.

3.4.5 Hepatic hTST overexpression does not impact the glucose tolerance of male or female mice after 20 weeks of GAN diet intervention

To evaluate the effect of elevated hepatic hTST levels on glucose tolerance and insulin secretion after 20-week dietary intervention, OGTTs were performed and indicated that hepatic overexpression of hTST did not affect glucose tolerance in male mice (Figure 3.12, a and c) or female mice (Figure 3.12, e, and g). It also did not affect insulin secretion across the OGTT in male mice (Figure 3.12, b and d) or female mice (Figure 3.12, f, and h) after 20 weeks of diet intervention.

Notably, after 20-week GAN diet, a sex-specific difference emerged; female mice of both genotypes on GAN diet displayed signs of impaired glucose tolerance characterised by a larger glucose AOC (Figure 3.12, e, and g) and insulin AOC (Figure 3.12, f and h), whereas their male counterparts do not exhibit a comparable impairment in glucose tolerance (Figure 3.12, a and c) or insulin secretion (Figure 3.12, b and d).

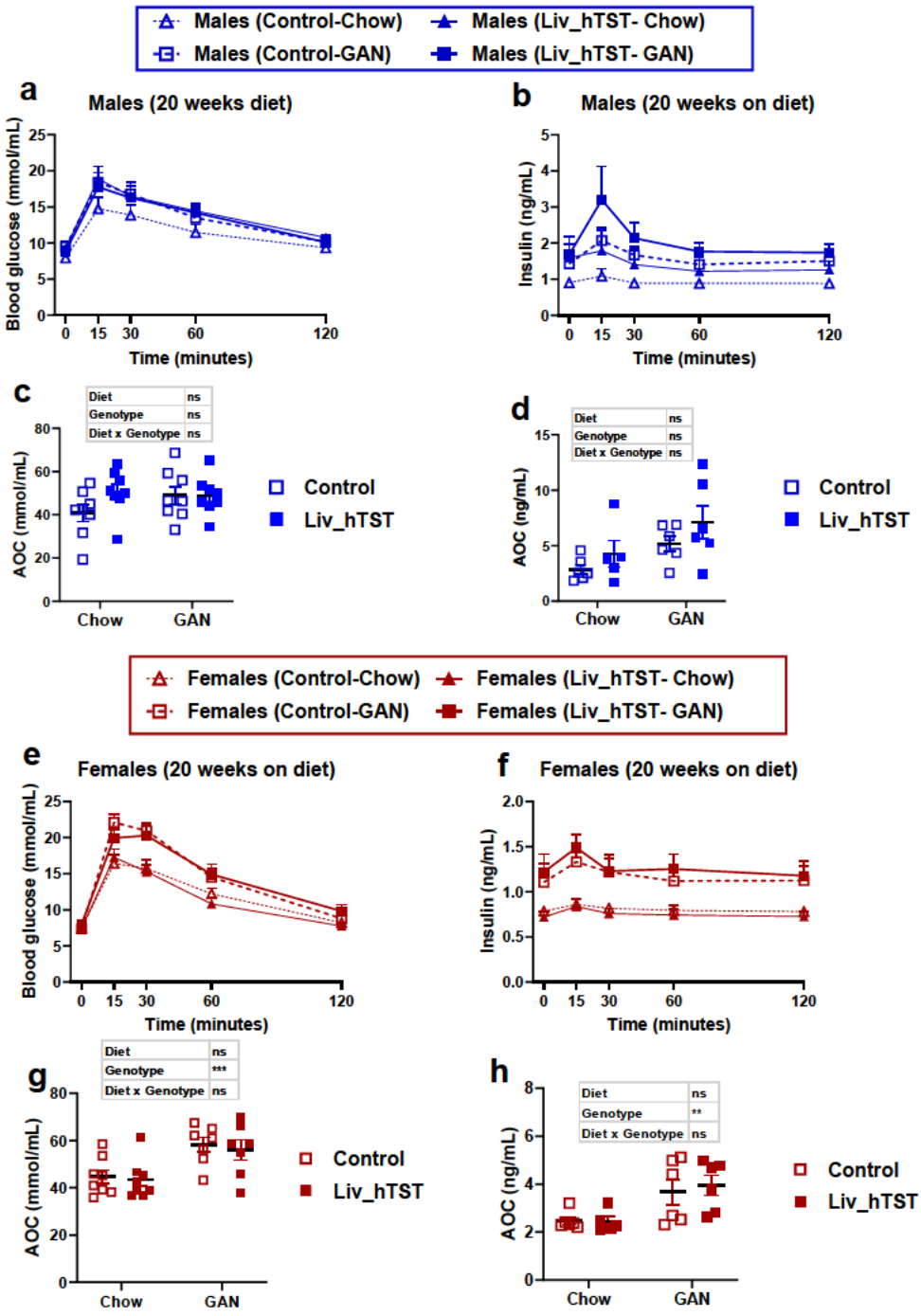

Figure 3.12 Glucose tolerance in Liv_hTST and WT male and female mice after 20 weeks of GAN or chow control diet

Glucose and insulin concentrations during oral glucose tolerance tests (OGTTs) performed on male (a and b respectively) and female (e and f respectively) control and Liv_hTST mice after 20 weeks on either a control (chow) or GAN diet. Glucose, and insulin area of the curve for males (c and d respectively) and females (g and h respectively). (n=8 per group). Data represented as mean ± SEM. Significant effects of diet or genotype were determined by two-way ANOVA or a fitted mixed model with Tukey's post hoc tests for each sex separately. ns: nonsignificant, *P≤ 0.05, **P≤ 0.01, ***P≤ 0.001. mmol: millimole, mL: millilitre, ng: nanogram, AOC: area of the curve.

3.4.6 Hepatic hTST overexpression does not protect mice from fat accumulation but mildly protects male mice from fibrosis

Following 20 weeks on GAN diet, male mice of both genotypes showed increased hepatic fat content (Figure 3.13 a) compared to their counterparts on chow diet, validating the GAN 20-week approach to induce steatosis. Interestingly, only control males on GAN had significantly higher fibrosis compared to their counterparts on chow (Figure 3.13 b).

All female mice had a significant increase in hepatic lipid content (Figure 3.13, c) with no effect of diet or genotype on fibrosis (Figure 3.13, d).

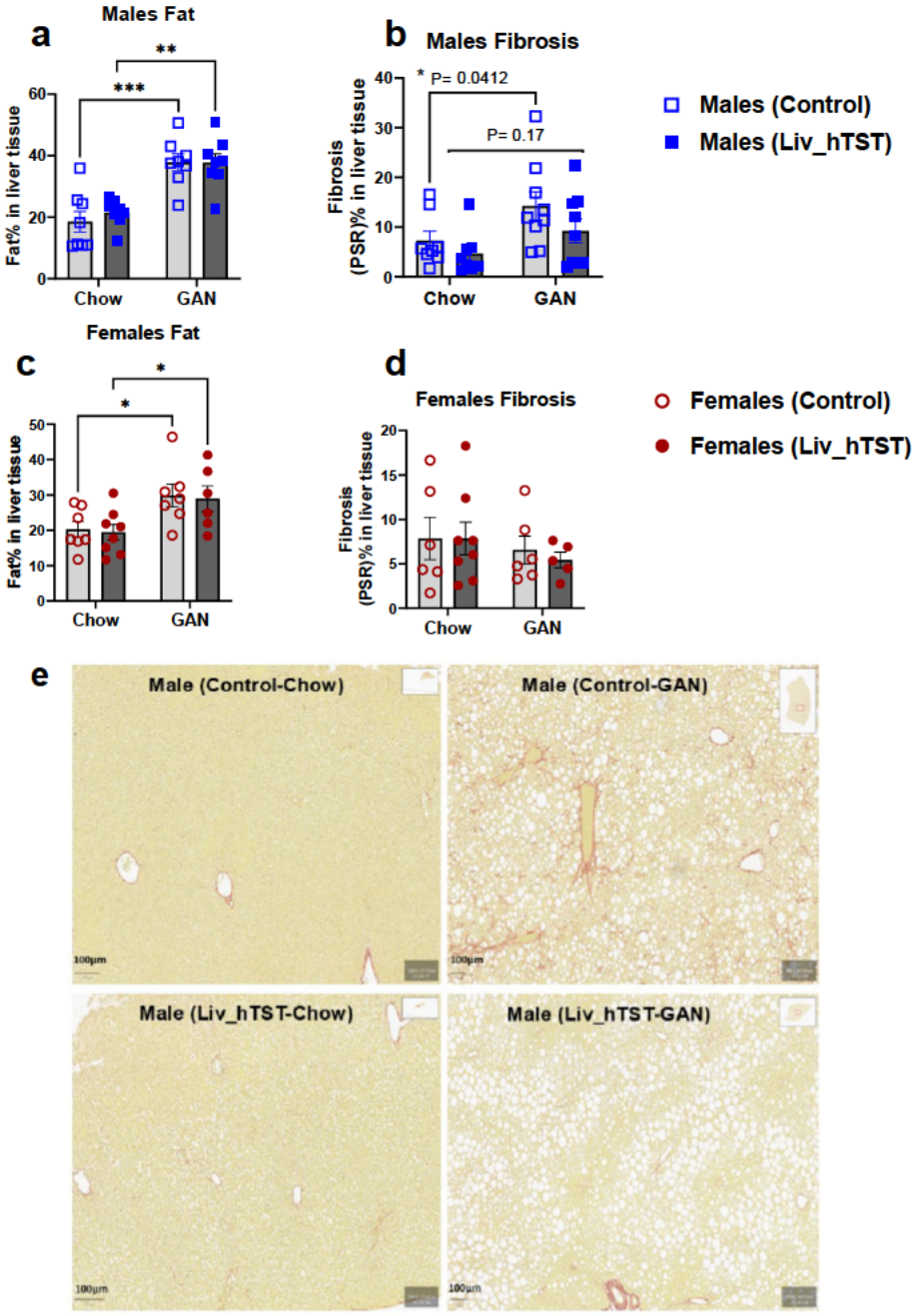

Figure 3.13 Quantification of Hepatic fat and fibrosis in male and female control and Liv_hTST mice after 20 weeks on GAN diet.

Quantification of hepatic fat in male (a) and female (c) mice. Quantification of PSR stain that indicates fibrosis in male (b) and female (d) mice. Representative images of liver sections (e) from control and Liv_hTST male mice fed either a control chow diet or a GAN diet for 20 weeks, scale bar; 100 micrometre, whole liver section is shown on the top right corner of each image, images are acquired as snapshots from Qupath. (n=8 per group). Data represented as mean ± SEM. Significant effects of diet or genotype were determined by two-way ANOVA with Tukey's post hoc tests for each sex separately. *P≤ 0.05, **P≤ 0.01, ***P ≤ 0.001. Fat and PSR quantification were carried out following multiple pixel classifiers as describes previously (245).

3.4.7 Endogenous TST protein is downregulated in males after GAN diet

To investigate the impact of chow and GAN diet on the endogenous mouse TST (mTST) levels in male and female mice with and without hepatic hTST overexpression, livers were collected at the end of the experiment and TST quantified using western blot. Endogenous mTST protein was significantly reduced after 20 weeks on GAN diet in control males (Figure 3.14 a and c) while the overexpressed hTST protein was unaffected (Figure 3.14 b and c). Notably, female mice did not exhibit the same pattern of changes in response to GAN diet (Figure 3.14, d, e, and f). MPST increased in response to GAN diet only in control females (Figure 3.15, c and d).

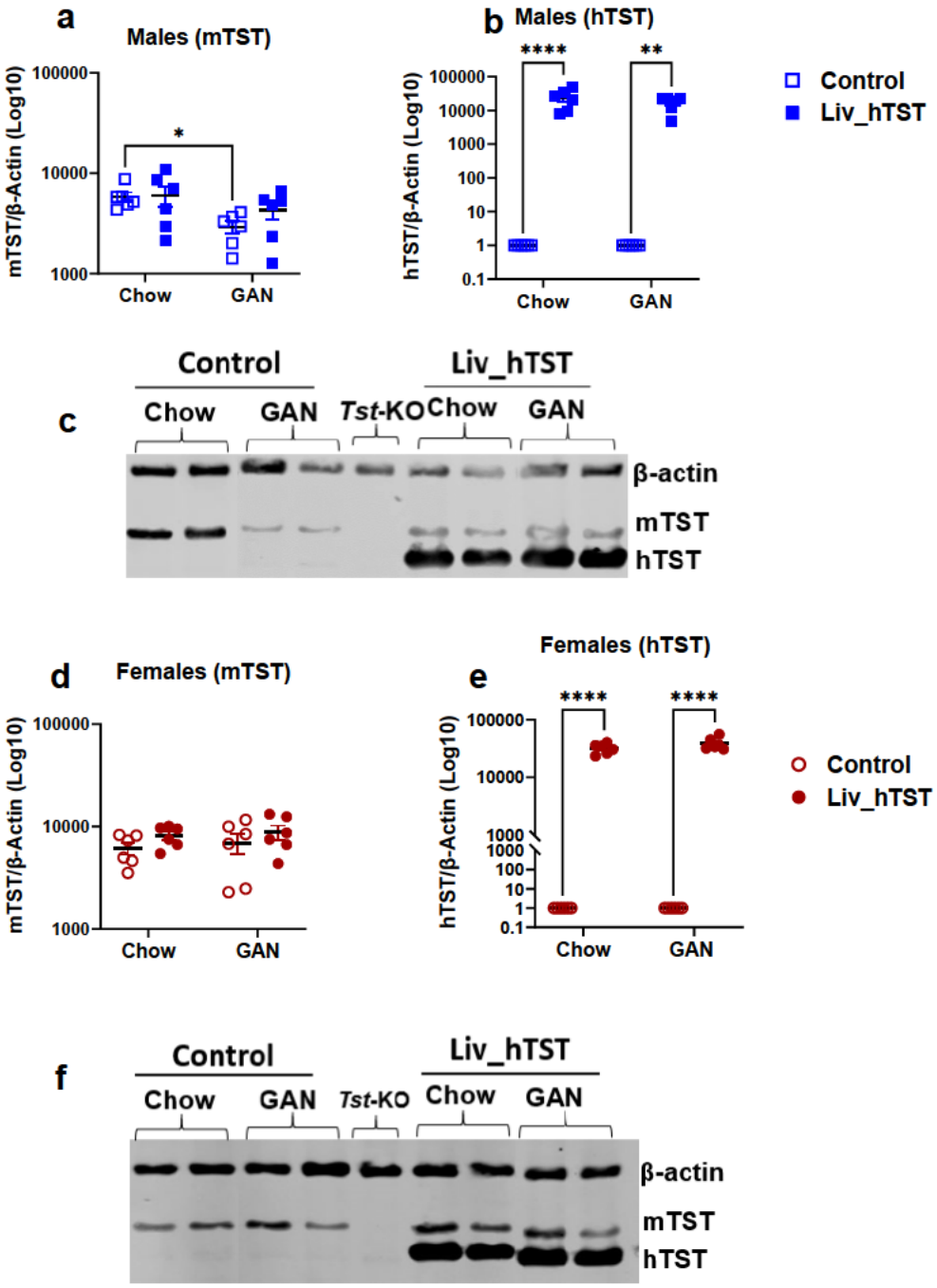

Figure 3.14 Western blot analysis of mouse and human TST protein (mTST and hTST respectively) relative to β-actin.

Western blot quantification depicting the protein levels of mouse TST (mTST) and human TST (hTST) in male mice (a and b respectively) and female mice (d and e respectively) on control or Liv_hTST backgrounds, fed either a control (chow) or GAN diet. (n=6 per group). Data represented as mean ± SEM. Representative blots for males and females on different genotypes and diets (c and f respectively). Data are shown as log10-transformed intensities to normalise the wide range of signal intensities. Two-way ANOVA, with Tukey's post hoc tests were performed on the original (non-transformed) intensity values to determine statistical significance for each sex separately. *$P \leq 0.05$.

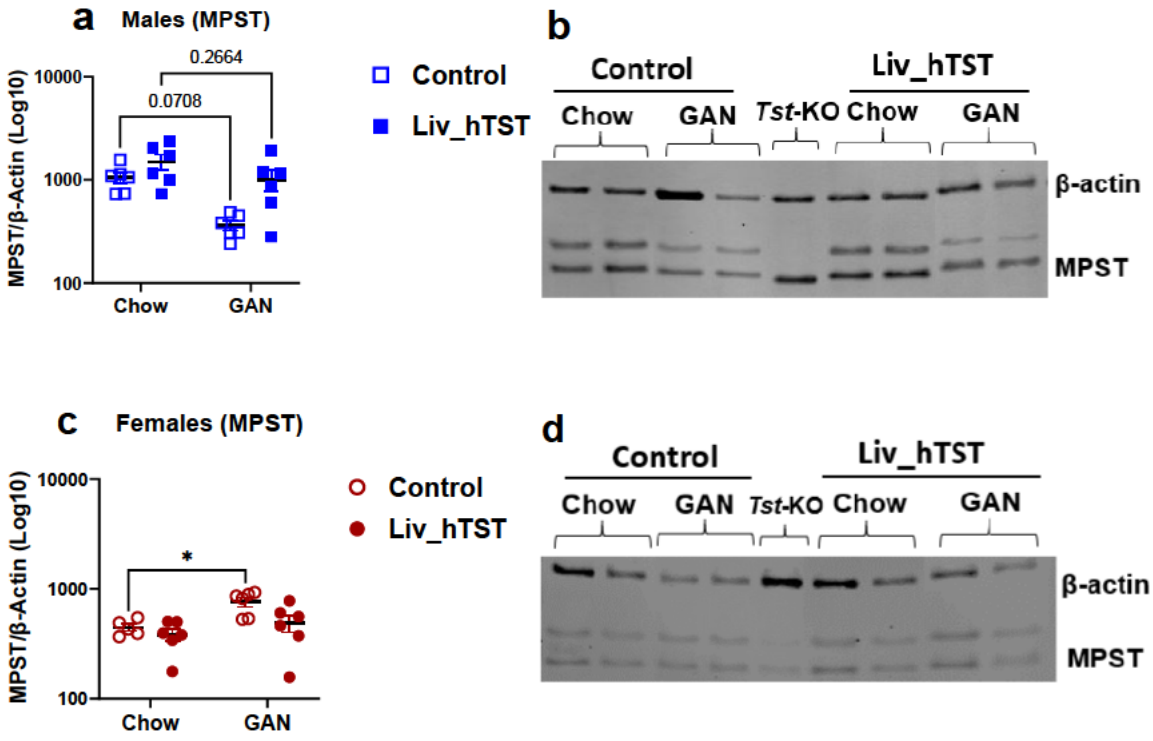

Figure 3.15 Western blot analysis of MPST relative to β-actin.

Western blot quantification depicting the protein levels of MPST in male mice (a) and female mice (b) on control or Liv_hTST backgrounds, fed either a control (chow) or GAN diet. Representative blots for males (c) and females (f) on different genotypes and diets. (n=6 per group). Data represented as mean ± SEM. Data are shown as log10-transformed intensities to normalise the wide range of signal intensities. Two-way ANOVA, with Tukey's post hoc tests were performed on the original (non-transformed) intensity values to determine statistical significance for each sex separately. *$P \leq 0.05$.

3.5 Discussion

This chapter explored the hypothesised protective role of elevated hepatic TST on MASLD progression. We established that TST expression increased at the steatosis/MASH boundary in humans and in the STAM mouse models. To test whether elevated TST is protective against disease progression, a liver-specific TST overexpression mouse model (Liv_hTST) was developed and subjected to a 20-week GAN diet, which induced steatosis, fibrosis, fat mass gain and impaired glucose tolerance. I have assessed systemic and hepatic sulfide and thiosulfate levels, weight, fat, and lean mass gain, and glucose tolerance at baseline and after 20 weeks on GAN diet.

3.5.1 TST is upregulated at the early stages of MASLD-MASH transition

This study demonstrated a significant upregulation of *TST* mRNA in human MASLD patients and increased TST protein levels in the STAM mouse model, particularly during the early stages of the disease. These findings suggest that TST may play a role in the initial response to liver damage. Previous research from our group further supports this, as *Tst*-deficient mice exhibited increased hepatic gluconeogenesis and dyslipidemia under baseline chow diet conditions, even without dietary intervention (168). These mice also showed elevated plasma triglyceride levels and increased hepatic lipid content (168). This highlighted an important role of TST in hepatic lipid metabolism, with its absence leading to disrupted lipid homeostasis, fatty liver, and a diabetogenic profile.

Based on these findings, I hypothesised that TST overexpression during the early steatosis-to-MASH transition would provide protection against GAN diet-induced hepatic fat accumulation and impaired glucose tolerance *in vivo*. This hypothesis aligns with previous research showing that mice overexpressing TST in adipose tissue were resistant to fat mass gain and diabetes when exposed to diet-induced obesity (194).

3.5.2 TST/ MPST interaction in the Liv_hTST mouse model

To investigate whether hepatic overexpression of TST is protective against GAN diet-induced MASH, a novel mouse model, Liv_hTST, was developed. This model features liver-specific overexpression of the human TST gene (*hTST*). The overexpression of *hTST* was validated through genotyping, and protein quantification, confirming that the elevated hTST protein levels were confined to the liver, as overexpression was not detected in other organs such as

the kidney or heart, ensuring that the effects observed in this model are attributed specifically to hepatic hTST overexpression. The Liv_hTST mice exhibited approximately six-fold higher levels of hTST compared to endogenous mouse mTST, providing a reliable model for studying the impact of increased hepatic hTST expression.

In addition to hTST overexpression, I observed an upregulation of MPST, with increases of 1.4-fold in male Liv_hTST mice and 1.7-fold in female Liv_hTST mice compared to their control counterparts. This upregulation suggests a potential compensatory response within the sulfur metabolism pathway, possibly driven by shared regulatory mechanisms or feedback loops aimed at maintaining metabolic homeostasis. The liver and kidney are known to exhibit the highest MPST activities, and co-regulation of TST and MPST is plausible due to their close genomic proximity on mammalian chromosomes. This co-regulation was previously noted in global *Tst* knockout mice that despite having decreased *Mpst* mRNA levels, exhibited increased protein levels of MPST (168). Additionally, studies by Nagahara *et al.* (185) showed upregulation of hepatic TST at both the gene and protein levels in an *Mpst*-knockout mouse model. Interestingly, Akahoshi *et al.* (258) generated an *Mpst*-knockout mouse model using a targeted deletion restricted to exon 2, located further from the shared promoter region with TST and did not find any changes in TST protein levels. This suggested that shared promoter elements between the juxtaposed genes leads to transcriptional co-regulation under certain circumstances.

3.5.3 Systemic and hepatic sulfide dynamics

The role of TST in sulfide metabolism has been previously explored by studies demonstrating elevated systemic sulfide and thiosulfate levels in TST-deficient mice (168), suggesting that TST plays a critical role in sulfide breakdown. Based on this, I hypothesised that hepatic overexpression of human TST (hTST) might enhance sulfide clearance, thereby impacting systemic and hepatic sulfide and thiosulfate levels. However, our findings indicate that hepatic hTST overexpression did not alter systemic or hepatic sulfide or thiosulfate levels in either male or female mice, regardless of dietary intervention.

The unexpected lack of change in systemic or hepatic H_2S levels with hepatic TST overexpression in this study contrasts with the marked elevation of systemic H_2S levels in $Tst^{-/-}$ mice (168). Carter *et al.* (168) reported that elevated circulating sulfide levels led to impaired glucose homeostasis, and increased hepatic fat in $Tst^{-/-}$ mice compared to C57BL/6J

mice. This divergence suggests that compensatory mechanisms may be activated to tightly regulate sulfide metabolism when TST is overexpressed, preventing fluctuations in H_2S concentrations. In *Tst*$^{-/-}$ mice, the liver compensates for the absence of TST by upregulating mitochondrial enzymes such as MPST and altering GSH and cysteine metabolism, primarily increasing their export to manage sulfide levels (168). It is plausible that similar pathways are engaged in the Liv_hTST model to maintain homeostasis, despite increased TST activity. One potential compensatory mechanism is reduced mitochondrial regulation of sulfide disposal, possibly involving MPST, which may mitigate the impact of increased TST on H_2S levels. Western blot analysis showed that MPST levels were significantly higher in the Liv_hTST livers compared to control livers in males and females by 1.4 and 1.7-fold respectively. Carter *et al.* also reported an increase in protein level of MPST in the livers of *Tst*$^{-/-}$ mice despite a reduces mRNA level, suggesting the activation of a post-transcriptional cellular sulfide-sensing mechanism. It is unclear why Liv_hTST mice would also show an increased MPST activity, one explanation would be the fact that *Mpst* and *Tst* share a promoter and the targeted overexpression of *Tst* unintentionally led to the overexpression of *Mpst.* In this study, I did not measure the gene expression of *Tst* or *Mpst.* MPST have been reported both as a sulfide-producing (185, 259, 260) and as a possible sulfide- disposal enzyme (168). Our results suggest that MPST might be functioning as a sulfide-producing enzyme to compensate for the increased H_2S clearance caused by the overexpression of TST. To test this, future work should investigate the effects of *Mpst* deletion on H_2S metabolism in the context of TST overexpression by crossing the Liv_hTST mice with *Mpst*-knockout mice. This approach would help determine whether MPST compensates for TST activity in sulfide production, as knocking out MPST should lead to reduced H_2S levels. Importantly, other sulfide- producing enzymes particularly CSE could be upregulated in response to the overexpression of TST, due to time constraints I did not quantify the full pathway of sulfide metabolism in the Liv_hTST mouse model which is a major limitation in interpreting these results.

Another possibility for the unchanged sulfide levels in the Liv_hTST mouse model is that hepatic cysteine and GSH export, which supports sulfide clearance in *Tst*$^{-/-}$ mice, is similarly modulated in TST-overexpressing mice, though without overt changes in sulfide levels. In response to reduced H_2S levels, the body might have compensated by altering cysteine and GSH metabolism. Cysteine, a precursor for H_2S, may be diverted toward GSH synthesis, enhancing antioxidant defences to mitigate oxidative stress (261). This shift helps preserve

cellular redox balance and ensures the continued availability of sulfur for other critical metabolic processes, even in the context of diminished H_2S production. Furthermore, the deficiency in H_2S triggers modifications in broader amino acid metabolism, particularly pathways involving methionine and cysteine. These pathways may be reprogrammed to prioritise alternative sulfur metabolism routes, ensuring the production of essential sulfur-containing molecules such as taurine and sulfates, thereby maintaining cellular and metabolic homeostasis in the face of altered H_2S levels. All these changes could have happened to restore sulfide levels to normal.

Furthermore, the role of thiosulfate metabolism in this context requires further investigation, particularly regarding localised shifts within mitochondrial or cytosolic compartments that might prevent systemic alterations in H_2S levels. These findings highlight the complexity of sulfide regulation and suggest that sulfide homeostasis is tightly controlled by interconnected pathways. Future studies should focus on investigating these compensatory mechanisms, including exploration of mitochondrial function, MPST activity, and sulfur-related metabolite dynamics will be critical in understanding the broader implications of TST modulation in metabolic regulation.

Sulfide changes: sex- specific response to dietary intervention

A strength of this study is the examination of both sexes, and indeed, this proved significant in discovering sex-specific responses to dietary interventions. Male mice of both genotypes on a chow diet exhibited a significant increase in systemic sulfide levels, an effect that was prevented by the GAN diet. In contrast, female mice displayed an increase in systemic sulfide levels on the GAN diet, with no significant response to the chow diet. Further analysis combining control and Liv_hTST mice reinforced the observed sex-specific effects of diet on systemic sulfide levels. This observation points to a major difference between males and females in sulfur metabolism in response to obesogenic diet.

This variation aligns with findings from Peh *et al.* (262) who reported that plasma sulfide levels increase with age in male mice, independent of diet. However, they also observed a decline in sulfide production in key tissues such as the liver, kidney, and lung following HFD, linked to reduced levels of the enzyme CSE in these tissues. My findings indicate that systemic sulfide levels increase under chow conditions in males which is disrupted by the GAN diet, one possible explanation that requires further verification is that the disruption in response to GAN

diet is due to the oxidative and metabolic stress imposed by the GAN diet, or the downregulation of CSE. Notably, while Peh *et al.* (262) measured sulfide in plasma obtained through cardiac puncture, I utilised whole blood from the tail vein to assess "systemic" sulfide levels, which may explain some differences in our findings. Importantly, Peh *et al.* (262) did not include female mice in their study so the response of female mice to HFD in terms of sulfide levels remains unclear. In female mice, Fu *et al.* (263) demonstrated that oestrogen can elevate plasma sulfide levels by activating CSE, suggesting a potential protective mechanism against atherosclerosis in female mice. If the GAN diet-induced weight gain leads to increased oestrogen levels, this may explain the elevated sulfide levels observed in females on the GAN diet, indicating a similar protective response. The GAN diet contains approximately 2% cholesterol by weight, significantly higher than standard HFD, which typically lacks added cholesterol. Since cholesterol is a precursor to all steroid hormones, including oestrogen (264), the high cholesterol content in the GAN diet could lead to increased oestrogen production, further contributing to the observed sulfide elevation. To the best of my knowledge, this study is the first to demonstrate sex differences in sulfide levels in response to GAN diet or HFD in general in mice.

Over the lifespan, sex differences in H_2S metabolism may also be linked to hormonal regulation and aging-related declines in metabolic function. Evidence from human studies suggests that circulating H_2S levels decrease with age, correlating with reduced vascular and metabolic health (265, 266). In males, this reduction may exacerbate age-related diseases such as cardiovascular dysfunction. In contrast, females might experience transient protective effects of oestrogen-mediated CSE activation during reproductive years (267), potentially mitigating age-associated declines in H_2S metabolism. However, postmenopausal reductions in oestrogen levels could diminish this protective effect (267), aligning female H_2S metabolism more closely with that observed in males.

Regarding thiosulfate, my data showed a lack of effect of genotype or diet on systemic thiosulfate levels in male mice. However, in female mice, I observed a reduction in thiosulfate levels after 20 weeks, independent of dietary intervention. Since thiosulfate is typically formed from sulfide oxidation, this reduction with ageing may suggest impaired sulfide oxidation develops in females, potentially due to the GAN diet or aging. High-fat diets, such as the GAN diet, might impair enzymes involved in sulfide oxidation, such as sulfide SQOR or TST, although our study did not quantify SQOR and did not find diet-dependent reduction in TST

levels in females. Notably, all liver samples used for western blot analysis in this study were from mice at the end of the experiment (around 7 months old), and we lack data on how these enzyme levels change with aging, independent of diet.

In summary, our data indicate that hepatic hTST overexpression does not significantly influence systemic or hepatic sulfide and thiosulfate levels under chow or GAN diet conditions. However, the observed sex-specific differences in response to dietary interventions suggests that the regulation of sulfide metabolism is complex and influenced by sex-related factors. These findings contribute to the growing body of knowledge on the role of diet and sex in sulfide metabolism, emphasising the need for further research to elucidate the underlying mechanisms of these processes.

3.5.4 Hepatic TST overexpression does not impact weight gain or body composition or glucose tolerance at baseline or after 20 weeks of diet intervention

In this study, I observed a significant increase in body weight and fat mass in both male and female mice subjected to the GAN diet compared to those on the chow diet. This observation is consistent with previous research that demonstrated the GAN diet induces adiposity and weight gain in rodent models (93, 94). The increase in fat mass was consistent across both genotypes and sexes, indicating that elevated hepatic hTST levels did not prevent diet-induced obesity or fat mass gain.

Interestingly, lean mass increased significantly only in Liv_hTST female mice on GAN diet. This finding points to a potential sex-specific adaptation in female mice, which may involve an increase in muscle mass as a compensatory mechanism to counteract the worsening insulin sensitivity typically associated with the GAN diet (93, 94). This study is the first to characterise the effects of the GAN diet in female mice, as prior research has predominantly focused on male mice. The results suggest that elevated hepatic TST may influence lean mass differently between sexes under chow and GAN diet conditions, potentially reflecting distinct metabolic adaptations in response to the diet.

Hepatic overexpression of hTST did not influence baseline glucose tolerance or insulin secretion in either sex, both before and after 20 weeks on the GAN diet. This finding indicates that while hTST may affect body composition in female mice, it does not appear to directly impact glucose metabolism or insulin sensitivity. Previous studies have demonstrated that the absence of TST leads to glucose intolerance in male mice, even in the absence of a HFD

challenge (168). Additionally, overexpression of TST in adipose tissue has been shown to protect against HFD-induced metabolic disturbances (194). However, in this study, liver-specific overexpression of TST did not confer the anticipated protective effects on glucose tolerance, insulin secretion, or weight gain. One possible explanation for this outcome is that the liver, while central to glucose and lipid metabolism, may not be the primary site where TST exerts its protective effects under HFD conditions, even though TST is highly expressed in the liver. The protective effects of TST overexpression observed in adipose tissue suggest that TST's role in modulating metabolic responses might be more effective in specialised adipose tissue. In contrast, the liver might require a more complex or coordinated interaction with other pathways or tissues to achieve similar protective effects. It is also possible that other compensatory mechanisms within the liver might have negated the potential benefits of TST overexpression, especially that I did not observe the expected reduction in systemic or hepatic sulfide levels in mice with elevated hepatic hTST. Interestingly, while hTST protein levels remained upregulated during the 20 weeks of the experiment timeline, endogenous mTST levels decreased in control male mice on GAN diet. This finding suggests that the 20-week intervention may extend beyond the "early steatosis/MASH transition" phase, complicating the potential protective role of TST at this later stage. Moreover, while the core function of TST in detoxification and sulfur metabolism is conserved, there may be species-specific roles that the enzyme plays in mice versus humans. The regulation of TST by other proteins, small molecules, or transcription factors might differ between species, leading to differences in how the enzyme is activated or inhibited, which could explain why the overexpression of hTST did not exert obvious changes in glucose tolerance in either sex.

Notably, independent of hepatic hTST overexpression, a sex-specific difference emerged after the 20-week GAN diet intervention. Female mice on GAN diet exhibited impaired glucose tolerance and reduced insulin secretion compared to their male counterparts. This impairment was evident from a larger area-of-the-curve (AOC) values calculated from the oGTT curves. These results suggest that female mice may be more susceptible to the metabolic disruptions caused by the GAN diet. Whether this increased susceptibility is related to the elevated sulfide levels observed in female mice in response to the GAN diet remains unclear.

3.5.5 Hepatic hTST overexpression does not affect hepatic fat content in male or female mice but slightly protects male mice from GAN- induced fibrosis

This study showed increased hepatic fat content in male mice of both genotypes after the GAN diet, confirming the effectiveness of the diet in inducing steatosis. Interestingly, fibrosis was significantly higher only in control males on the GAN diet compared to chow diet-fed counterparts. This observation suggests that while elevated hTST level did not impact overall hepatic fat content, it might have influenced fibrosis development differently. In contrast, all female mice exhibited increased hepatic lipid content with no significant differences in fibrosis due to diet or genotype. This aligns with previous studies that found sex differences in the progression of liver disease, where females might have different fibrotic responses to dietary-induced steatosis, Chen *et al.* (268) suggests that females, particularly premenopausal women, are generally more protected from fibrosis compared to males and postmenopausal women. The protective effect is largely attributed to oestrogen, which inhibits the activation of hepatic stellate cells, the primary cells involved in the development of fibrosis (269).

The choice of the GAN model over simpler dietary interventions like a HFD in this study was guided by its ability to replicate advanced MASLD features, including fibrosis and MASH. While HFD induces steatosis, the GAN model encompasses the metabolic and pathological spectrum of MASLD progression (94) enabling a deeper investigation of TST's role in fibrosis development. This is particularly relevant given that alterations in TST and other sulfide metabolism genes occur early in MASLD but may have different impact during advanced disease stages. Moreover, the methionine- and choline-deficient diet (MCD) effectively models steatohepatitis, but it lacks the ability to replicate obesity and insulin resistance, which are crucial in human MASLD (85). While sulfur plays a critical role in methionine metabolism, the systemic metabolic disruptions in the GAN and STAM models provide a more comprehensive framework for studying the interplay between sulfide metabolism and MASLD. Future studies could incorporate MCD to specifically investigate the intersection of methionine metabolism, sulfur dynamics, and TST function, particularly in earlier disease stages. These approaches collectively ensure that both early and advanced stages of MASLD are captured, providing a nuanced understanding of the mechanisms underlying sex- and diet-specific differences in liver pathology.

3.6 Limitations and recommendations for future work

Permanent TST overexpression: This study utilised a genetic model with lifelong hepatic TST overexpression, which may not fully reflect the gradual, environmentally driven progression of MASLD seen in humans. The persistent upregulation of TST from birth could lead to early-life reprogramming of hepatic sulfide and intermediary metabolism, potentially altering the disease trajectory. Temporal activation methods, such as AAV-Cre delivery or tamoxifen-inducible Cre systems, could address this limitation by enabling precise control of TST expression at critical disease stages, such as the steatosis-to-MASH transition. These approaches would allow investigation into whether late-stage activation of TST is sufficient to mitigate hepatic fat accumulation and glucose intolerance. Furthermore, administration of small-molecule TST activators, such as those characterised by Al-Dahmani *et al.* (270), offers a pharmacological alternative to genetic approaches. These activators could be employed to transiently enhance TST activity at specific time points, mimicking the dynamic regulation that occurs in human disease. Combined with viral-Cre recombinase delivery to activate an inducible allele, these strategies could provide valuable insights into the timing-dependent effects of TST modulation.

Compensatory mechanisms: Long-term TST overexpression may have triggered compensatory mechanisms, as evidenced by the observed MPST upregulation. Further studies are needed to explore the full impact of TST elevation on sulfide metabolism, including the roles of enzymes such as CSE and CBS, as well as mitochondrial regulation of sulfide production and disposal.

Incomplete metabolic profiling: The study primarily measured systemic and hepatic sulfide and thiosulfate levels but did not assess other critical aspects of metabolism such as oxidative stress markers, detailed lipid profiles, inflammation markers, or liver function tests. Future research should include these factors to gain a more comprehensive understanding of TST's effect on systemic metabolism in response to GAN diet.

Limited analysis of fibrosis mechanisms: Although male Liv_hTST mice showed modest resistance to fibrosis, the study did not explore the underlying mechanisms in detail due to time constraints. Future studies should use advanced imaging techniques and additional histological analyses to better understand how TST overexpression affects fibrotic processes, this could include qPCR and western blot analysis of fibrosis markers such as collagen type I alpha 1

(Col1a1), alpha-smooth muscle actin (α-SMA/Acta2), and transforming growth factor beta 1 (TGF-β1).

TST activity: This study demonstrated an upregulation of TST protein levels in the Liv_hTST mouse model. However, an increase in protein abundance does not necessarily correlate with enhanced enzymatic activity. Future research should include assessments of TST enzymatic activity in the liver tissues of the mice studied to clarify the functional implications of the observed protein level changes. In addition to investigating the phosphorylation of TST which might have affected its function in this context.

3.7 Conclusions

In this study, I explored the role of elevated hepatic TST expression in the progression of MASLD. The findings provide insights into how TST is regulated during the steatosis-to-MASH transition and the potential interactions between TST and other components of the sulfur metabolism pathway. Although TST was upregulated in both human MASLD patients and in the STAM mouse model, suggesting an early protective role, hepatic overexpression of TST in the Liv_hTST mouse model did not confer the anticipated protective effects against diet-induced obesity, fat mass gain, or glucose intolerance.

Notably, sex-specific differences were observed in both systemic sulfide dynamics and metabolic responses to the GAN diet, with female mice showing distinct adaptations compared to males. Additionally, while TST overexpression did not affect hepatic lipid content, male mice exhibited modest protection against fibrosis development, a finding that warrants further exploration.

4 Chapter 4: The effect of TST overexpression on HepaRG cells challenged with a fatty diet

4.1 Introduction

4.1.1 Cell and organoid models for MASLD/MASH research

HepaRG cells are particularly valuable for studying MASLD and MASH *in vitro* due to their unique ability to closely mimic human liver function and pathology. Originating from a human hepatic progenitor cell line, HepaRG cells can differentiate into hepatocyte-like cells that retain essential hepatic functions, including drug metabolism, lipid processing, and bile acid production (99). They demonstrate a higher abundance of proteins involved in insulin signalling and resistance pathways compared to HepG2 cells, with levels comparable to primary human hepatocytes (PHH). These include key components of insulin signalling pathways, such as IRS1/2, PI3K, PDPK1, IKBKB, FOXO1, and PCK1/2, as well as glucagon signalling components like PRKACB, which is more abundant in HepaRG than in PHH (99).

A notable feature of HepaRG cells is their ability to differentiate into both hepatocyte-like and cholangiocyte-like cells, which enhances their utility in studying liver function, drug metabolism, hepatotoxicity, and bile duct diseases (271, 272). Their genetic stability and extended culture viability ensure reproducibility and scalability, offering a practical advantage over primary hepatocytes, which are often limited by donor variability and a short lifespan. Additionally, HepaRG cells are highly susceptible to lipid accumulation under fatty acid exposure, effectively mirroring the steatosis characteristic of early-stage MASLD (271, 272). This lipid build-up, combined with their responsiveness to inflammatory stimuli, makes them a robust model for investigating MASLD progression to more severe forms, such as MASH and fibrosis. However, the slower growth rate and specific differentiation requirements of HepaRG cells pose challenges for high-throughput studies.

In addition to HepaRG cells, alternative models provide complementary advantages for MASLD research, these models and their advantages are revied in section 1.1.5. For instance, 3D hepatic organoids derived from primary human cells or induced pluripotent stem cells (iPSCs) replicate the structural and functional complexity of the liver, including hepatocyte polarisation, bile canaliculi formation, and interactions with non-parenchymal cells like

Kupffer and hepatic stellate cells (107, 108). These organoids enable the study of fibrosis, inflammation, and steatosis in a physiologically relevant context but require resource-intensive optimisation for reproducibility.

Primary human hepatocytes cultured in a collagen matrix sandwich remain the gold standard for studying hepatocyte-specific processes, such as lipid metabolism, insulin signalling, and fibrosis. This configuration supports hepatocyte polarization, bile canaliculi formation, and cytochrome P450 activity (273). However, primary hepatocytes face limitations, including donor variability, a short *in vitro* lifespan, and the absence of systemic interactions with other liver cell types or tissues.

Immortalised cell lines like HepG2 and AML12 are more scalable and cost-effective but lack key hepatic functions, including proper insulin and glucagon signalling and cytochrome P450 enzyme activity, making them less suitable for comprehensive MASLD studies. A critical consideration across all models is the expression and regulation of proteins like TST and MPST. HepaRG cells robustly express these proteins, offering a platform for investigating their roles in sulfide metabolism and oxidative stress in MASLD. While primary hepatocytes exhibit more accurate expression profiles, their short viability limits long-term studies of chronic conditions like MASLD (271, 272).

The complexity and resource demands of hepatic organoids and primary hepatocytes in collagen sandwiches provide a middle ground between simple cell lines and animal models. Integrating these systems with advanced tools like CRISPR-based genetic editing or RNA interference could further clarify the roles of proteins like TST and MPST. For example, organoids with CRISPR-mediated knockout or overexpression of these proteins, or co-culture systems incorporating hepatic stellate cells and macrophages, could deepen insights into fibrosis and inflammation mechanisms.

In addition to their functional relevance, HepaRG cells offer practical advantages over primary human hepatocytes. They exhibit significant genetic stability and can be cultured for extended periods without losing functionality, ensuring reproducibility and consistency across experiments. Unlike primary hepatocytes, which are often limited by donor variability and a short lifespan *in vitro*, HepaRG cells provide a reliable and scalable model that is commercially available and easier to culture. However, it is important to note that while HepaRG cells

comprehensively express the necessary molecular equipment, they may still have limitations in fully representing the functionality of primary human hepatocytes, particularly in the context of MASLD/MASH (274).

4.1.2 The LPON treatment to induce MASLD-like phenotype

To mimic MASLD *in vitro*, I used a cocktail of lactate (L), and pyruvate (P) which are key players in gluconeogenesis and *de novo* lipogenesis, and octanoate (O), a medium-chain fatty acid that can diffuse into mitochondria independently of carnitine palmitoyl transferase (CPT), enabling more efficient mitochondrial β-oxidation, in addition to ammonia (N) as its metabolism *via* the urea cycle or glutamine pathways increases NADH formation, further promoting mitochondrial activity and lipid accumulation. This cocktail was previously validated for its ability to recapitulate the characteristics of MASLD *in vitro* (275, 276). The LPON cocktail induces a metabolic environment within HepaRG cells that closely mimics the conditions observed in liver of MASLD patients, including disruptions in glucose metabolism and fatty acid overload, and induces changes on transcriptional and metabolomic levels consistent with those present in human MASLD patients (275). This model leads to significant intracellular lipid accumulation, mirroring the hepatic steatosis seen in MASLD, and triggers lipotoxicity, which is critical for studying the transition from simple steatosis to more advanced stages like MASH (275, 276). The LPON model also effectively simulates oxidative stress and mitochondrial dysfunction, two central features of MASLD pathogenesis. The induced metabolic stress not only results in increased ROS production but also compromises mitochondrial integrity, allowing for the study of these critical processes in a controlled *in vitro* setting. Additionally, the LPON treatment activates inflammatory pathways and the release of pro-inflammatory cytokines, replicating the inflammatory environment seen in MASH (Unpublished data from Dr. Lenny Nelson's lab, University of Edinburgh). The LPON model of MASLD, while useful for studying metabolic stress and mitochondrial dysfunction, has several limitations. The model is a simplified system that lacks the complexity of the liver microenvironment, including the interactions between different cell types like Kupffer cells and hepatic stellate cells, which are important in disease progression (275, 276).

4.1.3 The role of TST in lipid accumulation, oxidative stress, and mitochondrial function

While ROS are essential signalling molecules in processes like cell growth, autophagy, and immune function, excessive levels cause oxidative stress, damaging lipids, proteins, and nucleic acids, and contribute to diseases such as cardiovascular and liver disease, neurodegeneration, diabetes, and aging. Cells have developed antioxidant defence systems, including ROS scavengers and enzymes like superoxide dismutase and catalase, to balance ROS's beneficial and harmful effects and maintain redox homeostasis (277).

The mitochondria play a crucial role in lipid metabolism and ROS detoxification by coordinating bioenergetic functions and maintaining cellular homeostasis. During the early stages of MASLD, mitochondria help protect against oxidative stress by converting harmful FFAs into triglycerides (278). In response to increased fat deposition, hepatocytes initially increase GSH and thioredoxin to counter lipid and protein oxidation (279). However, as steatosis progresses, mitochondrial GSH rapidly depletes, making hepatocytes more vulnerable to inflammation and TNF-α-induced cell death, which is linked to insulin resistance and liver inflammation (279). Mitochondrial thioredoxin also decreases over time, impacting NO regulation and further contributing to oxidative stress in MASLD (43, 280, 281). In MASLD, increased fatty acid import and oxidation in hepatocytes leads to elevated NADH and FADH2 levels, which fuel the ETC for ATP production. However, about 2% of electrons leak from the ETC, reacting with oxygen to form superoxide radicals, the primary source of mitochondrial ROS (44, 280). The excess ROS overwhelms antioxidant defences, causing oxidative stress, which damages the mitochondrial membrane, DNA, and ETC components. This damage reduces ATP production and increases electron leakage, further boosting ROS levels (44, 280).

TST is integral to both oxidative stress management and mitochondrial function, acting through its phosphorylation state and interactions with various cellular components. Specifically, TST can be phosphorylated at serine 124, which induces a conformational change in TST, altering the accessibility of key cysteine residues (Cys-247, Cys-254, and Cys-263) (187). This change can lead to the formation of a disulfide bridge, impairing TST's ability to metabolise sulfane sulfur donors. In this phosphorylated state, TST extracts labile sulfide from iron-sulfur centres in the ETC, which results in decreased electron transport rates and ATP production due to reduced stability of iron-sulfur clusters (187). In contrast, when TST is dephosphorylated, it can catalyse the reverse reaction, promoting increased electron transport and ATP synthesis.

This dynamic phosphorylation-dephosphorylation cycle enables mitochondria to adjust oxidative metabolism rates according to energetic demands. TST's interactions with ETC enzymes, such as succinate dehydrogenase and NADH dehydrogenase, highlight its direct role in regulating mitochondrial respiratory activity (187, 282). Moreover, TST was found to be critical to in importing 5 S Ribosomal RNA into human mitochondria, which is essential for maintaining the integrity of mitochondrial processes like ATP production, thereby ensuring adequate energy supply for cellular functions (282).

There is growing pre-clinical evidence suggesting TST might have a protective role against oxidative stress and mitochondrial dysfunction. *Tst* was discovered as a driver of "healthy leanness" in mice, the overexpression of *Tst* in adipose tissue protected mice from HFD-induced obesity and glucose intolerance (194). Importantly, when fed HFD, mice with adipose tissue- specific overexpression of *Tst* were found to have higher protein levels of mitochondrial antioxidant enzymes superoxide dismutase 2 (SOD2) in their adipose tissue, and higher mRNA levels of peroxiredoxin 3 (*Prdx3*) (194). While the knockdown of *Tst* in 3T3-L1 adipocytes *in vitro* resulted in higher levels of mitochondrial ROS after cells were exposed to oxidative stress (194). This suggests that *Tst* is interacting with mitochondrial ROS, enhancing the production of these mitochondrial-specific antioxidants in response to HFD. Morton *et al.* (194) suggested that *Tst*-mediated leanness likely results from a shift in mitochondrial substrate preference, along with effective clearance of ROS and sulfide, which helps maintain insulin sensitivity in adipose tissue (194).

Tst global deletion also modifies mitochondrial respiration, increases ATP production, and elevates ROS levels in the brain cortex in mice, reflecting a significant alteration in mitochondrial function and oxidative stress regulation in response to lack of *Tst* (283). Moreover, Al-Dahmani *et al.* (270) have identified a small molecule activator of human *TST* which was found to enhance mitochondrial respiration, as demonstrated by increased oxygen consumption in isolated brain mouse mitochondria. These findings suggest that TST activation may offer therapeutic benefits for metabolic disorders primarily through the alleviation of oxidative stress and enhancing mitochondrial function.

4.2 Hypothesis and aims

Hypothesis: TST overexpression in HepaRG cells is protective against fat accumulation, oxidative stress and mitochondrial dysfunction caused by the LPON diet.

Aims:

1. Induce stable transfection of *TST* and control lentivirus in HepaRG cells to drive the overexpression of *TST*.
2. Test whether TST overexpression protects HepaRG cells from LPON- induced lipid accumulation
3. Test whether TST overexpression protects HepaRG cells from LPON- induced ROS accumulation
4. Test whether TST overexpression protects HepaRG cells from LPON- induced mitochondrial dysfunction.

4.3 Experimental design

4.3.1 Inducing stable overexpression of TST in HepaRG cells using lentivirus stable transfection.

To achieve stable overexpression of *TST* in HepaRG cells, control and *TST* lentiviral vectors (Figure 4.1, a and b, respectively) were obtained from Vector Builder, Edinburgh, UK. Undifferentiated HPR101 cells were used for lentiviral transduction to drive *TST* overexpression. One week before transduction, progenitor HPR101 cells were seeded, and lentivirus was added at a multiplicity of infection (MOI) of approximately 1.6 (10 million infectious units to 6 million cells). Five days post-transduction, lentiviral uptake was confirmed by imaging the GFP reporter in both plasmids under a microscope. Cells were then sorted *via* FACS based on GFP expression, to select cells with high GFP expression for further culture. Finally, the transfected HPR101 cells were differentiated into HepaRG cells as detailed in section 2.8.1.

To confirm the successful trasnfection of HepaRG cells with a lentivirus carrying an overexpression construct for *TST* (TST.LV), alongside a control plasmid (CT.LV), cells were lysed and TST quantified by western blot which confirmed the overexpression of TST in the

TST.LV transfected HepaRG cells compared to the CT.LV transfected HepaRG cells (Figure 4.2 a and b). Additionally, successful transfection was visually confirmed by the presence of GFP (green) in HepaRG (TST.LV) cells and mCherry (red) reporters in HepaRG (CT.LV) cells (Figure 4.2 c).

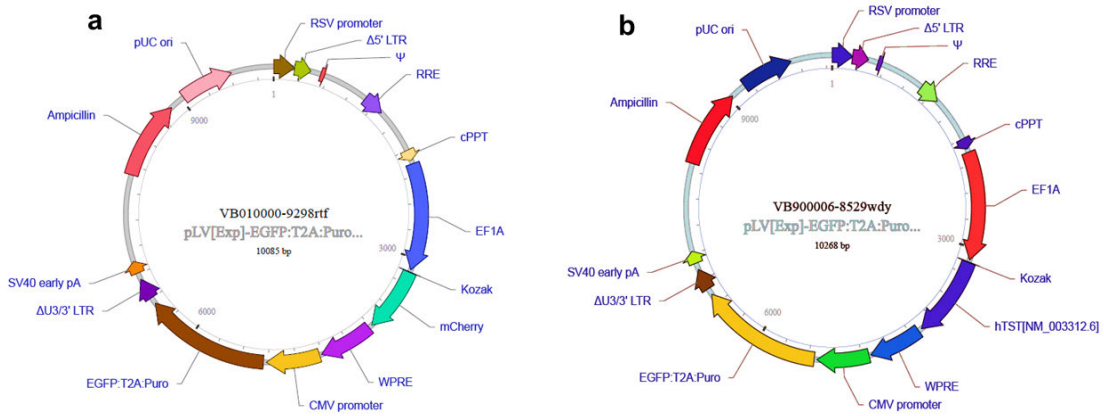

Figure 4.1 Plasmid maps for lentivirus packaging

(a) Control plasmid. (b) TST plasmid. Both plasmids are under the control of the CMV promoter and exhibit ampicillin and puromycin resistance and contain a GFP reporter.

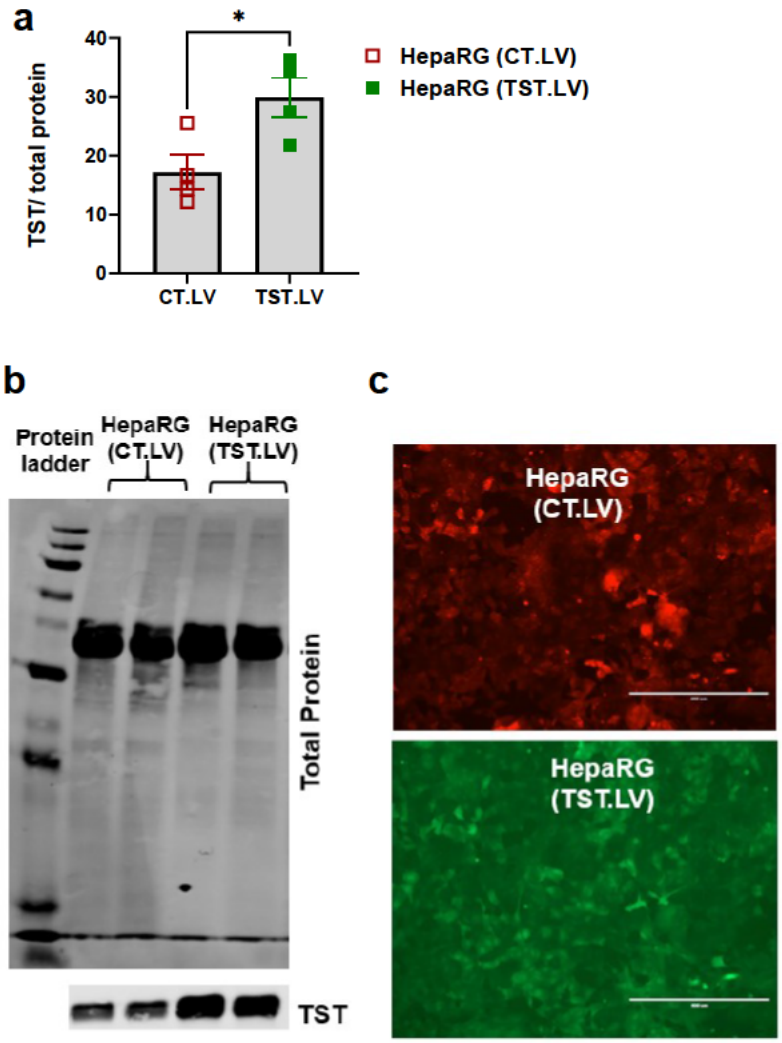

Figure 4.2 The stable transfection of differentiated HepaRG cells with TST and control lentivirus.

(a) Western blot quantification of transfected HepaRG cells with TST or control lentivirus. (n=3 biological replicates/group; 3 technical replicates). Data plotted as mean± SEM. (b) Representative western blot image showing the overexpression of TST in TST.LV transfected HepaRG cells compared to CT.LV transfected cells, relative to total protein. (c) Representative images of HepaRG cells expressing the GFP (green) and the mCherry (red) reporters indicating successful transfection, scale bar = 400 µm. Paired Student t-test was used for statistical testing. ns; $P > 0.05$, *$P \leq 0.05$. µm: micrometre, CT.LV: HepaRG cells transfected with a control lentivirus. TST.LV: HepaRG cells transfected with a lentivirus driving the overexpression of TST, TST: thiosulfate sulfurtransferase.

4.3.2 Experimental design

The schematic in Figure 4.3 illustrates the experimental design and timeline for HepaRG cells used in this study. For all experiments in this chapter, "oleate only" treatment was employed as a control to establish a clear baseline for studying lipid accumulation without the confounding effects of additional metabolic stressors. As a monounsaturated fatty acid, oleate is less toxic compared to saturated fatty acids like palmitate, making it effective for inducing simple steatosis in hepatocytes (284). This mirrors the early stages of MASLD by promoting lipid accumulation without causing significant cellular stress or death. Using oleate alone allows to benchmark the level of lipid accumulation in hepatocytes, providing a point of comparison for more complex treatments like LPON, which introduce further metabolic challenges and simulate advanced disease states, such as MASH.

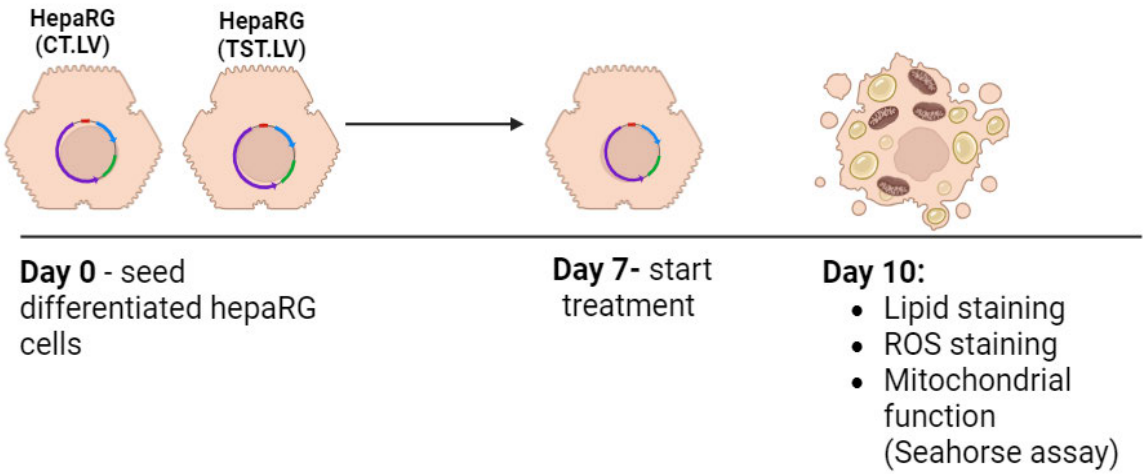

Figure 4.3 The experimental timeline for HepaRG cells used in this study

HepaRG cells, transfected with either a control or a TST lentivirus, were cultured as described in 2.8.2. Intracellular lipid accumulation was induced as previously described (275). Briefly, at day 7, HepaRG cells were incubated in medium only (untreated), or BSA-conjugated oleate only (0.25 mM), or medium containing a cocktail of sodium l-lactate (L; 10 mM), sodium pyruvate (P; 1 mM) and octanoic acid (O; 2 mM), and Ammonia (N; 4 mM) (LPON) for a period of 72 hours. After 72 hours of treatment (Day 10), lipid staining, ROS staining and seahorse assay were performed. CT.LV: HepaRG cells transfected with a control lentivirus. TST.LV: HepaRG cells transfected with a lentivirus driving the overexpression of TST, TST: thiosulfate Sulfurtransferase, ROS: reactive oxygen species, mM: millimolar.

4.4 Results

4.4.1 HepaRG cells overexpressing TST accumulate more lipids compared to control cells, augmented by LPON treatment

Lipid accumulation is central to the development of MASLD, to investigate the effect of oleate and LPON treatment on intracellular lipid accumulation, untreated HepaRG and HepaRG treated with oleate or LPON for 72 hours were stained for neutral lipids using LipidTox Deep Red stain and quantified using Opera imaging system. Fluorescence images revealed an increased accumulation of neutral lipids in HepaRG cells overexpressing TST across all treatment conditions, including untreated, oleate, and LPON treatments (Figure 4.4 a). Quantification of the lipid content confirmed these observations, with statistically significant increases in lipid retention in HepaRG cells overexpressing TST compared to controls even when untreated, and the worsening of lipid accumulation with the LPON treatment (Figure 4.4 b). Notably, oleate only did not cause a significant increase in lipids in either control or TST overexpressing cells.

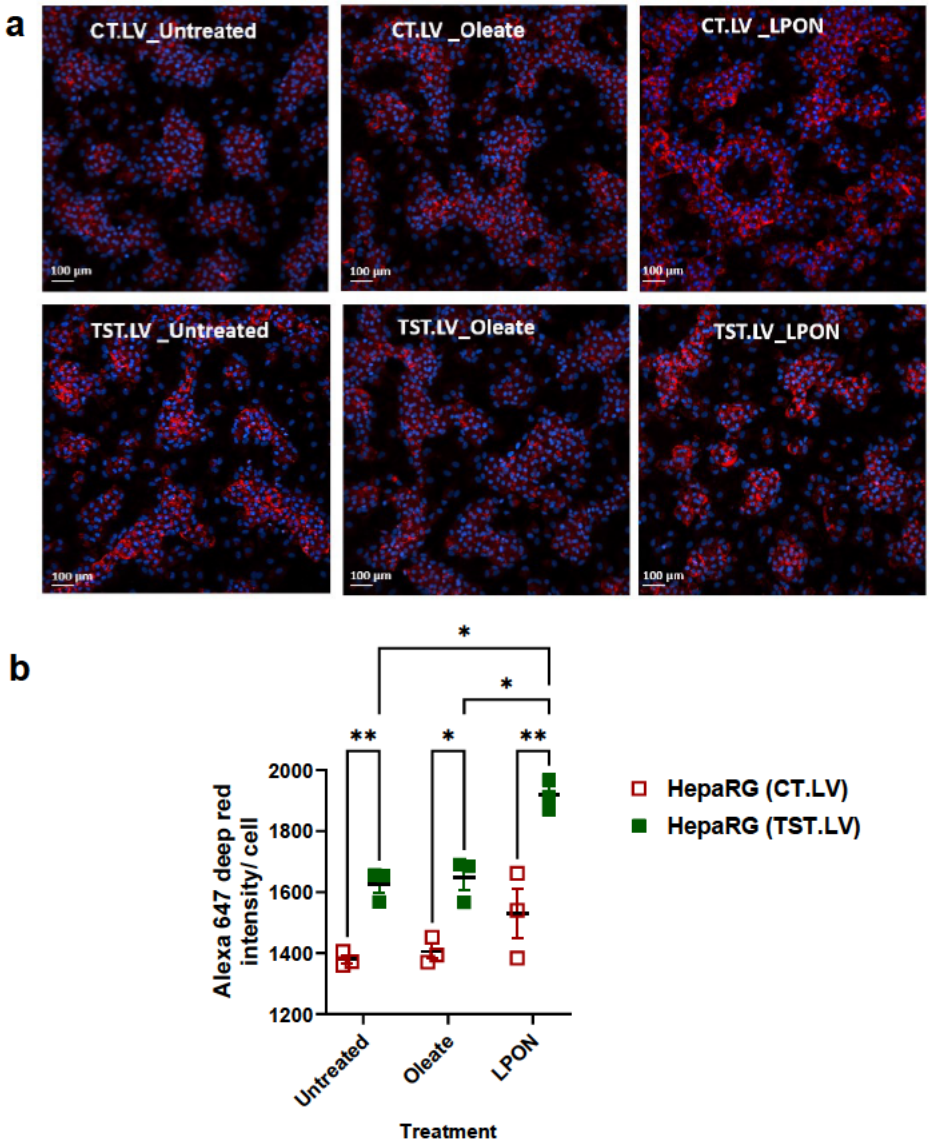

Figure 4.4 Neutral lipid staining and quantification in HepaRG cells transfected with TST or control lentivirus under untreated, oleate and LPON treatments.

(a) Images of HepaRG cells transfected with either TST or control lentivirus stained for neutral lipid with LipidTox (deep red, Alexa Fluor 647 dye) and Hoechst nucleus staining (blue) following different treatment conditions; untreated, oleate only (0.25 mM), LPON; a cocktail of lactate (L) (10 mM); pyruvate (P) (1 mM); octanoate (O) (2 mM) and ammonia (N) (4 mM). All treatments lasted for 72 hours. (b) Quantification of LipidTox deep red stain using opera image analysis system. (n=3 biological replicates/group; 3 technical replicates). Data plotted as mean± SEM. Significant effects of TST overexpression and/or treatment were determined by two-way ANOVA with Tukey's post hoc tests. *P≤ 0.05, **P≤ 0.01. Scale bar, 100 µm. CT.LV: HepaRG cells transfected with a control lentivirus. TST.LV: HepaRG cells transfected with a lentivirus driving the overexpression of TST, TST: thiosulfate sulfurtransferase, mM: millimolar.

4.4.2 HepaRG cells overexpressing TST exhibit less oxidative stress compared to control cells

To investigate the effect of oleate and LPON treatment on ROS accumulation, untreated HepaRG and HepaRG treated with oleate or LPON for 72 hours were stained for ROS using Abcam ROS Deep Red stain and quantified using Opera imaging system.

Despite the higher content of lipids in HepaRG cells overexpressing TST (TST.LV), significantly lower levels of ROS were detected in HepaRG (TST.LV) compared to HepaRG (CT.LV) control cells. As shown in Figure 4.5 a and b, fluorescence images revealed a reduction in ROS accumulation in TST-overexpressing cells under all treatment conditions, including untreated, oleate, and LPON treatments, and quantification of ROS levels supported these findings, showing a significant decrease in ROS in TST-overexpressing cells relative to controls. Interestingly, LPON treatment did not cause more production of ROS in HepaRG cells overexpressing TST or control cells.

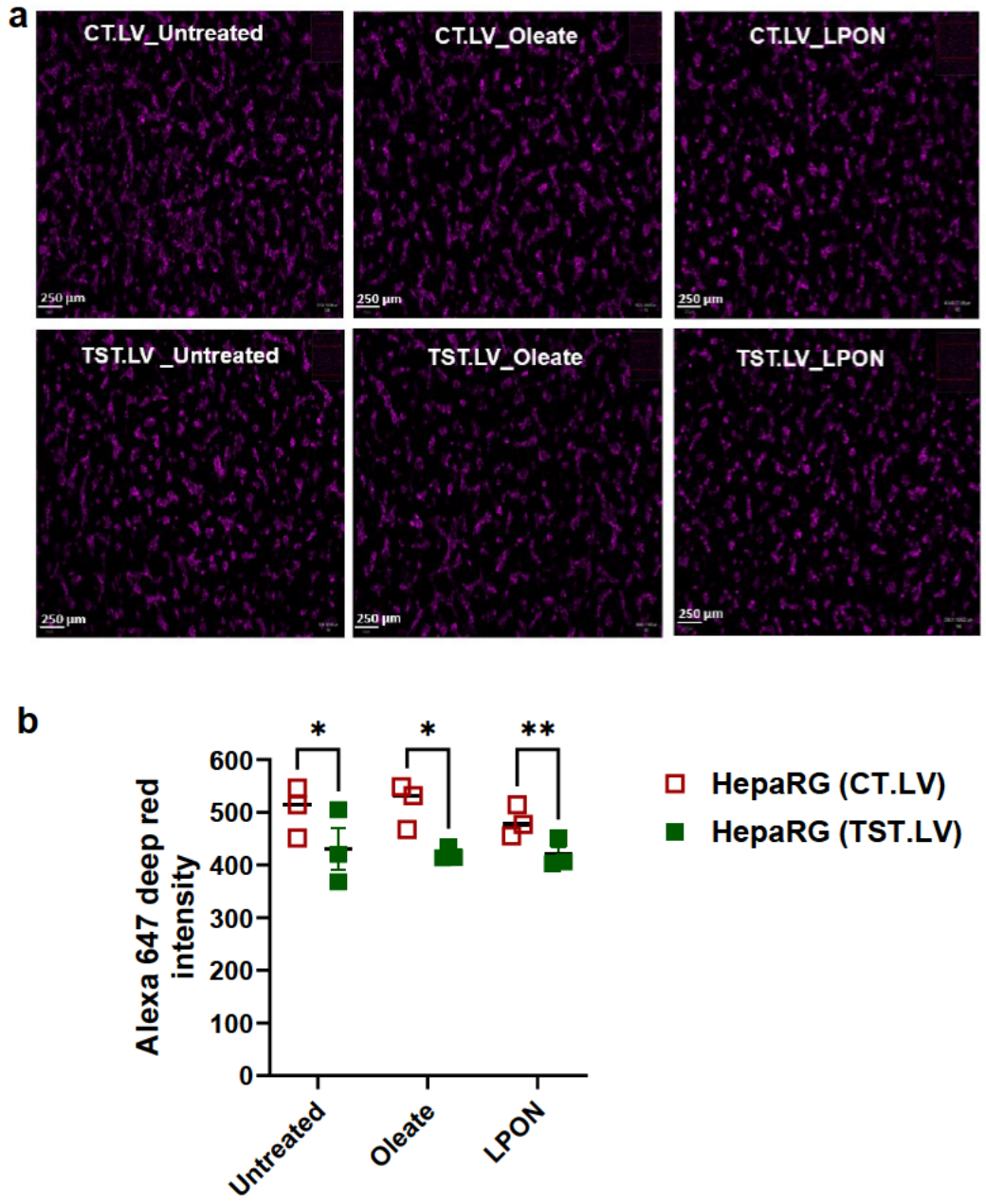

Figure 4.5 ROS staining and quantification in HepaRG cells transfected with TST or control lentivirus under untreated, oleate and LPON treatments conditions.

(a) Images of HepaRG cells transfected with either TST or control lentivirus stained for ROS with Abcam deep red stain (Alexa Fluor 647 dye) following different treatment conditions; untreated, oleate only (0.25 mM), LPON; a cocktail of lactate (L) (10 mM); pyruvate (P) (1 mM); octanoate (O) (2 mM) and ammonia (N) (4 mM). All treatments lasted for 72 hours. (b) Quantification of deep red stain using Opera image analysis system. (n=3 biological replicates/group; 3 technical replicates). All data plotted as mean± SEM. Significant effects of TST overexpression and/or treatment were determined by two-way ANOVA with Tukey's post hoc tests. *P≤ 0.05, **P ≤ 0.01. Scale bar, 250 µm. CT.LV: HepaRG cells transfected with a control lentivirus, TST.LV: HepaRG cells transfected with a lentivirus driving the overexpression of TST.TST: thiosulfate Sulfurtransferase, mM: millimolar.

4.4.3 HepaRG cells overexpressing TST exhibit basal and LPON-induced mitochondrial dysfunction

To test whether TST overexpression provides a protective effect to the mitochondria against the LPON treatment, evaluation of mitochondrial metabolism was performed on HepaRG cells with and without TST overexpression using the seahorse mitochondrial stress test.

HepaRG cells overexpressing TST showed signs of impaired mitochondrial function compared to control cells, and this was worsened by LPON treatment for 72hrs. Figure 4.6, b and c show the reduced basal respiration and ATP production, respectively, in HepaRG (TST.LV) compared to HepaRG (CT.LV) cells even when cells were untreated and unchallenged by oleate or LPON treatment. Maximal respiration and spare respiratory capacity were reduced in response to LPON treatment in HepaRG (TST.LV) and HepaRG (CT.LV) cells (Figure 4.6, d, and f). Proton leak was reduced only in HepaRG (TST.LV) cells in response to LPON treatment (Figure 4.6, e), while no changes were observed in non-mitochondrial oxygen consumption in response to LPON or caused by TST's overexpression (Figure 4.6 g).

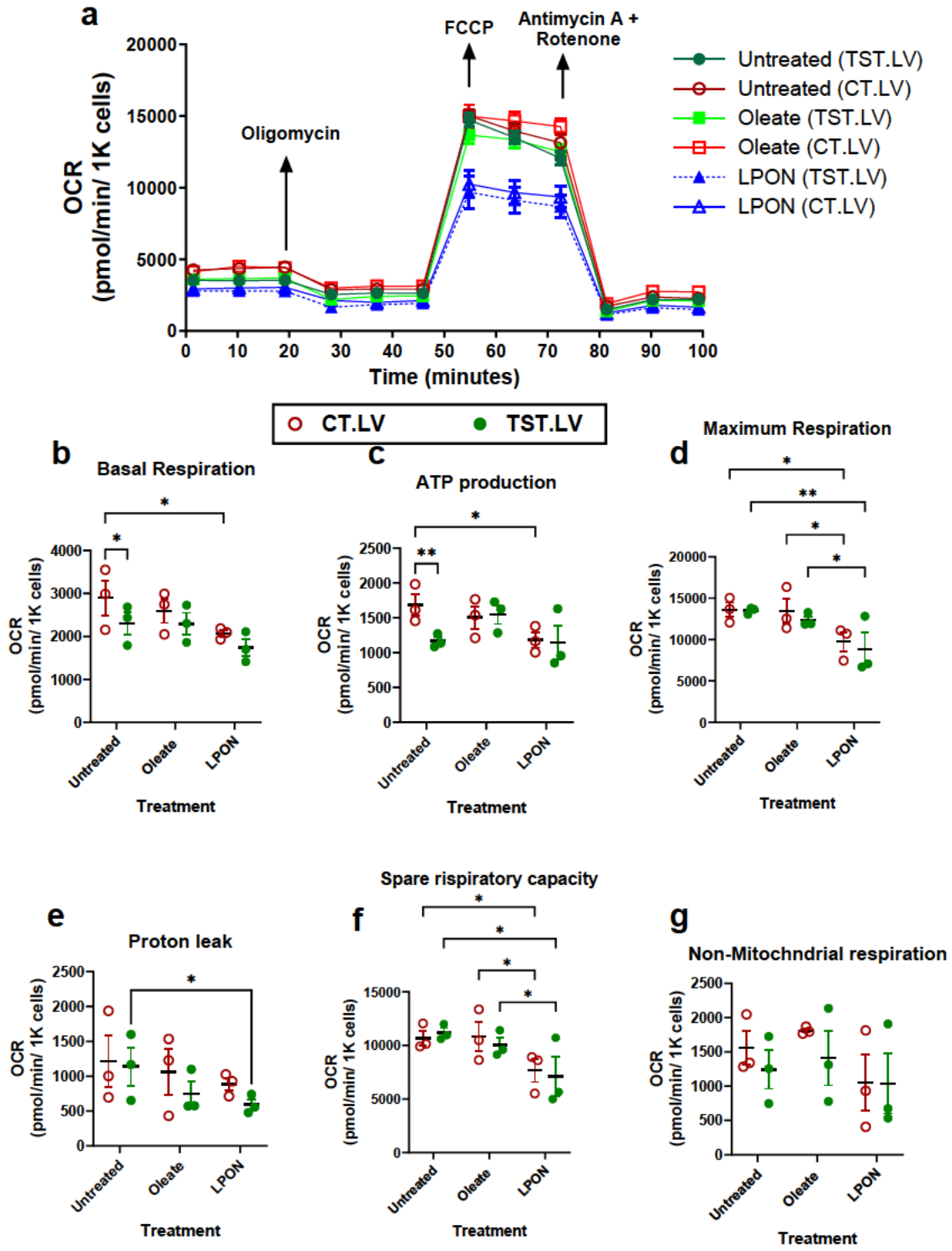

Figure 4.6 Mitochondrial stress test in HepaRG cells transfected with TST or control lentivirus under untreated, oleate and LPON treatments.

(a) A summary trace showing a standard mitochondrial stress test performed on HepaRG under different treatment conditions; untreated, oleate only (0.25 mM), LPON; a cocktail of lactate (L) (10 mM); pyruvate (P) (1 mM); octanoate (O) (2 mM) and ammonia (N) (4 mM). All treatments lasted for 72

hours. The time of addition for each drug compound is marked with arrows. Calculated (b) basal, (c) ATP-linked, (d) maximal uncoupled respirations, (e) proton leak, (f) spare respiratory capacity, and (g) non-mitochondrial respiration. (n=3 biological replicates/group; 4 technical replicates). Data are plotted as mean ± SEM. Data analysed by two-way ANOVA with Tukey's post hoc tests: *P<0.05, **P ≤ 0.01. OCR: oxygen consumption rate, FCCP: carbonyl cyanide-ptrifluoromethoxyphenylhydrazone, CT.LV: HepaRG cells transfected with a control lentivirus. TST.LV: HepaRG cells transfected with a lentivirus driving the overexpression of TST, TST: thiosulfate sulfurtransferase, mM: millimolar.

4.5 Discussion

This study investigated the hypothesised protective role of TST in regulating lipid accumulation, oxidative stress, and mitochondrial function in HepaRG cells within the context of MASLD. The results showed that TST overexpression led to increased lipid accumulation even without external fatty acid treatment, exacerbated by LPON treatment, and suggested that TST impacts lipid metabolism potentially through its effects on mitochondrial processes. Despite showing reduced oxidative stress, TST-overexpressing cells exhibited diminished basal respiration and ATP production, indicating potential mitochondrial dysfunction. Notably, these cells demonstrated unchanged proton leak, suggesting specific issues with ATP synthase or proton gradient coupling rather than general mitochondrial uncoupling. This work points to the complex and possibly context-dependent role of TST, which appears to balance between reducing oxidative stress and impairing mitochondrial function.

Our results demonstrated that HepaRG cells overexpressing TST accumulate significantly more lipids compared to control cells, even in the absence of external fatty acid treatment. This lipid accumulation was further exacerbated by LPON treatment, a treatment designed to mimic the metabolic environment of MASLD *in vitro* (275). The increased lipid retention in TST-overexpressing cells suggests that TST may play a role in lipid metabolism, potentially through its interactions with mitochondrial processes that affect the handling of fatty acids. Given that TST can influence the ETC and fatty acid oxidation, it is plausible that its overexpression may disrupt the balance of lipid metabolism, leading to excessive lipid accumulation. This aligns with previous studies that indicate TST's involvement in regulating mitochondrial substrate preference (194), which could contribute to the altered lipid metabolism observed in this study.

One way by which TST overexpression can affect lipid metabolism is by altering sulfide levels that disrupt normal lipid metabolism, leading to an increased accumulation of lipids within the cells. Since TST works on the oxidation of sulfide in the mitochondria, I hypothesised that

TST's overexpression would reduce sulfide levels, which could explain the impairment in lipid metabolism. There is evidence that reduced sulfide levels, achieved by CSE knockout, increases lipid accumulation *in vivo* (285), and the administration of sulfide donors alleviate this lipid accumulation (286). However, in this study, sulfide levels in cell culture were not measured, future studies should aim to quantify sulfide and thiosulfate levels in HepaRG cells in untreated conditions and in response to LPON treatment to test whether the observed lipid metabolism dysfunction is caused by altered H_2S levels.

Interestingly, despite the increased lipid content, HepaRG cells overexpressing TST exhibited significantly lower levels of ROS compared to control cells across all treatment conditions. Previous research has shown that TST enhances the production of mitochondrial-specific antioxidants like SOD2 and PRDX3 (194), reduction in ROS levels observed in TST-overexpressing cells supports the hypothesis that TST modulates oxidative stress, possibly by influencing the activity of these antioxidant enzymes. This protective effect against ROS could be particularly beneficial in preventing the progression of MASLD to more severe stages, such as MASH, where oxidative stress plays a central role in disease pathogenesis. It is important to acknowledge that the measurements of ROS in this study were performed without a positive control to confirm the assay's specificity, future work should include positive controls and include other oxidative stress markers such as the quantification of lipid peroxidation, quantification of GSH and SOD2 to gain a wider perspective on the oxidative stress state in these cells.

The impact of TST overexpression on mitochondrial function appears to be more complex. While TST-overexpressing cells showed reduced ROS, they also exhibited signs of mitochondrial dysfunction, even under basal conditions. This was evident by reduced basal respiration and ATP production in HepaRG cells overexpressing TST, which was further exacerbated by LPON treatment. The reduced basal respiration and ATP production was not accompanied by reduced proton leak, which could indicate a problem specifically with ATP synthase or the mechanisms coupling proton gradient to ATP synthesis. This typically points to issues with the ETC's efficiency or ATP synthase activity rather than general mitochondrial uncoupling or proton leakage. Additionally, it is possible that the observed mitochondrial dysfunction in TST-overexpressing cells could be linked to a reduction in mitochondrial content or structural abnormalities. Investigating mitochondrial biogenesis markers, such as PGC-1α and NRF1, or assessing mitochondrial number through mtDNA quantification, would

provide valuable insights into whether TST overexpression affects mitochondrial quantity or quality.

One possible explanation for the reduced basal respiration is the reduced levels of sulfide because of TST's overexpression, multiple studies have illustrated that increased sulfide signalling, either by exogenously administrating sulfide (287-289) or overexpression of the sulfide producing CBS protein (290) result in increased basal mitochondrial respiration. It is possible that the decrease in sulfide levels because of TST's overexpression might achieve the opposite. Although sulfide levels were not measured in this experiment, so this remains unknown. Future studies should aim to quantify H_2S in HepaRG cell culture treated as described in this study to identify the involvement of H_2S in the observed phenotypes. Moreover, considering that sulfide donors have been shown to alleviate lipid accumulation and mitochondrial dysfunction in other models, it would be worthwhile to explore whether H_2S supplementation could mitigate the detrimental effects of TST overexpression observed in this study. Such interventions might clarify whether the phenotypes are directly driven by altered H_2S metabolism.

The overexpression TST can disrupt the delicate balance of cellular metabolism by diverting metabolic resources away from oxidative phosphorylation (OXPHOS) and toward pathways like lipogenesis. Normally, oxidative phosphorylation is the primary pathway through which cells produce ATP, the energy currency, by utilising substrates like glucose and fatty acids in the mitochondria. However, in TST-overexpressing cells, a shift in metabolic regulation may reduce the efficiency of OXPHOS, leading to impaired mitochondrial oxidation of fatty acids and other substrates. One key consequence of this shift is that fatty acids, instead of being oxidised in the mitochondria through β-oxidation, are redirected into lipogenesis pathways, which result in the synthesis and storage of lipids. This redirection contributes to the accumulation of lipids within the cell. As lipogenesis is a highly energy-demanding process, the decreased mitochondrial oxidation further exacerbates this shift, as cells increasingly rely on anabolic pathways to store excess substrates as triglycerides and fatty acids, a process documented in multiple studies that report reduced mitochondrial oxidation can lead to decreased β-oxidation of fatty acids, potentially resulting in an accumulation of lipids within the cell (291, 292). This dual effect of TST-reducing oxidative stress while compromising mitochondrial function- highlights the unique role of TST in cellular metabolism and suggests that its overexpression could lead to a "metabolic trade-off". The reduction in maximal

respiration (revealed by the addition of the uncoupling compound FCCP), and spare respiratory capacity observed in TST-overexpressing cells further supports the notion that increased levels of TST influences mitochondrial function detrimentally under conditions of metabolic stress.

Studies have shown that at low concentrations, sulfide can enhance cellular respiration by donating electrons to cytochrome c oxidase (COX), which boosts ETC activity, while at higher concentrations, sulfide inhibits COX activity (293). This inhibition occurs through binding to the Fe3+-a3 and CuB subunits of COX, which disrupts its enzymatic function, or by forming stable inhibitory complexes that reduce the enzyme's ability to transfer electrons and consume oxygen (293, 294). Identifying the exact concertation at which sulfide is beneficial for hepatocytes is challenging and requires further experiments. In this study, I used a lentivirus-driven stable overexpression of TST which might have reduced sulfide levels below beneficial levels. Further studies should investigate how different levels of TST expression or activity influence oxidative stress and mitochondrial function and the progression of MASLD in HepaRG cells or other *in vitro* models.

Collectively, these results suggest that TST plays a role in the balance between lipid metabolism, oxidative stress management, and mitochondrial function in hepatocytes. While TST overexpression may confer protection against oxidative stress, it also appears to compromise mitochondrial function, which could contribute to the progression of MASLD. The findings that TST-overexpressing cells accumulate more lipids and exhibit mitochondrial dysfunction align with the concept that mitochondrial dysfunction and oxidative stress are key drivers of MASLD progression. However, the reduction in ROS levels suggests that TST may have a complex, context-dependent role in disease pathogenesis, where it modulates oxidative stress but at the potential cost of mitochondrial function.

4.6 Limitations and recommendation for future work

This chapter offers valuable insights into the complex role of TST in regulating lipid accumulation, oxidative stress, and mitochondrial function in HepaRG cells under conditions that simulate MASLD. However, several limitations of this study should be acknowledged to guide future research.

Measurement of sulfide levels: A significant limitation of this study is the lack of direct measurement of sulfide levels in cell culture. Given TST's role in sulfide oxidation, oxidative

stress, and lipid oxidation (160, 286, 295), understanding how TST overexpression affects sulfide concentrations is crucial. Future work should incorporate methods to accurately quantify sulfide and thiosulfate levels in HepaRG cells, both in untreated conditions and following LPON treatment. This will help clarify whether changes in sulfide levels contribute to the observed alterations in lipid metabolism and mitochondrial function following TST's overexpression.

Incomplete characterisation of lipid metabolism: While this study provided evidence of increased lipid accumulation in TST-overexpressing cells, it did not directly measure lipogenesis rates or assess how changes in mitochondrial function impact lipogenesis. Future experiments should evaluate lipogenesis through assays using the incorporation of labelled substrates into lipids or using lipogenesis assays. This could help determine whether reduced mitochondrial oxidation leads to increased lipogenesis and lipid storage.

Dose-dependent effects of sulfide: Finally, considering the reported dual effects of sulfide donors (160, 286, 295), it is essential to define the optimal sulfide concentrations that balance their beneficial and detrimental impacts. This involves testing varying doses of sulfide donors in *in vitro* models to investigate how different sulfide levels influence mitochondrial function and cellular metabolism. For future experiments, I propose using the slow-releasing sulfide donor GYY 4137. HepaRG cells overexpressing TST should be treated with different concentrations of GYY 4137, and subsequent observations should include assessments of lipid accumulation, oxidative stress, and mitochondrial respiration. This approach will help identify the optimal sulfide dose that achieves a beneficial balance.

4.7 Conclusions

This study provided mechanistic insights into how the overexpression of TST affects lipid metabolism, oxidative stress, and mitochondrial function in HepaRG cells challenged with fatty acid treatment to mimic MASLD. Overexpression of TST led to significant lipid accumulation, potentially by disrupting mitochondrial fatty acid oxidation and diverting metabolic resources towards lipogenesis. Despite the reduction in oxidative stress, as indicated by lower ROS levels, TST overexpression impaired mitochondrial function, evidenced by reduced basal respiration and ATP production. These findings suggest a "metabolic trade-off" in TST-overexpressing cells, where oxidative stress is mitigated at the expense of mitochondrial respiration, which could promote MASLD progression. Future studies should

focus on investigating the role of sulfide metabolism in this context and explore the impact of different TST expression levels on mitochondrial function and disease progression. Overall, this work highlights the complex and dose-dependent effects of TST on cellular metabolism.

5 Chapter 5: The impact of TST deficiency on the metabolic benefits on calorie restriction in mice

5.1 Introduction

Calorie restriction (CR), defined as a reduction in calorie intake without malnutrition, first observed to extend lifespan in rodents, has since been shown to enhance metabolic health, stress resistance, and cellular repair across various organisms, including yeast, worms, flies, rodents, and primates (202, 204, 216, 296), and humans (210). CR improves insulin sensitivity, glucose metabolism, lipid profiles, and may protect against metabolic diseases, cognitive decline, and neurodegeneration (297-299). While human studies support CR's benefits, such as weight loss and reduced free radical production, its application should be individualised due to challenges in compliance and potential adverse effects.

5.1.1 The transsulfuration pathway mediates the benefits of CR

The transsulfuration pathway (TSP) converts homocysteine into cysteine, a process facilitated by CSE and CBS (116). In addition to its critical role in protein synthesis, cysteine is a key component of the important antioxidant GSH which serves as a powerful antioxidant on its own (261). This conversion also results in the production of the gaseous signalling molecule H_2S and other sulfur metabolites (130). H_2S have been shown to facilitate a range of physiological benefits, including promoting stress resistance and extending lifespan in model organisms (127).

A series of ground breaking papers led by the late Dr. James R. Mitchell and Dr. Christopher Hine have identified H_2S production as a potentially conserved mechanism behind the longevity and health span improvements induced by CR in yeast, worms, fruit flies, and mice (233-236). In mice, Hine *et al.* (236) reported that 50% CR for 7 days increased expressions of CSE and CBS, resulting in the increased endogenous production of H_2S, leading to the conclusion that CR benefits were mediated by the endogenous upregulation of H_2S production in the liver. Their investigation also illustrated that genetic manipulation of TSP components can either amplify or block the advantages conferred by CR, underscoring the central role of H_2S production in mediating the favourable outcomes associated with CR (236). The regulation of H_2S production involves gene expression changes triggered by cysteine (Cys) deprivation, which may be influenced by stress responses and the mTORC1 pathway (236). The potential

mechanisms through which H_2S confers CR benefits include protecting against ischemic reperfusion injury (IRI) and oxidative damage, possibly by interacting with mitochondrial components. H_2S may also contribute to lifespan extension by counteracting vascular issues like atherosclerosis (300). Hine *et al.* (236) reported that supplementing with sulfur amino acids (SAA) or inhibiting CSE in the liver diminishes H_2S production and eliminates the protective effects of CR against liver injury. This study showed that restricting cysteine is the key factor behind the resistance to IRI and the reduction of liver damage markers after reperfusion, when compared to *ad libitum* mice (236).

The study also suggested that the protective effects of H_2S are mediated by the persulfidation of SQOR, a mitochondrial enzyme involved in transferring electrons from H_2S to the ETC, as the protective effects of H_2S against IRI were not observed when SQOR was deleted (236). This observation was confirmed by other studies that linked reduced SQOR activity to mitochondrial dysfunction in Leigh's disease, where mutations that inactivate SQOR can lead to elevated H_2S levels, subsequently inhibiting complex IV in the ETC (301). Moreover, transcriptomics analysis of graded CR interventions showed that hepatic *Cse* was upregulated in mice after 2 weeks on 10%, 20%, 30% or 40% CR, indicating an activation in the H_2S production pathway (237). In conclusion, the activation of the transsulfuration pathway and H_2S production seem to be essential to the benefits of CR, including enhanced stress resistance and protection against IRI.

5.1.2 *Tst*$^{-/-}$ male mice present with elevated plasma H_2S levels and a prediabetic phenotype

Morton *et al.* (194) unexpectedly identified TST, a member of the TSP as a genetic factor associated with "healthy leanness" in mice. The increased expression of TST specifically in adipose tissue conferred protective effects against HFD in mice (194). These effects included a significant reduction in fat mass gain, improved insulin sensitivity, mitigation of hyperglycemia, and a decrease in adipocyte size (194). *TST* expression in humans was negatively correlated with body mass index (BMI) and positively correlated with insulin receptor substrate 1 (IRS1) and secretion of the metabolically protective hormone adiponectin (195) in humans (194). The deletion of the *Tst* gene in mice resulted in viable, grossly normal mice despite a marked elevation of circulating H_2S levels (168). However, *Tst*$^{-/-}$ male mice exhibited a fatty liver profile when fed normal chow diet under *ad libitum* feeding conditions and without any other interventions (168). This phenotype includes elevated plasma NEFA and

VLDL, and increased lipid content in the liver tissue as quantified by oil red O staining. In addition, these mice exhibited impaired glucose tolerance and dyslipidaemia (168). This phenotype revealed a central role for hepatic TST in H_2S disposal and pointed to a maladaptive compensatory metabolic response when TST was absent. Hepatocytes from *Tst*$^{-/-}$ mice exhibited increased export of cysteine and GSH and enhanced mitochondrial respiratory clearance of H_2S, revealing induction of multiple routes for increased disposal to maintain hepatic sulfide homeostasis (168). Given the critical role of elevated hepatic sulfide in conferring beneficial metabolic effects of CR, I tested the hypothesis that TST deficiency, by elevating circulating H_2S, but maintaining hepatic H_2S, improves the beneficial metabolic effects of CR in mice.

Importantly, Carter *et al.* (168) did not include female mice in their study, therefore the effects of TST deficiency on female mice are still unknown, this chapter aims to explore the metabolic profile of *Tst*$^{-/-}$ male and female mice at baseline (*ad libitum*) and after 4 weeks of 30% CR intervention compared to their C57BL/6J counterparts.

5.2 Hypothesis and Aims

Hypothesis: TST deficiency leads to a pronounced improvement in response to calorie restriction due to elevated systemic sulfide levels.

Aims:

1. Assessment of the metabolic profile of *Tst*$^{-/-}$ male and female mice at baseline (*ad libitum* diet).
2. Assessment of the metabolic profile of *Tst*$^{-/-}$ male and female mice after 4 weeks of 30% CR.
3. Assessment of the lipid content in the livers of *Tst*$^{-/-}$ male and female mice after 4 weeks of 30% CR.

5.3 Study design

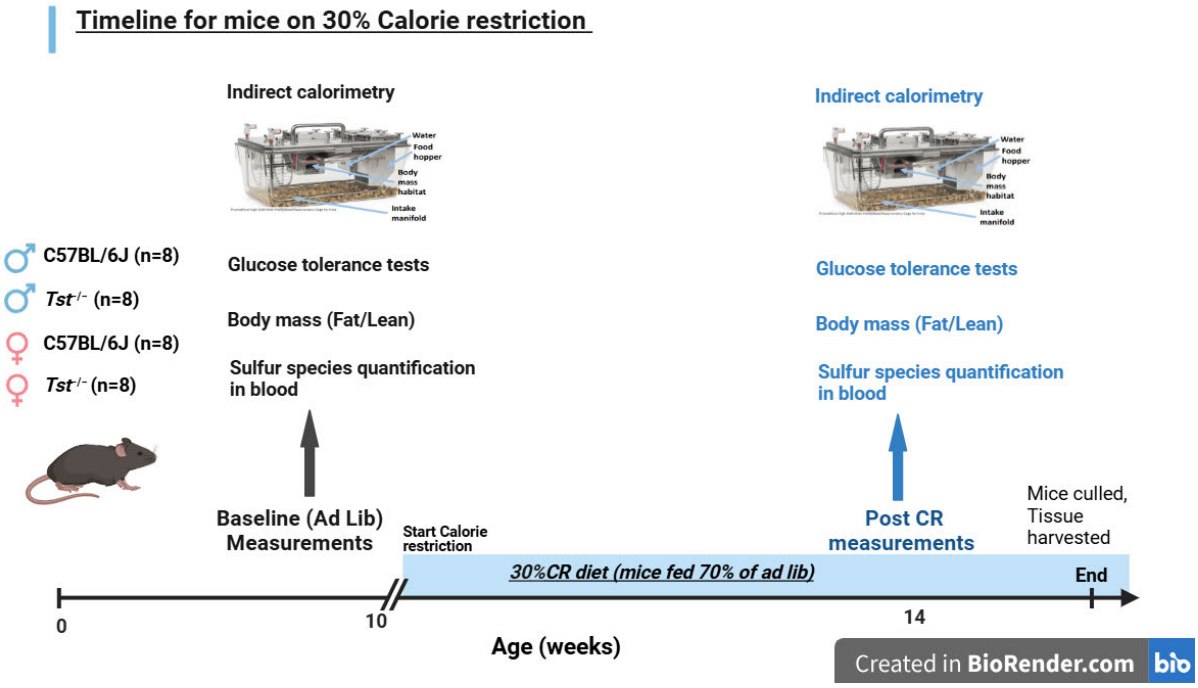

Figure 5.1 A schematic view of the timeline for the calorie restriction animal study. Created in BioRender.com.

The study aims to assess the effects of TST deficiency on metabolic response to 30% calorie restriction (CR). 4 experimental groups were used; C57BL/6J males, C57BL/6J females, *Tst*$^{-/-}$ males, *Tst*$^{-/-}$ females, n=8 each, and underwent the following protocol:

Prior to the start of the experiment, mice were single- housed and daily food intake for mouse was measured by measuring the food provided in each cage and subtracting the weight of the remaining food after 24 hours, this process was repeated for a week and the average food intake/day for each mouse was calculated.

Basal measurements (*ad libitum*): littermate mice – aged 10 weeks– were switched to a control diet similar to chow diet (Research Diets D09100304). Body weight and composition were assessed by TD-NMR. Weekly body weight measurements were recorded. Week 1: Indirect calorimetry using the Promethion metabolic cage system to measure metabolic rates. Week 2: Oral glucose tolerance tests (OGTTs) were performed. Blood and plasma samples were collected for further analysis.

Calorie restriction (CR) phase (Weeks 2-6): Mice received 70% of their *ad libitum* daily intake based on the measurements calculated for each mouse individually. Food was provided between 4-4:30 PM. Body weight was measured 3 times per week.

Post-CR measurements (Weeks 7-8): Body weight was recorded 3 times a week and TD-NMR measurements were monitored every week. Indirect calorimetry was measured using the Promethion metabolic cage system. Glucose tolerance tests were performed again.

Finally, mice were culled by Schedule 1 method, in a fasted state. Blood, brain, liver, adipose tissue, skeletal muscle, heart, and kidney were collected for analysis.

5.4 Results

5.4.1 CR did not induce changes in blood or hepatic sulfide levels in male or female mice

Given the critical role ascribed to elevated hepatic sulfide in CR's metabolic benefits, I assessed concentrations of sulfide, thiosulfate (an oxidation product of sulfide), GSH, and cysteine (all quantified in whole blood) in both C57BL/6J and *Tst*$^{-/-}$ mice, at baseline and after a 4-week 30% CR intervention.

At baseline, *Tst*$^{-/-}$ males and females exhibited higher systemic levels of sulfide (Figure 5.2 a) and thiosulfate (Figure 5.2 b) relative to C57BL/6J males and females. Upon completion of the 4-week 30% CR intervention, systemic sulfide levels were comparable to their respective baseline levels in all groups (Figure 5.2 a). Thiosulfate levels were significantly elevated above baseline in *Tst*$^{-/-}$ male and female mice following CR, in contrast to C57BL/6J mice (Figure 5.2 b). Glutathione (GSH) and cysteine levels were comparable between genotypes and were not affected by CR (Figure 5.2 c and d).

Sulfide levels in the liver tissue taken from mice after 4 weeks on CR did not show difference between genotypes, however, thiosulfate shows a slight elevation following CR only in *Tst*$^{-/-}$ mice (males and females combined) (Figure 5.2 e and f).

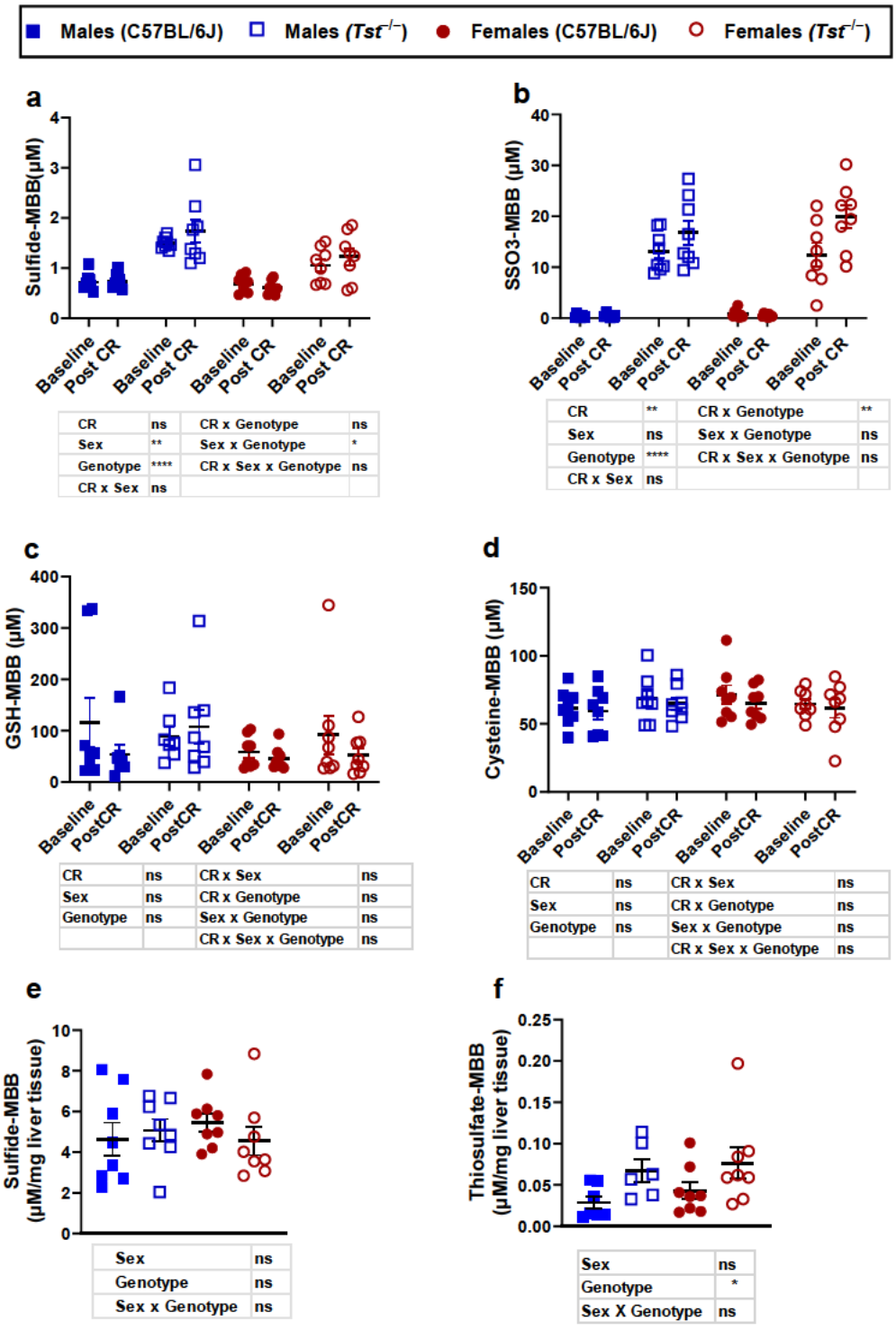

Figure 5.2 The impact of calorie restriction on systemic and hepatic sulfide and thiosulfate levels in C57BL/6J and *Tst*$^{-/-}$male and female mice.

Sulfide (a), thiosulfate (b), reduced glutathione (GSH) (c), and cysteine (d) concentration in whole blood taken from the tail vein of *ad libitum* -fed mice (Baseline) and again after 4 weeks on 30% calorie restriction (Post CR). Hepatic sulfide (e), and hepatic thiosulfate (f) concentration (µM/mg) in liver tissue taken after 4 weeks on 30% calorie restriction (Post CR). All compounds are measured after

derivatisation with MBB and detected using liquid chromatography-mass spectrometry. (n= 8 per group). Data are plotted as mean± SEM. Significant effects of CR and/or sex and/ or genotype were determined by three-way ANOVA or a mixed effects model with Tukey's post hoc tests. ns; P> 0.05, *P≤ 0.05, **P≤ 0.01, ****P≤ 0.0001. CR: calorie restriction (30%), GSH: the reduced form of glutathione, µM: micromolar, mg: milligram, MBB: monobromobimane.

5.4.2 *Tst*$^{-/-}$ male mice are resistant to CR-induced whole-body fat mass loss, despite hepatic fat loss

Weight loss was more pronounced in male C57BL/6J mice compared to *Tst*$^{-/-}$ males across the 4-week CR period (Figure 5.3 a and b). Male *Tst*$^{-/-}$ mice exhibited a weight loss pattern akin to that observed in female mice of both genotypes, charactrised by an initial weight loss at week1 followed by a stabilisation of weight loss until the end of the 4 weeks (Figure 5.3 a and b).

To examine whether the differences in weight loss among sexes and genotypes, particularly in male mice, was due to alterations in fat mass and/or lean mass, I conducted weekly assessments of body composition using TD-NMR. Males of both genotypes exhibited a rapid decline in fat mass during the initial 2 weeks of CR, followed by a stabilisation from the 3rd week onwards. Beyond this point, C57BL/6J males sustained this stablisation in fat mass loss, while *Tst*$^{-/-}$ males displayed a reversal in fat mass dynamics, leading to a restoration of fat mass levels similar to their baseline measurements by week 4 of CR (Figure 5.3 c and d). This happened despite these mice losing hepatic fat following the CR weeks (Figure 5.4).

Among female mice of both genotypes, resistance to fat mass loss was apparent over the 4-week CR period (Figure 5.3 c and d). Nonetheless, females exhibited a reduction in lean mass, accounting for their overall loss in body weight (Figure 5.3 f and g).

The weight loss observed in both C57BL/6J and *Tst*$^{-/-}$ male subjects gave rise to substantial differences in body composition. Specifically, C57BL/6J males experienced a greater reduction in fat mass compared to lean mass, resulting in a higher proportion of lean mass relative to body composition after the 4-week CR intervention. In contrast, *Tst*$^{-/-}$ males did not exhibit significant loss in fat mass by the end of the study; rather, there was a reduction in lean mass, contributing to a higher percentage of fat mass (9.85% compared to 5.64% in C57BL/6J males, P=0.02) and a lower percentage of lean mass (67% compared to 70% in C57BL/6J males, (P= 0.003) (Figure 5.3 e and h).

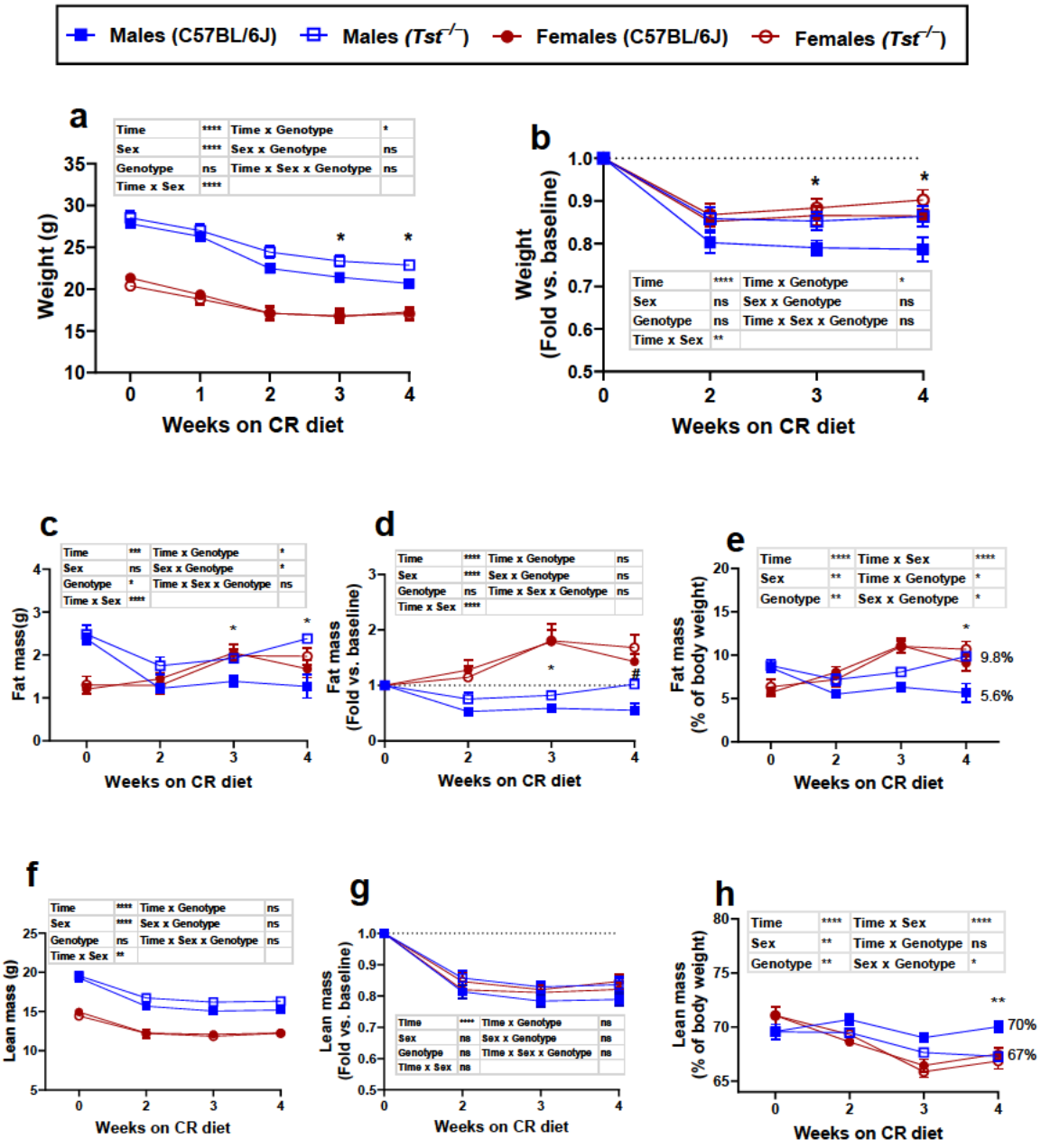

Figure 5.3 The impact of *Tst* deficiency on weight, fat, and lean mass in male and female mice at baseline and after 4 weeks of 30% calorie restriction

Weight loss for male and female C57BL/6J and *Tst*$^{-/-}$ mice over 4 weeks of 30% caloric restriction, plotted as whole weight (a), and as a fold change vs. baseline (b). Changes in fat mass are plotted as whole-body fat mass (c), as fold change vs. baseline (d), and as a percentage of whole weight (e). Lean mass plotted as whole-body lean mass (f), as fold change vs. baseline (g), and as a percentage of whole weight (h). (n= 8 per group). Data plotted as mean± SEM. Significant effects of genotype were determined by three-way ANOVA with Tukey's post hoc tests. All stars annotated on the graph refer to comparisons of *Tst*$^{-/-}$ males vs. C57BL/6J males, the rest of the comparisons are presented in the ANOVA table within each graph. ns; $P > 0.05$, *$P \leq 0.05$, **$P \leq 0.01$, ***$P \leq 0.001$, ****$P \leq 0.0001$. CR: calorie restriction (30%), g: gram, Tst: thiosulfate sulfurtransferase.

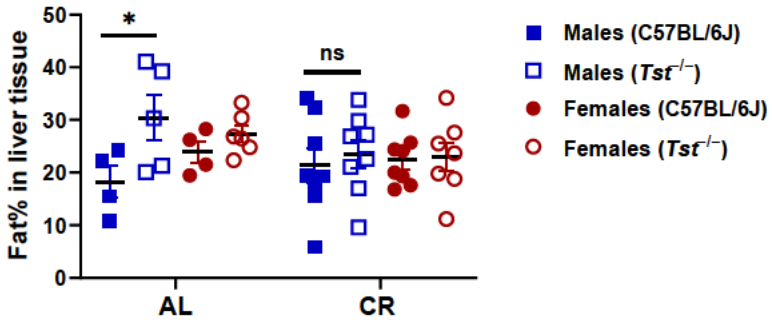

Figure 5.4 Hepatic fat quantified in C57BL/6J and *Tst*$^{-/-}$ mice after 4 weeks of CR compared to age, sex, and genotype-matched mice on *ad libitum* diet.

Quantification of hepatic fat in male and female C57BL/6J and *Tst*$^{-/-}$mice (n=8 post CR, n= 5 AL). Data are presented as mean ± SEM. Significant effects of CR, sex, or genotype were determined by two-way ANOVA with Tukey's post hoc tests. ns; P> 0.05, *P≤ 0.05. Hepatic fat quantifications were carried out following multiple pixel classifiers as describes previously (245). CR: calorie restriction (30%), AL: *ad libitum.*

5.4.3 *Tst*$^{-/-}$ males, but not females, have impaired glucose tolerance at baseline (*ad libitum*), corrected after 4 weeks of CR

The impaired glucose tolerance observed in male *Tst*$^{-/-}$ mice under *ad libitum* conditions was documented previously by our group (168), and confirmed in this study (Figure 5.5 a and e). Furthermore, there appears to be a lack of first-phase insulin secretion during OGTT was observed in *Tst*$^{-/-}$ mice (as indicated by the apparent peak in the C57BL/6J mice at 15 minutes) (Figure 5.5 c). Interestingly, *Tst*$^{-/-}$ female mice did not demonstrate any abnormalities in terms of glucose (Figure 5.5 a) or insulin (Figure 5.5 c) homeostasis compared to C57BL/6J females.

To investigate the impact of a 4-week 30% CR on glucose tolerance and insulin secretion, I conducted OGTTs at baseline and during the fourth week of CR for each mouse. After undergoing the 4-week CR protocol, *Tst*$^{-/-}$ male mice exhibited improved glucose tolerance compared to their *ad libitum* status (glucose AOC reduced following CR, 2-way ANOVA, P<0.0001) (Figure 5.5 e) and no significant increase was observed in first phase insulin secretion of *Tst*$^{-/-}$ males after CR, although it became comparable to their C57BL/6J counterparts (Figure 5.5 c, d, and f). Female mice did not exhibit any significant changes in terms of glucose tolerance or insulin secretion following CR (Figure 5.5 e and f).

Based on the blood glucose and plasma insulin concentration data, two metrics were employed: the HOMA-IR as described by Matthews *et al.* (241), and the Matsuda Index of insulin

sensitivity introduced by Matsuda and DeFronzo (242). Following the CR intervention, males from both genotypes displayed enhanced insulin sensitivity, as evidenced by reduced HOMA-IR values and elevated Matsuda Index scores (Figure 5.5 g and h). Whilst C57BL/6J females exhibited resistance to CR-induced improvements in insulin sensitivity, *Tst*$^{-/-}$ females experienced beneficial effects, although this discrepancy was predominantly evident in the Matsuda Index (Figure 5.5 h) rather than the HOMA-IR score (Figure 5.5 g).

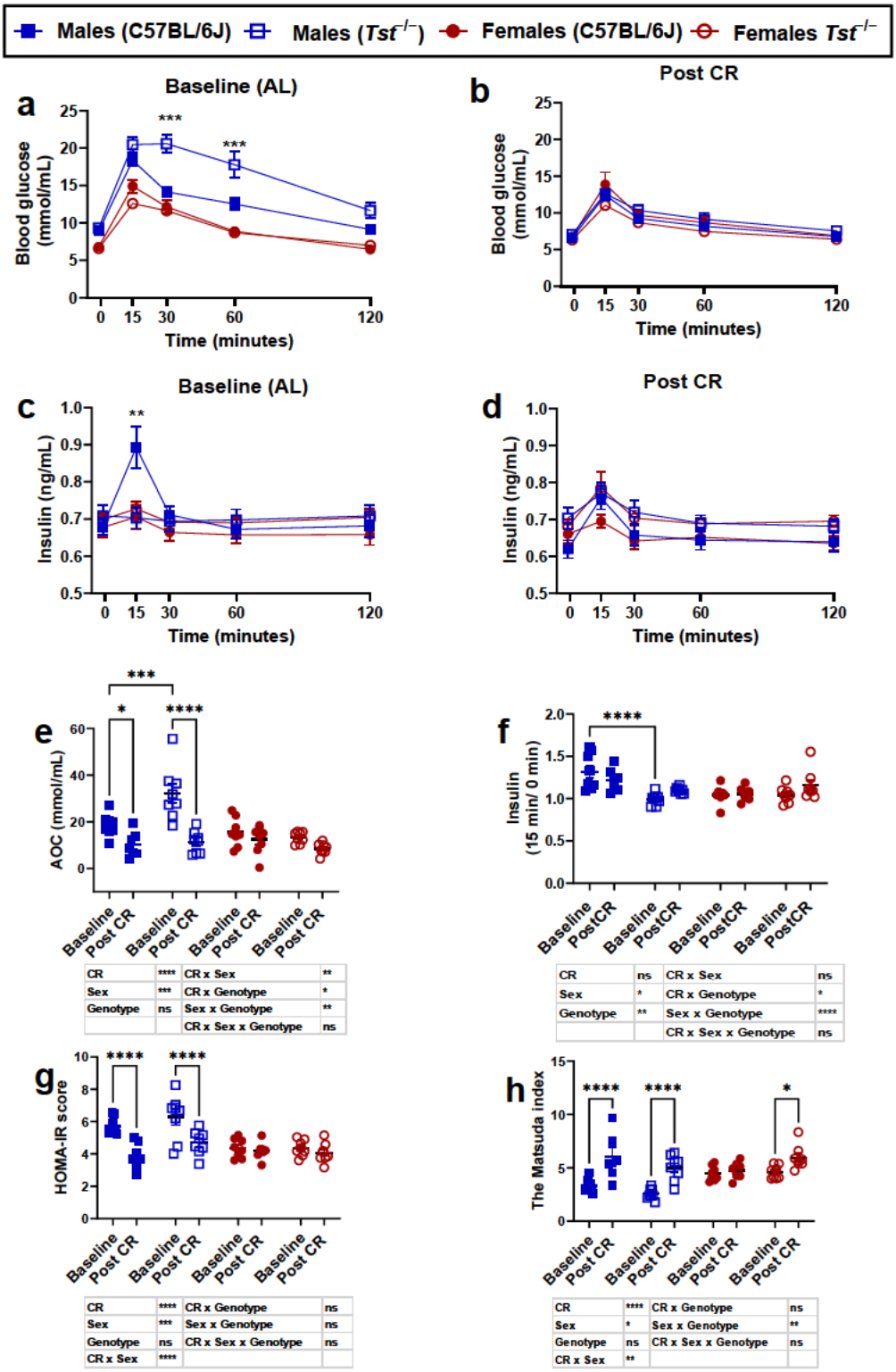

CR	****	CR x Sex	**
Sex	***	CR x Genotype	*
Genotype	ns	Sex x Genotype	**
		CR x Sex x Genotype	ns

CR	ns	CR x Sex	ns
Sex	*	CR x Genotype	*
Genotype	**	Sex x Genotype	****
		CR x Sex x Genotype	ns

CR	****	CR x Genotype	ns
Sex	***	Sex x Genotype	ns
Genotype	ns	CR x Sex x Genotype	ns
CR x Sex	****		

CR	****	CR x Genotype	ns
Sex	*	Sex x Genotype	**
Genotype	ns	CR x Sex x Genotype	ns
CR x Sex	**		

Figure 5.5 The effects of TST deficiency on glucose homeostasis in male and female mice at baseline and after 4 weeks of 30% calorie restriction.

Oral glucose tolerance tests (OGTTs) were conducted at (a) baseline (mice on an *ad libitum* diet) and (b) after 4 weeks of 30% calorie restriction (CR). Insulin levels in plasma were quantified using ELISA

at baseline (c) and after 4 weeks of CR (d). (f) The area of the curve (AOC) was calculated for each group. Insulin fold-changes at 15 minutes relative to 0 minutes were calculated (e). Panels (g) and (h) show HOMA-IR and Matsuda indices calculated from glucose and insulin concentrations during the OGTTs. C57BL/6J and *Tst*$^{-/-}$ male and female mice (n = 8 per group) were used. Data are plotted as mean ± SEM. Significant effects of CR, sex, and/or genotype were determined using three-way ANOVA followed by Tukey's post hoc tests. ns; P> 0.05, * P ≤ 0.05, ** P ≤ 0.01, *** P ≤ 0.001, **** P ≤ 0.0001. CR: calorie restriction (30%), AOC: area of the curve; min: minutes, AL: *ad libitum*, Tst: thiosulfate sulfurtransferase.

5.4.4 Energy expenditure and substrate utilisation are comparable in C57BL/6J and *Tst*$^{-/-}$ mice

I then explored whether differences in energy expenditure (EE) or fuel utilisation (measured by respiratory exchange ratio: RER) contribute to the observed improvement in glucose tolerance in male mice in response to CR. To investigate this, indirect calorimetry was performed on mice at baseline and 4 weeks post CR.

At baseline, male mice of both genotypes exhibited higher EE during day time, night time, and postprandial periods compared to females (Figure 5.6 a and c). No genotype effects on EE were detected within either sex at baseline. Following the initiation of CR, both male and female mice, regardless of genotype, experienced reductions in EE during daytime, night time, and postprandial periods (Figure 5.6 b and c). Postprandial intervals were defined as 7-10 pm under *ad libitum* conditions and 4:30-7:30 pm during the CR diet. These reductions in EE were confirmed to be independent of genotype, as indicated by three-way ANOVA analysis.

Analysis of covariance (ANCOVA) was used to examine whether the relationship between lean mass and total EE differed significantly between sexes and genotypes at both baseline and after CR. At baseline, there were no significant differences in EE for a given lean mass between C57BL/6J and *Tst*$^{-/-}$ mice in either sex (Figure 5.6 d). However, after CR, ANCOVA revealed a significant reduction in total EE for *Tst*$^{-/-}$ females compared to C57BL/6J females, whereas no significant differences were observed in males after CR (Figure 5.6 e).

Total physical activity, measured over 24-hour periods and during specific intervals (daytime, night time, and postprandial), did not differ between genotypes within each sex (Figure 5.7). CR did not significantly affect physical activity in either male or female mice at any time point measured. As expected, physical activity peaked during night time across all groups.

RER analysis was conducted to determine the effects of CR and TST deficiency on the oxidation of carbohydrates and fats. At baseline, under *ad libitum* feeding, RER peaked at the onset of the nocturnal phase, corresponding with increased food intake and physical activity (Figure 5.8 a). Conversely, after CR, the peak in RER was observed around 4-5 pm, coinciding with the time when the daily food ration was provided (Figure 5.8 b).

Further analysis of average RER during daytime, night time, and postprandial periods showed no significant effects of sex or genotype (Figure 5.8 c and d). Specifically, postprandial RER values under *ad libitum* conditions (7-10 pm) were below 0.7, indicating predominant lipid utilisation. In contrast, postprandial RER values after CR (4:30-7:30 pm) exceeded 1, reflecting a shift towards carbohydrate oxidation in all groups (Figure 5.8 c).

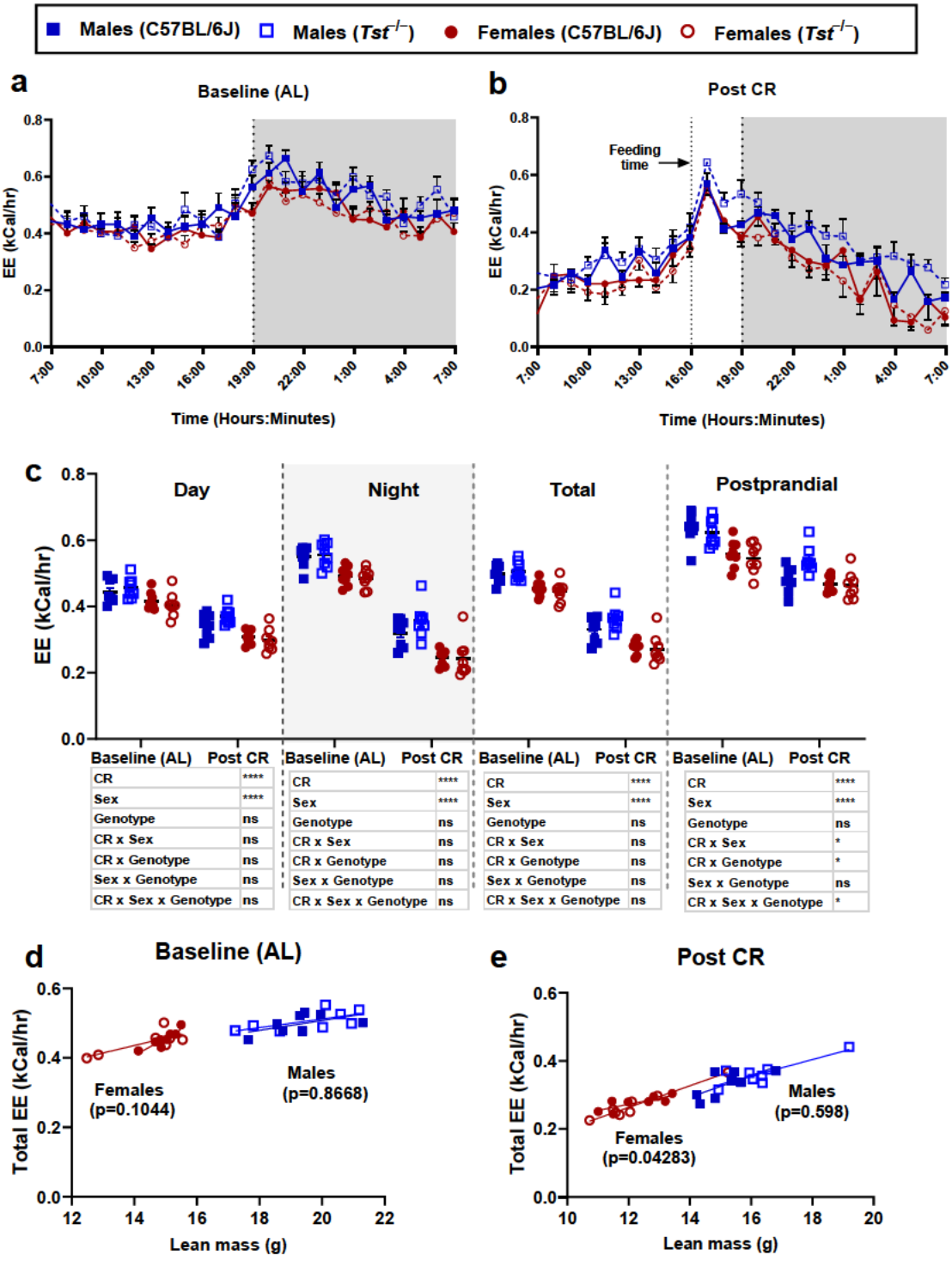

Figure 5.6 The impact of TST deficiency on energy expenditure in male and female mice at baseline and after 4 weeks of calorie restriction

Energy expenditure (EE) is presented as a 24-hour profile at baseline (a) and after 4 weeks of CR (b). Panel (c) shows average energy expenditure values over the 12-hour light (day) and 12-hour dark (night) periods, the total average over 24 hours, and the postprandial period (defined as 7-10 pm at "baseline" and as 4:30- 7:30 pm at "Post CR" period); "baseline" data were collected at week 0 (*ad libitum* feeding), and "Post CR" data were obtained at week 4. Panels (d) and (e) show linear regressions of

lean mass versus total energy expenditure (kcal/24 hours) during baseline and post-CR conditions, respectively. P-values for differences in slope are displayed below the graphs. Male and female C57BL/6J and *Tst*$^{-/-}$ mice (n= 8 per group) were used. Data are plotted as mean ± SEM. Significant effects of CR, sex, and/or genotype were assessed using three-way ANOVA followed by Tukey's post hoc tests, *P< 0.05, **P< 0.01, ***P< 0.001). EE: energy expenditure, kcal/hr: kilocalories per hour, CR: calorie restriction (30%), AL: *ad libitum*, Tst: thiosulfate sulfurtransferase.

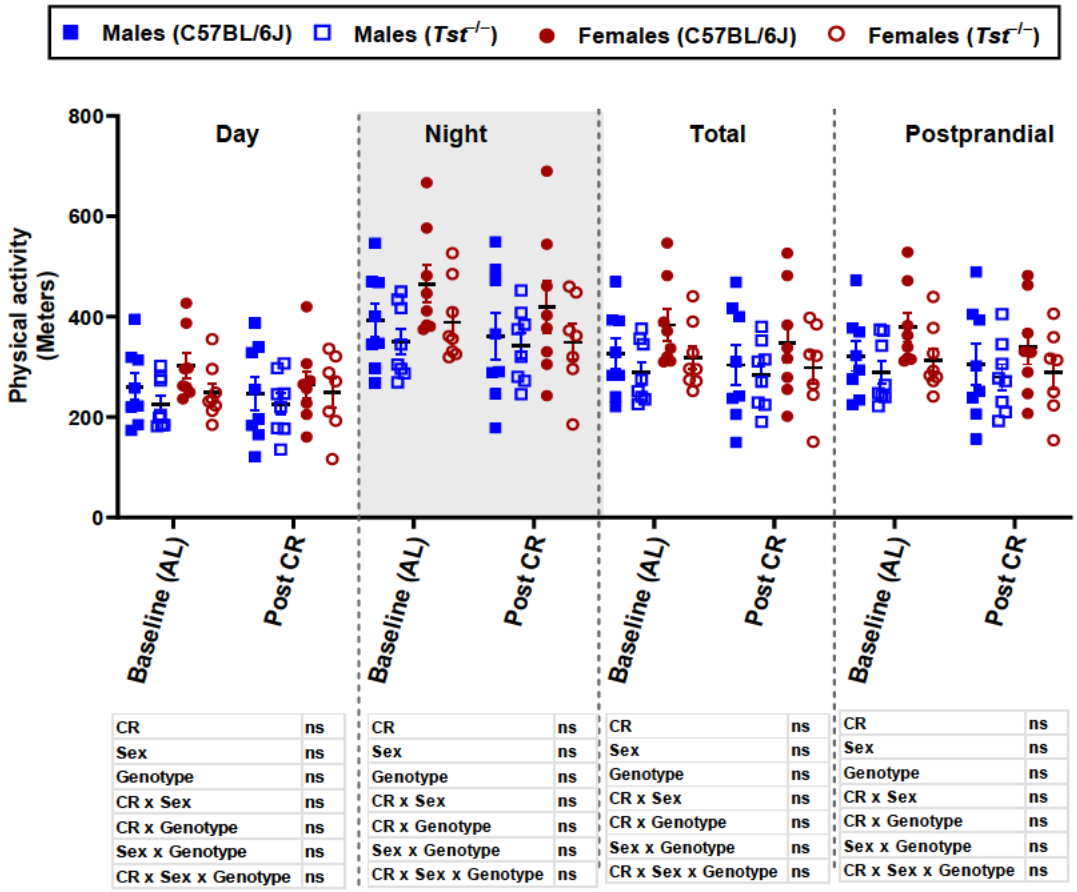

Figure 5.7 The impact of TST deficiency on physical activity in male and female mice at baseline and after 4 weeks of calorie restriction.

Physical activity is presented as average values over the 12-hour light (day) and 12-hour dark (night) periods, the total average over 24 hours, and the postprandial period (defined as 7-10 pm at "baseline" and as 4:30- 7:30 pm at "Post CR" period); "baseline" data were collected at week 0 (*ad libitum* feeding), and "Post CR" data were obtained at week 4. Male and female C57BL/6J and *Tst*$^{-/-}$ mice (n= 8 per group) were used. Data are plotted as mean ± SEM. Significant effects of CR, sex, and/or genotype were assessed using three-way ANOVA. AL: *ad libitum*, CR: calorie restriction (30%), Tst: thiosulfate sulfurtransferase.

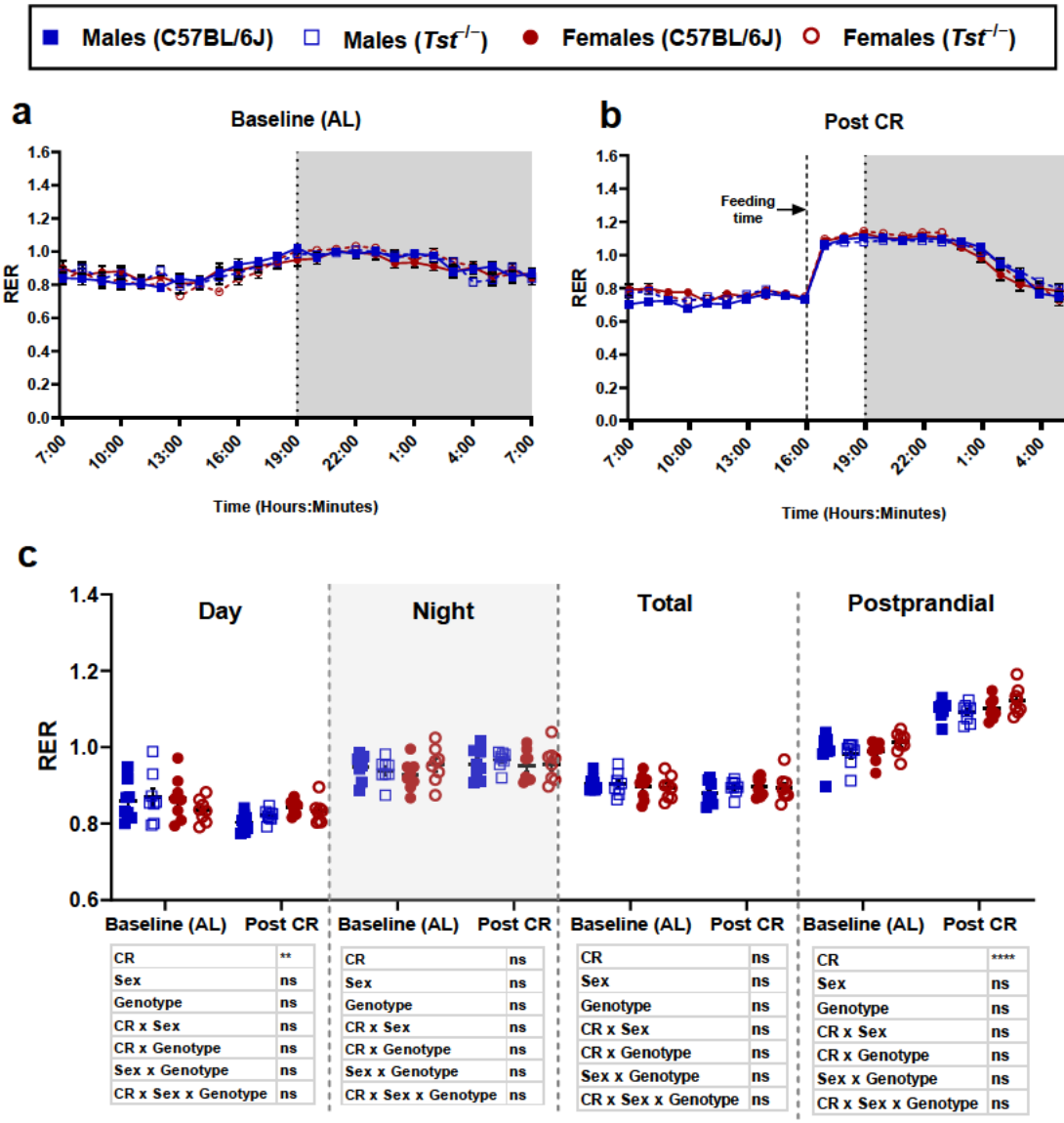

Figure 5.8 The impact of TST deficiency on substrate utilisation in mice in male and female mice at baseline and after 4 weeks of calorie restriction.

Respiratory exchange ratio (RER) is presented as a 24-hour profile at baseline (a) and after 4 weeks of CR (b). Panel (c) shows average RER values over the 24-hour light (day) and dark (night) periods, the total average over 24 hours, and the postprandial period (defined as 7-10 pm at "baseline" and as 4:30-7:30 pm at "Post CR" period); "baseline" data were collected at week 0 (*ad libitum* feeding), and "Post CR" data were obtained at week 4. Male and female C57BL/6J and *Tst*$^{-/-}$ mice (n= 8 per group) were used. Data are plotted as mean ± SEM. Significant effects of CR, sex, and/or genotype were assessed using three-way ANOVA followed by Tukey's post hoc tests, **P< 0.01, ****P< 0.0001. RER: respiratory exchange ratio, CR: calorie restriction (30%), AL: *ad libitum*, Tst: thiosulfate Sulfurtransferase.

5.4.5 CR did not alter the levels of hepatic hydrogen sulfide production and oxidation enzymes in the liver

Subsequently, I investigated the impact of CR on the key enzymes integral to the enzymatic pathways of the synthesis and clearance of H_2S. To address this question, C57BL/6J and *Tst*$^{-/-}$ mice were age and sex-matched with mice on *ad libitum* diet, thus ensuring a reliable dataset for my analysis.

There was a notable sexual dimorphism in enzyme levels, with females exhibiting consistently lower levels of sulfide-producing enzymes, including CSE, CBS, and MPST (Figure 5.9 a-c), irrespective of dietary intervention or genotype. Furthermore, female mice were characterised by reduced levels of TST (Figure 5.9 g).

The only alteration that could be ascribed to genotype manifested in the context of MPST levels. Specifically, elevated MPST expression was evident in *Tst*$^{-/-}$ male mice, independent of dietary conditions (Figure 5.9 c), consistent with previous studies (168).

The only significant effect of CR was increased levels of SQRDL in females of both genotypes ($P<0.01$) compared to *ad libitum* condition.

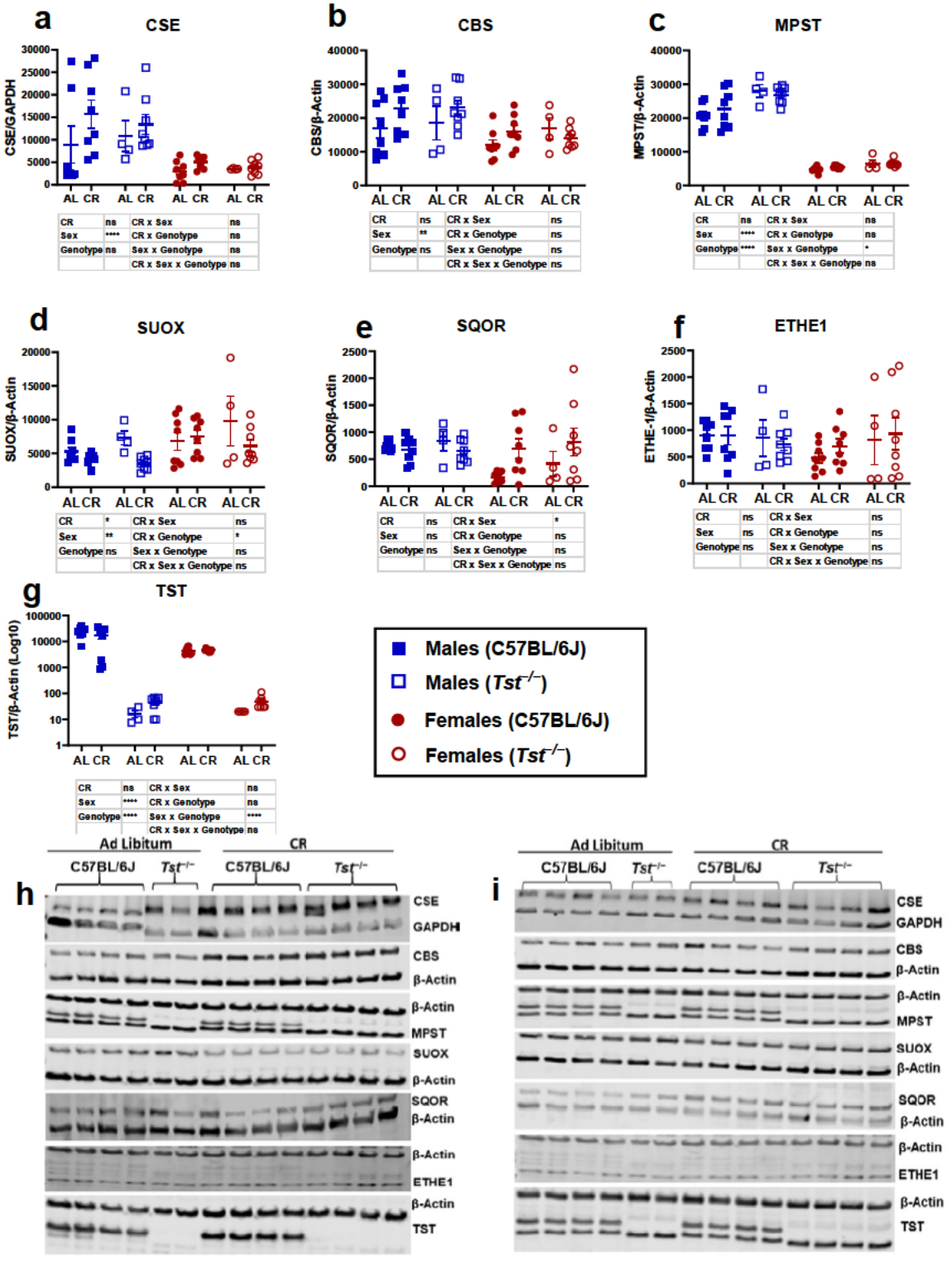

Figure 5.9 Western Blot quantification of protein levels involved in hydrogen sulfide production and clearance in the livers of male and female C57BL/6J and *Tst*$^{-/-}$ mice under *ad libitum* diet and after 4 weeks of caloric restriction.

Western blot quantification depicting the expression levels of enzymes (a) Cystathionine γ-lyase (CSE), (b) Cystathionine β-synthase (CBS), and (c) 3-Mercaptopyruvate sulfurtransferase (MPST), (d) Sulfite oxidase (SUOX), (e) sulfide quinone oxidoreductase (SQRDL), (f) ETHE1 Persulfide Dioxygenase (ETHE1), and (g) Thiosulfate sulfur transferase (TST). Representative western blot images for (h) males and (i) females. Male and female C57BL/6J and *Tst*$^{-/-}$ mice (n= 6 per group) were used, in addition to age, sex and genotype- matched mice that were fed *ad libitum* (n=6 per group). Data are plotted as mean ± SEM. Data in g are shown as log10-transformed intensities to normalise the wide range of signal intensities. Two-way ANOVA, with Tukey's post hoc tests were performed on the original (non-transformed) intensity values to determine statistical significance. *P< 0.05, **P< 0.01), *** P<0.001, ****P<0.0001. CR: calorie restriction (30%), AL: *ad libitum*.

5.5 Discussion

This study aimed to investigate the metabolic impact of TST deficiency on the benefits of CR in male and female mice, with the hypothesis that TST deficiency in *Tst*$^{-/-}$ mice will enhance the metabolic benefits of 30% CR for 4 weeks. I have used a genetic model of TST deficiency, proven to represent a state of elevated systemic sulfide with homeostatic hepatic sulfide levels to test the hypothesis that the metabolic benefits of CR require elevation of hepatic sulfide.

5.5.1 CR did not further elevate systemic or hepatic sulfide levels

Building on the findings of Hine *et al.* (236), who demonstrated the importance of hepatic H_2S elevation in the metabolic benefits of CR in mice, I hypothesised that *Tst*$^{-/-}$ mice, characterised by elevated H_2S levels, would experience greater benefits from CR compared to C57BL/6J mice. This study aimed to explore this hypothesis using a four-week mild CR (30% reduction in caloric intake).

The results showed that CR did not elevate systemic sulfide levels in either C57BL/6J or *Tst*$^{-/-}$ mice. Although *Tst*$^{-/-}$ mice had higher baseline systemic sulfide levels, CR did not further increase these levels. However, a modest rise in both systemic and hepatic thiosulfate levels was observed in *Tst*$^{-/-}$ mice following CR, indicating a potential increase in sulfide turnover in these animals. No changes in systemic levels of glutathione or cysteine were detected in either genotype, or sex. Thiosulfate, a by-product of H_2S oxidation, is known for its protective role against IRI, possibly through conversion back to H_2S. Despite the lack of a CR-induced increase in H_2S levels, a significant rise in systemic thiosulfate was observed exclusively in *Tst*$^{-/-}$ mice after four weeks, suggesting a genotype-specific response. This may be attributed to the already elevated baseline H_2S levels in *Tst*$^{-/-}$ mice, influencing thiosulfate accumulation.

It is important to note that "systemic" measurements refer to blood samples taken from the tail vein at a specific time of day, providing only a snapshot of sulfide levels. While this approach was consistent across all mice, it may not fully reflect the dynamic changes in sulfide levels in the blood or liver.

Due to the longitudinal design of this study, baseline hepatic sulfide levels could not be measured directly. However, previous research has comprehensively assessed these levels and reported them to be comparable between genotypes in male mice under basal *ad libitum* conditions (168). In this study, CR did not alter the relative hepatic sulfide levels between genotypes in either sex. These findings challenge the concept that elevation of hepatic sulfide is required for the beneficial metabolic effects of CR since we observed an improvement in glucose homeostasis in all mice, consistent with previous CR studies (217, 302-304), without elevation of hepatic sulfide. Notably, the most pronounced protective metabolic effect was observed in *Tst*$^{-/-}$ mice that presented with baseline impairment of glucose tolerance, as was observed previously (168, 194).

Since systemic sulfide levels remained unchanged and hepatic sulfide levels were unlikely to differ from baseline, increased hepatic sulfide does not appear to account for the improved glucose tolerance in either genotype. The complete correction of glucose intolerance in *Tst*$^{-/-}$ mice suggests alternative mechanisms driving this metabolic improvement. One potential explanation for the differences between my findings and those reported by Hine *et al.* (236) lies in the differing experimental conditions. Hine *et al.* (236) employed a 50% dietary restriction for one week, whereas I utilised a mild 30% CR over a 4-week period. It is possible that the acute increase in CSE activity leading to elevated H_2S levels reported by Hine *et al.* (236) may be a transient response rather than a sustained adaptation to CR. Additionally, Hine *et al.* (236) assessed CR benefits through resistance to IRI and reduced liver damage markers, while this study evaluated distinct parameters including glucose tolerance, weight loss, energy expenditure, and substrate utilisation. Moreover, methodological differences may contribute to the observed differences in results. Hine *et al.* (236) employed the lead sulfide method for measuring H_2S, which relies on the reaction of H_2S with lead salts to form a black precipitate, indicative of H_2S levels. This method has limitations due to potential interference from other sulfide compounds. In contrast, I – in collaboration with the mass spec core facility at the University of Edinburgh – have modified and utilised a method that relies on MBB derivatisation of sulfur species followed by LC-MS quantification for measurements in liver

tissue and whole blood. This method is more complicated and laborious but provides high sensitivity and specificity for detecting low levels of H_2S, and provides a certain level of consistency throughout all samples which were analysed at the same time

Carter *et al.* (168) suggested that the liver engages in increased respiratory sulfide disposal and enhanced exportation of cysteine and GSH to deal with the excess sulfide levels. In doing so the liver also activates pathways that lead to a more diabetic phenotype in *Tst*$^{-/-}$ males. One of the most striking observations in the baseline *Tst*$^{-/-}$ mice was their complete lack of an early-phase insulin release, compared to male C57BL/6J mice. This could point to a key role for the pancreas and regulation of insulin secretion as a potential explanation. Thus, the observed partial restoration of insulin secretion in CR, a small but meaningful insulin excursion on the background of increased insulin sensitivity with CR, could account for improved glucose tolerance. However, this cannot easily be ascribed to altered sulfide exposure in the pancreatic islets. Several studies have shown that H_2S is synthesised in pancreatic β cells by CSE and CBS, although their expression levels vary by specie, in male mice, immunohistochemistry revealed that while CBS and CSE expression levels were similar in the exocrine part of the pancreas, CBS expression was significantly higher in endocrine islets compared to CSE (305). *In vivo* and *in vitro* studies have demonstrated that increased H_2S levels can suppress glucose stimulated insulin secretion, in Zucker diabetic fatty (ZDF) rats, Wu *et al.* (306) observed impaired insulin secretion, increased pancreatic CSE levels, increased H_2S production, hyperglycemia, and insulin resistance compared to control rats. In cell culture, multiple studies showed that the overexpression of CSE to increase H_2S production results in reduced insulin secretion in response to high glucose doses in INS-1E cells (138) and in HIT-T15 Syrian hamster insulinoma cells (307). Overall, these findings indicate that increased H_2S produced in pancreatic islets plays a role in inhibiting glucose-stimulated insulin secretion. To know if this is the case with this study, intra-islet sulfide would need to be measured, which is challenging to achieve given the lengthy process required to isolate pancreatic islets, and consequent loss of true *in vivo* sulfide levels. The balance of H_2S generating and oxidising enzymes would also be informative in this context. Nevertheless, if altered sulfide does not explain either hepatic or islet effects, and by analogy, sulfide exposure remains unchanged in skeletal muscle, the conclusion remains that elevated sulfide is unlikely to explain the rescue of the impaired *Tst*$^{-/-}$ glucose intolerance phenotype.

An important consideration is whether methionine or cysteine restriction, rather than overall calorie restriction, could better elucidate the role of sulfur metabolism in glucose homeostasis. Methionine-restricted diets have been shown to elevate H_2S levels and promote metabolic health benefits, including enhanced glucose tolerance, reduced adiposity, and improved mitochondrial function (308-311). Since methionine is a precursor for H_2S production, a restriction in this amino acid may amplify changes in sulfur metabolism and provide more targeted insights into its role in CR-induced metabolic improvements. A similar rationale applies to cysteine restriction, which has been linked to beneficial effects on redox homeostasis and energy metabolism (109, 261, 310). Future studies comparing CR with methionine- or cysteine-restricted diets could clarify whether the observed improvements in glucose tolerance are dependent on changes in sulfur metabolism.

5.5.2 *Tst*$^{-/-}$ male mice are resistant to CR-induced weight loss, not explained by differences in EE or fuel utilisation

Tst$^{-/-}$ mice resisted the expected fat mass loss observed in male C57BL/6J mice. As an observation, this is interesting and requires further mechanistic investigation, but it does not readily explain the marked improvement in glucose tolerance unless greater fat mass in this case acts as a sink for glucose uptake during the glucose tolerance test. These observations align with previous studies indicating a role for TST in modulating body composition, likely through its influence on energy metabolism pathways (168), and showing *TST* mRNA levels in adipose tissue have a strong negative correlation with fat mass (194)**.** TST is known to modulate various metabolic pathways, including mitochondrial function and oxidative stress responses, which are integral to energy homeostasis (312). Our results suggest that TST deficiency may impair the utilisation of fat stores during CR, leading to a reliance on lean mass for energy production in *Tst*$^{-/-}$ males. Under normal conditions, CR triggers hormonal shifts, such as reduced insulin and increased growth hormone levels, which promote fat oxidation and protect muscle mass (313). However, in *Tst*$^{-/-}$ mice, this process is impaired, compromising fat oxidation and forcing the body to turn to proteolysis to generate glucose through gluconeogenesis (168). Carter *et al.* (168) provided evidence of increased hepatic gluconeogenesis in *Tst*$^{-/-}$ mice in *ad libitum* conditions, which further drives this reliance on lean mass for energy, as their elevated phosphoenolpyruvate carboxykinase (PEPCK) activity and enhanced pyruvate metabolism to oxaloacetate indicate increased glucose production from non-carbohydrate sources (168). Moreover, the deficiency in TST may interfere with key

pathways like ketogenesis, reducing the availability of fat-derived ketones and further promoting the breakdown of lean tissue to meet energy demands during CR. Combined with impaired lipid metabolism and increased triglycerides, all these factors could explain why *Tst*$^{-/-}$ male mice exhibit resistance to fat loss and an increased loss of lean mass.

To investigate whether this resistance to weight loss is due to higher EE, or changed fuel utilisation, I have measured EE and substrate utilisation and did not find genotype difference that would imply a simple increase or change in calorie burning accounts for the protective glycaemic effect. Both genotypes and genders showed the expected changes in EE and substrate utilisation after CR, suggesting on a gross level that lifelong adjustment to higher sulfide does not alter EE or fuel utilisation.

Consistent with our findings, previous studies have shown that females tend to resist fat mass loss during calorie restriction in mice (217, 314-316) and humans (206, 207, 317). These sex-specific responses to calorie restriction are attributed to hormonal factors, particularly oestrogen in females, which influences several aspects of fat metabolism, including lipolysis, lipogenesis, and adipocyte size and distribution (318). Oestrogen levels drive changes in fat storage between the sexes; in females, it drives subcutaneous adipose tissue (SAT) accumulation with limited visceral adipose tissue (VAT) accumulation which is thought to protect females from metabolic dysfunction caused by excess VAT accumulation (319).

This sex- specific response raises an important question of whether CR-induced metabolic benefits inherently limited or masked in female mice due to their unique metabolic characteristics. Female mice, in general, display a greater baseline resistance to metabolic dysregulation (217, 314-316), which may reduce the measurable impact of CR. Consistent with this, female mice in this study exhibited lower baseline levels of H_2S-producing enzymes (CSE, CBS, and MPST), a pattern observed regardless of dietary conditions. Interestingly, this sexual dimorphism did not correlate with baseline systemic sulfide levels, suggesting alternative regulatory mechanisms at play in females. The CR-induced increase in SQRDL in females may reflect a sex-specific adaptive response to maintain redox homeostasis rather than driving improvements in H_2S production or glucose tolerance.

In females, the inherent metabolic advantages may obscure the effects of CR, while in *Tst*$^{-/-}$ mice, alternative pathways, such as enhanced sulfide turnover or changes in insulin dynamics, may account for improved glucose tolerance. Future studies should focus on the interplay

between sulfide metabolism, hormonal regulation, and tissue-specific adaptations to CR, integrating measures of mitochondrial function, redox balance, and non-hepatic contributions to glucose homeostasis. Given the distinct metabolic adaptations in female mice, such as prioritising gluconeogenesis over oxidative pathways and resisting hepatic triglyceride reductions (168), it is unclear whether CR can yield measurable metabolic benefits under the current model. These sex-specific differences suggest that CR's effects may be inherently limited or less quantifiable in females compared to males.

Moreover, the age, body composition, and duration of intervention are critical factors that could influence these findings. Previous studies have shown that older, heavier mice may exhibit greater body-weight changes in response to CR due to larger fat reserves and increased metabolic dysregulation (320, 321). Additionally, longer intervention periods may allow for more pronounced shifts in metabolic pathways, including changes in H_2S metabolism, which could have been missed in this four-week study. Extending the CR duration to eight weeks or longer, or employing older, diet-induced obese mice, could help clarify whether the resistance to fat loss and enhanced glucose tolerance in *Tst*$^{-/-}$ mice are sustained or emerge more prominently under different experimental conditions. These factors are particularly relevant given the gradual adaptation of sulfur metabolism pathways and potential lag in observable phenotypic effects (310).

5.5.3 No significant effects of CR on hepatic H_2S metabolism enzymes, and evidence for sexual dimorphism

In this study, I investigated the impact of CR on hepatic H_2S production and oxidation enzymes using age- and sex-matched C57BL/6J and *Tst*$^{-/-}$ mice to ensure a reliable dataset for analysis. The results revealed that CR did not alter the levels of key hepatic enzymes involved in H_2S synthesis and clearance. Specifically, the levels of CSE, CBS, and MPST were unaffected by CR in both genotypes and both sexes. This challenges previous findings by Hine *et al.* (236), which suggested that increased H_2S production through CSE is critical for the metabolic benefits of CR. The lack of changes in enzyme levels indicates that the capacity for hepatic H2S production and metabolism may not be a major factor in mediating CR's effects on glucose homeostasis, as previously proposed.

An intriguing aspect of this study is the observed sexual dimorphism in enzyme levels, with female mice exhibiting consistently lower levels of CSE, CBS, and MPST, regardless of dietary

intervention. This finding points to inherent differences in H_2S metabolism between sexes, which may influence their response to metabolic challenges such as CR. Lower baseline levels of these enzymes in females could suggest a reduced capacity for H_2S production, which is unlikely since I found the levels of sulfide in males and females at baseline were similar, or a different regulatory mechanism for sulfide metabolism which is a more likely explanation. Understanding the biological basis for this sexual dimorphism, such as hormonal regulation or differences in metabolic rate, could provide insights into sex-specific responses to CR.

Notably, MPST levels were elevated in *Tst*$^{-/-}$ male mice compared to controls, independent of dietary conditions. This supports previous work by Carter *et al.* (168) suggesting a compensatory mechanism in the absence of TS. The upregulation of MPST in *Tst*$^{-/-}$ males may represent an adaptive response to maintain sulfide homeostasis despite the absence of TST activity, which could have broader implications for understanding how sulfide metabolism adapts in pathological states.

In contrast to the unchanged levels of most enzymes, CR was associated with an increase in SQRSL levels in female mice of both genotypes. This suggests a sex-specific adaptive response to CR that may involve enhanced sulfide oxidation. The functional implications of increased SQRDL require further study, but it could represent a compensatory mechanism to maintain sulfide homeostasis under conditions of reduced caloric intake. Given that SQRDL is involved in the detoxification of H_2S, its upregulation might also reflect a broader metabolic adaptation to CR, potentially linked to shifts in mitochondrial function or redox balance.

Overall, these findings indicate that while CR does not significantly impact hepatic H_2S production and oxidation enzyme levels, it does induce sex-specific changes in SQRDL. This underscores the complexity of H_2S metabolism regulation and suggests that factors beyond hepatic enzyme expression, such as cellular localisation, enzyme activity, or other tissues' contributions, may play a role. The observed sexual dimorphism and genotype-specific responses highlight the need for further investigation into the mechanisms driving these variations and their potential impact on metabolic health and disease outcomes.

Future research should explore the activity of H_2S -metabolising enzymes, the role of non-hepatic tissues, and the interplay between hormonal regulation and H_2S metabolism in the context of CR. Additionally, linking these findings to functional outcomes such as

mitochondrial activity, oxidative stress, and overall metabolic flexibility could provide a more comprehensive understanding of the role of H_2S in CR-mediated health benefits.

5.6 Limitations and recommendations for future work

Global *Tst* knockout vs. liver-specific effects

The *Tst* knockout used in this study is global, meaning TST deficiency affects all tissues, not just the liver. I recommend future studies to develop liver-specific *Tst* knockout models to isolate the hepatic role of TST in glucose regulation and energy metabolism. This would help clarify whether the impaired glucose tolerance and its correction during CR in $Tst^{-/-}$ male mice are directly related to hepatic H_2S levels or other functions of TST.

Lack of intra-tissue H_2S measurements

Although systemic measurements of sulfide and thiosulfate levels in blood provided valuable insights into whole-body H_2S dynamics. This study did not measure H_2S levels in tissues critical for glucose homeostasis and fat metabolism, such as pancreatic islets, skeletal muscle, and kidneys. This limits our understanding of how TST deficiency impacts local H_2S metabolism in these tissues, particularly their roles in insulin secretion and glucose utilisation. I recommend future studies should measure H_2S levels within pancreatic islets, muscle, and kidney tissues under both *ad libitum* and CR conditions. Islet-specific measurements of H_2S could help investigate the role of sulfide in insulin secretion dynamics, while kidney and muscle measurements may provide insights into tissue-specific metabolic changes contributing to the CR response.

Lack of insulin sensitivity data

In this study, I have found significant indications of improved insulin sensitivity such as the increased insulin secretion during the OGTTs and the improved HOMAIR and Matsuda index scores after CR. However, direct assessments of insulin sensitivity were not performed, leaving a gap in understanding how CR influences insulin dynamics in $Tst^{-/-}$ mice. I recommend future studies to conduct insulin tolerance tests (ITTs) and glucose-stimulated insulin secretion (GSIS) tests in both C57BL/6J and $Tst^{-/-}$ male mice before and after 4 weeks of CR to

comprehensively assess changes in insulin sensitivity. These tests would help determine the extent to which improved glucose tolerance in *Tst*$^{-/-}$ mice is driven by changes in insulin action.

Incomplete analysis of fatty acid oxidation and lipid metabolism

Although I found a significant reduction in hepatic fat in *Tst*$^{-/-}$ male mice after CR and a resistance to whole-body fat mass loss during CR. This study did not investigate key markers of fatty acid oxidation or quantify TGs, limiting the ability to explain the resistance to fat loss in *Tst*$^{-/-}$ mice and their reliance on lean mass for energy. I recommend future work to quantify serum TGs and measure the expression of genes involved in fatty acid oxidation (e.g., LCAD, Cyp4a14) before and after CR. This would help determine whether altered lipid metabolism or impaired fat oxidation explains the increased reliance on lean mass for energy production in *Tst*$^{-/-}$ mice during CR.

5.7 Conclusions

This study aimed to test the hypothesis that *Tst*$^{-/-}$ mice, which have impaired glucose tolerance and high liver fat content, would experience more pronounced metabolic benefits from 30% CR compared to C57BL/6J mice. The findings did not fully support this hypothesis, as CR improved glucose tolerance in both *Tst*$^{-/-}$ and C57BL/6J mice, but without significant differences between the genotypes. Importantly, the expected increase of hepatic sulfide levels in *Tst*$^{-/-}$ mice did not occur with CR, and glucose tolerance improved independently of hepatic sulfide elevation. While *Tst*$^{-/-}$ mice exhibited resistance to CR-induced fat mass loss, this resistance did not account for their improved glucose tolerance. These results suggest that the metabolic benefits of CR in *Tst*$^{-/-}$ mice are mediated by alternative mechanisms other than hepatic sulfide elevation. Since our findings challenge existing hypotheses regarding the role of sulfide metabolism in mediating the metabolic effects of CR, future studies should explore alternative mechanisms underlying the metabolic benefits of CR, including alterations in nutrient-sensing pathways, mitochondrial function, and oxidative stress responses especially in the context of mild but chronic CR.

6 Final discussion

6.1 Main findings

This PhD project aimed to investigate the role of thiosulfate sulfurtransferase (TST) in liver metabolism and its implications for metabolic-associated steatotic liver disease (MASLD) and calorie restriction. This interest was triggered by the discovery of *TST* as a gain-for-function genetic driver of "healthy leanness" in mice and by the protective metabolic effects observed in mice overexpressing TST in the adipose tissue (194), and the impaired glucose tolerance and fatty liver observed in the global *Tst* knockout model (168). The three studies in this thesis collectively highlight the complicated role of TST in liver metabolism, and its implications for MASLD and metabolic regulation.

The first study in chapter 3 aimed to test the hypothesis that elevated hepatic TST levels is protective against the metabolic dysfunction associated with MASLD *in vivo*. The results revealed that despite elevated hepatic TST expression in both early human MASLD patients and the early stages of MASLD in the STAM mouse model, overexpression of TST in our liver-specific mouse model did not provide the expected protective effects against diet-induced obesity, fat mass gain, or glucose intolerance. A mild protection from fibrosis in male mice with hepatic TST overexpression was observed warranting further research to confirm this protection and explore the mechanisms behind it. Furthermore, an interesting sex- specific response to GAN diet emerged where only female mice developed glucose intolerance over the period of 20 weeks, in addition to opposite systemic sulfide- diet dynamics in males and females regardless of TST overexpression.

The second study in chapter 4 explored the mechanistic effects of TST overexpression in HepaRG cells, showing that TST overexpression led to increased intralipid accumulation and impaired mitochondrial function despite reduced ROS production, these effects were true with and without challenges with the LPON fatty acid treatment. This suggests a metabolic trade-off where TST's potential to reduce oxidative stress comes at the cost of mitochondrial function, contributing to lipid accumulation and potentially promoting MASLD progression.

The third study in chapter 5 assessed the impact of 30% CR on $Tst^{-/-}$ mice compared to C57BL/6J mice, finding that CR improved glucose tolerance in both genotypes without significantly altering hepatic sulfide levels. This challenges the hypothesis that hepatic sulfide

elevation mediates the metabolic benefits of CR and suggests that other mechanisms may drive these benefits.

6.2 Implications of these findings

6.2.1 TST and glucose- insulin dynamics

In this project I have evaluated the impact of TST overexpression and deficiency on glucose tolerance in male and female mice within two different contexts, dietary overload (MASLD-inducing GAN diet) and calorie restriction.

The oral glucose tolerance test (OGTT) is an essential tool for assessing glucose metabolism and diagnosing diabetes and other glucose-related disorders. Its significance lies in its ability to provide a controlled, measurable challenge to the body's glucose-handling mechanisms by introducing a fixed glucose load. The OGTT is widely recognised for its sensitivity and precision in diagnosing conditions like impaired glucose tolerance and gestational diabetes mellitus, conditions that are critical for early intervention and preventing more severe metabolic issues, such as T2D and cardiovascular disease (322).

This study's findings have important implications for understanding the role of hepatic TST in glucose tolerance. In chapter 5 involving *Tst* knockout, $Tst^{-/-}$ male mice displayed impaired glucose tolerance under baseline *ad libitum* conditions, indicating the crucial role of TST in maintaining normal glucose metabolism, this impairment was accompanied by reduced insulin secretion as measured during the OGTTs especially the early response phase at 15 minutes after glucose administration. Interestingly, this impairment was corrected after a 4-week of 30% CR intervention, which significantly improved glucose tolerance in $Tst^{-/-}$ males despite their systemic sulfide levels still being higher than their C57BL/6J counterparts, and restored insulin secretion to comparable levels as the C57BL/6J counterparts.

Interestingly, female $Tst^{-/-}$ mice did not show any significant disruptions in glucose or insulin homeostasis, either at baseline or after CR. This highlights a potential sex-specific effect of TST on glucose regulation, where males seem more vulnerable to glucose intolerance in the absence of TST, but benefit more from dietary interventions like CR. The impaired glucose tolerance in $Tst^{-/-}$ male mice have been documented by Carter *et al.* and mechanisms behind it were studied in detail (168). Briefly, this impairment in $Tst^{-/-}$ males was suggested to be a result

of the liver engaging in compensatory mechanisms in response to the elevated H_2S levels caused by TST deficiency (168), such as reduced glutathione S-transferases (GST), which inhibit gluconeogenesis and the activation of NRF2, which suppresses gluconeogenesis in *Tst*$^{-/-}$ males. These mechanisms -aimed at increased export of H_2S out of the liver- also accidently reduce gluconeogenesis and increase the export of glucose, VLDL and TG to the bloodstream causing glucose impairment (168).

This study is the first to characterise the metabolic consequences of TST deficiency in female mice, my work demonstrated the striking lack of impact of TST deficiency on glucose tolerance in female mice compared to males, in the context of *ad libitum* and CR conditions. This points to a possible interaction between sex hormones, caloric intake, and the role of TST in glucose regulation, suggesting that female mice may possess different compensatory mechanisms in response to metabolic challenges. Interestingly, CR improved glucose tolerance and insulin sensitivity in both genotypes of male mice, but the effects in females were more subtle. The lack of glucose tolerance improvement by female mice after 30% CR was reported recently by Suchacki *et al.* (217). Suchacki *et al.* demonstrated that while CR enhances hepatic fatty acid oxidation in both sexes, only males utilise acetyl-CoA to support the TCA cycle and ATP production, leading to better glucose metabolism, whereas females direct acetyl-CoA towards gluconeogenesis to maintain blood glucose. Additionally, males exhibit changes in hepatic gene expression linked to the TCA cycle and oxidative phosphorylation, while females do not, limiting their glucose tolerance benefits (217). CR also affects hepatic sphingolipids differently, with males showing increases in insulin-sensitivity-related ceramides, which is not seen in females. Furthermore, females resist reductions in hepatic triglycerides during CR, a change associated with improved insulin sensitivity in males, potentially contributing to their lack of metabolic improvement (217). Together, these sex-specific liver adaptations explain why CR fails to enhance glucose tolerance in female mice.

In contrast to the glucose tolerance impairment caused by TST deficiency, the overexpression of TST in the liver did not impact the glucose tolerance. Both male and female mice with liver-specific TST overexpression did not exhibit improvements in glucose tolerance or insulin secretion under baseline conditions or following 20 weeks on GAN diet. These findings suggest that while TST plays a critical role in glucose homeostasis, its effects may be more pronounced in other tissues, such as adipose tissue as reported by Morton *et al.* (194), rather than in the liver. One possible reason for the lack of glucose tolerance improvement in this study could be

that the liver may not be the primary site where TST exerts protective effects on glucose metabolism. While the liver plays a central role in regulating glucose and lipid metabolism, TST's protective effects might be more effectively mediated in specialised tissues such as adipose tissue. Another consideration is the possibility of compensatory mechanisms in the liver that offset any potential benefits of TST overexpression. In this study, systemic and hepatic sulfide levels were not reduced in mice with elevated hepatic TST, despite continued overexpression of hTST throughout the 20 weeks of the experiment. This might suggest a complex interaction between TST and other metabolic pathways in the liver, preventing it from exerting the same effects observed in adipose tissue (194).

I also uncovered a sex-specific difference in glucose metabolism. After the 20-week GAN diet intervention, female mice exhibited impaired glucose tolerance and reduced insulin secretion compared to male mice, independent of hepatic TST overexpression. This suggests that female mice may be more vulnerable to the metabolic disruptions caused by the GAN diet. To the best of my knowledge, this study is the first to characterise the metabolic consequences of 20 weeks-GAN diet on female mice.

The findings from this project have significant implications for therapeutic targeting of TST in glucose and insulin regulation. First, the impaired glucose tolerance in *Tst*$^{-/-}$ male mice under *ad libitum* conditions, accompanied by reduced insulin secretion, suggests that TST plays a crucial role in maintaining normal glucose metabolism, particularly in males. The observation that CR restored glucose tolerance and insulin secretion in *Tst*$^{-/-}$ males highlights the potential of dietary interventions in mitigating glucose dysregulation caused by TST deficiency. This suggests that targeting TST function could be beneficial in developing metabolic therapies, particularly for conditions like impaired glucose tolerance or diabetes in males.

Female *Tst*$^{-/-}$ mice did not show glucose tolerance disruptions, even after CR, implying different compensatory mechanisms in females. This highlights the importance of considering sex differences when developing TST-targeted treatments, as females may not benefit from TST modulation in the same way males do. Moreover, overexpression of TST in the liver did not improve glucose tolerance in either sex after GAN diet. This suggests that the liver - despite having the highest expression of TST- may not be the primary site where TST exerts its protective effects on glucose metabolism, directing future research toward adipose tissue or other specialised tissues where TST may play a more pronounced role.

6.2.2 TST and lipid metabolism, weight gain and weight loss

This study provides important insights into the complex roles of TST in lipid metabolism, weight gain, and weight loss, offering new perspectives on how metabolic processes are regulated under different dietary conditions. In both male and female mice, the MASLD-inducing GAN diet led to significant increases in body weight and fat mass, a finding consistent with previous research showing that this diet induces adiposity (93, 94). However, liver-specific overexpression of TST did not prevent weight gain or fat accumulation, suggesting that TST's influence on lipid metabolism is not straightforward, especially in the liver. In fact, *in vitro* experiments with HepaRG cells in chapter 4 further revealed that TST overexpression led to a marked increase in lipid accumulation, even in the absence of external fatty acids, suggesting a direct influence on lipid metabolism. This excessive lipid retention was exacerbated by treatments mimicking MASLD, indicating that TST may disrupt normal mitochondrial processes responsible for fatty acid oxidation. While the overexpression of TST reduced oxidative stress, it simultaneously impaired mitochondrial function, particularly in ATP production and basal respiration. This metabolic imbalance suggests that TST overexpression may shift cellular energy use away from fatty acid oxidation, contributing to lipid accumulation and weight gain.

Interestingly, female mice on the GAN diet exhibited a unique metabolic adaptation with a significant increase in lean mass, possibly as a compensatory response to counteract the insulin resistance typically associated with a high-fat diet. This highlights a potential sex-specific mechanism in lipid metabolism, where female mice may increase muscle mass to buffer against the negative metabolic effects of excessive fat intake. In contrast, male mice did not show such an adaptation, but TST overexpression slightly protected them from developing fibrosis, pointing to a nuanced role for TST in modulating different aspects of metabolic health across sexes. In the context of weight loss, TST-deficient male mice displayed resistance to CR-induced fat mass loss, a phenomenon that was not explained by changes in energy expenditure or substrate utilisation as these were comparable between $Tst^{-/-}$ and C57BL/6J mice.

These findings suggest that TST plays a role in regulating fat metabolism during periods of caloric deficit. TST-deficient male mice seemed have impaired fat oxidation and altered glucose metabolism, which forced a greater reliance on gluconeogenesis from non-fat sources (168). This shift in energy production highlights the complex role of TST in balancing fat

storage and utilisation, as well as its potential impact on body composition during both weight gain and weight loss.

Collectively, these results suggest that TST exerts a multifaceted influence on lipid metabolism, where its overexpression in the liver promotes lipid accumulation and impairs mitochondrial function *in vitro*, and its deficiency alters fat utilisation during CR and promotes resistance to fat mass loss. These findings highlight the need for further research into how TST interacts with other metabolic pathways and how these interactions might differ between tissues and sexes, especially in the context of therapeutic interventions aimed at managing weight gain, obesity, and MASLD.

6.2.3 Implications for therapeutic approaches

Sulfide plays a dual role in cellular metabolism, acting as both a beneficial and detrimental molecule depending on its concentration and context (323). In this study, modulation of sulfide levels, particularly through the overexpression of TST, points to the complex role of sulfide in lipid metabolism, mitochondrial function, and oxidative stress regulation. At lower concentrations, sulfide serves as a signalling molecule, enhancing mitochondrial function by donating electrons to COX in the ETC, thereby promoting cellular respiration and ATP synthesis (160, 295). This is supported by evidence demonstrating that exogenous low sulfide levels can augment mitochondrial respiration and improve energy production. This role of sulfide is especially critical in tissues with high energy demands, such as the liver, where sulfide helps balance energy production and oxidative stress.

Conversely, at higher concentrations, sulfide becomes toxic by inhibiting mitochondrial function. This occurs *via* interference with COX activity, specifically through binding to the enzyme's Fe3+-a3 and CuB subunits, which disrupts electron transfer and oxygen consumption (169). Such inhibition leads to mitochondrial damage, reduced ATP production, and potential cellular dysfunction. The present study illustrates that TST overexpression, which clears out sulfide by facilitating its oxidation, led to impaired mitochondrial function in HepaRG cells, as evidenced by decreased basal respiration and ATP production. This suggests a metabolic trade-off: while sulfide reduction may alleviate oxidative stress, it can simultaneously compromise mitochondrial function. Therefore, identifying the dose at which sulfide exerts its beneficial effects is central to developing effective therapeutic approaches.

Another notable finding with important implications is the sex-specific response to the GAN diet, which induces MASLD. The study reveals that males exhibit higher systemic sulfide levels when fed a standard chow diet, but this effect is prevented by the GAN diet. In contrast, females experience a significant increase in systemic sulfide levels when exposed to the GAN diet. This has important therapeutic implications, particularly for treatments aimed at increasing sulfide levels, such as sulfide donors for MASLD alleviation. If females with MASLD already have elevated systemic sulfide, further increasing sulfide could have detrimental effects, a risk that may not manifest in male subjects. These findings add to the growing research emphasising the need for sex-specific therapeutic strategies when developing interventions targeting MASLD.

7 Concluding Remarks

This thesis provides new insights into the complex role of thiosulfate sulfurtransferase (TST) in liver metabolism and its implications for metabolic-associated steatotic liver disease (MASLD) and calorie restriction (CR). Although TST has been associated with "healthy leanness" and beneficial metabolic effects in previous studies, the findings here challenge the assumed protective role of TST in the liver. Elevated TST expression was observed in early MASLD stages in humans and mouse models; however, overexpression in a liver-specific mouse model did not prevent diet-induced obesity, fat accumulation, or glucose intolerance. Some protection against fibrosis was noted in males.

Mechanistic studies in HepaRG cells revealed that TST overexpression led to lipid accumulation and impaired mitochondrial function, despite lowering oxidative stress. This suggests a metabolic trade-off where TST's ability to reduce oxidative stress may come at the cost of mitochondrial function, potentially exacerbating lipid storage and MASLD progression.

In *Tst* knockout mice, impaired glucose tolerance and reduced insulin secretion were evident in males under normal conditions, with CR intervention significantly improving glucose regulation. Interestingly, female $Tst^{-/-}$ mice showed no such impairments, pointing to sex-specific metabolic adaptations that might buffer against TST deficiency. The lack of improvement in glucose tolerance among liver-specific TST overexpression models further suggests that TST's beneficial metabolic effects may be more prominent in tissues other than the liver, such as adipose tissue.

The findings also illuminate TST's role in lipid metabolism, where its overexpression *in vitro* promotes lipid accumulation, and its deficiency alters fat metabolism during CR, leading to resistance to fat loss. These results highlight TST's complex role in balancing lipid storage and energy use, particularly under different dietary conditions. Moreover, a unique sex-specific response to the MASLD-inducing GAN diet was identified, where females exhibited increased systemic sulfide levels, raising considerations for therapeutic strategies involving sulfide modulation.

These studies have significant implications for the therapeutic targeting of TST and sulfide metabolism. The dual role of sulfide as a beneficial and toxic molecule suggests that precise modulation of its levels is essential. The observed sex-specific responses to dietary challenges

underscore the need for personalised therapeutic approaches that consider individual metabolic contexts.

In conclusion, this thesis challenges the current understanding of TST's role in metabolic regulation, highlighting its complicated influence on glucose tolerance, lipid metabolism, and the effects of dietary interventions. These findings pave the way for future research to explore TST's tissue-specific roles, sex differences, and potential of manipulating the transsulfuration pathway as a therapeutic target for managing metabolic diseases like MASLD.

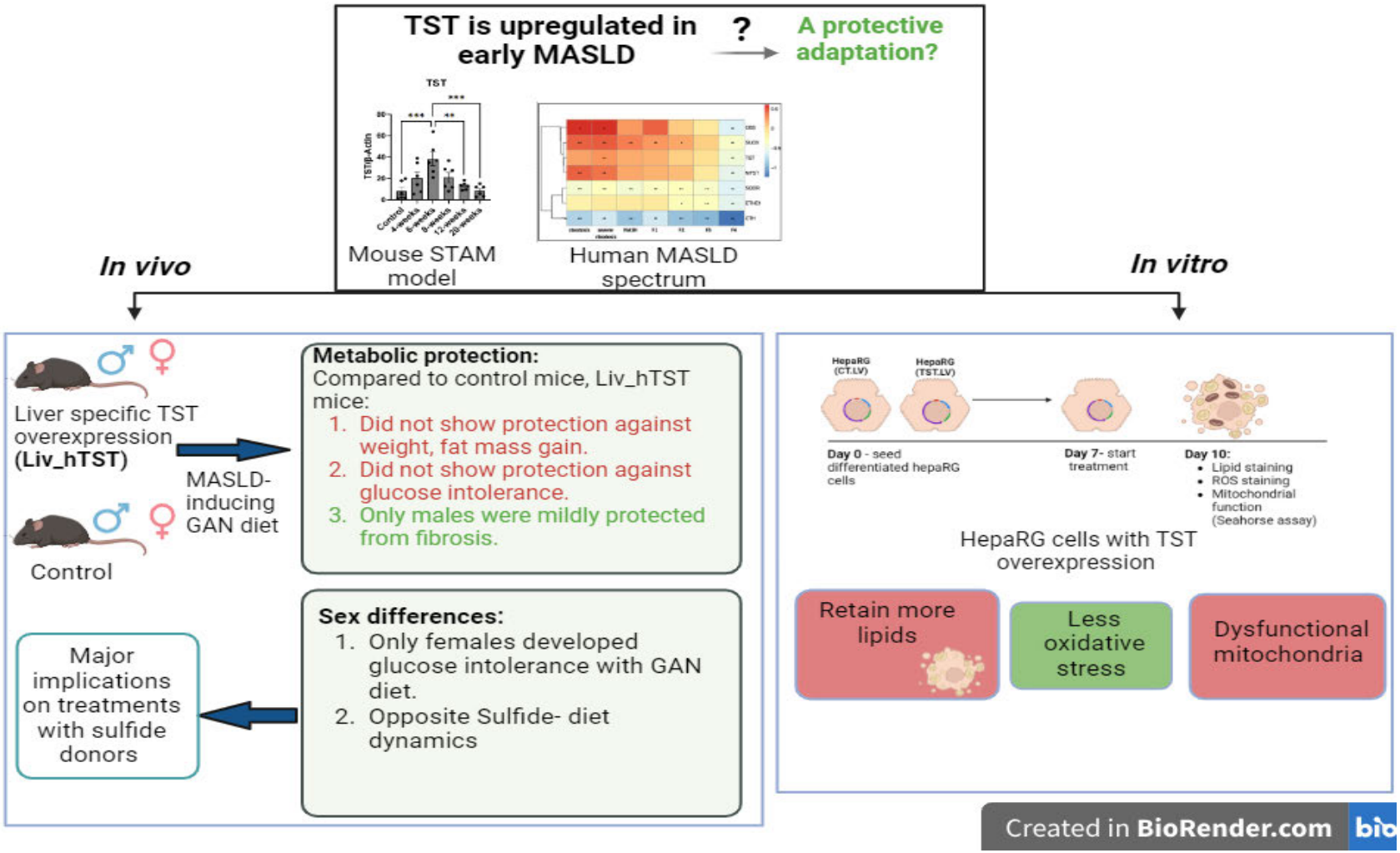

Figure 7.1 A schematic summary of the studies investigating the protective role of TST in MASLD. Created in BioRender.com

TST: Thiosulfate sulfurtransferase, Liv_hTST: liver specific TST overexpression, MASLD: Metabolic dysfunction-associated steatotic liver disease.

8 References

1. Rinella ME, Sookoian S. From nafld to masld: Updated naming and diagnosis criteria for fatty liver disease. Journal of lipid research. 2024;65(1):100485.

2. Malnick SDH, Zamir D. From non-alcoholic fatty liver disease to metabolic-associated steatotic liver disease: Rationale and implications for the new terminology. World Journal of Hepatology. 2024;16(6):863-6.

3. Staufer K, Stauber RE. Steatotic liver disease: Metabolic dysfunction, alcohol, or both? Biomedicines. 2023;11(8):2108.

4. Rinella ME, Lazarus JV, Ratziu V, Francque SM, Sanyal AJ, Kanwal F, et al. A multisociety delphi consensus statement on new fatty liver disease nomenclature. Hepatology. 2023;78(6):1966-86.

5. Kim GA, Moon JH, Kim W. Critical appraisal of metabolic dysfunction-associated steatotic liver disease: Implication of janus-faced modernity. Clinical Molecular Hepatology. 2023;29(4):831-43.

6. Masoodi M, Gastaldelli A, Hyötyläinen T, Arretxe E, Alonso C, Gaggini M, et al. Metabolomics and lipidomics in nafld: Biomarkers and non-invasive diagnostic tests. Nature reviews Gastroenterology & hepatology. 2021;18(12):835-56.

7. Castera L, Friedrich-Rust M, Loomba R. Noninvasive assessment of liver disease in patients with nonalcoholic fatty liver disease. Gastroenterology. 2019;156(5):1264-81.e4.

8. Teng ML, Ng CH, Huang DQ, Chan KE, Tan DJ, Lim WH, et al. Global incidence and prevalence of nonalcoholic fatty liver disease. Clinical Molecular Hepatology. 2023;29(Suppl):S32-s42.

9. Le MH, Yeo YH, Li X, Li J, Zou B, Wu Y, et al. 2019 global nafld prevalence: A systematic review and meta-analysis. Clinical Gastroenterology and Hepatology. 2022;20(12):2809-17. e28.

10. Bellentani S, Scaglioni F, Marino M, Bedogni G. Epidemiology of non-alcoholic fatty liver disease. Digestive Diseases. 2010;28(1):155-61.

11. Younossi ZM, Golabi P, Paik JM, Henry A, Van Dongen C, Henry L. The global epidemiology of nonalcoholic fatty liver disease (nafld) and nonalcoholic steatohepatitis (nash): A systematic review. Hepatology. 2023;77(4):1335-47.

12. Estes C, Razavi H, Loomba R, Younossi Z, Sanyal AJ. Modeling the epidemic of nonalcoholic fatty liver disease demonstrates an exponential increase in burden of disease. Hepatology. 2018;67(1):123-33.

13. Ito T, Ishigami M, Zou B, Tanaka T, Takahashi H, Kurosaki M, et al. The epidemiology of nafld and lean nafld in japan: A meta-analysis with individual and forecasting analysis, 1995–2040. Hepatology international. 2021;15:366-79.

14. Hagström H, Nasr P, Ekstedt M, Hammar U, Stål P, Hultcrantz R, et al. Fibrosis stage but not nash predicts mortality and time to development of severe liver disease in biopsy-proven nafld. Journal of hepatology. 2017;67(6):1265-73.

15. Day CP, James OF. Steatohepatitis: A tale of two "hits"? Gastroenterology. 1998;114(4):842-5.

16. Buzzetti E, Pinzani M, Tsochatzis EA. The multiple-hit pathogenesis of non-alcoholic fatty liver disease (nafld). Metabolism. 2016;65(8):1038-48.

17. Listenberger LL, Han X, Lewis SE, Cases S, Farese RV, Jr., Ory DS, et al. Triglyceride accumulation protects against fatty acid-induced lipotoxicity. Proceedings of the National Academy of Sciences. 2003;100(6):3077-82.

18. Mota M, Banini BA, Cazanave SC, Sanyal AJ. Molecular mechanisms of lipotoxicity and glucotoxicity in nonalcoholic fatty liver disease. Metabolism. 2016;65(8):1049-61.

19. Sanyal AJ, Kaplan LM, Frias JP, Brouwers B, Wu Q, Thomas MK, et al. Triple hormone receptor agonist retatrutide for metabolic dysfunction-associated steatotic liver disease: A randomized phase 2a trial. Nature Medicine. 2024;30(7):2037-48.

20. Petersen MC, Shulman GI. Mechanisms of insulin action and insulin resistance. Physiological reviews. 2018;98(4):2133-223.

21. Santoro A, McGraw TE, Kahn BB. Insulin action in adipocytes, adipose remodeling, and systemic effects. Cell Metabolism. 2021;33(4):748-57.

22. Soto A, Spongberg C, Martinino A, Giovinazzo F. Exploring the multifaceted landscape of masld: A comprehensive synthesis of recent studies, from pathophysiology to organoids and beyond. Biomedicines. 2024;12(2):397.

23. Zámbó V, Simon-Szabó L, Szelényi P, Kereszturi E, Bánhegyi G, Csala M. Lipotoxicity in the liver. World Journal of Hepatology. 2013;5(10):550-7.

24. Lee YA, Friedman SL. Inflammatory and fibrotic mechanisms in nafld—implications for new treatment strategies. Journal of Internal Medicine. 2022;291(1):11-31.

25. Geng Y, Faber KN, de Meijer VE, Blokzijl H, Moshage H. How does hepatic lipid accumulation lead to lipotoxicity in non-alcoholic fatty liver disease? Hepatology international. 2021;15(1):21-35.

26. Sekizkardes H, Chung ST, Chacko S, Haymond MW, Startzell M, Walter M, et al. Free fatty acid processing diverges in human pathologic insulin resistance conditions. The Journal of clinical investigation. 2020;130(7):3592-602.

27. Lipke K, Kubis-Kubiak A, Piwowar A. Molecular mechanism of lipotoxicity as an interesting aspect in the development of pathological states-current view of knowledge. Cells. 2022;11(5).

28. Juanola O, Martínez-López S, Francés R, Gómez-Hurtado I. Non-alcoholic fatty liver disease: Metabolic, genetic, epigenetic and environmental risk factors. International Journal of Environmental Research and Public Health. 2021;18(10).

29. Fontana L, Eagon JC, Trujillo ME, Scherer PE, Klein S. Visceral fat adipokine secretion is associated with systemic inflammation in obese humans. Diabetes. 2007;56(4):1010-3.

30. Merz KE, Thurmond DC. Role of skeletal muscle in insulin resistance and glucose uptake. Comprehensive Physiology. 2020;10(3):785-809.

31. Park SS, Seo YK. Excess accumulation of lipid impairs insulin sensitivity in skeletal muscle. International Journal of Molecular Sciences 2020;21(6).

32. Kim JK, Michael MD, Previs SF, Peroni OD, Mauvais-Jarvis F, Neschen S, et al. Redistribution of substrates to adipose tissue promotes obesity in mice with selective insulin resistance in muscle. The Journal of clinical investigation. 2000;105(12):1791-7.

33. Di Ciaula A, Calamita G, Shanmugam H, Khalil M, Bonfrate L, Wang DQ, et al. Mitochondria matter: Systemic aspects of nonalcoholic fatty liver disease (nafld) and diagnostic assessment of liver function by stable isotope dynamic breath tests. International Journal of Molecular Sciences. 2021;22(14).

34. Moore MP, Cunningham RP, Meers GM, Johnson SA, Wheeler AA, Ganga RR, et al. Compromised hepatic mitochondrial fatty acid oxidation and reduced markers of mitochondrial turnover in human nafld. Hepatology. 2022;76(5):1452-65.

35. Pérez-Carreras M, Del Hoyo P, Martín MA, Rubio JC, Martín A, Castellano G, et al. Defective hepatic mitochondrial respiratory chain in patients with nonalcoholic steatohepatitis. Hepatology. 2003;38(4):999-1007.

36. Martin J, Maurhofer O, Bellance N, Benard G, Graber F, Hahn D, et al. Disruption of the histidine triad nucleotide-binding hint2 gene in mice affects glycemic control and mitochondrial function. Hepatology. 2013;57(5):2037-48.

37. Amjad S, Nisar S, Bhat AA, Shah AR, Frenneaux MP, Fakhro K, et al. Role of nad(+) in regulating cellular and metabolic signaling pathways. Molecular metabolism. 2021;49:101195.

38. Hirschey MD, Shimazu T, Goetzman E, Jing E, Schwer B, Lombard DB, et al. Sirt3 regulates mitochondrial fatty-acid oxidation by reversible enzyme deacetylation. Nature. 2010;464(7285):121-5.

39. Pereira CV, Lebiedzinska M, Wieckowski MR, Oliveira PJ. Regulation and protection of mitochondrial physiology by sirtuins. Mitochondrion. 2012;12(1):66-76.

40. Sullivan EM, Pennington ER, Green WD, Beck MA, Brown DA, Shaikh SR. Mechanisms by which dietary fatty acids regulate mitochondrial structure-function in health and disease. Advances in Nutrition. 2018;9(3):247-62.

41. Ahmadpour ST, Mahéo K, Servais S, Brisson L, Dumas JF. Cardiolipin, the mitochondrial signature lipid: Implication in cancer. International Journal of Molecular Sciences. 2020;21(21).

42. Zorov DB, Juhaszova M, Sollott SJ. Mitochondrial reactive oxygen species (ros) and ros-induced ros release. Physiological reviews. 2014;94(3):909-50.

43. Masarone M, Rosato V, Dallio M, Gravina AG, Aglitti A, Loguercio C, et al. Role of oxidative stress in pathophysiology of nonalcoholic fatty liver disease. Oxidative Medicine and Cellular Longevity. 2018;2018(1):9547613.

44. Prasun P, Ginevic I, Oishi K. Mitochondrial dysfunction in nonalcoholic fatty liver disease and alcohol related liver disease. Translational Gastroenterology and Hepatology. 2021;6:4.

45. Rives C, Fougerat A, Ellero-Simatos S, Loiseau N, Guillou H, Gamet-Payrastre L, et al. Oxidative stress in nafld: Role of nutrients and food contaminants. Biomolecules. 2020;10(12).

46. Arroyave-Ospina JC, Wu Z, Geng Y, Moshage H. Role of oxidative stress in the pathogenesis of non-alcoholic fatty liver disease: Implications for prevention and therapy. Antioxidants (Basel, Switzerland). 2021;10(2).

47. Smirne C, Croce E, Di Benedetto D, Cantaluppi V, Comi C, Sainaghi PP, et al. Oxidative stress in non-alcoholic fatty liver disease. Livers. 2022;2(1):30-76.

48. Makrecka-Kuka M, Liepinsh E, Murray AJ, Lemieux H, Dambrova M, Tepp K, et al. Altered mitochondrial metabolism in the insulin-resistant heart. Acta Physiologica. 2020;228(3):e13430.

49. Dabravolski SA, Bezsonov EE, Baig MS, Popkova TV, Orekhov AN. Mitochondrial lipid homeostasis at the crossroads of liver and heart diseases. International Journal of Molecular Sciences. 2021;22(13).

50. Weiskirchen R, Tacke F. Cellular and molecular functions of hepatic stellate cells in inflammatory responses and liver immunology. Hepatobiliary Surgery and Nutrition. 2014;3(6):344-63.

51. Wu KJ, Qian QF, Zhou JR, Sun DL, Duan YF, Zhu X, et al. Regulatory t cells (tregs) in liver fibrosis. Cell Death Discovery. 2023;9(1):53.

52. Chen Z, Tian R, She Z, Cai J, Li H. Role of oxidative stress in the pathogenesis of nonalcoholic fatty liver disease. Free Radical Biology and Medicine. 2020;152:116-41.

53. Ortiz C, Schierwagen R, Schaefer L, Klein S, Trepat X, Trebicka J. Extracellular matrix remodeling in chronic liver disease. Current Tissue Microenvironment Reports. 2021;2(3):41-52.

54. Ignat SR, Dinescu S, Hermenean A, Costache M. Cellular interplay as a consequence of inflammatory signals leading to liver fibrosis development. Cells. 2020;9(2).

55. Araya J, Rodrigo R, Videla LA, Thielemann L, Orellana M, Pettinelli P, et al. Increase in long-chain polyunsaturated fatty acid n - 6/n - 3 ratio in relation to hepatic steatosis in patients with non-alcoholic fatty liver disease. Clinical Science 2004;106(6):635-43.

56. Chalasani N, Guo X, Loomba R, Goodarzi MO, Haritunians T, Kwon S, et al. Genome-wide association study identifies variants associated with histologic features of nonalcoholic fatty liver disease. Gastroenterology. 2010;139(5):1567-76, 76.e1-6.

57. Kozlitina J, Smagris E, Stender S, Nordestgaard BG, Zhou HH, Tybjærg-Hansen A, et al. Exome-wide association study identifies a tm6sf2 variant that confers susceptibility to nonalcoholic fatty liver disease. Nature genetics. 2014;46(4):352-6.

58. Umano GR, Martino M, Santoro N. The association between pediatric nafld and common genetic variants. Children (Basel). 2017;4(6).

59. Benedict M, Zhang X. Non-alcoholic fatty liver disease: An expanded review. World Journal of Hepatology. 2017;9(16):715-32.

60. Amangurbanova M, Huang DQ, Loomba R. Review article: The role of hsd17b13 on global epidemiology, natural history, pathogenesis and treatment of nafld. Alimentary pharmacology & therapeutics. 2023;57(1):37-51.

61. Mahmood S, Morrice N, Thompson D, Milanizadeh S, Wilson S, Whitfield PD, et al. Hydroxysteroid 17-beta dehydrogenase 13 (hsd17b13) knockdown attenuates liver steatosis in high-fat diet obese mice. bioRxiv. 2024:2024.02.27.582262.

62. Yang JD, Abdelmalek MF, Pang H, Guy CD, Smith AD, Diehl AM, et al. Gender and menopause impact severity of fibrosis among patients with nonalcoholic steatohepatitis. Hepatology. 2014;59(4):1406-14.

63. Romeo S, Kozlitina J, Xing C, Pertsemlidis A, Cox D, Pennacchio LA, et al. Genetic variation in pnpla3 confers susceptibility to nonalcoholic fatty liver disease. Nature genetics. 2008;40(12):1461-5.

64. Abdelmalek MF, Suzuki A, Guy C, Unalp-Arida A, Colvin R, Johnson RJ, et al. Increased fructose consumption is associated with fibrosis severity in patients with nonalcoholic fatty liver disease. Hepatology. 2010;51(6):1961-71.

65. Perseghin G, Lattuada G, De Cobelli F, Ragogna F, Ntali G, Esposito A, et al. Habitual physical activity is associated with intrahepatic fat content in humans. Diabetes Care. 2007;30(3):683-8.

66. Boursier J, Mueller O, Barret M, Machado M, Fizanne L, Araujo-Perez F, et al. The severity of nonalcoholic fatty liver disease is associated with gut dysbiosis and shift in the metabolic function of the gut microbiota. Hepatology. 2016;63(3):764-75.

67. Du Y, Zhang W, Qiu H, Xiao C, Shi J, Reid LM, et al. Mouse models of liver parenchyma injuries and regeneration. Frontiers in Cell and Developmental Biology. 2022;10:903740.

68. Denk H, Abuja PM, Zatloukal K. Animal models of nafld from the pathologist's point of view. Biochimica et Biophysica Acta (BBA)-Molecular Basis of Disease. 2019;1865(5):929-42.

69. Santhekadur PK, Kumar DP, Sanyal AJ. Preclinical models of non-alcoholic fatty liver disease. Journal of hepatology. 2018;68(2):230-7.

70. Hummel KP, Dickie MM, Coleman DL. Diabetes, a new mutation in the mouse. Science. 1966;153(3740):1127-8.

71. Bell-Anderson KS, Aouad L, Williams H, Sanz F, Phuyal J, Larter C, et al. Coordinated improvement in glucose tolerance, liver steatosis and obesity-associated inflammation by cannabinoid 1 receptor antagonism in fat aussie mice. International journal of obesity. 2011;35(12):1539-48.

72. Arsov T, Silva DG, O'Bryan MK, Sainsbury A, Lee NJ, Kennedy C, et al. Fat aussie—a new alstrom syndrome mouse showing a critical role for alms1 in obesity, diabetes, and spermatogenesis. Molecular endocrinology. 2006;20(7):1610-22.

73. Arsov T, Larter CZ, Nolan CJ, Petrovsky N, Goodnow CC, Teoh NC, et al. Adaptive failure to high-fat diet characterizes steatohepatitis in alms1 mutant mice. Biochemical and Biophysical Research Communications. 2006;342(4):1152-9.

74. Aravani D, Kassi E, Chatzigeorgiou A, Vakrou S. Cardiometabolic syndrome: An update on available mouse models. Thrombosis and Haemostasis. 2021;121(06):703-15.

75. Bieghs V, Van Gorp PJ, Wouters K, Hendrikx T, Gijbels MJ, van Bilsen M, et al. Ldl receptor knock-out mice are a physiological model particularly vulnerable to study the onset of inflammation in non-alcoholic fatty liver disease. PloS one. 2012;7(1):e30668.

76. Subramanian S, Goodspeed L, Wang S, Kim J, Zeng L, Ioannou GN, et al. Dietary cholesterol exacerbates hepatic steatosis and inflammation in obese ldl receptor-deficient mice. Journal of lipid research. 2011;52(9):1626-35.

77. Sullivan PM, Mezdour H, Quarfordt SH, Maeda N. Type iii hyperlipoproteinemia and spontaneous atherosclerosis in mice resulting from gene replacement of mouse apoe with human apoe* 2. The Journal of clinical investigation. 1998;102(1):130-5.

78. Baron M, Leroyer AS, Majd Z, Lalloyer F, Vallez E, Bantubungi K, et al. Pparα activation differently affects microparticle content in atherosclerotic lesions and liver of a mouse model of atherosclerosis and nash. Atherosclerosis. 2011;218(1):69-76.

79. Schierwagen R, Maybüchen L, Zimmer S, Hittatiya K, Bäck C, Klein S, et al. Seven weeks of western diet in apolipoprotein-e-deficient mice induce metabolic syndrome and non-alcoholic steatohepatitis with liver fibrosis. Scientific reports. 2015;5(1):12931.

80. Lo Sasso G, Schlage WK, Boué S, Veljkovic E, Peitsch MC, Hoeng J. The apoe(-/-) mouse model: A suitable model to study cardiovascular and respiratory diseases in the context of cigarette smoke exposure and harm reduction. Journal of Translational Medicine. 2016;14(1):146.

81. Tsuchida T, Lee YA, Fujiwara N, Ybanez M, Allen B, Martins S, et al. A simple diet-and chemical-induced murine nash model with rapid progression of steatohepatitis, fibrosis and liver cancer. Journal of hepatology. 2018;69(2):385-95.

82. Sharma L, Gupta D, Abdullah ST. Thioacetamide potentiates high cholesterol and high fat diet induced steato-hepatitic changes in livers of c57bl/6j mice: A novel eight weeks model of fibrosing nash. Toxicology Letters. 2019;304:21-9.

83. Flessa CM, Nasiri-Ansari N, Kyrou I, Leca BM, Lianou M, Chatzigeorgiou A, et al. Genetic and diet-induced animal models for non-alcoholic fatty liver disease (nafld) research. International Journal of Molecular Sciences. 2022;23(24).

84. Lau JKC, Zhang X, Yu J. Animal models of non-alcoholic fatty liver disease: Current perspectives and recent advances. The Journal of pathology. 2017;241(1):36-44.

85. Soret PA, Magusto J, Housset C, Gautheron J. In vitro and in vivo models of non-alcoholic fatty liver disease: A critical appraisal. Journal of Clinical Medicine. 2020;10(1).

86. dela Peña A, Leclercq I, Field J, George J, Jones B, Farrell G. Nf-κb activation, rather than tnf, mediates hepatic inflammation in a murine dietary model of steatohepatitis. Gastroenterology. 2005;129(5):1663-74.

87. Matsuzawa N, Takamura T, Kurita S, Misu H, Ota T, Ando H, et al. Lipid-induced oxidative stress causes steatohepatitis in mice fed an atherogenic diet. Hepatology. 2007;46(5):1392-403.

88. Henkel J, Coleman CD, Schraplau A, Jöhrens K, Weber D, Castro JP, et al. Induction of steatohepatitis (nash) with insulin resistance in wild-type b6 mice by a western-type diet containing soybean oil and cholesterol. Molecular Medicine. 2017;23:70-82.

89. Zheng S, Hoos L, Cook J, Tetzloff G, Davis Jr H, van Heek M, et al. Ezetimibe improves high fat and cholesterol diet-induced non-alcoholic fatty liver disease in mice. European journal of pharmacology. 2008;584(1):118-24.

90. Kohli R, Kirby M, Xanthakos SA, Softic S, Feldstein AE, Saxena V, et al. High-fructose, medium chain trans fat diet induces liver fibrosis and elevates plasma coenzyme q9 in a novel murine model of obesity and nonalcoholic steatohepatitis. Hepatology. 2010;52(3):934-44.

91. Tsuchiya H, Ebata Y, Sakabe T, Hama S, Kogure K, Shiota G. High-fat, high-fructose diet induces hepatic iron overload via a hepcidin-independent mechanism prior to the onset of liver steatosis and insulin resistance in mice. Metabolism. 2013;62(1):62-9.

92. Oligschlaeger Y, Shiri-Sverdlov R. Nafld preclinical models: More than a handful, less of a concern? Biomedicines. 2020;8(2):28.

93. Boland ML, Oró D, Tølbøl KS, Thrane ST, Nielsen JC, Cohen TS, et al. Towards a standard diet-induced and biopsy-confirmed mouse model of non-alcoholic steatohepatitis: Impact of dietary fat source. World journal of gastroenterology. 2019;25(33):4904-20.

94. Hansen HH, Ægidius HM, Oró D, Evers SS, Heebøll S, Eriksen PL, et al. Human translatability of the gan diet-induced obese mouse model of non-alcoholic steatohepatitis. BMC gastroenterology. 2020;20(1):1-12.

95. Ramos MJ, Bandiera L, Menolascina F, Fallowfield JA. In vitro models for non-alcoholic fatty liver disease: Emerging platforms and their applications. iScience. 2022;25(1):103549.

96. Wang Y-J, Liu H-L, Guo H-T, Wen H-W, Liu J. Primary hepatocyte culture in collagen gel mixture and collagen sandwich. World journal of gastroenterology. 2004;10(5):699.

97. Lőrincz T, Deák V, Makk-Merczel K, Varga D, Hajdinák P, Szarka A. The performance of hepg2 and heparg systems through the glass of acetaminophen-induced toxicity. Life (Basel). 2021;11(8).

98. Allard J, Bucher S, Massart J, Ferron P-J, Le Guillou D, Loyant R, et al. Drug-induced hepatic steatosis in absence of severe mitochondrial dysfunction in heparg cells: Proof of multiple mechanism-based toxicity. Cell Biology and Toxicology. 2021;37(2):151-75.

99. Tascher G, Burban A, Camus S, Plumel M, Chanon S, Le Guevel R, et al. In-depth proteome analysis highlights heparg cells as a versatile cell system surrogate for primary human hepatocytes. Cells. 2019;8(2).

100. Thomas RJ, Bhandari R, Barrett DA, Bennett AJ, Fry JR, Powe D, et al. The effect of three-dimensional co-culture of hepatocytes and hepatic stellate cells on key hepatocyte functions in vitro. Cells Tissues Organs. 2006;181(2):67-79.

101. Abu-Absi SF, Hansen LK, Hu W-S. Three-dimensional co-culture of hepatocytes and stellate cells. Cytotechnology. 2004;45:125-40.

102. Zinchenko YS, Schrum LW, Clemens M, Coger RN. Hepatocyte and kupffer cells co-cultured on micropatterned surfaces to optimize hepatocyte function. Tissue engineering. 2006;12(4):751-61.

103. Rose KA, Holman NS, Green AM, Andersen ME, LeCluyse EL. Co-culture of hepatocytes and kupffer cells as an in vitro model of inflammation and drug-induced hepatotoxicity. Journal of pharmaceutical sciences. 2016;105(2):950-64.

104. Pingitore P, Sasidharan K, Ekstrand M, Prill S, Lindén D, Romeo S. Human multilineage 3d spheroids as a model of liver steatosis and fibrosis. International Journal of Molecular Sciences. 2019;20(7):1629.

105. Park Y, Thadasina D, Bolujo I, Isidan A, Cross-Najafi AA, Lopez K, et al., editors. Three-dimensional organoids as a model to study nonalcoholic fatty liver disease. Seminars in Liver Disease; 2022: Thieme Medical Publishers, Inc.

106. Wang Y, Wang H, Deng P, Tao T, Liu H, Wu S, et al. Modeling human nonalcoholic fatty liver disease (nafld) with an organoids-on-a-chip system. ACS Biomaterials Science & Engineering. 2020;6(10):5734-43.

107. Duwaerts CC, Le Guillou D, Her CL, Phillips NJ, Willenbring H, Mattis AN, et al. Induced pluripotent stem cell–derived hepatocytes from patients with nonalcoholic fatty liver disease display a disease-specific gene expression profile. Gastroenterology. 2021;160(7):2591-4. e6.

108. Pareja E, Gómez-Lechón MJ, Tolosa L. Induced pluripotent stem cells for the treatment of liver diseases: Challenges and perspectives from a clinical viewpoint. Annals of translational medicine. 2020;8(8).

109. Carter RN, Morton NM. Cysteine and hydrogen sulphide in the regulation of metabolism: Insights from genetics and pharmacology. The Jornal of Pathology. 2016;238(2):321-32.

110. Comas F, Moreno-Navarrete JM. The impact of h(2)s on obesity-associated metabolic disturbances. Antioxidants (Basel, Switzerland). 2021;10(5):633.

111. Yang J, Minkler P, Grove D, Wang R, Willard B, Dweik R, et al. Non-enzymatic hydrogen sulfide production from cysteine in blood is catalyzed by iron and vitamin b(6). Communications biology. 2019;2:194-.

112. Bianco CL, Savitsky A, Feelisch M, Cortese-Krott MM. Investigations on the role of hemoglobin in sulfide metabolism by intact human red blood cells. Biochemical Pharmacology. 2018;149:163-73.

113. Cortese-Krott MM. Red blood cells as a “central hub” for sulfide bioactivity: Scavenging, metabolism, transport, and cross-talk with nitric oxide. Antioxidants & Redox Signaling. 2020;33(18):1332-49.

114. Jensen B, Fago A. A novel possible role for met hemoglobin as carrier of hydrogen sulfide in the blood. Antioxidants & Redox Signaling. 2019;32(4):258-65.

115. Fräsdorf B, Radon C, Leimkühler S. Characterization and interaction studies of two isoforms of the dual localized 3-mercaptopyruvate sulfurtransferase tum1 from humans. The Journal of biological chemistry. 2014;289(50):34543-56.

116. Kabil O, Vitvitsky V, Xie P, Banerjee R. The quantitative significance of the transsulfuration enzymes for h2s production in murine tissues. Antioxidants & Redox Signaling. 2011.

117. Mustafa AK, Gadalla MM, Snyder SH. Signaling by gasotransmitters. Science signaling. 2009;2(68):re2-re.

118. Mani S, Li H, Yang G, Wu L, Wang R. Deficiency of cystathionine gamma-lyase and hepatic cholesterol accumulation during mouse fatty liver development. Science Bulletin. 2015;60(3):336-47.

119. Shibuya N, Tanaka M, Yoshida M, Ogasawara Y, Togawa T, Ishii K, et al. 3-mercaptopyruvate sulfurtransferase produces hydrogen sulfide and bound sulfane sulfur in the brain. Antioxidants & Redox Signaling. 2008;11(4):703-14.

120. Yuan X, Zhang J, Xie F, Tan W, Wang S, Huang L, et al. Loss of the protein cystathionine β-synthase during kidney injury promotes renal tubulointerstitial fibrosis. Kidney and Blood Pressure Research 2017;42(3):428-43.

121. Jiang J, Chan A, Ali S, Saha A, Haushalter KJ, Lam W-LM, et al. Hydrogen sulfide-mechanisms of toxicity and development of an antidote. Scientific reports. 2016;6:20831-.

122. Singh SB, Lin HC. Hydrogen sulfide in physiology and diseases of the digestive tract. Microorganisms. 2015;3(4):866-89.

123. Goubern M, Andriamihaja M, Nübel T, Blachier F, Bouillaud F. Sulfide, the first inorganic substrate for human cells. Faseb journal. 2007;21(8):1699-706.

124. Suzuki K, Sagara M, Aoki C, Tanaka S, Aso Y. Clinical implication of plasma hydrogen sulfide levels in japanese patients with type 2 diabetes. Internal medicine (Tokyo, Japan). 2017;56(1):17-21.

125. Andrés CMC, Pérez de la Lastra JM, Andrés Juan C, Plou FJ, Pérez-Lebeña E. Chemistry of hydrogen sulfide-pathological and physiological functions in mammalian cells. Cells. 2023;12(23).

126. Rodkin S, Nwosu C, Sannikov A, Tyurin A, Chulkov VS, Raevskaya M, et al. The role of gasotransmitter-dependent signaling mechanisms in apoptotic cell death in cardiovascular, rheumatic, kidney, and neurodegenerative diseases and mental disorders. International Journal of Molecular Sciences. 2023;24(7).

127. Wilkie SE, Borland G, Carter RN, Morton NM, Selman C. Hydrogen sulfide in ageing, longevity and disease. Biochemical Journal. 2021;478(19):3485-504.

128. Filipovic MR. Persulfidation (s-sulfhydration) and h2s. In: Moore PK, Whiteman M, editors. Chemistry, biochemistry and pharmacology of hydrogen sulfide. Cham: Springer International Publishing; 2015. p. 29-59.

129. Mustafa AK, Gadalla MM, Sen N, Kim S, Mu W, Gazi SK, et al. H2s signals through protein s-sulfhydration. Science signaling. 2009;2(96):ra72-ra.

130. Paul BD, Snyder SH. H2s signalling through protein sulfhydration and beyond. Nature reviews Molecular cell biology. 2012;13(8):499-507.

131. Paul BD, Snyder SH. H2s: A novel gasotransmitter that signals by sulfhydration. Trends in biochemical sciences. 2015;40(11):687-700.

132. Filipovic MR, Zivanovic J, Alvarez B, Banerjee R. Chemical biology of h2s signaling through persulfidation. Chemical Reviews. 2018;118(3):1253-337.

133. Yang CT, Devarie-Baez NO, Hamsath A, Fu XD, Xian M. S-persulfidation: Chemistry, chemical biology, and significance in health and disease. Antioxidants & Redox Signaling. 2020;33(15):1092-114.

134. Yang G, Zhao K, Ju Y, Mani S, Cao Q, Puukila S, et al. Hydrogen sulfide protects against cellular senescence via s-sulfhydration of keap1 and activation of nrf2. Antioxidants & Redox Signaling. 2013;18(15):1906-19.

135. Hourihan JM, Kenna JG, Hayes JD. The gasotransmitter hydrogen sulfide induces nrf2-target genes by inactivating the keap1 ubiquitin ligase substrate adaptor through formation of a disulfide bond between cys-226 and cys-613. Antioxidants & Redox Signaling. 2013;19(5):465-81.

136. Liu H, Negoita F, Brook M, Sakamoto K, Morton NM. Quantification of persulfidation on specific proteins: Are we nearly there yet? Essays In Biochemistry. 2024.

137. Tang G, Wu L, Liang W, Wang R. Direct stimulation of k(atp) channels by exogenous and endogenous hydrogen sulfide in vascular smooth muscle cells. Molecular Pharmacology. 2005;68(6):1757-64.

138. Yang W, Yang G, Jia X, Wu L, Wang R. Activation of katp channels by h2s in rat insulin-secreting cells and the underlying mechanisms. The Journal of physiology. 2005;569(2):519-31.

139. Huang D, Jing G, Zhu S. Regulation of mitochondrial respiration by hydrogen sulfide. Antioxidants. 2023;12(8):1644.

140. Wen Y-D, Wang H, Kho S-H, Rinkiko S, Sheng X, Shen H-M, et al. Hydrogen sulfide protects huvecs against hydrogen peroxide induced mitochondrial dysfunction and oxidative stress. PloS one. 2013;8(2):e53147.

141. Wei G, Zhang W, Cao H, Yue S, Li P, Yang H. Effects hydrogen sulfide on the antioxidant system and membrane stability in mitochondria of malus hupehensis under nacl stress. Biol Plant. 2019;63:228-36.

142. Abe K, Kimura H. The possible role of hydrogen sulfide as an endogenous neuromodulator. Journal of Neuroscience. 1996;16(3):1066-71.

143. Hosoki R, Matsuki N, Kimura H. The possible role of hydrogen sulfide as an endogenous smooth muscle relaxant in synergy with nitric oxide. Biochemical and Biophysical Research Communications. 1997;237(3):527-31.

144. Kimura Y, Kimura H. Hydrogen sulfide protects neurons from oxidative stress. Faseb journal. 2004;18(10):1165-7.

145. Zhang J, Chen S, Liu H, Zhang B, Zhao Y, Ma K, et al. Hydrogen sulfide prevents hydrogen peroxide-induced activation of epithelial sodium channel through a pten/pi (3, 4, 5) p3 dependent pathway. PloS one. 2013;8(5):e64304.

146. Wallace JL, Blackler RW, Chan MV, Da Silva GJ, Elsheikh W, Flannigan KL, et al. Anti-inflammatory and cytoprotective actions of hydrogen sulfide: Translation to therapeutics. Antioxidants & Redox Signaling. 2015;22(5):398-410.

147. Wu D, Zheng N, Qi K, Cheng H, Sun Z, Gao B, et al. Exogenous hydrogen sulfide mitigates the fatty liver in obese mice through improving lipid metabolism and antioxidant potential. Medical gas research. 2015;5(1):1-.

148. Wu D, Wang J, Li H, Xue M, Ji A, Li Y. Role of hydrogen sulfide in ischemia-reperfusion injury. Oxidative Medicine and Cellular Longevity. 2015;2015:186908.

149. Giovinazzo D, Bursac B, Sbodio JI, Nalluru S, Vignane T, Snowman AM, et al. Hydrogen sulfide is neuroprotective in alzheimer's disease by sulfhydrating gsk3β and inhibiting tau hyperphosphorylation. Proceedings of the National Academy of Sciences. 2021;118(4):e2017225118.

150. Humphreys BD, Xu F, Sabbisetti V, Grgic I, Naini SM, Wang N, et al. Chronic epithelial kidney injury molecule-1 expression causes murine kidney fibrosis. The Journal of clinical investigation. 2013;123(9):4023-35.

151. Yuan X, Zhang J, Xie F, Tan W, Wang S, Huang L, et al. Loss of the protein cystathionine β-synthase during kidney injury promotes renal tubulointerstitial fibrosis. Kidney and Blood Pressure Research. 2017;42(3):428-43.

152. HOUSE DJ, BROSNAN EM, BROSNAN TJ. Characterization of homocysteine metabolism in the rat kidney. Biochemical Journal. 1997;328(1):287-92.

153. Nagahara N, Ito T, Kitamura H, Nishino T. Tissue and subcellular distribution of mercaptopyruvate sulfurtransferase in the rat: Confocal laser fluorescence and immunoelectron microscopic studies combined with biochemical analysis. Histochemistry and Cell Biology. 1998;110(3):243-50.

154. Bazhanov N, Ansar M, Ivanciuc T, Garofalo RP, Casola A. Hydrogen sulfide: A novel player in airway development, pathophysiology of respiratory diseases, and antiviral defenses. American journal of respiratory cell and molecular biology. 2017;57(4):403-10.

155. Khattak S, Zhang Q-Q, Sarfraz M, Muhammad P, Ngowi EE, Khan NH, et al. The role of hydrogen sulfide in respiratory diseases. Biomolecules. 2021;11(5):682.

156. Szabo C, Papapetropoulos A. International union of basic and clinical pharmacology. Cii: Pharmacological modulation of h2s levels: H2s donors and h2s biosynthesis inhibitors. Pharmacological reviews. 2017;69(4):497-564.

157. Mani S, Cao W, Wu L, Wang R. Hydrogen sulfide and the liver. Nitric Oxide. 2014;41:62-71.

158. Norris EJ, Culberson CR, Narasimhan S, Clemens MG. The liver as a central regulator of hydrogen sulfide. Shock (Augusta, Ga). 2011;36(3):242.

159. Wang R. Physiological implications of hydrogen sulfide: A whiff exploration that blossomed. Physiological reviews. 2012;92(2):791-896.

160. Sun H-J, Wu Z-Y, Nie X-W, Wang X-Y, Bian J-S. Implications of hydrogen sulfide in liver pathophysiology: Mechanistic insights and therapeutic potential. Journal of Advanced Research. 2021;27:127-35.

161. Watanabe M, Osada J, Aratani Y, Kluckman K, Reddick R, Malinow MR, et al. Mice deficient in cystathionine beta-synthase: Animal models for mild and severe homocyst(e)inemia. Proceedings of the National Academy of Sciences of the United States of America. 1995;92(5):1585-9.

162. Namekata K, Enokido Y, Ishii I, Nagai Y, Harada T, Kimura H. Abnormal lipid metabolism in cystathionine β-synthase-deficient mice, an animal model for hyperhomocysteinemia. Journal of Biological Chemistry. 2004;279(51):52961-9.

163. Li M, Xu C, Shi J, Ding J, Wan X, Chen D, et al. Fatty acids promote fatty liver disease via the dysregulation of 3-mercaptopyruvate sulfurtransferase/hydrogen sulfide pathway. Gut. 2018;67(12):2169-80.

164. Wei W, Wang C, Li D. The content of hydrogen sulfide in plasma of cirrhosis rats combined with portal hypertension and the correlation with indexes of liver function and liver fibrosis. Experimental and Therapeutic Medicine. 2017;14(5):5022-6.

165. Robert K, Nehmé J, Bourdon E, Pivert G, Friguet B, Delcayre C, et al. Cystathionine β synthase deficiency promotes oxidative stress, fibrosis, and steatosis in mice liver. Gastroenterology. 2005;128(5):1405-15.

166. Ci L, Yang X, Gu X, Li Q, Guo Y, Zhou Z, et al. Cystathionine γ-lyase deficiency exacerbates ccl4-induced acute hepatitis and fibrosis in the mouse liver. Antioxidants & Redox Signaling. 2017;27(3):133-49.

167. Zhang L, Yang G, Untereiner A, Ju Y, Wu L, Wang R. Hydrogen sulfide impairs glucose utilization and increases gluconeogenesis in hepatocytes. Endocrinology. 2013;154(1):114-26.

168. Carter RN, Gibbins MTG, Barrios-Llerena ME, Wilkie SE, Freddolino PL, Libiad M, et al. The hepatic compensatory response to elevated systemic sulfide promotes diabetes. Cell Reports. 2021;37(6):109958.

169. Murphy B, Bhattacharya R, Mukherjee P. Hydrogen sulfide signaling in mitochondria and disease. The FASEB Journal 2019;33(12):13098-125.

170. Hine C, Zhu Y, Hollenberg AN, Mitchell JR. Dietary and endocrine regulation of endogenous hydrogen sulfide production: Implications for longevity. antioxidants & redox signalling. 2018;28(16):1483-502.

171. Miękus N, Marszałek K, Podlacha M, Iqbal A, Puchalski C, Świergiel AH. Health benefits of plant-derived sulfur compounds, glucosinolates, and organosulfur compounds. Molecules. 2020;25(17).

172. Martelli A, Citi V, Testai L, Brogi S, Calderone V. Organic isothiocyanates as hydrogen sulfide donors. Antioxidants & Redox Signaling. 2020;32(2):110-44.

173. Powell CR, Dillon KM, Matson JB. A review of hydrogen sulfide (h(2)s) donors: Chemistry and potential therapeutic applications. Biochemical Pharmacology. 2018;149:110-23.

174. Kang K, Zhao M, Jiang H, Tan G, Pan S, Sun X. Role of hydrogen sulfide in hepatic ischemia-reperfusion–induced injury in rats. Liver Transplantation. 2009;15(10):1306-14.

175. Jha S, Calvert JW, Duranski MR, Ramachandran A, Lefer DJ. Hydrogen sulfide attenuates hepatic ischemia-reperfusion injury: Role of antioxidant and antiapoptotic signaling. American Journal of Physiology-Heart and Circulatory Physiology. 2008;295(2):H801-H6.

176. Chen Y, Yuan S, Cao Y, Kong G, Jiang F, Li Y, et al. Gasotransmitters: Potential therapeutic molecules of fibrotic diseases. Oxidative Medicine and Cellular Longevity. 2021;2021(1):3206982.

177. McFarlane L, Nelson P, Dugbartey GJ, Sener A. Pre-treatment of transplant donors with hydrogen sulfide to protect against warm and cold ischemia-reperfusion injury in kidney and other transplantable solid organs. International Journal of Molecular Sciences. 2023;24(4).

178. Papapetropoulos A, Pyriochou A, Altaany Z, Yang G, Marazioti A, Zhou Z, et al. Hydrogen sulfide is an endogenous stimulator of angiogenesis. The Proceedings of the National Academy of Sciences (PNAS). 2009;106(51):21972-7.

179. Kruithof PD, Lunev S, Aguilar Lozano SP, de Assis Batista F, Al-dahmani ZM, Joles JA, et al. Unraveling the role of thiosulfate sulfurtransferase in metabolic diseases. Biochimica et Biophysica Acta (BBA) - Molecular Basis of Disease. 2020;1866(6):165716.

180. Alsohaibani R, Claudel AL, Perchat-Varlet R, Boutserin S, Talfournier F, Boschi-Muller S, et al. Rhodanese-fold containing proteins in humans: Not just key players in sulfur trafficking. Antioxidants (Basel, Switzerland). 2023;12(4).

181. Pedre B, Dick TP. 3-mercaptopyruvate sulfurtransferase: An enzyme at the crossroads of sulfane sulfur trafficking. Biological Chemistry. 2021;402(3):223-37.

182. Bordo D, Bork P. The rhodanese/cdc25 phosphatase superfamily. EMBO reports. 2002;3(8):741-6.

183. Libiad M, Sriraman A, Banerjee R. Polymorphic variants of human rhodanese exhibit differences in thermal stability and sulfur transfer kinetics. Journal of Biological Chemistry. 2015;290(39):23579-88.

184. Gliubich F, Berni R, Colapietro M, Barba L, Zanotti G. Structure of sulfur-substituted rhodanese at 1.36 å resolution. Acta Crystallographica Section D. 1998;54(4):481-6.

185. Nagahara N, Tanaka M, Tanaka Y, Ito T. Novel characterization of antioxidant enzyme, 3-mercaptopyruvate sulfurtransferase-knockout mice: Overexpression of the evolutionarily-related enzyme rhodanese. Antioxidants. 2019;8(5):116.

186. Baskin SI, Horowitz AM, Nealley EW. The antidotal action of sodium nitrite and sodium thiosulfate against cyanide poisoning. The Journal of Clinical Pharmacology. 1992;32(4):368-75.

187. Buonvino S, Arciero I, Melino S. Thiosulfate-cyanide sulfurtransferase a mitochondrial essential enzyme: From cell metabolism to the biotechnological applications. International Journal of Molecular Sciences. 2022;23(15).

188. Billaut-Laden I, Allorge D, Crunelle-Thibaut A, Rat E, Cauffiez C, Chevalier D, et al. Evidence for a functional genetic polymorphism of the human thiosulfate sulfurtransferase (rhodanese), a cyanide and h2s detoxification enzyme. Toxicology. 2006;225(1):1-11.

189. Nagahara N. Catalytic site cysteines of thiol enzyme: Sulfurtransferases. Journal of Amino Acids. 2011;2011:709404.

190. Ploegman JH, Drent G, Kalk KH, Hol WGJ, Heinrikson RL, Keim P, et al. The covalent and tertiary structure of bovine liver rhodanese. Nature. 1978;273(5658):124-9.

191. Luo G-X, Horowitz PM. The sulfurtransferase activity and structure of rhodanese are affected by site-directed replacement of arg-186 or lys-249. Journal of Biological Chemistry. 1994;269(11):8220-5.

192. Hornbeck PV, Kornhauser JM, Tkachev S, Zhang B, Skrzypek E, Murray B, et al. Phosphositeplus: A comprehensive resource for investigating the structure and function of experimentally determined post-translational modifications in man and mouse. Nucleic Acids Research. 2012;40(Database issue):D261-70.

193. Herzig S, Shaw RJ. Ampk: Guardian of metabolism and mitochondrial homeostasis. Nature reviews Molecular cell biology. 2018;19(2):121-35.

194. Morton NM, Beltram J, Carter RN, Michailidou Z, Gorjanc G, McFadden C, et al. Genetic identification of thiosulfate sulfurtransferase as an adipocyte-expressed antidiabetic target in mice selected for leanness. Nature Medicine. 2016;22(7):771-9.

195. Yanai H, Yoshida H. Beneficial effects of adiponectin on glucose and lipid metabolism and atherosclerotic progression: Mechanisms and perspectives. International Journal of Molecular Sciences. 2019;20(5):1190.

196. Tiranti V, Viscomi C, Hildebrandt T, Di Meo I, Mineri R, Tiveron C, et al. Loss of ethe1, a mitochondrial dioxygenase, causes fatal sulfide toxicity in ethylmalonic encephalopathy. Nature Medicine. 2009;15(2):200-5.

197. McCay CM, Crowell MF, Maynard LA. The effect of retarded growth upon the length of life span and upon the ultimate body size: One figure. The Journal of Nutrition. 1935;10(1):63-79.

198. Larson-Meyer DE, Heilbronn LK, Redman LM, Newcomer BR, Frisard MI, Anton S, et al. Effect of calorie restriction with or without exercise on insulin sensitivity, beta-cell function, fat cell size, and ectopic lipid in overweight subjects. Diabetes Care. 2006;29(6):1337-44.

199. Guarente L. Calorie restriction and sir2 genes—towards a mechanism. Mechanisms of ageing and development. 2005;126(9):923-8.

200. Houthoofd K, Vanfleteren JR. The longevity effect of dietary restriction in caenorhabditis elegans. Experimental Gerontology 2006;41(10):1026-31.

201. Partridge L, Piper MD, Mair W. Dietary restriction in drosophila. Mechanisms of ageing and development. 2005;126(9):938-50.

202. Taormina G, Mirisola MG. Calorie restriction in mammals and simple model organisms. Biomedical research international. 2014;2014:308690.

203. Heilbronn LK, Ravussin E. Calorie restriction and aging: Review of the literature and implications for studies in humans. The American Journal of Clinical Nutrition. 2003;78(3):361-9.

204. Ramsey JJ, Harper M-E, Weindruch R. Restriction of energy intake, energy expenditure, and aging. Free Radical Biology and Medicine. 2000;29(10):946-68.

205. Colman RJ, Beasley TM, Kemnitz JW, Johnson SC, Weindruch R, Anderson RM. Caloric restriction reduces age-related and all-cause mortality in rhesus monkeys. Nature Communications. 2014;5(1):3557.

206. Fontana L, Klein S, Holloszy JO. Effects of long-term calorie restriction and endurance exercise on glucose tolerance, insulin action, and adipokine production. AGE. 2010;32:97-108.

207. Das SK, Roberts SB, Bhapkar MV, Villareal DT, Fontana L, Martin CK, et al. Body-composition changes in the comprehensive assessment of long-term effects of reducing intake of energy (calerie)-2 study: A 2-y randomized controlled trial of calorie restriction in nonobese humans. The American Journal of Clinical Nutrition. 2017;105(4):913-27.

208. Stewart TM, Bhapkar M, Das S, Galan K, Martin CK, McAdams L, et al. Comprehensive assessment of long-term effects of reducing intake of energy phase 2 (calerie phase 2) screening and recruitment: Methods and results. Contemporary Clinical Trials. 2013;34(1):10-20.

209. Fontana L, Klein S, Holloszy JO. Long-term low-protein, low-calorie diet and endurance exercise modulate metabolic factors associated with cancer risk. The American Journal of Clinical Nutrition. 2006;84(6):1456-62.

210. Redman LM, Smith SR, Burton JH, Martin CK, Il'yasova D, Ravussin E. Metabolic slowing and reduced oxidative damage with sustained caloric restriction support the rate of living and oxidative damage theories of aging. Cell Metabolism. 2018;27(4):805-15.e4.

211. Promrat K, Kleiner DE, Niemeier HM, Jackvony E, Kearns M, Wands JR, et al. Randomized controlled trial testing the effects of weight loss on nonalcoholic steatohepatitis. Hepatology. 2010;51(1):121-9.

212. Levine ME, Suarez JA, Brandhorst S, Balasubramanian P, Cheng C-W, Madia F, et al. Low protein intake is associated with a major reduction in igf-1, cancer, and overall mortality in the 65 and younger but not older population. Cell Metabolism. 2014;19(3):407-17.

213. Hambly C, Speakman JR. Contribution of different mechanisms to compensation for energy restriction in the mouse. Obesity Research. 2005;13(9):1548-57.

214. Blanc Sp, Schoeller D, Kemnitz J, Weindruch R, Colman R, Newton W, et al. Energy expenditure of rhesus monkeys subjected to 11 years of dietary restriction. The Journal of Clinical Endocrinology & Metabolism. 2003;88(1):16-23.

215. Ramsey JJ, Roecker EB, Weindruch R, Kemnitz JW. Energy expenditure of adult male rhesus monkeys during the first 30 mo of dietary restriction. American Journal of Physiology-Endocrinology and Metabolism. 1997;272(5):E901-E7.

216. Heilbronn LK, de Jonge L, Frisard MI, DeLany JP, Larson-Meyer DE, Rood J, et al. Effect of 6-month calorie restriction on biomarkers of longevity, metabolic adaptation, and oxidative stress in overweight individualsa randomized controlled trial. JAMA. 2006;295(13):1539-48.

217. Suchacki KJ, Thomas BJ, Ikushima YM, Chen K-C, Fyfe C, Tavares AAS, et al. The effects of caloric restriction on adipose tissue and metabolic health are sex- and age-dependent. eLife. 2023;12:e88080.

218. Sinclair DA. Toward a unified theory of caloric restriction and longevity regulation. Mechanisms of Ageing and Development 2005;126(9):987-1002.

219. Calabrese EJ, Mattson MP. Hormesis provides a generalized quantitative estimate of biological plasticity. Journal of Cell Communication and Signaling. 2011;5(1):25-38.

220. Tapia PC. Sublethal mitochondrial stress with an attendant stoichiometric augmentation of reactive oxygen species may precipitate many of the beneficial alterations in cellular physiology produced by caloric restriction, intermittent fasting, exercise and dietary phytonutrients: "Mitohormesis" for health and vitality. Medical Hypotheses. 2006;66(4):832-43.

221. Tucci P. Caloric restriction: Is mammalian life extension linked to p53? Aging (Albany NY). 2012;4(8):525.

222. Pan H, Finkel T. Key proteins and pathways that regulate lifespan. Journal of Biological Chemistry. 2017;292(16):6452-60.

223. Tulsian R, Velingkaar N, Kondratov R. Caloric restriction effects on liver mtor signaling are time-of-day dependent. Aging (Albany NY). 2018;10(7):1640-8.

224. Sadria M, Layton AT. Interactions among mtorc, ampk and sirt: A computational model for cell energy balance and metabolism. Cell Communication and Signaling. 2021;19(1):57.

225. Packer M. Longevity genes, cardiac ageing, and the pathogenesis of cardiomyopathy: Implications for understanding the effects of current and future treatments for heart failure. European Heart Journal 2020;41(39):3856-61.

226. Palikaras K, Lionaki E, Tavernarakis N. Balancing mitochondrial biogenesis and mitophagy to maintain energy metabolism homeostasis. Cell Death & Differentiation. 2015;22(9):1399-401.

227. Lettieri Barbato D, Baldelli S, Pagliei B, Aquilano K, Ciriolo MR. Caloric restriction and the nutrient-sensing pgc-1α in mitochondrial homeostasis: New perspectives in neurodegeneration. International Journal of Cell Biology. 2012;2012:759583.

228. Kobayashi M, Deguchi Y, Nozaki Y, Higami Y. Contribution of pgc-1α to obesity- and caloric restriction-related physiological changes in white adipose tissue. International Journal of Molecular Sciences. 2021;22(11).

229. Qiu X, Brown K, Hirschey MD, Verdin E, Chen D. Calorie restriction reduces oxidative stress by sirt3-mediated sod2 activation. Cell Metabolism. 2010;12(6):662-7.

230. Hallows WC, Yu W, Smith BC, Devires MK, Ellinger JJ, Someya S, et al. Sirt3 promotes the urea cycle and fatty acid oxidation during dietary restriction. Molecular cell. 2011;41(2):139-49.

231. Dhillon RS, Qin YA, van Ginkel PR, Fu VX, Vann JM, Lawton AJ, et al. Sirt3 deficiency decreases oxidative metabolism capacity but increases lifespan in male mice under caloric restriction. Aging cell. 2022;21(12):e13721.

232. Ristow M, Schmeisser K. Mitohormesis: Promoting health and lifespan by increased levels of reactive oxygen species (ros). Dose Response. 2014;12(2):288-341.

233. Hine CM, Mitchell JR. Nrf2 and the phase ii response in acute stress resistance induced by dietary restriction. Journal of Clinical and Experimental Pathology. 2012;S4(4).

234. Longchamp A, Mirabella T, Arduini A, MacArthur MR, Das A, Trevino-Villarreal JH, et al. Amino acid restriction triggers angiogenesis via gcn2/atf4 regulation of vegf and h2s production. Cell. 2018;173(1):117-29. e14.

235. Hine C, Mitchell JR. Calorie restriction and methionine restriction in control of endogenous hydrogen sulfide production by the transsulfuration pathway. Experimental Gerontology. 2015;68:26-32.

236. Hine C, Harputlugil E, Zhang Y, Ruckenstuhl C, Lee BC, Brace L, et al. Endogenous hydrogen sulfide production is essential for dietary restriction benefits. Cell. 2015;160(1-2):132-44.

237. Derous D, Mitchell SE, Wang L, Green CL, Wang Y, Chen L, et al. The effects of graded levels of calorie restriction: Xi. Evaluation of the main hypotheses underpinning the life extension effects of cr using the hepatic transcriptome. Aging (Albany NY). 2017;9(7):1770-824.

238. Greenhalgh SN, Conroy KP, Henderson NC. Cre-ativity in the liver: Transgenic approaches to targeting hepatic nonparenchymal cells. Hepatology. 2015;61(6):2091-9.

239. Virtue S, Vidal-Puig A. Gtts and itts in mice: Simple tests, complex answers. Nat Metab. 2021;3(7):883-6.

240. Künnecke B, Verry P, Bénardeau A, von Kienlin M. Quantitative body composition analysis in awake mice and rats by magnetic resonance relaxometry. Obesity Research. 2004;12(10):1604-15.

241. Matthews DR, Hosker JP, Rudenski AS, Naylor BA, Treacher DF, Turner RC. Homeostasis model assessment: Insulin resistance and beta-cell function from fasting plasma glucose and insulin concentrations in man. Diabetologia. 1985;28(7):412-9.

242. Matsuda M, DeFronzo RA. Insulin sensitivity indices obtained from oral glucose tolerance testing: Comparison with the euglycemic insulin clamp. Diabetes Care. 1999;22(9):1462-70.

243. Gu X, Ma Y, Liu Y, Wan Q. Measurement of mitochondrial respiration in adherent cells by seahorse xf96 cell mito stress test. STAR Protocols. 2021;2(1):100245.

244. Espinosa JA, Pohan G, Arkin MR, Markossian S. Real-time assessment of mitochondrial toxicity in hepg2 cells using the seahorse extracellular flux analyzer. Current protocols. 2021;1(3):e75.

245. Kendall TJ, Jimenez-Ramos M, Turner F, Ramachandran P, Minnier J, McColgan MD, et al. An integrated gene-to-outcome multimodal database for metabolic dysfunction-associated steatotic liver disease. Nature Medicine. 2023;29(11):2939-53.

246. Bankhead P, Loughrey MB, Fernández JA, Dombrowski Y, McArt DG, Dunne PD, et al. Qupath: Open source software for digital pathology image analysis. Scientific reports. 2017;7(1):1-7.

247. Fiorucci S, Antonelli E, Mencarelli A, Orlandi S, Renga B, Rizzo G, et al. The third gas: H2s regulates perfusion pressure in both the isolated and perfused normal rat liver and in cirrhosis. Hepatology. 2005;42(3):539-48.

248. Luo ZL, Tang LJ, Wang T, Dai RW, Ren JD, Cheng L, et al. Effects of treatment with hydrogen sulfide on methionine-choline deficient diet-induced non-alcoholic steatohepatitis in rats. Journal of Gastroenterology and Hepatology. 2014;29(1):215-22.

249. Wu D, Zhong P, Wang Y, Zhang Q, Li J, Liu Z, et al. Hydrogen sulfide attenuates high-fat diet-induced non-alcoholic fatty liver disease by inhibiting apoptosis and promoting autophagy via reactive oxygen species/phosphatidylinositol 3-kinase/akt/mammalian target of rapamycin signaling pathway. Frontiers in pharmacology. 2020;11:585860.

250. Sun L, Zhang S, Yu C, Pan Z, Liu Y, Zhao J, et al. Hydrogen sulfide reduces serum triglyceride by activating liver autophagy via the ampk-mtor pathway. American Journal of Physiology-Endocrinology and Metabolism. 2015;309(11):E925-35.

251. Zhao C, Yu N, Li W, Cai H, Liu M, Hu Y, et al. Slow-release h(2)s donor anethole dithiolethione protects liver from lipotoxicity by improving fatty acid metabolism. Frontiers in pharmacology. 2020;11:549377.

252. Feng X, Zhang H, Shi M, Chen Y, Yang T, Fan H. Toxic effects of hydrogen sulfide donor nahs induced liver apoptosis is regulated by complex iv subunits and reactive oxygen species generation in rats. Environmental Toxicology. 2020;35(3):322-32.

253. Bonomi F, Pagani S, Cerletti P, Cannella C. Rhodanese-mediated sulfur transfer to succinate dehydrogenase. European Journal of Biochemistry. 1977;72(1):17-24.

254. Pagani S, Galante YM. Interaction of rhodanese with mitochondrial nadh dehydrogenase. Biochimica et Biophysica Acta (BBA). 1983;742(2):278-84.

255. Nandi DL, Horowitz PM, Westley J. Rhodanese as a thioredoxin oxidase. The International Journal of Biochemistry & Cell Biology. 2000;32(4):465-73.

256. Begum M, Choubey M, Tirumalasetty MB, Arbee S, Mohib MM, Wahiduzzaman M, et al. Adiponectin: A promising target for the treatment of diabetes and its complications. Life (Basel). 2023;13(11).

257. Fujii M, Shibazaki Y, Wakamatsu K, Honda Y, Kawauchi Y, Suzuki K, et al. A murine model for non-alcoholic steatohepatitis showing evidence of association between diabetes and hepatocellular carcinoma. Medical Molecular Morphology. 2013;46(3):141-52.

258. Akahoshi N, Minakawa T, Miyashita M, Sugiyama U, Saito C, Takemoto R, et al. Increased urinary 3-mercaptolactate excretion and enhanced passive systemic anaphylaxis in mice lacking mercaptopyruvate sulfurtransferase, a model of mercaptolactate-cysteine disulfiduria. International Journal of Molecular Sciences. 2020;21(3):818.

259. Szabo C, Ransy C, Módis K, Andriamihaja M, Murghes B, Coletta C, et al. Regulation of mitochondrial bioenergetic function by hydrogen sulfide. Part i. Biochemical and physiological mechanisms. British Journal of Pharmacology. 2014;171(8):2099-122.

260. Yadav PK, Yamada K, Chiku T, Koutmos M, Banerjee R. Structure and kinetic analysis of h2s production by human mercaptopyruvate sulfurtransferase*. Journal of Biological Chemistry. 2013;288(27):20002-13.

261. Chiang FF, Chao TH, Huang SC, Cheng CH, Tseng YY, Huang YC. Cysteine regulates oxidative stress and glutathione-related antioxidative capacity before and after colorectal tumor resection. International Journal of Molecular Sciences. 2022;23(17).

262. Peh MT, Anwar AB, Ng DSW, Atan MSBM, Kumar SD, Moore PK. Effect of feeding a high fat diet on hydrogen sulfide (h2s) metabolism in the mouse. Nitric Oxide. 2014;41:138-45.

263. Fu X, Zhou K, Gao Q, Zheng S, Chen H, Li P, et al. 17β-estradiol attenuates atherosclerosis development: The possible role of hydrogen sulfide. International Journal of Cardiology. 2013;167(3):1061-3.

264. Hu J, Zhang Z, Shen WJ, Azhar S. Cellular cholesterol delivery, intracellular processing and utilization for biosynthesis of steroid hormones. Nature Metabolism 2010;7:47.

265. Nicholson CK, Calvert JW. Hydrogen sulfide and ischemia-reperfusion injury. Pharmacological Research. 2010;62(4):289-97.

266. Piragine E, Malanima MA, Lucenteforte E, Martelli A, Calderone V. Circulating levels of hydrogen sulfide (h(2)s) in patients with age-related diseases: A systematic review and meta-analysis. Biomolecules. 2023;13(7).

267. Fu M, Zhang W, Wu L, Yang G, Li H, Wang R. Hydrogen sulfide (h2s) metabolism in mitochondria and its regulatory role in energy production. Proceedings of the National Academy of Sciences of the United States of America. 2012;109(8):2943-8.

268. Chen XY, Wang C, Huang YZ, Zhang LL. Nonalcoholic fatty liver disease shows significant sex dimorphism. World Journal of Clinical Cases. 2022;10(5):1457-72.

269. Wang Y, Wu C, Zhou J, Fang H, Wang J. Overexpression of estrogen receptor β inhibits cellular functions of human hepatic stellate cells and promotes the anti-fibrosis effect of calycosin via inhibiting stat3 phosphorylation. BMC Pharmacology and Toxicology. 2022;23(1):77.

270. Al-Dahmani ZM, Hadian M, Ruiz-Moreno AJ, Maria S-GA, Batista FA, Zhang R, et al. Identification and characterization of a small molecule that activates thiosulfate sulfurtransferase and stimulates mitochondrial respiration. Protein Science. 2023;32(11):e4794.

271. Maseko TE, Elkalaf M, Peterová E, Lotková H, Staňková P, Melek J, et al. Comparison of heparg and hepg2 cell lines to model mitochondrial respiratory adaptations in non-alcoholic fatty liver disease. International Journal of Molecular Medicine. 2024;53(2).

272. Diprospero TJ, Brown LG, Fachko TD, Lockett MR. Heparg cells undergo increased levels of post-differentiation patterning in physiologic conditions when maintained as 3d cultures in paper-based scaffolds. Research Square. 2023.

273. Ströbel S, Kostadinova R, Fiaschetti-Egli K, Rupp J, Bieri M, Pawlowska A, et al. A 3d primary human cell-based in vitro model of non-alcoholic steatohepatitis for efficacy testing of clinical drug candidates. Scientific reports. 2021;11(1):22765.

274. Rezvani M, Vallier L, Guillot A. Modeling nonalcoholic fatty liver disease in the dish using human-specific platforms: Strategies and limitations. Cellular and molecular gastroenterology and hepatology. 2023;15(5):1135-45.

275. Lyall MJ, Cartier J, Thomson JP, Cameron K, Meseguer-Ripolles J, O'Duibhir E, et al. Modelling non-alcoholic fatty liver disease in human hepatocyte-like cells. Philosophical Transactions of the Royal Society B: Biological Sciences. 2018;373(1750):20170362.

276. Lockman KA, Baren JP, Pemberton CJ, Baghdadi H, Burgess KE, Plevris-Papaioannou N, et al. Oxidative stress rather than triglyceride accumulation is a determinant of mitochondrial dysfunction in in vitro models of hepatic cellular steatosis. Liver International. 2012;32(7):1079-92.

277. Ngo V, Duennwald ML. Nrf2 and oxidative stress: A general overview of mechanisms and implications in human disease. Antioxidants (Basel, Switzerland). 2022;11(12).

278. Donnelly KL, Smith CI, Schwarzenberg SJ, Jessurun J, Boldt MD, Parks EJ. Sources of fatty acids stored in liver and secreted via lipoproteins in patients with nonalcoholic fatty liver disease. The Journal of clinical investigation. 2005;115(5):1343-51.

279. Vairetti M, Di Pasqua LG, Cagna M, Richelmi P, Ferrigno A, Berardo C. Changes in glutathione content in liver diseases: An update. Antioxidants (Basel, Switzerland). 2021;10(3).

280. Grattagliano I, de Bari O, Bernardo TC, Oliveira PJ, Wang DQH, Portincasa P. Role of mitochondria in nonalcoholic fatty liver disease-from origin to propagation. Clinical Biochemistry. 2012;45(9):610-8.

281. Bessone F, Razori MV, Roma MG. Molecular pathways of nonalcoholic fatty liver disease development and progression. Cellular and Molecular Life Sciences. 2019;76:99-128.

282. Smirnov A, Comte C, Mager-Heckel AM, Addis V, Krasheninnikov IA, Martin RP, et al. Mitochondrial enzyme rhodanese is essential for 5 s ribosomal rna import into human mitochondria. Journal of Biological Chemistry. 2010;285(40):30792-803.

283. Luo Y, Chatre L, Melhem S, Al-Dahmani ZM, Homer NZM, Miedema A, et al. Thiosulfate sulfurtransferase deficiency promotes oxidative distress and aberrant nrf2 function in the brain. Redox Biology. 2023;68:102965.

284. Malhi H, Gores GJ. Molecular mechanisms of lipotoxicity in nonalcoholic fatty liver disease. Seminars in Liver Disease 2008;28(4):360-9.

285. Ligi S, Ali A, Yang G. Cystathionine gamma-lyase deficiency exaggerates diethylnitrosamine-induced liver damage in mice. Nitric Oxide. 2024;151:1-9.

286. Li X, Jiang K, Ruan Y, Zhao S, Zhao Y, He Y, et al. Hydrogen sulfide and its donors: Keys to unlock the chains of nonalcoholic fatty liver disease. International Journal of Molecular Sciences. 2022;23(20):12202.

287. Gerő D, Torregrossa R, Perry A, Waters A, Le-Trionnaire S, Whatmore JL, et al. The novel mitochondria-targeted hydrogen sulfide (h(2)s) donors ap123 and ap39 protect against hyperglycemic injury in microvascular endothelial cells in vitro. Pharmacological Research. 2016;113(Pt A):186-98.

288. Módis K, Coletta C, Erdélyi K, Papapetropoulos A, Szabo C. Intramitochondrial hydrogen sulfide production by 3-mercaptopyruvate sulfurtransferase maintains mitochondrial electron flow and supports cellular bioenergetics. The FASEB Journal. 2013;27(2):601-11.

289. Reily C, Mitchell T, Chacko BK, Benavides G, Murphy MP, Darley-Usmar V. Mitochondrially targeted compounds and their impact on cellular bioenergetics. Redox Biology. 2013;1(1):86-93.

290. Szabo C, Coletta C, Chao C, Módis K, Szczesny B, Papapetropoulos A, et al. Tumor-derived hydrogen sulfide, produced by cystathionine-β-synthase, stimulates bioenergetics, cell proliferation, and angiogenesis in colon cancer. The Proceedings of the National Academy of Sciences (PNAS). 2013;110(30):12474-9.

291. Guerra IMS, Ferreira HB, Melo T, Rocha H, Moreira S, Diogo L, et al. Mitochondrial fatty acid β-oxidation disorders: From disease to lipidomic studies-a critical review. International Journal of Molecular Sciences. 2022;23(22).

292. Gumucio JP, Qasawa AH, Ferrara PJ, Malik AN, Funai K, McDonagh B, et al. Reduced mitochondrial lipid oxidation leads to fat accumulation in myosteatosis. The FASEB Journal 2019;33(7):7863-81.

293. Koenitzer JR, Isbell TS, Patel HD, Benavides GA, Dickinson DA, Patel RP, et al. Hydrogen sulfide mediates vasoactivity in an o2-dependent manner. American Journal of Physiology-Heart and Circulatory Physiology. 2007;292(4):H1953-H60.

294. Nicholls P, Marshall DC, Cooper CE, Wilson MT. Sulfide inhibition of and metabolism by cytochrome c oxidase. Portland Press Ltd.; 2013.

295. Paul BD, Snyder SH, Kashfi K. Effects of hydrogen sulfide on mitochondrial function and cellular bioenergetics. Redox Biology. 2021;38:101772.

296. Pifferi F, Terrien J, Marchal J, Dal-Pan A, Djelti F, Hardy I, et al. Caloric restriction increases lifespan but affects brain integrity in grey mouse lemur primates. Communications biology. 2018;1(1):30.

297. Pak HH, Haws SA, Green CL, Koller M, Lavarias MT, Richardson NE, et al. Fasting drives the metabolic, molecular and geroprotective effects of a calorie-restricted diet in mice. Nature Metabolism. 2021;3(10):1327-41.

298. Dias IR, Santos CdS, Magalhães CODe, de Oliveira LRS, Peixoto MFD, De Sousa RAL, et al. Does calorie restriction improve cognition? IBRO Reports. 2020;9:37-45.

299. Omodei D, Fontana L. Calorie restriction and prevention of age-associated chronic disease. FEBS letters. 2011;585(11):1537-42.

300. Corvino A, Frecentese F, Magli E, Perissutti E, Santagada V, Scognamiglio A, et al. Trends in h2s-donors chemistry and their effects in cardiovascular diseases. Antioxidants. 2021;10(3):429.

301. Friederich MW, Elias AF, Kuster A, Laugwitz L, Larson AA, Landry AP, et al. Pathogenic variants in sqor encoding sulfide: Quinone oxidoreductase are a potentially treatable cause of leigh disease. Journal of inherited metabolic disease. 2020;43(5):1024-36.

302. Pires RC, Souza EE, Vanzela EC, Ribeiro RA, Silva-Santos JC, Carneiro EM, et al. Short-term calorie restriction improves glucose homeostasis in old rats: Involvement of ampk. Applied physiology, nutrition, and metabolism. 2014;39(8):895-901.

303. Mezhnina V, Kondratov R. Regulation of glucose homeostasis by calorie restriction and periodic fasting. Aging (Albany NY). 2020;12(23):23422.

304. Mayurasakorn K, Hasanah N, Homma T, Homma M, Rangel IK, Garza AE, et al. Caloric restriction improves glucose homeostasis, yet increases cardiometabolic risk in caveolin-1-deficient mice. Metabolism. 2018;83:92-101.

305. Kaneko Y, Kimura T, Taniguchi S, Souma M, Kojima Y, Kimura Y, et al. Glucose-induced production of hydrogen sulfide may protect the pancreatic beta-cells from apoptotic cell death by high glucose. FEBS letters. 2009;583(2):377-82.

306. Wu L, Yang W, Jia X, Yang G, Duridanova D, Cao K, et al. Pancreatic islet overproduction of h2s and suppressed insulin release in zucker diabetic rats. Laboratory investigation. 2009;89(1):59-67.

307. Ali MY, Whiteman M, Low C-M, Moore PK. Hydrogen sulphide reduces insulin secretion from hit-t15 cells by a katp channel-dependent pathway. Journal of endocrinology. 2007;195(1):105-12.

308. Ruckenstuhl C, Netzberger C, Entfellner I, Carmona-Gutierrez D, Kickenweiz T, Stekovic S, et al. Lifespan extension by methionine restriction requires autophagy-dependent vacuolar acidification. PLoS Genet. 2014;10(5):e1004347.

309. Miller RA, Buehner G, Chang Y, Harper JM, Sigler R, Smith-Wheelock M. Methionine-deficient diet extends mouse lifespan, slows immune and lens aging, alters glucose, t4, igf-i and insulin levels, and increases hepatocyte mif levels and stress resistance. Aging cell. 2005;4(3):119-25.

310. Richie JP, Jr., Komninou D, Leutzinger Y, Kleinman W, Orentreich N, Malloy V, et al. Tissue glutathione and cysteine levels in methionine-restricted rats. Nutrition. 2004;20(9):800-5.

311. Orentreich N, Matias JR, DeFelice A, Zimmerman JA. Low methionine ingestion by rats extends life span. The Journal of Nutrition. 1993;123(2):269-74.

312. Kabil O, Banerjee R. Enzymology of h2s biogenesis, decay and signaling. Antioxidants & Redox Signaling. 2014;20(5):770-82.

313. Selman C, Lingard S, Gems D, Partridge L, Withers DJ. Comment on" brain irs2 signaling coordinates life span and nutrient homeostasis". Science. 2008;320(5879):1012-.

314. Shi H, Strader AD, Woods SC, Seeley RJ. Sexually dimorphic responses to fat loss after caloric restriction or surgical lipectomy. American Journal of Physiology-Endocrinology and Metabolism. 2007;293(1):E316-E26.

315. Piotrowska K, Tarnowski M, Zgutka K, Pawlik A. Gender differences in response to prolonged every-other-day feeding on the proliferation and apoptosis of hepatocytes in mice. Nutrients. 2016;8(3):176.

316. Li X, Cope MB, Johnson MS, Smith Jr DL, Nagy TR. Mild calorie restriction induces fat accumulation in female c57bl/6j mice. Obesity. 2010;18(3):456-62.

317. Evans EM, Mojtahedi MC, Thorpe MP, Valentine RJ, Kris-Etherton PM, Layman DK. Effects of protein intake and gender on body composition changes: A randomized clinical weight loss trial. Nutrition & metabolism. 2012;9:1-9.

318. Kuryłowicz A. Estrogens in adipose tissue physiology and obesity-related dysfunction. Biomedicines. 2023;11(3).

319. Chang E, Varghese M, Singer K. Gender and sex differences in adipose tissue. Current Diabetes Reports. 2018;18(9):69.

320. Mitchell SJ, Madrigal-Matute J, Scheibye-Knudsen M, Fang E, Aon M, González-Reyes JA, et al. Effects of sex, strain, and energy intake on hallmarks of aging in mice. Cell Metabolism. 2016;23(6):1093-112.

321. Anderson RM, Shanmuganayagam D, Weindruch R. Caloric restriction and aging: Studies in mice and monkeys. Toxicologic pathology. 2009;37(1):47-51.

322. Lages M, Barros R, Moreira P, Guarino MP. Metabolic effects of an oral glucose tolerance test compared to the mixed meal tolerance tests: A narrative review. Nutrients. 2022;14(10).

323. Sun HJ, Wu ZY, Nie XW, Wang XY, Bian JS. Implications of hydrogen sulfide in liver pathophysiology: Mechanistic insights and therapeutic potential. Journal of Advanced Research 2021;27:127-35.